CVD/CVI pulsée du pyrocarbone : application aux matériaux composites thermostructuraux

Pascal Dupel

N° d'ordre : 927

THESE

PRESENTEE A

L'UNIVERSITE BORDEAUX I

ECOLE DOCTORALE DE SCIENCES CHIMIQUES

Par M. Pascal DUPEL

POUR OBTENIR LE GRADE DE

DOCTEUR

SPECIALITE : SCIENCES DES MATERIAUX

CVD/CVI pulsée du pyrocarbone
Application aux matériaux composites thermostructuraux

Soutenue le : 24 mai 1993

Après avis de : MM J. LAHAYE..... *Rapporteurs*
L. VANDENBULCKE.....

Devant la commission d'examen formée de :

MM.	J. LAHAYE	*Président*
	M. L. HITCHMAN.....	*Examinateurs*
	B. DARRIET.....	
	F. CHRISTIN.....	
	R. NASLAIN.....	
	R. PAILLER.....	
	L. VANDENBULCKE.....	

- 1993 -

N° d'ordre : 927

THESE

PRESENTEE A

L'UNIVERSITE BORDEAUX I

ECOLE DOCTORALE DE SCIENCES CHIMIQUES

Par M. Pascal DUPEL

POUR OBTENIR LE GRADE DE

DOCTEUR

SPECIALITE : SCIENCES DES MATERIAUX

CVD/CVI pulsée du pyrocarbone
Application aux matériaux composites thermostructuraux

Soutenue le : 24 mai 1993

Après avis de : MM J. LAHAYE..... *Rapporteurs*
L. VANDENBULCKE.....

Devant la commission d'examen formée de :

MM.	J. LAHAYE	*Président*
	M. L. HITCHMAN.....	*Examinateurs*
	B. DARRIET.....	
	F. CHRISTIN.....	
	R. NASLAIN.....	
	R. PAILLER.....	
	L. VANDENBULCKE.....	

- 1993 -

Cette étude a été réalisée au Laboratoire des Composites Thermostructuraux (Unité Mixte de Recherche 47 CNRS-Société Européenne de Propulsion-Université de Bordeaux I).

Monsieur le Professeur Roger NASLAIN, Directeur du Laboratoire des Composites Thermostructuraux, m'a accueilli au sein de son équipe de recherche et m'a encouragé dans mon travail. Je tiens à l'assurer de ma profonde reconnaissance.

Monsieur le Professeur Jacques LAHAYE, du Centre de Recherches sur la Physico-Chimie des Surfaces Solides de Mulhouses, m'a fait l'honneur de juger ce travail. Qu'il trouve ici l'expression de mes plus vifs remerciemments.

Monsieur Lionel VANDENBULCKE, Directeur de Recherches au Laboratoire de Combustion et Systèmes Réactifs d'Orléans, m'a fait le plaisir de juger cette étude, ce dont je le remercie chaleureusement.

Monsieur le Professeur, Michael L. HITCHMAN, de l'Université de Stathclyde, m'a fait l'honneur de participer à mon jury de thèse. Je le prie d'accepter l'expression de m'a respectueuse reconnaissance.

Monsieur le Professeur Bernard DARRIET, de l'Université de Bordeaux, a aimablement accepté de participer à mon jury de thèse. Je lui adresse mes sincères remerciements.

Monsieur François CHRISTIN, Chef du département développement matériaux de la S.E.P., a aimablement accepté de représenter notre partenaire industriel au sein du jury de thèse. Je lui adresse mes remerciements les plus sincères.

Monsieur René PAILLER, Ingénieur de Recherches au CNRS, a dirigé ce travail. Grâce à ses compétences scientifiques et techniques et à sa patience infinie, il m'a permis de mener à bien cette étude. Je tiens a lui exprimer ma profonde estime et ma sincère reconnaissance.

Messieurs X. BOURRAT et Francis LANGLAIS, Chargés de Recherches au CNRS, et Monsieur Jacques LAMON, Directeur de Recherches au CNRS, du Laboratoire des Composites Thermostructuraux, ont participé à ce travail de recherches. Qu'ils soient remerciés pour leur précieuse collaboration et pour la disponibilité dont ils ont fait preuve.

Monsieur Stéphane GOUJARD, Ingénieur à la Société Européenne de Propulsion, m'a conseillé tout au long de ce travail. Qu'il soit remercié pour son aimable collaboration.

Que tous les menbres du Laboratoire soient sincèrement remerciés. J'aimerais citer en particulier Nathalie RICCA, Cathy RACAULT, Christine LABRUGERE, Laurent GUILLAUMAT, Franck LAMOUROUX, Raphaël BODET, Jean Louis BOBET... et tous les autres, car chacun, par sa collaboration amicale et sa gentillesse, a permis de créer une ambiance de travail chaleureuse et agréable.

Je remercie Bruno HUMEZ et Muriel ALRIVIE pour leur constante disponibilité et pour l'aide qu'ils m'ont apporté lors des ess
-ais mécaniques et lors de la préparation des échantillons pour la microscopie électronique à transmission.

A l'ensemble de ces remerciements j'associe Madame Josette FORGET et Mesdemoiselles Florence DUCASSE ET Cécile DUPOUY, qui ont dactylographié le texte de ce mémoire, ainsi qu'à M. COIGNARD, pour toute l'aide qu'ils m'ont apporté durant mon séjour au Laboratoire.

Je remercie enfin la Société Européenne de Propulsion qui ma permis de conduire cette étude en me faisant bénéficier d'une bourse de recherche.

SOMMAIRE GENERALE

Chapître 1 : CVD/CVI OF PYROCARBON FROM PROPANE ON FLAT SUBSTRATES AND IN MODEL PORES WITH RECTANGULAR CROSS-SECTIONS

INTRODUCTION GENERALE

INTRODUCTION GENERALE

****

1- GENERALITES SUR LES MATERIAUX COMPOSITES

Un matériau composite est un assemblage intime d'au moins deux constituants de natures ou de structures différentes dont les propriétés individuelles se combinent et se complètent en donnant un matériau dont certaines performances globales sont améliorées vis à vis de celles de ses constituants pris individuellement.

C'est le développement des industries aérospatiales et aéronautiques, lors des 30 dernières années, qui a permis l'essor des matériaux composites obtenus en enrobant l'un des constituants (le renfort : fibres) par l'autre (la matrice).

Le champ d'application des composites apparaît être très vaste car, en théorie du moins, chacune des propriétés du matériau final peut être modulée par un choix adéquat des constituants initiaux. Il existe une large gamme de composites dont les propriétés dépendent (i) de la morphologie du matériau de renforcement (fibres longues, whiskers, sphères,..) qui conditionne le caractère isotrope ou anisotrope des propriétés, (ii) de la nature respective du renfort et de la matrice (organique, alliage métallique, verre ou céramique) dont dépend la température d'emploi du composite, et (iii) de la distribution relative des constituants (aléatoire, constituée de fibres alignées ou tissées,...).

Les composites les plus développés (90 % des applications) sont ceux qui associent une **matrice organique** (résine époxyde, polyester...) à des fibres de verre, de polyamide aromatique ou de carbone. Avec une fraction volumique de fibres de l'ordre de 60 %, leurs propriétés mécaniques sont équivalentes ou supérieures à celles d'aciers à haute résistance pour une masse volumique 4 fois plus faible. C'est pouquoi ils sont utilisés dans les industries automobile et aérospatiale en remplacement des alliages métalliques, ainsi que dans d'autres domaines tel celui des articles de sport. Cependant, leur faible stabilité thermique limite leur emploi aux applications à basse température (<300°C).

Les composites à **matrice métallique** permettent des températures d'utilisation plus élevées, de l'ordre de 600°C pour une matrice titane, mais présentent des problèmes à haute température, liés aux interactions chimiques entre les fibres et la matrice, qui réduisent le pouvoir renforçant des fibres. De plus, la plupart des fibres minérales sont mal mouillées par les métaux liquides, ce qui complique la réalisation de ce type de matériau.

Dans la gamme de température 600-1000°C, les composites à **matrice vitreuse** sont prometteurs grâce à une bonne inertie chimique, et à des propriétés mécaniques inaltérées jusque vers 1000°C (verre de silice-fibres d'alumine) [1], cependant, ils présentent une mauvaise résistance au fluage liée à la matrice.

Les céramiques présentent de grands avantages par rapport aux verres et aux métaux. C'est pourquoi une nouvelle gamme de matériaux composites associant des fibres minérales réfractaires à des matrices céramiques s'est développée ces dernières années : **les composites à matrice céramique (CMC).**

2 - LES COMPOSITES A MATRICE CERAMIQUE

2.1 - Principaux avantages et inconvénients

Les CMC se sont développés sous l'impulsion de l'industrie aérospatiale qui a besoin de matériaux permettant (i) d'alléger les éléments constituant les moteurs thermiques, et (ii) une température de fonctionnement de plus en plus élevée, ce qui n'est pas le cas des métaux réfractaires caractérisés par leur forte densité, leur recristallisation et/ou leur oxydation à haute température.

Les CMC présentent d'autres propriétés intéressantes qui justifient leur développement, entre autres, une dureté importante (pièces d'usure et d'abrasion), une bonne inertie chimique (le carbure de silicium résiste en atmosphère oxydante au-delà de 1500°C), une mauvaise conduction de la chaleur (barrière thermique efficace) et une mauvaise conduction électrique. Par ailleurs, au contraire de certains alliages spéciaux qu'ils sont susceptibles de remplacer, les CMC sont fabriqués à partir d'éléments courants facilement approvisionnables.

Le principal inconvénient des céramiques monolithiques est leur **fragilité**. Les systèmes de glissement étant peu nombreux dans les céramiques, elles ne présentent pas de déformation plastique comme les métaux, et sont donc très sensibles aux effets d'entaille et aux défauts de fabrication. La taille et la distribution des défauts étant aléatoires, une grande dispersion de la résistance à la rupture est observée [2].

Les différences entre les coefficients de dilatation thermique de la fibre et de la matrice, ainsi que les interactions chimiques entre les constituants

posent des problèmes dans leur choix. De plus, les caractéristiques mécaniques du composite doivent rester intéressantes à haute température.

2.2 - Les divers composites à matrice céramique

Les premiers CMC ayant été développés de façon industrielle sont les composites **carbone-carbone**. Ils sont utilisés pour leurs propriétés thermomécaniques (tuyères d'engin de propulsion, boucliers thermiques des corps de rentrée), pour leurs remarquables caractéristiques de friction (système de freinage dans l'aéronautique), et pour leur biocompatibilité (chirurgie orthopédique et dentaire). Les propriétés des composites carbone-carbone leur permettraient un vaste domaine d'utilisation s'ils ne s'oxydaient pas à l'air à partir de 500°C.

C'est pourquoi de nouvelles matrices furent développées pour pallier cet inconvénient : matrice carbure SiC [3], TiC [4], B_4C [5], matrice nitrure BN [6], matrice oxyde Al_2O_3 [7], et ZrO_2 [8]. La nature des fibres s'est également diversifiée (carbure de silicium, alumine, nitrure de silicium...).

2.3 - Méthodes d'élaboration des CMC

Les fibres étant très sensibles aux effets d'environnement, l'incorporation de la matrice dans le réseau constitué par le renfort doit se faire en utilisant des procédés basse température et basse pression. Trois types de méthodes sont généralement utilisés : voie solide, voie liquide, voie gazeuse.

L'élaboration en **phase solide** est réservée aux fibres courtes, trichytes ou poudres, car cette technique utilise un cycle de compression-frittage qui endommagerait fortement des fibres longues [9].

La **voie liquide** est surtout employée dans le cas des matrices vitro-céramiques car à la température de mise en oeuvre du verre, la viscosité est suffisamment basse pour permettre l'imprégnation directe du renfort, sous l'action d'une pression élevée [10]. Dans le cas des matrices céramiques, leur réfractairité interdit tout procédé d'imprégnation directe à partir de céramique fondue, mais l'utilisation de précurseurs organo-métalliques [11] ou de voie sol-gel semble prometteuse mais n'est pas encore très développée industriellement [12].

Avec **la voie gazeuse**, le dépôt de la matrice se fait directement sur les fibres par réactions chimiques hétérogènes, à partir d'un ou plusieurs gaz précurseurs, au sein d'un réseau de pores de tailles très diverses. Cette technique est appelée infiltration chimique en phase vapeur ou CVI (Chemical Vapor Infiltration) [13,14].

3 - L'INFILTRATION CHIMIQUE EN PHASE VAPEUR

Le procédé de dépôt chimique en phase vapeur ou CVD (Chemical Vapor Deposition) a été principalement développé et industrialisé dans le secteur de la microélectronique pour l'élaboration de couches minces isolantes (SiO_2, Al_2O_3, BN ...), semi-conductrices (Si, AsGa ...), ou conductrices (W, WSi_2 ...) pour des circuits intégrés et des dispositifs optoélectroniques [15].

Son application à des revêtements de surface, puis à des matériaux composites en a fait la technique d'élaboration la plus utilisée pour les CMC. L'un des intérêts majeurs de la CVI réside dans le fait que sa mise en œuvre se fait à température très inférieure à la température de fusion ou de décomposition de la céramique à déposer (e.g. vers 1000°C pour le carbure de silicium qui se décompose vers 2500°C). Cette technique peut donc être considérée comme une méthode " douce " qui limite la dégradation du renfort fibreux, et par conséquent celle des propriétés mécaniques. La réaction chimique de dépôt peut être une simple décomposition, une réduction, une hydrolyse ou une oxydation. Elle est généralemment activée en chauffant le substrat. Certains précurseurs sont liquides à température ambiante tel le Méthyl-Trichloro-Silane (CH_3SiCL_3) ou MTS, précurseur du SiC.

Il existe au moins trois variantes de la méthode CVI. La première consiste à imposer un **gradient de pression** de part et d'autre de la pièce à infiltrer, ce qui force les gaz réactifs à traverser le réseau de porosités de la préforme. La seconde impose un **gradient de température** au niveau du substrat, la partie interne étant plus chaude que la partie externe. Cela permet une meilleure infiltration des porosités car les gaz réactifs auront tendance à pénétrer dans les pores avant de réagir. Cette méthode permet de densifier plus rapidement (2 fois plus vite) [16-17]. Le grand inconvénient de ces deux méthodes est qu'elles ne permettent pas d'infiltrer simultanément un grand nombre de pièces, de telle sorte qu'on leur préfére une troisième méthode dite procédé **isotherme/isobar** (I-CVI) qui est à notre connaissance la seule méthode développée industriellement. Le problème majeur de cette dernière technique est que le dépôt a tendance à se faire préférentiellement en surface et à l'entrée des pores, ceci malgré un choix de conditions opératoires telles que

la cinétique des réactions de dépôt soit faible en comparaison des vitesses de transfert de matière au sein de la porosité. La durée de densification d'une préforme fibreuse est donc longue, de l'ordre de quelques centaines d'heures, et, dans le cas de grosses pièces, il est nécessaire de faire plusieurs cycles d'infiltration avec un usinage de surface entre les cycles. De plus, la porosité résiduelle n'est pas négligeable. Deux types de fours d'infiltrations sont utilisés, le réacteur à **parois froides**, et le réacteur à **parois chaudes**. Dans le premier cas, seul le substrat est chauffé, ce qui limite les réactions en phase homogène et les dépôts sur les parois du four mais induit de forts gradients thermiques dans la phase gazeuse et rend sa composition difficile à contrôler à la surface du substrat. Dans le second cas, le réacteur permet d'avoir une phase gazeuse plus homogène mais il se produit un dépôt important sur les parois du four et une consommation accrue de gaz réactifs.

La synthèse par I-CVI d'un solide dans un réacteur à parois chaudes comprend une série de transports et de réactions chimiques décrite à la figure 1, [18-19] :

1- transport par convection forcée du mélange gazeux introduit dans le réacteur vers la zone chaude où se trouve le substrat,

2 - élévation de la température du mélange gazeux pouvant provoquer des réactions homogènes entre ces différents constituants. La nouvelle phase gazeuse peut être totalement différente de la phase initiale et composée d'espèces intermédiaires stables à cette température,

3 - transport par convection et par diffusion dans les porosités, des espèces intermédiaires,

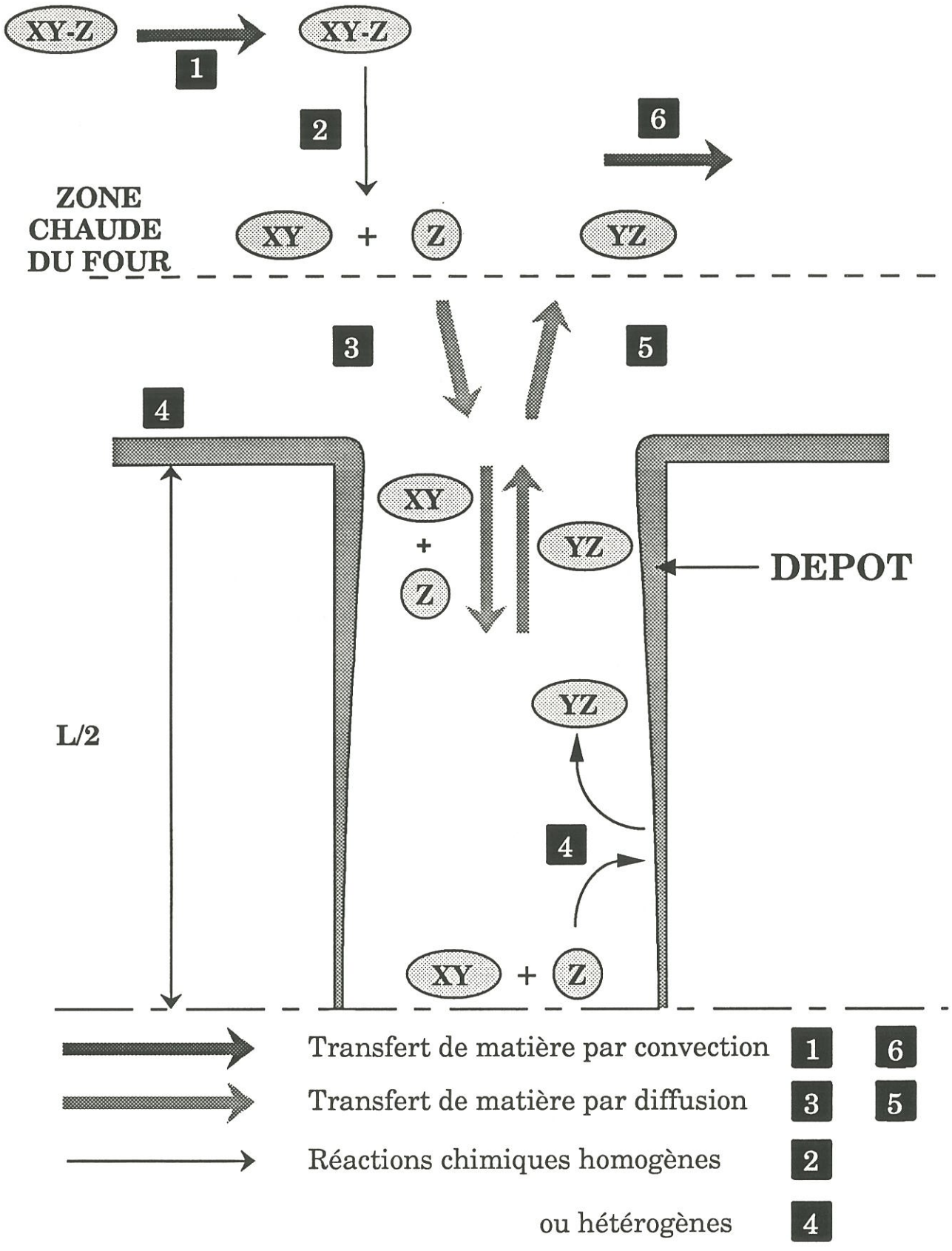

Fig. 1 : Schéma de principe du processus de dépôt dans un pore de dimension L d'un solide X à partir de l'espèce gazeuse source XYZ.

$$XYZ_{(g)} \longrightarrow X_{(s)} + YZ_{(g)}$$

4 - réactions chimiques hétérogènes de ces espèces au contact du substrat faisant intervenir :

(a) l'adsorption des espèces réactives,

(b) les réactions à la surface entre espèces adsorbées ou entre espèces adsorbées et espèces présentes dans la phase gazeuse,

(c) la désorption des espèces adsorbées, en particulier des espèces produites par les réactions à la surface du substrat,

5 - transport par diffusion des espèces produites, vers l'extérieur de la porosité,

6 - transport par convection forcée, de la zone réactionnelle vers la sortie du réacteur, des espèces produites et des espèces n'ayant pas réagi.

Dans la mesure où ces étapes sont séquentielles, la plus lente, appelée **étape limitante**, détermine la vitesse de dépôt de la céramique. Généralement, le processus est contrôlé soit par les transferts de masse (étapes 3 et 5), soit par les réactions de surface (étape 4).

Les étapes 3 et 4 sont couplées en tout point de la surface interne des pores. Pour obtenir une bonne infiltration, il faut, en première analyse, que les réactions de surface (étape 4) soient l'étape limitante du processus de dépôt afin que les espèces réactives aient le temps de diffuser au coeur de la porosité avant de réagir. Pour cela, il faut généralement que le dépôt soit réalisé à basse température et à basse pression. L'étape 5 est très importante dans la mesure où dans la plupart des cas les produits de réaction agissent en tant

qu'inhibiteur dans la réaction de surface. La difficulté consiste à évacuer ces espèces produites par les réactions de dépôt qui en s'accumulant au sein du pore inhibent la réaction de dépôt et s'opposent à la diffusion des espèces réactives, et par conséquent conduisent à une mauvaise densification à cœur du substrat .

Pour évacuer les espèces produites par les réactions de surface, il suffit d'arrêter l'introduction des gaz réactifs et de vider le réseau poreux par pompage. Cette idée a donné naissance à un nouveau type d'infiltration chimique en phase vapeur : **la CVI pulsée ou P-CVI** [20-26].

4 - L'INFILTRATION CHIMIQUE EN PHASE VAPEUR PULSEE

4.1 - Généralités

Contrairement à la CVI classique (I-CVI) où les paramètres de dépôt sont constants ou n'évoluent que très lentement au cours du temps, l'infiltration chimique en phase vapeur pulsée (P-CVI) consiste en une succession de cycles (ou pulse) composés de trois phases (figure 2).

Ce cyclage implique, par exemple, une variation périodique de la pression au sein du four qui passe de quelque Pa (vide primaire) à quelques dizaines de kPa très rapidemment. Il serait possible de faire varier d'autres paramètres, telle la température ou le débit, mais **la pression** est le paramètre le plus facile à faire varier instantanément.

L'étape **d'introduction** des gaz est très courte (< 0,2 s) car le gaz réactif peut être stocké sous pression. Les gaz réactifs peuvent être mélangés dans un réservoir avant introduction dans le four, ou bien introduits simultanément ou

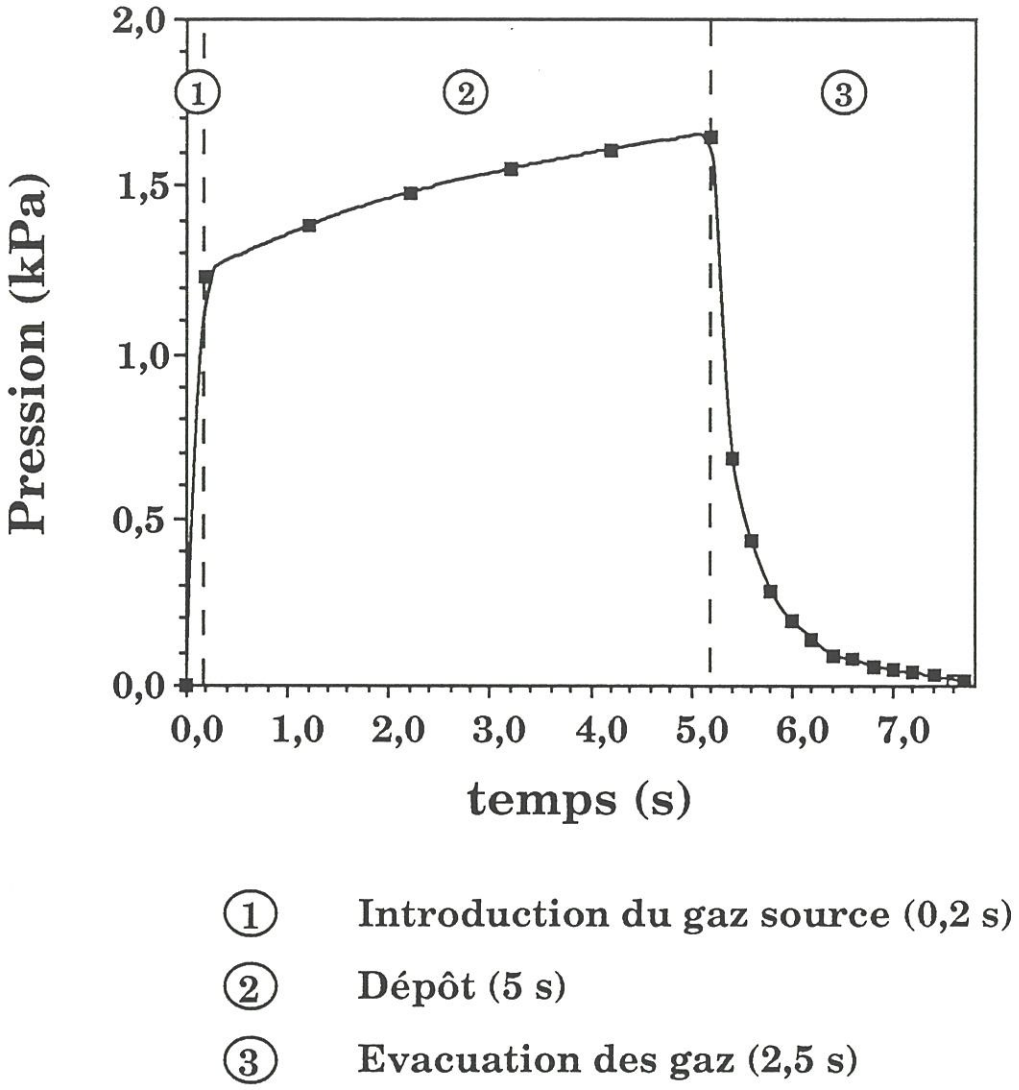

Fig. 2 : Evolution de la pression totale lors d'un pulse (durée de palier 5 s).

successivement. Cette seconde méthode permet d'injecter un gaz réactif dans un premier temps, puis un gaz inhibiteur de la réaction de dépôt dans un second temps, ceci dans le but de limiter le dépôt en surface du substrat.

La seconde étape qui correspond à la **phase de dépôt** proprement dite a une durée variant de 0,2 s à plusieurs minutes. Lors de cette étape, la pression augmente, suite aux réactions chimiques qui généralement produisent plus de moles de gaz qu'elles n'en consomment. Cette variation de pression n'est pas linéaire car les réactions s'effectuant dans un milieu clos, la phase gazeuse s'épuise.

L'évacuation des gaz s'effectue par pompage. C'est une période qui doit être la plus courte possible (e.g. quelques secondes) car il n'y a pas de dépôt lors de cette phase. Sa durée dépend, d'une manière générale, des possibilités de pompage et du volume mort, c'est à dire du volume inoccupé dans le four. Celui-ci doit être le plus faible possible.

L'introduction instantanée du gaz sous pression est sensée favoriser l'homogénéité de la composition gazeuse dans l'ensemble de la zone chaude du réacteur, et doit donc conduire à un dépôt uniforme au point de vue de la microstructure, de la composition, et de l'épaisseur. Ce procédé pourrait apporter un gain de temps important au niveau de l'infiltration des préformes car la phase gazeuse présente au sein des pores est sans cesse renouvelée. Son application industrielle pose toutefois un défi technologique car s'il est facile de remplir et de vider rapidemment un réacteur d'un volume de l'ordre de quelques litres, ce n'est plus le cas lorsqu'il fait plusieurs m^3.

4.2 - Travaux antérieurs

A ce jour, peu d'études consacrées à la P-CVI ont été publiées. A notre connaissance, le premier article concernant la P-CVI traite du dépôt de pyrocarbone sur des substrats en graphite poreux et date de 1970 [20]. Le gaz source utilisé était le 1,3-butadiène, les durées de pompage et de palier étant respectivement de 4 à 60 s et 0,5 à 1 s. Aucune comparaison n'est faite avec l'I-CVI, et l'influence du paramètre essentiel de la P-CVI, c'est à dire la durée du palier, n'est pas étudiée. Les deux résultats importants de cette étude sont : (i) la température, tout comme en I-CVI, ne doit pas être trop élevée pour bien infiltrer le substrat, (ii) le spectre de porosité initial du substrat conditionne les conditions optimales d'infiltration.

W.A.Bryant [21] a repris cette idée de cyclage en pression pour réaliser des dépôts uniformes en épaisseur sur des mandrins en cuivre. Ce qui intéressait l'auteur, était le renouvellement de la phase gazeuse, de façon à ce que les concentrations en espèces réactives restent constantes dans l'espace.

L'essentiel des recherches expérimentales publiées sur la P-CVI a été réalisé par K.Sugiyama et coll qui ont étudié l'infiltration de préformes de carbone par du carbure de silicium [22], ou du nitrure de titane [23], ainsi que le dépôt de BN sur des poudres compactées de Si_3N_4 [24].

Dans ces différentes études, l'auteur a montré que l'allure de la courbe de prise de masse de l'échantillon poreux en fonction de la durée du palier (t_R) dépend essentiellement de la température et de la pression, et ceci quel que soit le système chimique considéré. Une température d'infiltration élevée implique : (i) une vitesse importante des réactions chimiques conduisant à la formation du dépôt, (ii) un épuisement rapide de la phase gazeuse contenue dans le réacteur.

Par conséquent, quelle que soit la durée du palier, la prise de masse est constante. De plus, comme une grande partie du dépôt se fait sur les parois du four, l'augmentation de masse est plus faible que pour une température plus faible. C'est pourquoi dans le cas du dépôt de BN sur du Si_3N_4 (fig. 3), la courbe à 1473 K est en dessous de celle à 1273 K. A plus basse température, la vitesse réactionnelle est plus lente et la phase gazeuse s'épuise plus lentement d'où une prise de masse qui croît avec la durée de palier, puis devient constante lorsque la phase gazeuse est épuisée, c'est à dire lorsque la durée du palier est grande.

Il y aurait eu un grand intérêt à comparer l'infiltration obtenue en P-CVI et en I-CVI. K.Sugiyama [23] effectue un début de comparaison en infiltrant des substrats microporeux de graphite par du TiN. En P-CVI (P=80 kPa, Dp=3 s) la qualité de l'infiltration dépend fortement de la température qui doit être de l'ordre de 850°C pour éviter le dépôt de surface. En I-CVI, (80 kPa, débit H_2, N_2, et $TiCl_4$: respectivement 6.0, 3.0, et 0.08 cm^3/s) la vitesse de dépôt est faible, et il y a peu d'infiltration même à 850°C. Cette étude montrerait que l'infiltration de pores submicroniques est meilleure si l'on utilise la P-CVI.

Dans l'étude de Sugiyama et Ohzawa sur l'infiltration de substrats de graphites poreux par du carbure de silicium [22] aucune comparaison n'a été réalisée entre l'I-CVI et la P-CVI. Cependant, la température optimale d'infiltration apparaît être de l'ordre de 1000°C, mais aucune information n'est fournie sur l'effet de la durée du palier sur la qualité de l'infiltration. L'augmentation de la pression entraine un accroissement de la vitesse de dépôt, mais n'est ce pas au détriment de l'infiltration ?

Des travaux théoriques récents de Sotirchos et coll [25-26] ont montré que l'infiltration de SiC par P-CVI pourrait permettre de réduire de plusieurs

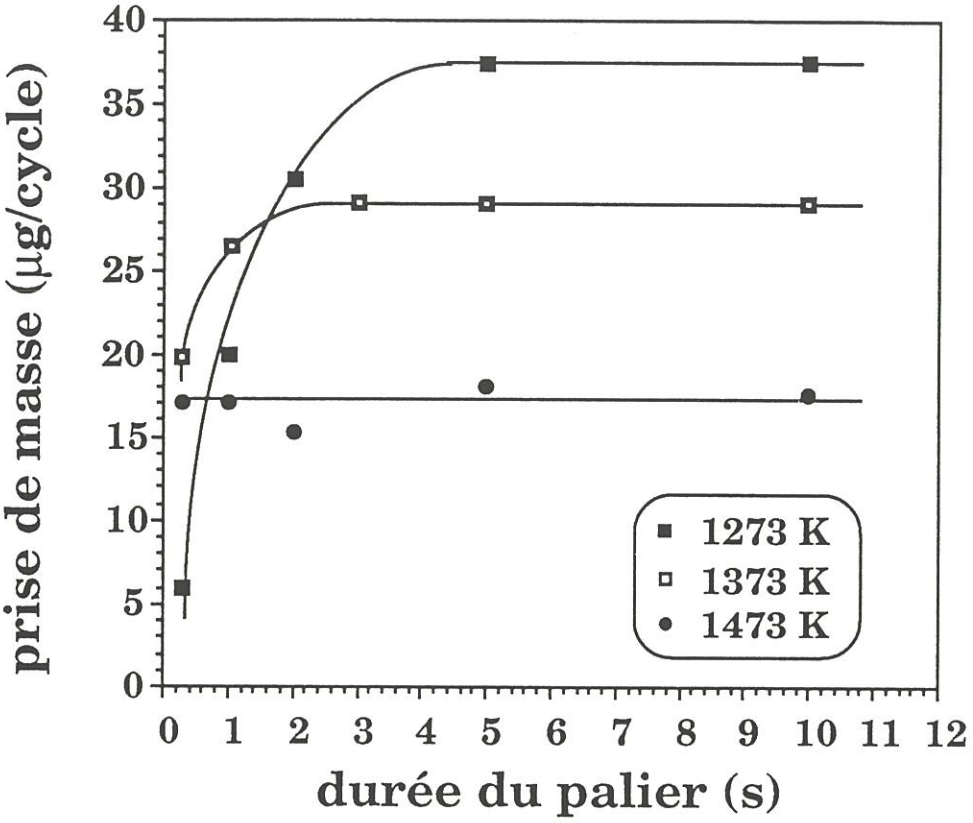

Fig. 3 : Relation entre la prise de masse par pulse et la durée du palier lors du dépôt de BN sur poudre de Si_3N_4 compactée [21].

ordres de grandeur le gradient de densité dans une préforme fibreuse par rapport à une infiltration menée en I-CVI dans les mêmes conditions. Toutefois, les durées de palier necessaires sont très petites (de l'ordre de 0,2 s voire moins). De plus, selon ces travaux, il existerait un diamètre de pore minimun en dessous duquel la P-CVI n'apporterait aucune amélioration en raison de l'augmentation de la résistance à la diffusion des espèces par convection lorsque la taille du pore diminue. Compte tenu de la publication trop récente de ces travaux théoriques, il n'a pas été possible d'établir une comparaison entre les résultats théoriques que cette méthode aurait pu fournir et ceux obtenus lors de notre expérimentation qui concerne le dépôt de pyrocarbone à partir de propane.

Comme les mécanismes régissant le dépôt de pyrocarbone par CVI se sont révélés prépondérants lors de notre étude, le paragraphe suivant en fera une synthèse bibliographique non exhaustive.

5- LES MODELES DE DEPOT DE PYROCARBONE PAR VOIE GAZEUSE

Le dépôt de pyrocarbone (PyC) à partir du craquage d'un hydrocarbure gazeux est un phénomène complexe qui met en jeu un nombre important d'espèces chimiques, ce qui explique le nombre élevé de mécanismes sur lesquels s'appuient les différents modèles de dépôt. La plupart des théories sur le dépôt de PyC s'appuie sur une expérimentation menée avec le **méthane** comme hydrocarbure précurseur, peu de travaux concernent le **propane**. Cependant, les mécanismes de base doivent être sensiblement les mêmes.

La première théorie concernant le dépôt de PyC a été donnée par Grisdale [27]. Selon cette théorie, il y a à tout moment dans l'atmosphère de

pyrolyse une série d'espèces moléculaires allant d'hydrocarbures légers gazeux aux molécules complexes de poids moléculaire élevé et comprenant peu d'hydrogène. La pression partielle de chaque espèce croît jusqu'à ce qu'il y ait condensation de gouttelettes qui, heurtant la surface, donnent naissance au dépôt. Selon la viscosité des gouttelettes, le dépôt sera plus ou moins dense et orienté.

Pour Bokros [28], il y a effectivement formation de gouttelettes, mais ce phénomène apparaît à une température située vers 1400°C. A plus basse température, le dépôt résulte de la condensation directe de molécules planes formées dans la phase gazeuse et dont la taille dépend des conditions opératoires. En 1988, Lee et Oh [29], pour expliquer les différentes microstructures observées lors du dépôt de PyC à partir de propane entre 900°C et 1200°C, reprennent ces deux processus de dépôt et selon les conditions opératoires, soit (i) les associent dans un processus de dépôt mixte de petites gouttelettes et de molécules planes complexes qui viennent s'aligner sur les gouttelettes, soit (ii) font intervenir seulement le dépôt de molécules planaires complexes et leur réarangement sur la surface du substrat.

Delhaes et coll [30] à partir d'observations réalisées au M.E.T envisagent la formation de petites gouttelettes en suspension dans un milieu confiné (préforme fibreuse). La microstructure du dépôt évolue avec le stade de polymérisation atteint par les gouttelettes. Le dépôt est soit laminaire rugueux en raison du dépôt de gouttelettes liquides présentant un caractére mésophasique et ne se solidifiant qu'au contact du substrat, soit isotrope si la polymérisation est moins avancée.

Linke et coll [31] proposent un modèle de dépôt à haute température (>1300°C) qui fait intervenir des agglomérats de différentes tailles, solides ou visqueux selon les conditions de dépôt.

Kaee [32] suggère que le dépôt est constitué à la fois par des particules solides formées dans le gaz et par des molécules planes se déposant sur le substrat. Il explique les variations de microstructure par un double mécanisme faisant intervenir la taille des particules (fonction du pourcentage d'hydrocarbure) et la probabilité que les molécules planes se déposent parallélement à la surface (fonction de la température).

Pierson et Lieberman [33] ont proposé un modèle basé sur les hypothèses suivantes :

(i) le dépôt résulte principalement, comme l'indique Diefendorf [33] du dépôt d'espèces aromatiques et acétylèniques, (ii) la concentration de ces espèces peut être estimée à partir de celles du benzène et de l'acétylène, et (iii) il existe un équilibre en phase gazeuse entre les différentes espèces. Ils s'appuient sur des calculs thermodynamiques pour estimer le rapport $R=(C_2H_2)/(C_6H_6)$ en fonction de la température, de la pression, et du rapport C/H. Expérimentalement, ils ont montré que dans le cas où il n'y a pas de formation de noir de carbone, la microstructure du dépôt de PyC évolue avec R : $R<5$ => PyC laminaire lisse, $5<R<70$ =>PyC laminaire rugueux, $R>70$=> PyC isotrope.

En résumé, selon les différents auteurs, le PyC pourrait se déposer à partir (i) de gouttelettes formées dans la phase gazeuse, (ii) de molécules planes aromatiques ou acétylèniques, (iii) d'agglomérats plus ou moins visqueux, (iv) de particules solides. Ces différents mécanismes impliquent tous un stade de polymérisation et de déhydrogénation avec formation de molécules

de poids moléculaire élevé, ce qui a été vérifié expérimentalement par Back et coll [35-36] lors de la pyrolyse du méthane au cours de laquelle a été observée la formation de molécules de fluoranthène $C_{16}H_{10}$.

6- OBJECTIFS ET CONTENU DU MEMOIRE

La présente étude s'inscrit dans le cadre général des travaux visant à améliorer le procédé de synthèse par voie gazeuse des matrices et des interphases des composites fibreux à matrices céramiques.

Elle a été abordée avec deux objectifs qui sont (i) l'étude systématique des principaux paramètres de la P-CVI de **pyrocarbone** (température, pression et durée de palier), (ii) la comparaison P-CVI et I-CVI, au niveau de la qualité de l'infiltration, de la vitesse de dépôt et de la microstructure du dépôt .

L'étude de la qualité de l'infiltration en fonction des conditions expérimentales, en P-CVI et en I-CVI pouvait difficilement se faire de façon précise à partir de l'infiltration de préformes fibreuses (dont le réseau de pores est très complexe et difficile à modèliser). C'est pourquoi, la majeure partie de ce travail s'appuie sur l'infiltration de **pores modèles** de dimensions bien définies (longueur : 20 mm, largeur : 2 mm, pour trois hauteurs : 60 µm, 120 µm et 320 µm) et relativement facile à exploiter.

Le choix du système chimique s'est porté principalement sur le **système C_3H_8/H_2**, ceci pour deux raisons : (i) le pyrocarbone est le principal matériau d'interphase utilisé dans les composites à matrice céramique, et (ii) la technologie de dépôt paraissait relativement simple à mettre en œuvre. Le choix du gaz précurseur s'est porté, après des essais préliminaires, sur le

propane car il s'agit d'un gaz plus réactif que le méthane, ce qui a permis de limiter la durée d'expérimentation déjà longue. Toutefois, quelques essais ont été également réalisés à partir d'autres hydrocarbures tels le méthane et le propylène.

Le présent mémoire comprend cinq chapitres **présentés sous forme de publications**.

Le premier chapitre concerne l'étude du dépôt de pyrocarbone à partir de propane en I-CVI. Trois points sont particulièrement étudiés : la qualité de l'infiltration, la cinétique de dépôt et la microstructure du dépôt . Ce travail a permis de définir dans le domaine expérimental considéré (P,T,Q) (i) les conditions optimales de densification associées à une qualité de dépôt déterminée, et (ii) une base de comparaison pour la P-CVI de PyC à partir de propane.

Les trois chapitres suivants traitent de la P-CVI du pyrocarbone à partir de propane (et de méthane) et mettent en évidence l'importance du degré de maturation de la phase gazeuse sur les processus de dépôt. Le second est axé sur les mécanismes de dépôt intervenant lors d'un pulse en fonction des conditions expérimentales. Le troisième présente les résultats des infiltrations de pores modèles en les comparant à ceux obtenus en I-CVI, corrèle les résultats expérimentaux avec les mécanismes mis en évidence au chapitre 2 et définit les conditions optimales d'infiltration P-CVI. Le quatrième chapitre rassemble les observations microstructurales effectuées sur les dépôts I-CVI et P-CVI (réalisées par observations en lumière polarisée au microscope optique et par microscopie électronique à transmission). Les différentes structures

observées sont corrélées à des mécanismes de croissance latérale ou colonnaire des couches de carbone.

La cinquième et dernière partie du mémoire expose les résultats d'une étude sur les propriétés mécaniques de composites unidirectionnels (C/PyC/SiC et SiC/PyC/SiC). Il montre que l'utilisation de la P-CVI dans la formation de l'interphase de PyC permet un accroissement notable des propriétés mécaniques des composites.

REFERENCES

[1] R. Naslain, "Introduction aux matériaux composites 2- Matrices métalliques et céramiques", Ed. du CNRS/IMC, Bordeaux, (1985).

[2] R. Labbens, "Introduction à la mécanique de la rupture", Ed Pluralis, Paris (1980).

[3] F. Christin, R. Naslain and C. Bernard, "A thermodynamic and experimental approach of silicon carbide-CVD. Application to the CVD infiltration of porous carbon-carbon composites", Proc. 7th Int. Conf. on CVD, (T.O. Sedgwick et al., eds.), The Electrochem. Soc., Princeton, 499-514 (1979).

[4] J.Y. Rossignol, F. Langlais, R. Naslain and C. Bernard, "A Tentative modelization of titanium carbide CVI. within the pore network of two-dimensional carbon-carbon composite preforms", Proc. 9th Int. Conf. on CVD, (Mc.D. Robinson et al., eds), The Electrochem. Soc., Pennington, 596-614 (1984).

[5] H. Hannache, F. Langlais and R. Naslain, "Kinetics of boron carbide chemical vapor deposition and infiltration", Proc. 5th European. Conf. on CVD, (J.O. Carlsson et al, eds), Uppsala, 219-233 (1985).

[6] H. Hannache, R. Naslain and C. Bernard, "Boron nitride chemical vapor infiltration of fibrous materials from BCl_3-NH_3-H_2 or BF_3-NH_3 mixtures : a thermodynamic and experimental approach", J. Less-Common Met., **95**, 221-246 (1983).

[7] R. Colmet, R. Naslain, P. Hagenmuller and C.Bernard, "Thermodynamic and experimental analysis of chemical vapor deposition of alumina from $AlCl_3$-H_2-CO_2 gas phase mixtures", Proc. 8th Int. Conf. on CVD, (J.M. Blocher et al, eds), The Electrochem. Soc., Pennington , 17-31 (1981).

[8] J. Minet, F. Langlais and R. Naslain, "On the chemical vapor deposition of zirconia from ZrO_2-H_2-CO_2-Ar gas mixture II : An experimental approach", J. Less-Common Met., **132**, 273-287 (1987).

[9] J.K. Guo, Z.Q. Mao, C.D. Bao, R.H. Wang and D.S. Yan, "Carbon fiber-reinforced silicon nitride composite", J. Mater. Sc., **117**, 3611-3616 (1982).

[10] K.M. Prewo, T.J. Brennan and G.K. Layden, "Fiber reinforced glasses and glass ceramics for high performance applications", Ceramic Bulletin, **65,** [2], (1986).

[11] S. Yajima, "Special heat-resisting materials from organometallic polymers", Ceramic Bulletin., **62**, 8, 893-915 (1983).

[12] R. Veltri, D. Scole, J. Vontell and F. Galasso, "Sol-gel derived matrix-composites", J. Powder Metallurgy International, **21**, [6], (1989).

[13] R. Naslain and F. Langlais, "Fundamental and practical aspects of the chemical vapor infiltration of porous substrates", High Temperatures Sc, (J.W. Hastie, ed), Humana Press, Clifton, New Jersey, **27**, 221-235 (1990).

[14] E. Fitzer, "Chemical vapor deposition - A review of 25 years of experience", Proc. of 8th European. Conf. on CVD, (M.L. Hitchman and N.J. Archer., eds.), Glasgow, 509-537 (1991).

[15] A. Sherman, "Chemical vapor deposition for microelectronics", Noyes Publications, (1987).

[16] T.M. Besmann, R.A. Lowden, D.P. Stinton and L.L. Starr, "A method for rapid chemical vapor infiltration of ceramic composites", Proc. 7th European Conf. on CVD, Journal de physique, Colloque C5, Supp. 5, **50**, 229-239 (1989).

[17] T.L. Starr, "Modelling of forced flow/thermal gradient CVI", Proc. Int. Conf. on Wiskers-and-Fiber-Thoughened Ceramics, Oak Ridge, USA (1988), (R.A Bradley et al., eds), ASM International, Oak Ridge, 243-252 (1988).

[18] K.E. Spear, "Thermochemical modeling of steady state CVD processes", Proc. 9thInt. Conf. CVD, Paris, France (1989), (Mc Robinson et al., eds.), The Electrochem. Soc., Pennington, 81-97 (1989).

[19] C.E. Morosanu, "Thin films in chemical vapor deposition", Elsevier Ed., Amsterdam-Oxford-New York-Tokyo, (1990).

[20] R.L. Beatty, "Gas pulse impregnation of graphite with carbon", J. Nuclear Applications&Technology., **8**, 488-495 (1970).

[21] W.A. Bryant, "Producing extended area deposits of uniform thickness by a new chemical vapor technique", J. Crystal Growth, **35**, 257-261 (1976).

[22] K. Sugiyama and Y. Ohzawa, "Pulse chemical vapor infiltration of SiC in porous or SiC particulate preform using an r.f. heating system", J. Mat. Sc. Let. , **25**, 4511-4517 (1990).

[23] K. Sugiyama and T. Nakamura, "Pulse CVI of porous carbon", J. Mat. Sc. Let., **6**, 331-333 (1987).

[24] K. Sugiyama and Y. Ohzawa, "Consolidation of Si_3N_4 powder-preform by infiltration of BN using the pulse CVI process", J. Mat. Sc. Let., **7**, 1221-224 (1988).

[25] S.V. Sotirchos and M. Tomadakis, "Modelling tranport, reaction, and pore structure evolution during densification of cellular or fibrous structures", Chemical Vapor Deposition of Refractory Metals and Ceramics, (T.M. Besmann and B.M. Gallois, eds), MRS, Pittsburgh, 73-78 (1990).

[26] S.V. Sotirchos, "Dynamic modeling of chemical vapor infiltration", AIChE J, **37**,9, 1365-1378 (1991).

[27] R.O. Grisdale, "The formation of black carbon", J. Applied Physics, **24**, [9], 1082-1091 (1953).

[28] J.C. Bokros, "Variation in the crystallinity of carbons deposited in fluidized bed", Carbon, **3**, 201-211 (1965).

[29] J.Y. Lee and S.E. Oh, "Structures of pyrolytic carbon matrices in carbon/carbon composites", Carbon, **26**, [6], 763-768 (1988).

[30] P. Delhaes, M. Trinquecoste, A. Pacault, J. Goma and J. Thebault,

"Matériaux composites carbone carbone. Conditions de fabrication par dépôt chimique en phase vapeur-Microstructures et propriétés physiques", J. Chim. Phys., **81**, [11/12], 809-817 (1984).

[31] J. Linke, K. Koizlik and H. Nickel, "Fundamentals on the agglomerate model and its relation to the physical properties of pyrocarbon", J. Nuclear Technology, **35**, 257-262 (1977).

[32] J.L. Kaae,"The mechanism of the deposition of pyrolytic carbon", Carbon, **23**, 6, 665-673 (1985).

[33] H.O. Pierson and M.L. Liebermann, "The chemical vapor deposition of carbon on carbon fibers", Carbon, **13**, 159-166 (1975).

[34] R.J. Diefendorf, "The deposition of pyrolytic graphite", J. Chim. Phys., **57**, 815-821 (1960).

[35] M.H. Back and R.A. Back, "Thermal decomposition and reactions of methane", in "Pyrolysis : Theory and Industrial Practise", (L.F. Albright, B.L. Crynes and W.H. Corcoran., eds), Academic Press, (1983).

[36] C.J. Chen and M.H. Back, "The simultaneous measurement of the rate of formation of carbon and hydrocarbon products in the pyrolysis of methane", Carbon, **17**, 175-180 (1979).

Chapître 1 : CVD/CVI OF PYROCARBON FROM PROPANE ON FLAT SUBSTRATES AND IN MODEL PORES WITH RECTANGULAR CROSS-SECTIONS

Il paraissait indispensable, dans le cadre de l'étude d'une nouvelle technique d'infiltration, de se référer, avant toute chose, à la méthode classique d'infiltration, c'est à dire l'I-CVI. C'est pourquoi une étude relativement simple et concernant un domaine expérimental limité a été entreprise. La première étape a consisté à développer un appareillage modulable pouvant servir aussi bien à déposer du pyrocarbone en I-CVI qu'en P-CVI. De même, le gaz source et la méthode de chargement du four sont identiques pour les deux méthodes de dépôt.

Ce travail n'avait pas pour but de faire une analyse exhaustive du **dépôt de pyrocarbone à partir de propane**, mais devait refléter les possibilités de l'I-CVI. Il a fourni d'intéressantes données sur la qualité de l'infiltration et sur la microstructure du dépôt qui a pu être reliée à un paramètre empirique fonction de la concentration en espèces aromatiques dans la phase gazeuse. Son originalité repose sur l'utilisation de **pore modèles**, d'un **plan d'expérience** qui permet de modéliser la qualité de l'infiltration et sur l'étude par spe**ctromètrie de masse** des espèces gazeuses présentes ou formées dans la zone chaude du réacteur.

Ce chapitre présente les résultats de cette étude sous forme d'un projet de publication adressée à la revue Carbon.

submitted to Carbon.

CVD/CVI OF PYROCARBON FROM PROPANE ON FLAT SUBSTRATES AND IN MODEL PORES WITH RECTANGULAR CROSS-SECTIONS

P. Dupel, R. Pailler, F. Langlais, R. Naslain
Laboratoire des Composites thermostructuraux
UMR-47 CNRS-SEP-UB1, Domaine Universitaire
3, allée de La Boëtie, 33600-Pessac, France.

A. Costecalde
Société Européenne de Propulsion (SEP)
BP. 37, 33165 Saint-Médard-en-Jalles, France.

ABSTRACT

The chemical vapor deposition (CVD) and infiltration (CVI) of pyrocarbon (PyC) resulting from the cracking of propane on the external surface and within the straight pores of model graphite substrates, are studied under conditions selected on the basis of a Doehlert experiment design, i.e. 900 < T < 1150°C ; 0.8 < P < 4.7 kPa and 20 < Q < 100 sccm. The main intermediate species in the gas phase are H_2, CH_4, C_2H_2, C_3H_8 and C_6H_6 as assessed by semi-quantitative mass-spectroscopy. The PyC-deposition, when rate-

controlled by the surface reactions, obeys a first order kinetic law with respect to propane with an activation energy of 150-200 $kJ.mol^{-1}$. The anisotropy of the PyC-deposit, as characterized by the value of the extinction angle (with $10 < Ae < 20$), correlates with the relative concentration of the pyrocarbogenic C_6H_6 intermediates. At a given pressure, the DL (Dark laminar) → SL (Smooth laminar) → RL (Rough laminar) sequence is observed as temperature is raised. Both temperature and pressure have a strong influence on the infiltration homogeneity of the model pores. The anisotropy of the PyC deposited in-depth is less pronounced than that of the deposit near the pore entrance.

KEY WORDS

Pyrocarbon, CVD/CVI, propane, kinetics, microtexture, experiment design, model pores.

1 - INTRODUCTION

Carbon carbon (C/C) composites, consisting of carbon fibers embedded in a carbon matrix, are now rather well-known structural materials. They are used in a variety of applications including rocket motor nozzles, spacecraft thermal protection, brake disks or prosthetic devices [1-4]. This broad field of application is related to the fact that most properties of C/C composites depend on the microstructure of their constituents, which can be either almost isotropic or strongly anisotropic (i.e. close to that of graphite) and is itself depending on the processing conditions of both the fibers and the matrix. As an example, the Young's modulus of carbon is related to the degree of graphitization. It has been reported to vary from a few 10 GPa to almost 1000 GPa (this latter value being close to that of graphite single crystal in the a-direction).

There are two classical ways for processing C/C composites. In the **liquid phase route**, a carbon fiber preform is impregnated with a liquid precursor of the carbon matrix (e.g. a polymeric resin or a pitch) and then it is submitted to a pyrolysis treatment during which the precursor is converted into carbon [5,6]. In the **gas phase route**, the carbon matrix is deposited on the fiber surface as the result of the cracking of a gaseous precursor (usually a hydrocarbon species such as CH_4) occurring within the open porosity of the fiber preform heated at a high enough temperature [1,7].

The chemical deposition of a solid from a gaseous precursor is referred to as CVD (chemical vapor deposition) when it is performed on the external surface of a substrate and as CVI (chemical vapor infiltration) when it takes place specifically (i.e. under conditions of low temperature and pressure) in the

open porosity of the substrate (here the highly porous fiber preform). In the most conventional version of the CVI-process, referred to as I-CVI (isothermal-isobaric CVI), the fiber preform is set in an isothermal infiltration furnace and the mass transfer of the reactant(s) and product(s) along the pores occurs mainly by diffusion (i.e. no pressure gradient is applied to the preform). The I-CVI-processing of a C/C composite is a rather slow process since both temperature and pressure have to be lowered (with respect to conventional CVD) in order to favor the in-depth deposition of the matrix, with consequently a lowering of the deposition rate. As a result, the infiltration conditions must be carefully optimized for each type of fiber preform. Although some modelling of the CVI-process has been done (for very simple pore morphology) [8,9], the optimization of the CVI-conditions for actual fiber preforms still remains based on an experimental approach and is time consuming. Two main points seem to presently limit the use of theoretical approaches : (i) the lack of accurate models depicting quantitavely the complex pore network of actual fiber preforms and (ii) the lack of reliable kinetic laws for the deposition of the matrix (here carbon resulting from the cracking of a given hydrocarbon precursor) under rather unusual T - P conditions. It was one of the objectives of the present work to propose a kinetic law for the deposition of carbon from propane under T-P I-CVI-conditions.

Very few studies have been published up to now on the **mechanisms** involved in the deposition of **pyrocarbon** (PyC) from a gaseous precursor in the pore network of a fiber preform [10,11]. Conversely, the CVD of PyC is better documented [12-19]. Generally speaking, the pyrolysis of a hydrocarbon species is a complex phenomenon : (i) it is based on a deshydrogenation/condensation process involving **many intermediates**, (ii) the relations that exist between the nature of the precursor, the CVD-conditions and the microstructure of the PyC

deposit are not straightforward and (iii) most theories are based on experiments often limited to the use of methane. As the deshydrogenation/condensation mechanism proceeds, intermediates with higher and higher molecular weights are formed in the gas phase either as minute droplets [11,12,13] or planar acetylenic/aromatic molecules [16,17] or more or less viscous aggregates [14] or solid particulates [15]. The microstructure of the carbon deposit is related to the nature of the mechanism actually involved (which in turn depends on the CVD-conditions) and to that of the substrate. It was another objective of the present work to depict quantitatively the **microstructure of the PyC deposited** from propane along **model straight pores** of various cross-sections (focusing on the anisotropy of the deposit) and to derive relationships between the nature of the deposit and the chemical composition of the gas phase. Finally, the present work being part of a more general study devoted to the CVI of porous bodies by PyC [20], a last objective was to optimize the CVI-parameters on the basis of an experiment design.

2 - EXPERIMENTAL

2.1 - CVD/CVI apparatus

The apparatus used for the CVD/CVI experiments is shown in fig. 1. Its main part is an inconel cylindrical deposition chamber, heated externally with an electrical resistance furnace and whose temperature is monitored with a thermocouple and a PID-unit. The substrate is set within a quasi isothermal zone 27 mm in diameter and 50 mm in height. The reactant, i.e. **pure propane** is injected on the top of the deposition chamber, its flowrate being controlled

1 - mass flow
2 - furnace
3 - pressure sensor
4 - substrate
5 - thermocouple
6 - liquid nitrogen trap
7 - pressure sensor
8 - pressure controller
9 - vacuum pump

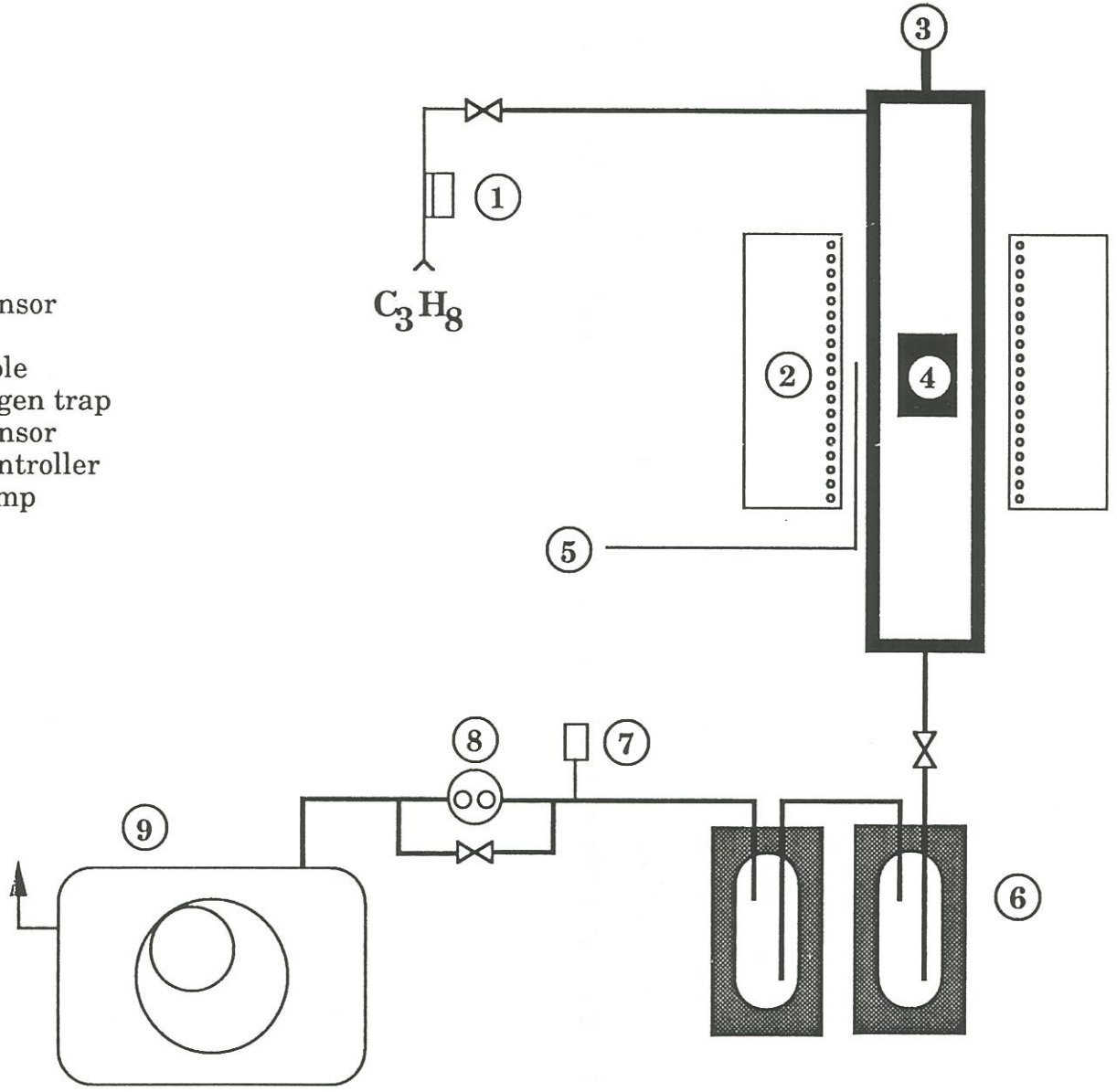

Fig. 1 : Apparatus used for the CVD/CVI of pyrocarbon (schematic).

with a mass flowmeter within the 10 - 100 sccm range. The total pressure is maintained at a constant value (lying between 0.8 and 5 kPa) with a rotary pump (residual pressure : 0.01 Pa), a membrane valve and a pressure sensor.

2.2 - The substrates

Two different substrates have been used : graphite substrates with model straight pores for the CVI-experiments and rectangular graphite substrates for the CVD-experiments.

The **model straight pore substrate** is shown schematically in fig. 2. The model pores are formed by the assembly of two plates made of purified graphite(1), one of the two being machined in order to exhibit three parallel grooves of rectangular cross-sections (their width being the same, i.e. 2 mm, but their height being different, i.e. 60 ; 120 and 320 μm) and of same length (20 mm). The two graphite plates are bolted with graphite screws and nuts (not shown in the figure). Owing to the surface roughness of the plates after machining and to the intrinsic residual porosity of the graphite, the height of the pore, h, is known with some uncertainty (e.g. h=60 ± 5 μm, for the thinnest pore). The main advantage of such model pores, e.g. with respect to cylindrical straight pores of same sizes, lies in the fact that they allow one to measure in a rather straightforward manner (e.g. by optical microscopy) the PyC-thickness profile along the longitudinal axis (i.e. in a longitudinal cross-section cut within the 2 mm width of the sample).

The substrates used for the kinetic study consist of **rectangular specimens** (10x10x5 mm^3) cut in purified graphite of same origin.

---

(1) from Polygraphite (Cevins, France)

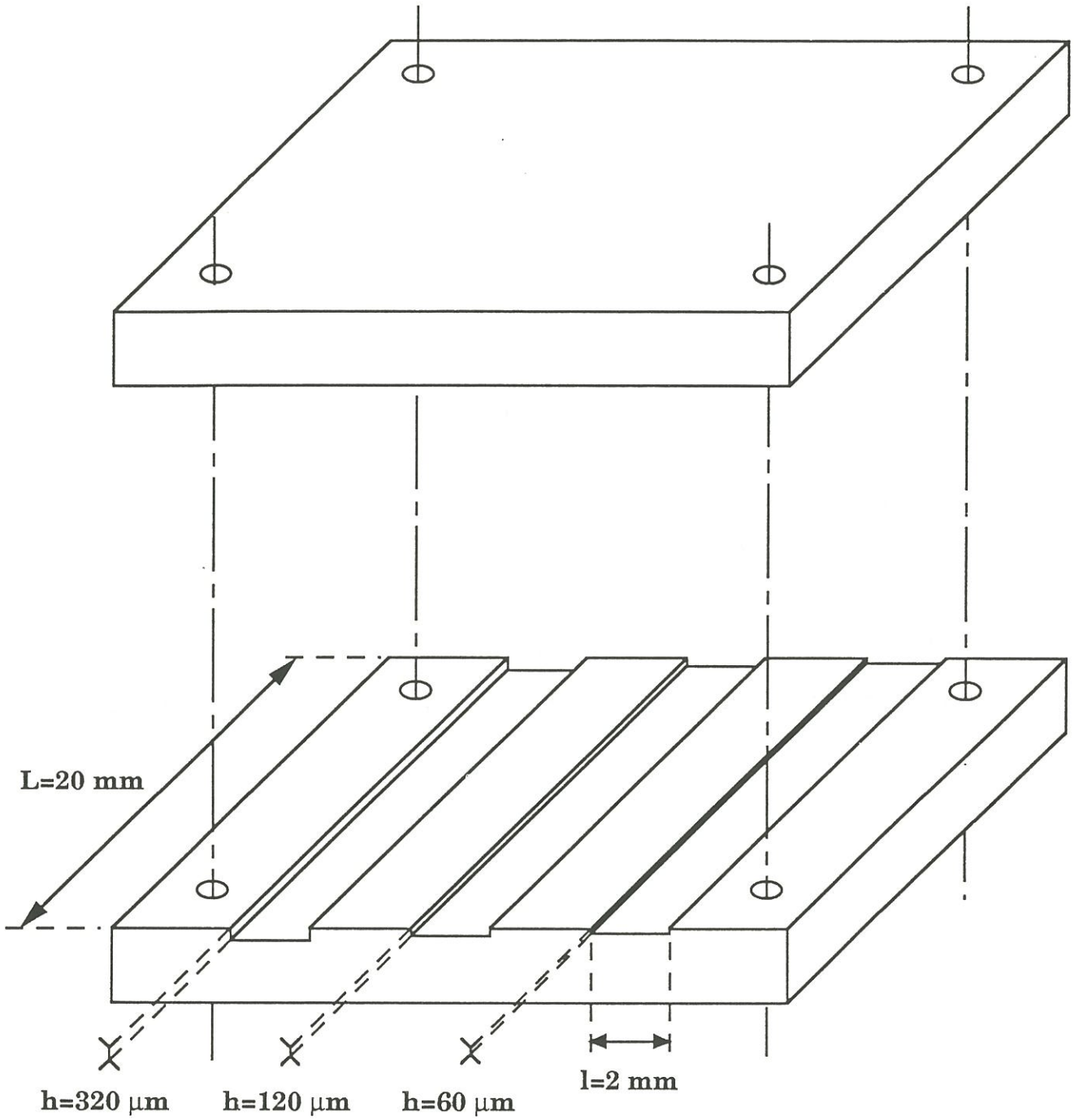

Fig. 2 : Schematic of the model graphite substrate with 3 straight pores with rectangular cross-sections.

2.3 - Experiment design

The optimization of the CVI-conditions, for the model pores, has been performed on the basis of an experiment design approach. Such an approach is known to provide an extremely efficient way of determining the influence of the various parameters while requiring a minimum of experiments . The choice of the methodology depends on the relationships between **the experimental response(s)**, here, the thickness **e** of the PyC-deposit along the pores, and the **parameters** being studied. In I-CVI, three parameters are known to control the kinetics of the infiltration process [8] : the substrate temperature, the total pressure and the source species gas flowrate. For practical reasons, the temperature has been fixed at 1050°C (experiments were run at other temperatures too, in order to assess the kinetic law, but the results were not taken into account in the I-CVI experiment design). Thus, the experiment design has only two variables, the total pressure and the propane gas flowrate, which were varied within the ranges 0.8-4.7 kPa and 20 - 100 sccm, respectively.

The Doehlert experiment design [21,22], whose matrix is symmetrical in the parameter space, has been used. The values of the parameters for the **seven experiments** which have been designed are shown in table 1, all the experiments being performed at the same temperature (i.e. 1050°C, as previously mentioned) and with the same duration (i.e. 100 hours, this duration being representative of infiltrations performed on actual fiber preforms and yielding deposits with high enough thicknesses). The equation of the **response surface**, e=f(P, Q), is polynomial of order two, which can be written as :

experiment code	1	2	3	5	4	6	7
P(kPa)	0.8	0.8	2.75	2.75	2.75	4.7	4.7
Q(sccm)	40	80	20	60	100	40	80

Table. 1 : Values of the pressure and propane flow rate for the seven experiments of the Doehlert experiment design.

P(kPa) Q(sccm)	0.8 40	0.8 80	2.75 20	2.75 60	2.75 100	4.7 40	4.7 80
V_{ds} (µm/h)	0.50	0.42	0.53	1.05	1.20	1.35	2.75
V_{dc320} (µm/h)	0.40	0.34	0.47	0.93	1.02	1.06	2.13
V_{dc120}(µm/h)	0.26	0.22	0.30	0.78	0.90	0.83	1.56
V_{dc60} (µm/h)	0.13	0.11	0.19	0.35	0.44	0.27	0.55

Table. 2 : Deposition rate at the substrate surface and model pore center as a function of the experimental P and Q parameters (with T=1050°C).

$$e = a + bP + cQ + dP^2 + eQ^2 + f\,PQ \qquad (1)$$

where a, b, c, d, e and f are constants which have been calculated from the experimental data, according to a numerical procedure(1), the response surface being drawn in the e - P - Q space with a computer(2). The validity and the dispersion of the results were checked by performing additional experiments under conditions already used.

2.4 - Characterization of the PyC-deposit

After each experiment, the substrate(s) and the deposit(s) were embedded in a resin(3) cut transversally (rectangular CVD-substrates) or longitudinally (substrates with model pores) with a diamond saw and the sections were polished with diamond pastes, according to a conventional procedure. The thicknesses of the PyC-deposit were measured with an optical microscope(4) equipped with a micrometer scale eyepiece, both at the substrate surface and along the longitudinal axes of the model pores. The homogeneity of the infiltration within a pore of size i (with i=h=60, 120 or 320 μm) was charaterized by a **R_i-parameter** defined as the ratio between the value of e at the center of the pore (i.e. at z=10 mm from the pore entrance, z being the pore longitudinal axis) and that at the pore entrance (i.e. at z=0).

The **anisotropy** of the PyC-microstructure was assessed quantitatively by measuring the extinction angle Ae on polished sections with an optical microscope in polarized light according to a procedure [23] which is described

---

(1) NEMROD software, from LPRA1 (Univ. Marseille)
(2) STRATGRAPHICS software, from UNIWARE
(3) from SRUERS
(4) MeF3 from REICHERT-JUNG

elsewhere [24]. The accuracy of the measurements was thought to be of the order of one degree. It is generally admitted that the pyrocarbon is isotropic (I) for Ae <4°, dark laminar (DL) for 4 < Ae < 12°, smooth laminar (SL) for 12 < Ae < 18° and rough laminar (RL) for 18 < Ae < 25°. Ae profiles depicting the variations of the PyC-anisotropy were drawn by performing the measurements along the pore longitudinal axes.

Finally, the morphology of the PyC-deposits was assessed through scanning electron microscopy(5)(SEM) analyses.

2.5 - Analysis of the gas phase by mass spectrometry

The chemical composition of the gas phase was semi-quantitatively assessed by probing the gas phase near the substrate surface with a capillary and analyzing the chemical species with a quadrupole mass-spectrometer(6). This procedure has obviously two weak points : (i) the gas phase sample is taken near the substrate surface and not along the pore axis (for I-CVI experiments performed with model pores) and (ii) the species entering the spectrometer may be somewhat different from those actually present near the substrate surface (owing to recombination of free radicals and condensation of heavy species during the transfer in the capillary). This procedure, despite its limitations, gave interesting semi-quantitative data on the main intermediates stable at the ambient temperature. The amount of each species was assessed in a **relative scale**, by injecting a constant flow of argon in the deposition chamber (argon giving two peaks (mass 20 and mass 40), that corresponding to mass 40 being used as standard).

---

(5) 840 from JEOL
(6) Anagaz 200 from KENOS

3 - RESULTS

3.1- PyC-deposition rate

The PyC-deposition rate, V_d, is defined as the thickness of PyC (expressed in μm) deposited in one hour. It has been measured first on the **external surfaces** of the two kinds of substrates (see section 2.2). Under such conditions, it has been observed to be constant vs time and will be referred to as V_{ds} in the following. The PyC-deposition rate has been also measured **at the centers of the model pores** for relatively short infiltration durations (i.e. 20 hours) corresponding to pores far from being fully filled. It will be referred to as V_{dc60} ; V_{dc120} and V_{dc320} for the pores with a height of 60 ; 120 and 320 μm, respectively. The data are shown in table 2 for the seven experiments performed at 1050°C with propane as carbon precursor. For P=0.8 kPa, the deposition rate does not vary significantly as the gas flowrate is increased, whatever the size of the pore and the location of the deposit. Conversely, for P > 0.8 kPa, the value of V_d depends on the gas flowrate Q, its variations with Q being more and more significant as P is raised.

The variations of the deposition rates as a function of the reciprocal temperature (Arrhenius plots) are shown in fig. 3, for P=3 kPa ; Q=60 sccm and 950 < T< 1150°C. They are linear whatever the location of the deposit, suggesting that the deposition process is thermally activated. The corresponding values of the apparent activation energy, Ea, are shown in table 3. It is worthy of note that Ea is slightly lower at the pore center than at the substrate external surface (160 vs 188 $kJ.mol^{-1}$ respectively).

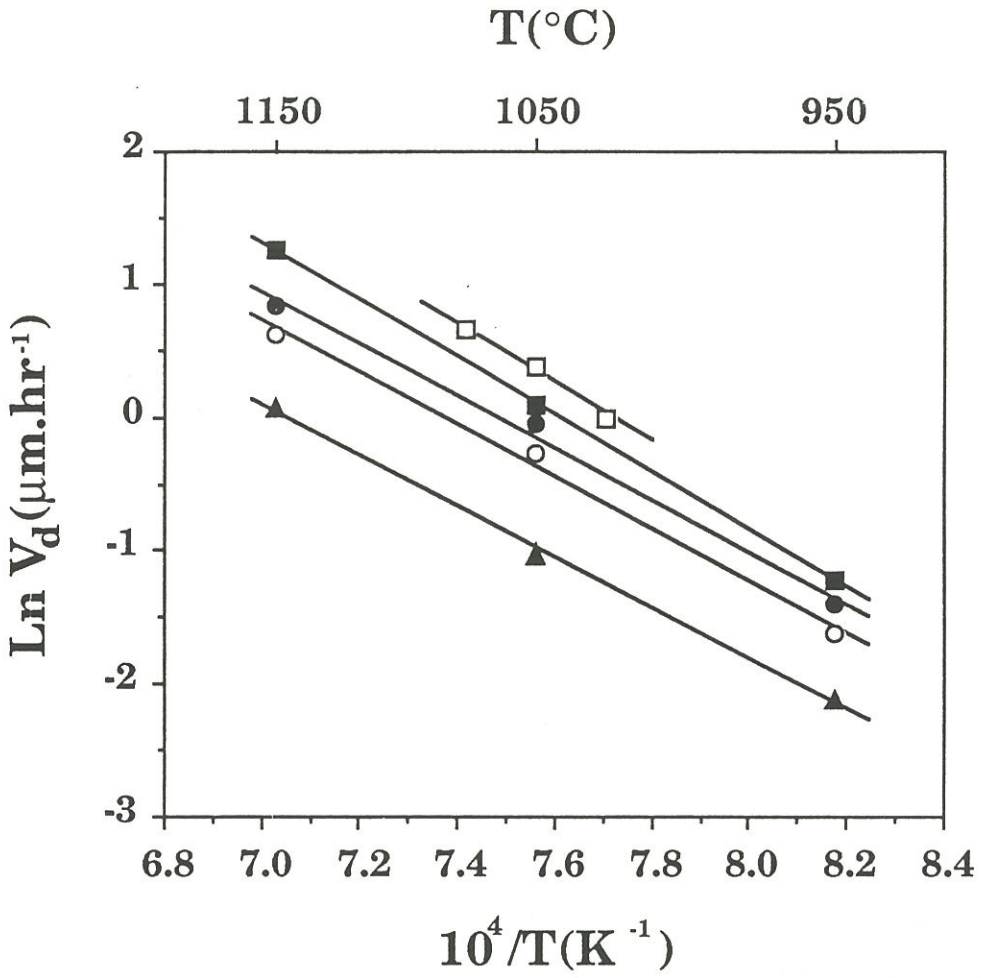

Fig. 3 : Arrhenius plots of the PyC-deposition rate for P=3 kPa and Q=60 sccm : □ on the external surface of the rectangular specimens; ■ on the external surface of the model pore substrate and at the centers of the model pores 320 μm (●) ; 120 μm (○) and 60 μm (▲) in height.

Deposit location	external surface		pore center		
	rectangular specimen	model pore specimen	320 μm	120 μm	60 μm
Ea (kJ.mol^{-1})	192	184	161	161	158

Table. 3 : Apparent activation energy for the deposition of PyC from propane at various substrate locations derived from fig. 3 data.

The variations of the PyC deposition rate on the external surface of the substrate, as a function of the propane pressure (i.e. the total pressure in our experiments) are shown in fig. 4 in a Ln/Ln scale, for a propane gas flowrate of 60 sccm and three different temperatures. Within the pressure range studied (i.e. $0.8 < P < 4.7$ kPa), these variations are linear in a first approximation, the mean slope of the straight lines corresponding to an overall apparent **reaction order close to one** (i.e. falling in the range 0.98 - 1.10).

3.2- Nature of the deposit

An optical micrograph of a cross-section of PyC deposited from propane near the entrance of one of the model pores is shown in fig. 5 in polarized light at two different magnifications. The PyC deposit thickness appears to be rather uniform in the pore cross-section whatever its location along the z-axis. The PyC-deposit has grown with a **cone/columnar microstructure**, the nucleation sites being located, with only very few exceptions, on the pore wall graphite surface whatever the infiltration conditions [25]. The PyC deposit consists of carbon layers parallel to the substrate surface and which appear only weakly bonded to one another, as shown in fig. 6.

The **anisotropy** of the PyC deposits can be assessed through the values of the extinction angle, Ae, for various infiltration conditions (table 4). These values fall within the range 10 - 20° suggesting that the PyC-deposit is either dark laminar ($4 < Ae < 12°$), smooth laminar ($12 < Ae < 18°$) or rough laminar ($18 < Ae < 20°$) depending on the location of the deposit, the size of the pore and the infiltration conditions. The effect of the gas flowrate on the PyC-anisotropy is rather weak. As an example, for P=2.75 kPa and T=1050°C, increasing the

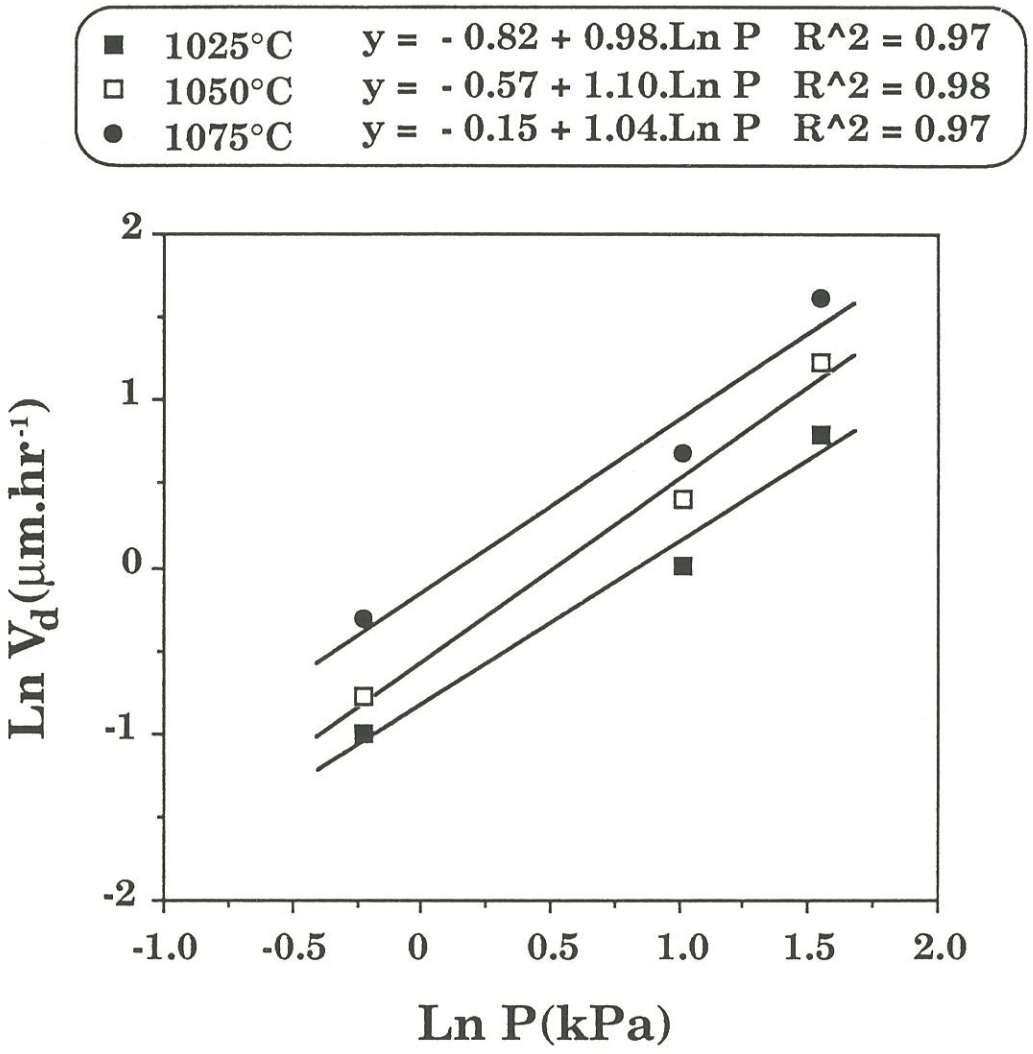

Fig. 4 : Variations of the PyC-deposition rate on the external surface of the substrates as a function of the propane pressure in a Ln-Ln scale, for Q=60 sccm.

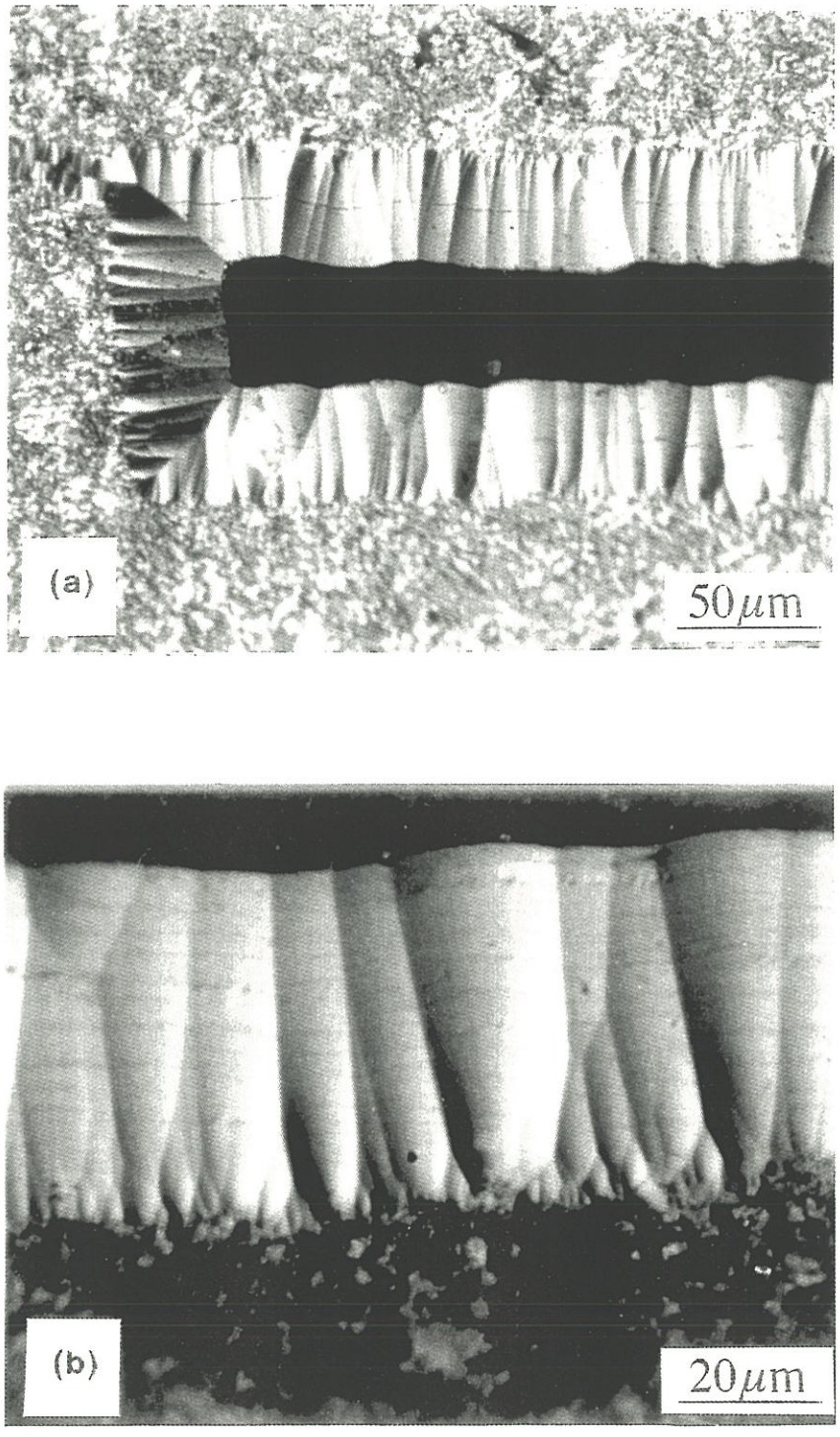

Fig. 5 : Optical micrographs (polarized light) of PyC deposited from propane near the entrance of a 120 μm-model pore : (a) at low magnification, (b) at higer magnification (T=1050°C; Q=20 sccm and P=2.75 kPa).

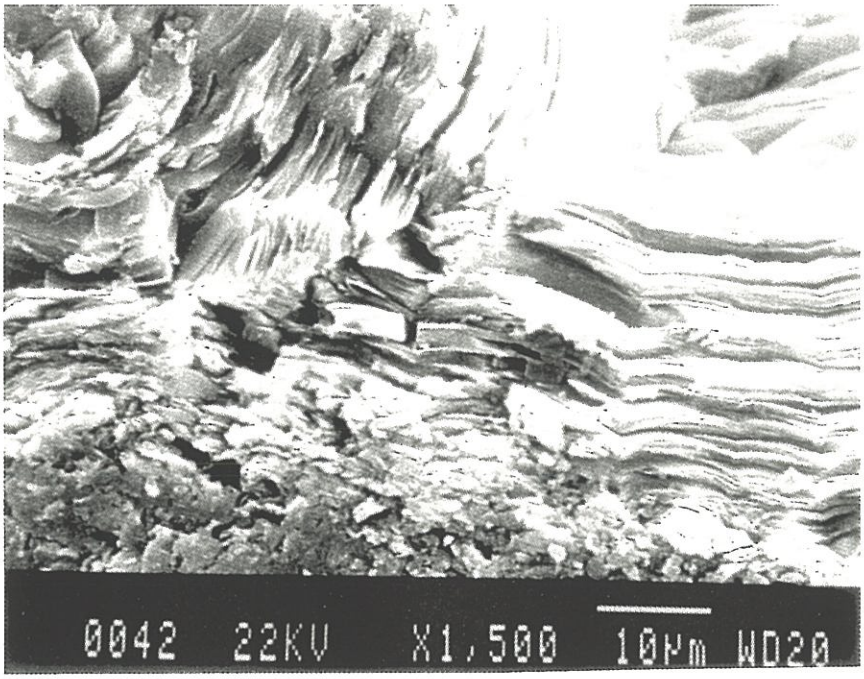

Fig. 6 : SEM micrograph of a PyC-deposit showing the layered microstructure (T=1050°C; P=2.75 kPa; Q=20 sccm).

T(°C)	P (kPa) Q (sccm)	Ae(°) (surface)	Ae (°)(pore center)		
			320 μm	120 μm	60 μm
950	3.0 60	11.5	11	10.5	10
1050	0.8 40/80	11.5	11	11	10.5
1050	2.75 20	19.5	15.5	12.5	10.5
1050	2.75 60	16.5	14	12.5	10
1050	2.75 100	15.5	14	12	10
1050	4.7 40	20	17	14	11.5
1050	4.7 80	20	17	13	11.5
1150	3.0 60	20	11	10	10.5

Table. 4 : Values of the extinction angle Ae of the PyC deposited on the external substrate surface and at the center of the model pores, for various infiltration conditions.

propane gas flowrate by a factor of 5 (i.e. from 20 to 100 sccm) only results in a 20% decrease of Ae (from 19.5 to 15.5). Pressure and temperature are the two parameters which mainly control the anisotropy of the deposit on the **external** surface of the substrates. As an example, increasing the temperature by 200°C (P and Q being constant) or the pressure by 4 kPa (T and Q being constant) raises the value of Ae by 9°. At the **pore center**, Ae is low when its value at the substrate external surface is itself low and when the pore is of small size. Furthermore, it is noteworthy that when the Ae value at the external surface is of the order of 11° (dark laminar PyC) it remains almost unchanged at the pore center whatever the pore size and the infiltration conditions.

3.3- Composition of the gas phase

The main chemical species present in the gas phase were observed to be H_2, CH_4, C_2H_2, C_2H_4, C_2H_6, C_3H_8 and C_6H_6, on the basis of mass spectrometry analyses. No chemical species with a mass higher than 78 (i.e. that of C_6H_6) was detected. However, tars were indeed present at the level of the cold parts of the infiltration chamber suggesting that heavy chemical species have been also formed.

For a given P-value, the concentration of a chemical species X at the infiltration chamber gas inlet will be referred to as C_x^0 (with $C_x^0=0$ when X is a species resulting from a chemical reaction involved in the deposition process). Its concentration in the hot zone near the external surface of the substrate, for given P, T values, C_x^T is derived from the treatment of the mass spectrometry signal, as mentioned in section 2.5. The rate of formation of a species X is written as :

$$dC_x/dt=(C_x^T - C_x^o)/t_R \quad (2)$$

where t_R is the residence time of X in the hot zone, defined as :

$$t_R= L.S/Q = \frac{L.S}{Q_o.\ (T/T_o)\ .\ (P_o/P)} \quad (3)$$

where L is the length of the hot zone (in cm), S the area of the infiltration furnace cross-section (in cm^2), T the deposition temperature (in K), P the pressure (in Pa), T_o=273 K, $P_o=10^5$ Pa, Q the propane gas flowrate and Q_o the gas flowrate under standard T, P conditions (both in sccm).

The thermal variations of the concentrations of the main species present in the hot zone of the infiltration chamber, near the substrate surface, are shown in fig. 7 as an Arrhenius plot. The data obey linear relationships which have been used to derive apparent activation energies for the formation of the various species, with the following results (in kJ. mol^{-1}) : $E_a(H_2)$=135 ; $E_a(CH_4)$=150 and $E_a(C_6H_6)$=286.

3.4- Optimization of the infiltration in the model pores

The pore entrance of the 60 μm model pore was observed to be always plugged by the PyC-deposit for the infiltration duration of 100 hours and the seven sets of conditions selected by the experiment design. Conversely, this was not systematically the case for the larger 120 and 320 μm pores, depending on the infiltration conditions. As already mentioned in section 2.3 the response used to assess the quality of the infiltration has been the thickness of the PyC-deposit at the 60 μm pore center. The variations of the PyC-thickness as a fonction of the distance along the pore, z (the origin being at the pore entrance)

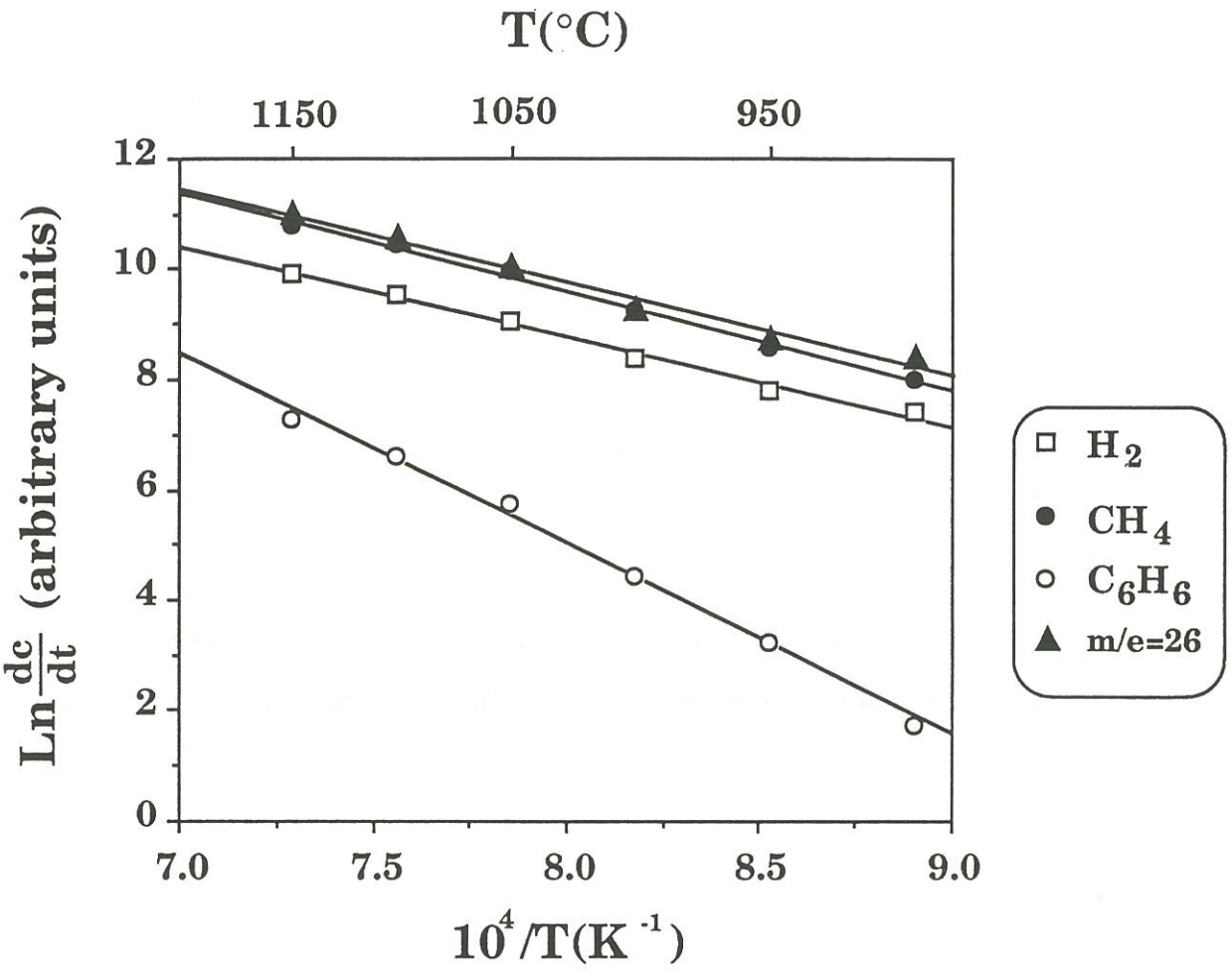

Fig. 7 : Thermal variations of the rates of formation of the main species present in the hot zone near the substrate surface during the deposition of PyC from propane (P=3 kPa; Q=60 sccm) as assessed from mass spectroscopy. The data corresponding to the mass 26 are related to several species (i.e. C_2H_2, C_2H_4 C_2H_6, acetylene being thought to be the most abundant).

are shown in fig. 8 and table 5, for the 60 μm pore. It appears that the influence of the propane gas flowrate on the PyC thickness profile along the pore is weak. Conversely, that of the pressure is very significant.

The values of the Ri-ratio (see section 2.4) are shown in table 6. Their variations as a function of both Q and P, for the three model pores, confirm the weak influence of the gas flowrate and the **strong influence of the propane pressure** on the quality of the infiltration, as already mentioned for the 60 μm pore (fig. 8a and table 5). Finally and as shown in fig. 8b, the **temperature has also a significant effect** on the PyC-thickness profile along the 60 μm model pore whereas the effect is less pronounced for the larger pores (table 7). All these features are classical in I-CVI and have been reported previously for the infiltration of SiC in model pores [9].

4- DISCUSSION

4.1- Kinetic law for the deposition of PyC from propane under I-CVI conditions

Our data show that the rate of deposition of the PyC resulting from the cracking of propane is thermally activated (see fig. 3 for P=3 kPa and Q=60 sccm). The apparent activation energy within the 950-1150°C range is of the order of **188 kJ.mol^{-1}** when the deposit occurs on the external surface of the substrate. This value is of the same order as that, 171 kJ.mol^{-1}, reported by Lee et al. in their study of the deposition of PyC from propane, within the temperature range 900-1230°C, but under different P - Q conditions (i.e. P=100 kPa ; P(C_3H_8)=10 to 100 kPa and Q=9 - 50 sccm) [26]. It is also not too different

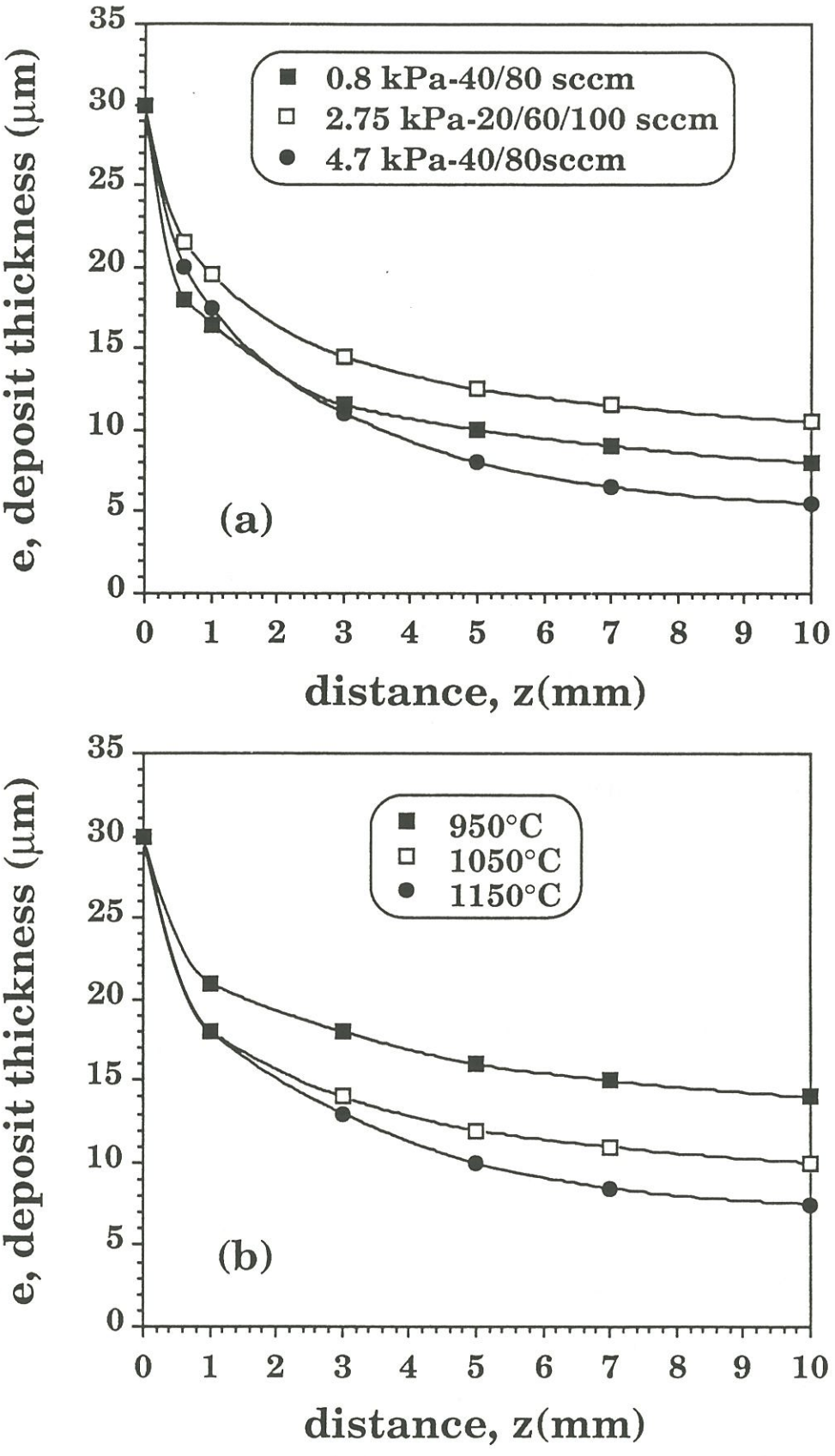

Fig. 8 : Thickness profiles along the 60 μm-model pore as a function of : (a) the pressure and gas flow rate (for T=1050°C) and (b) the temperature (for P=3 kPa and Q=60 sccm).

P (kPa) Q (sccm)	location along the pore axis, z(mm)					
	0	1	3	5	7	10
0.8 40	30	17	12	10	9	8
0.8 80	30	16	11	10	9	8
2.75 20	30	20	15	13	12	11
2.75 60	30	18	14	12	11	10
2.75 100	30	20	15	13	12	11
4.7 40	30	18	11	8	7	6
4.7 80	30	17	11	8	6	6

Table. 5 : Thickness of the PyC deposit (in μm) along the 60 μm model pore for the seven condition sets of the experiment design (T=1050°C; t=100 hours).

P (kPa) Q (sccm)	R_{320}	R_{120}	R_{60}
0.8 40	0.80	0.58	0.27
0.8 80	0.81	0.55	0.27
2.75 20	0.89	0.59	0.37
2.75 60	0.88	0.72	0.33
2.75 100	0.85	0.75	0.37
4.7 40	0.78	0.61	0.20
4.7 80	0.77	0.57	0.20

Table. 6 : Values of the Ri-ratio at the pore center for the three model pores and the seven condition sets of the experiment design (T=1050°C; t=100 hours).

T(°C)	R_{320}	R_{120}	R_{60}
950	0.92	0.74	0.46
1050	0.87	0.71	0.33
1150	0.65	0.55	0.20

Table. 7 : Values of the Ri-ratio at the pore center as a function of the temperature (P=3 kPa; Q=60 sccm) for the three model pores.

from the apparent activation energy associated with the decomposition of propane reported by Sundaram and Froment, i.e. 206 $kJ.mol^{-1}$ [27].

The values of the apparent activation energy are slightly lower at the pore center (158 - 161 $kJ.mol^{-1}$) than at the substrate external surface (184 - 192 $kJ.mol^{-1}$). This difference might be related to the uncertainty on the E_a-measurement (which is based on three temperatures only). It might be related too to the fact that some chemical species involved in the deposition process could be preferentially trapped near the pore entrance with the result that at the pore center the **deposition mechanism is different**, as suggested by the variations of the extinction angle along the pore (see table 4).

Generally speaking, a CVD-process can be rate-limited by the reactant(s) (or product(s)) **mass transfer** in the gas phase (regime of mass transfer or RMT) or by the kinetics of the **chemical reactions** (reaction regime or RR) [28,29]. When the deposition rate is observed to depend upon both temperature and pressure but remains constant as the gas flowrate is varied, the chemical surface reaction are the rate-limiting step of the deposition process. The data shown in table 2 (for T=1050°C) suggest that the rate-limiting step is the chemical surface reactions at low pressures, e.g. 0.8 kPa (deposition rate weakly depending on Q) and the mass transfer in the gas phase at high pressures, e.g. P > 4.7 kPa (deposition rate depending significantly on Q), whatever the pore size and the location of the deposit. For intermediate pressures (e.g. P=2.75 kPa), the deposition rate depends significantly upon the propane gas flowrate for Q < 60 sccm whereas it is no longer the case for Q > 60 sccm. Thus, the rate-limiting step for the deposition process could be the chemical surface reactions at high gas flowrates and the mass transfer in the gas phase at low gas flowrates.

4.2- Anisotropy of the PyC-deposit

The anisotropy of the PyC-deposits can be assessed through the value of the extinction angle Ae (table 4), as already mentioned in section 2.4. The combined influences of the deposition parameters (P, T, Q) on Ae will be discussed on the basis of an empirical factor, referred to as the **anisotropy potential** F_{ap} and proportional to the benzene concentration in the gas phase, benzene being considered as representative of the chemical intermediate species responsible for the formation of anisotropic PyC [16] :

$$F_{ap}=\alpha \,.[C_6H_6]_{T,P,\,Q} \qquad (4)$$

The benzene concentration has been measured in a relative scale by mass-spectroscopy near the **external substrate surface**, as explained in sections 2.5 and 3.3, within the temperature range 900 - 1150°C but only for P_s=3 kPa and Q_s=60 sccm. Assuming that the concentration of C_6H_6 formed in the hot wall deposition chamber is, at least in a first approximation, proportional to the pressure and to the residence time (and thus to the reciprocal gas flowrate according to equation (3)), the concentration of benzene at P, T, Q can be derived from that measured by mass-spectrometry at P_s, Q_s, T, according to the following equation :

$$[C_6H_6]_{P,Q,T}= A.[C_6H_6]_{Ps,Qs,T} \cdot \frac{Q_s}{Q} \cdot \frac{P}{P_s} \qquad (5)$$

where A is constant, Q_s=60 sccm (standard conditions) and P_s=3 kPa. Q, the actual gas flowrate in the deposition chamber can be expressed in the standard conditions as a function of both T and P assuming that the gas mixture obeys the perfect gas law :

$$Q = Q_o \frac{T}{T_o} \frac{P_o}{P} \qquad (6)$$

Substituting (6) in (5) and (5) in (4) leads to :

$$F_{ap} = \frac{a.\,[C_6H_6]_{Ps,Qs,T} \,.\, P^2}{T.Q_o} \qquad (7)$$

where **a** is a scale constant, P, the total pressure, T, the substrate temperature, Qo, the gas flowrate and $[C_6H_6]_{Ps,Qs,T}$, the relative apparent benzene concentration in the gas phase, measured by mass-spectroscopy for P_s=3 kPa and Q_s=60 sccm. It appears from equation (7) that a low value of F_{ap} corresponds to low pressure values. Finally, it is noteworthy that the F_{ap} factor is valid only when the supersaturation of the gas phase in pyrocarbogenic species is not too high and does not result in the formation of carbon black soot in the gas phase.

4.2.1- Anisotropy of PyC deposited on the external substrate surface

The values of F_{ap} have been calculated for the Q, P, T conditions corresponding to the experiments listed in table 4, as well as for two complementary experiments performed at T=1100°C, P=3 kPa and for Q=110 sccm (with Ae=12°) and Q=190 sccm (with Ae=13°) respectively, in order to enlarge the gas flowrate range. The variations of Ae as a function of F_{ap}, are shown in fig. 9, with the following main features : (i) Ae is constant and equal to about 11.5°, i.e. the pyrocarbon remains **isotropic**, when F_{ap} is less than 10, (ii) Ae is constant and equal to about 20, i.e. the deposits consist of **anisotropic** PyC (rough laminar) when F_{ap} is higher than 130 and (iii) for intermediate

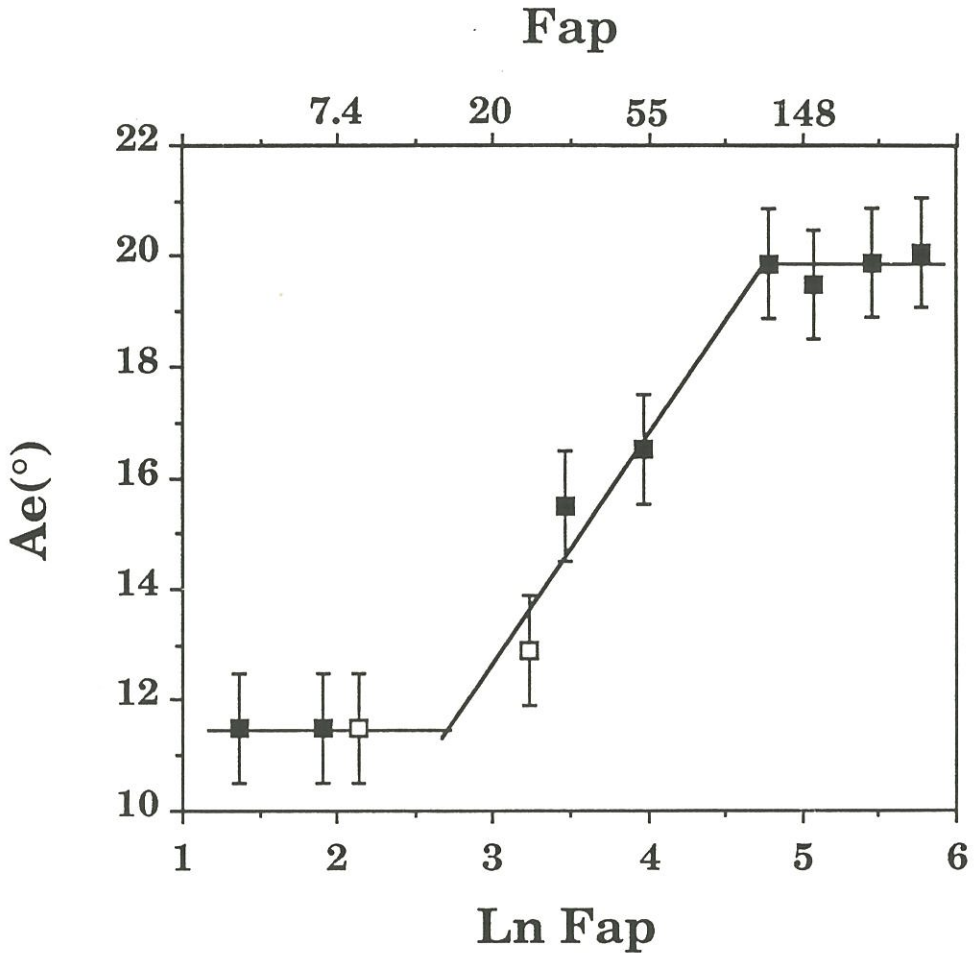

Fig. 9 : Variations of the extinction angle Ae measured for PyC deposits on the external substrate surface as a function of the anisotropy potential Fap, plotted in an arithmetic/logarithmic scale : ■ data derived from table 4; □ additional data (see text).

values of F_{ap}, i.e. $10 < F_{ap} < 130$, Ae increases from 11.5 to 20°, which means that the anisotropy of the PyC deposit increases as F_{ap} is progressively raised.

These results suggest that the **residence time** t_R of the chemical species in the deposition chamber (which is function of Q) has to be increased in order to observe a well organized carbon on the external surface of the model pore substrate, as P and T are lowered. Conversely, short residence times become acceptable when both T and P are raised. There is thus a compensating effect between the residence time, on the one hand, and both the temperature and the pressure, on the other hand. Increasing both T and P results in a larger number of collisions between the molecules in the gas phase and a higher chemical reactivity. Thus, it seems that the variations of the deposit microstructure as a function of T, P and Q are related to those of the interactions between the chemical species in the gas phase : the chemical species yielding actually the PyC-deposit being in a more or less "achieved" state depending on the experimental conditions.

Pierson and Liebermann have proposed a model predicting the microstructure of pyrocarbon on the basis of the value of the ratio, R, between the concentration of C_2H_2 and that of C_6H_6 in the gas phase, the microstructure being successively smooth laminar (SL) for $R < 5$, rough laminar (RL) for $5 < R < 70$ and finally isotropic (I) for $R > 70$ [16]. This sequence is not in agreement with the results of present work. Assuming that C_2H_2 is the main species of the 26 mass signal, the data shown in fig. 7 suggest that the R-ratio decreases as temperature is raised. Thus, according to the model of Pierson and Liebermann, the sequence should be RL and then SL which contrasts with the SL → RL sequence observed in present work. We propose here the following sequence, : DL → SL → RL for $950 < T < 1150$° and $1 <$

P < 5 kPa which is in agreement with that derived by Goma from TEM analysis results [30]. In a similar manner, Lajzerowicz, has reported a SL → RL transition as temperature is increased in PyC deposited under low pressures from methane, within the same temperature range as that studied here [31].

The value of Ae, observed in present work for T=1050 - 1150°C and P=3 kPa is of the order of 20° and corresponds to a RL - microstructure. The result contrasts with the conclusions of Lee according to which the PyC microstructure is reported to be SL and even a SL + I mixture, for the same P-T domain [10]. This disagreement could be related to the fact that Lee's experiments have been performed at a **pressure of 100 kPa** (argon/propane mixture), a condition under which the number of the effective collisions yielding the formation of pyrocarbogenic molecules is thought to be less and, furthermore, his experimental reactor was different (tumbling bed). However, the apparent activation energy reported by Lee for the PyC-deposition from propane, E_a=171 kJ.mol^{-1} and the apparent reaction order with respect to propane, are close to those observed in present work.

4.2.2- Anisotropy of the PyC deposited along the model pores

As shown in table 4, when the anisotropy of the PyC deposited on the external surface of the model pore substrates is high (i.e. Ae=20°), that of the deposit at the pore center is systematically **less pronounced** (Ae < 15°), whatever the pore size. This important feature could be explained as follows : (i) diffusion in the gas phase along the pore results in a selection of the intermediate pyrocarbogenic molecules : the molecules with a high aromatic character (i.e. containing several aromatic rings), assumed to diffuse with difficulty tend to be deposited flat on the pore wall near the pore entrance

(yielding anisotropic PyC) whereas the H-rich molecules (with a low aromatic character) diffuse in-depth in the pore (yielding at the pore center less-anisotropic PyC) and (ii) the in-depth deposition process increases the hydrogen concentration at the pore center and yields a H-gradient along the pore which is unfavorable to the "maturation" of highly aromatic intermediate species far from the pore entrance and to their in-depth diffusion.

4.3- Optimization of the I-CVI of the model pores

Within the domain of the experiment design (T=1050°C ; 0.8 < P < 4.7 kPa and 20 < Q < 100 sccm), the deposit thickness and R_i-ratio data listed in tables 5 and 6, clearly show that the quality of the pore infiltration mainly depends on the total pressure, at a given temperature, whereas the influence of the gas flowrate is low. Conversely, **both** the total pressure and the gas flowrate have a strong influence upon the deposition rate either at the external surface of the substrate or at the pore center, as shown in fig. 10a and b.

The constant terms i (with i=a, b, c, d, e, f) in equation (1) have been computed from the PyC deposit thicknesses measured at the center of the 60 µm-pore (which is always sealed by the deposit, as previously mentioned) for the T, P, Q conditions of the experiment design (table 5 ; z=10 mm) and equation (1) rewritten as :

$$e=4.45 + 0.186 \times 10^{-6}.\mathbf{Q} + 5.273.\mathbf{P} - 0.219 \times 10^{-8}.\mathbf{Q}^2 - 1.1052.\mathbf{P}^2 - 0.13087.10^{-6}.\mathbf{P.Q} \quad (1)$$

showing that the values of the i constant terms (with i=b, d, f) associated with Q are very low, a result which emphasizes the fact that the propane flowrate has but a very limited influence on the quality of the pore infiltration. The

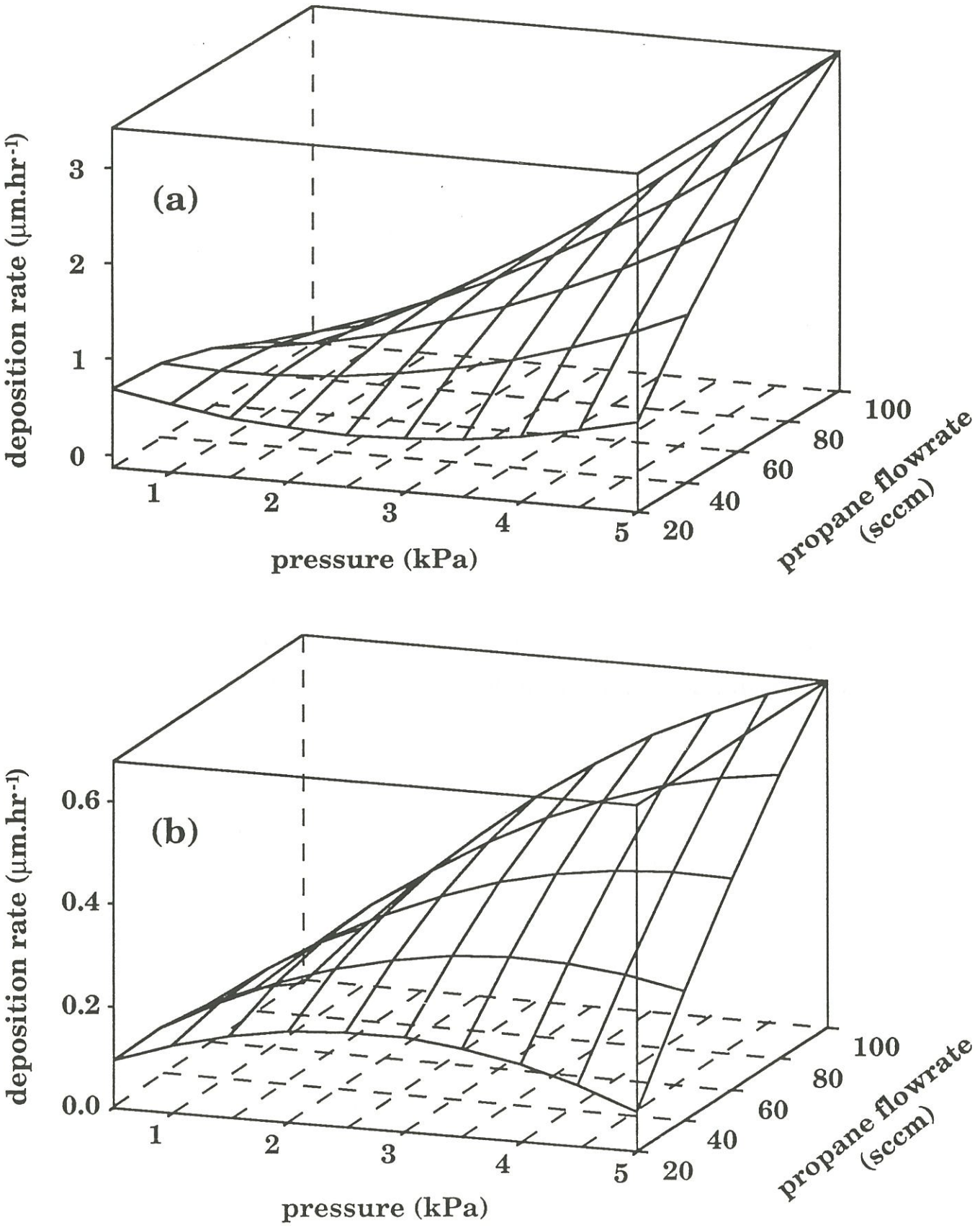

Fig. 10 : Variations of the PyC-deposition rate as a function of both total pressure and propane flowrate : (a) at the external surface of the substrate and (b) at the 60 µm-model pore center for the T-P-Q conditions of the experiment design.

variations of **e** as a function of both P and Q are shown in fig. 11. They clearly show that the infiltration quality undergoes an optimum for a total pressure of about 3 kPa, for the 60 μm-pore, a result which can be extended to the other model pores (120 and 320 μm in diameters) on the basis of the Ri data listed in table 6.

The reproductibility of the experiments has been quantitatively assessed by repeating twice the infiltration of the 60 μm-pore under the following conditions : P=2.75 kPa ; Q=60 sccm and T=1050°C. The values of e_{10} (thickness of the PyC-deposit at z=10 mm) were observed to be 10 and 11 μm respectively (as compared to 10 μm for the initial experiment ; tables 4 and 5). Thus, the accuracy of the model is of the order of 10%, the dispersion of the results, for given PTQ conditions, being mainly related to the error on the thickness measurement.

Finally, experiments performed at $T \neq 1050°C$ (and thus not included in the experiment design, as already mentioned), have shown (see table 4) that temperature is a parameter as important as pressure for the quality of the pore infiltration. This result corroborates the conclusions drawn by previous authors for the infiltration of SiC and appears to be a general feature of the I-CVI-process [8].

5- CONCLUSION

On the basis of the experimental data shown in section 3 and of the discussion presented in section 4, the following main conclusions can be drawn on the CVD/CVI of PyC from propane performed at $900 < T < 1150°C$; $0.8 < P < 4.7$ kPa and $20 < Q < 100$ sccm :

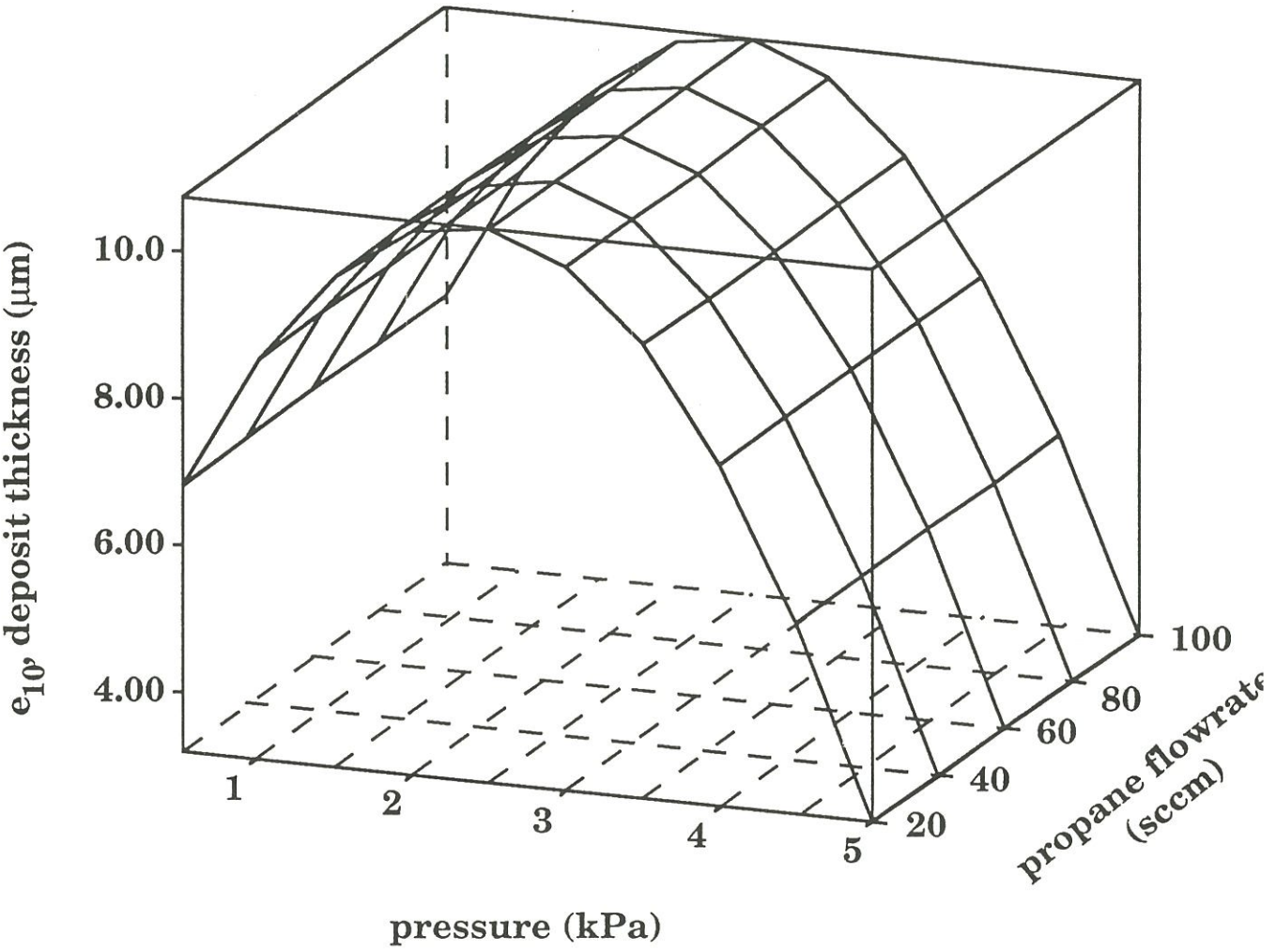

Fig. 11 : Variations of the PyC-thickness deposited at the center of the 60 µm-model po (measured after pore-sealing) as a function of both the totale pressure and the propane gas flowrate, for the T-P-Q conditions of the experiment design.

(i) the main intermediate species formed in the gas phase near the hot substrate are H_2, CH_4, C_2H_2, C_3H_8 and C_6H_6 (and possibly heavy molecules undetectable by simple mass-spectrometry),

(ii) the PyC-deposition, when it is rate-controlled by the surface reactions obeys a **first order kinetic law** with respect to propane with an apparent activation energy slightly different at the pore center ($E_a \approx 160$ kJ.mol^{-1}) than at the pore entrance ($E_a \approx 188$ kJ.mol^{-1}). For Q = 60 sccm, the value of the kinetic constant (i.e. the pre-exponential term) is 13725 μm.h^{-1}.Pa^{-1},

(iii) both temperature and pressure have a strong influence on the homogeneity of the infiltration of the model pores whereas the gas flowrate has a much more limited effect. At 1050°C, the optimum pressure is close to 3 kPa whatever the pore size,

(iv) the nature of the PyC-microstructure correlates with the value of an empirical factor, referred to as the **anisotropy potential factor** F_{ap} which depends on the benzene concentration and the deposition parameters (T, P, Q). When $F_{ap} < 10$, the microstructure is isotropic (Ae < 12) whereas for $F_{ap} > 130$ (Ae > 18°), it is rough laminar. For intermediate F_{ap} values, i.e. $10 < F_{ap} < 130$, the microstructure is smooth laminar. When F_{ap} increases, e.g. when temperature is raised (at constant P, Q), the sequence DL → SL → RL occurs,

(v) the F_{ap} factor expresses the combined influences of various parameters. At low P.T (i.e. under I-CVI-conditions), the residence time of the gaseous precursor in the hot deposition chamber should be high enough in order to permit the maturation of the intermediate species (i.e. molecules with a high aromatic character) responsible for the deposition of anisotropic PyC (rough laminar). Unfortunately, in the I-CVI of PyC from propane, the deposit

occurring in-depth is less anisotropic than that near the pore entrance owing to the facts that the large aromatic molecules are trapped at the pore entrance and the high H-concentration at the pore center prevents the in-depth formation and diffusion of these aromatic molecules.

ACKNOWLEDGEMENTS

This work has been supported by Société Européenne de Propulsion (SEP) through a grant given to P.Dupel. The authors are indebted to X. Bourrat (LCTS) and S. Goujard (SEP) for valuable discussions of the experiments and results.

REFERENCES

[1] J.J. Choury, "SEP carbon and ceramic composites in aeronautics and space applications", Proc. 1st. Int. Symp. Functionally Gradient Materials (M. Yamanouchi, M. Koizumi, T. Hirai and I. Shiota, eds.), p. 157, Soc. Non Tradit. Technology, Tokyo, (1990).

[2] B. Broquere, B. Buttazzoni and J.J. Choury, "Carbon/carbon composites and their industrial applications" (in french), in "Introduction aux matériaux composites"-Vol.2 (R. Naslain, ed.), p. 405, Co-édition, CNRS/IMC, Paris and Bordeaux, (1985).

[3] J.P. Belmonte, "Technology of carbon and graphite fiber composites", p. 388, Van Nostrand Reinhold Cº, New York, (1981).

[4] P. Lamicq, "Properties and uses of carbon-carbon composites" (in french), J. Chimie Physique, 81, [11/12], 735 (1984).

[5] Y.Gremic, "Les composites multidirectionnels dans les véhicules balistiques et spatiaux", Matériaux et Techniques, n°spécial Mater. Composites, p. 33 (1984).

[6] M. Heyn and E. Fitzer, "Carbon fiber reinforced carbon", in "Processing and uses of carbon fiber reinforced plastics", p. 85, V. d. I. Verlag GmbH, Düsseldorff, (1981).

[7] W. V. Kotlensky, "Deposition of pyrolytic carbon in porous solids", J. Chem. Phys. Carbon, 9, 173 (1973).

[8] R. Naslain and F. Langlais, "CVD-processing of ceramic-ceramic composite materials", in "Tailoring multiphase and composite

ceramics" (R.E. Tressler, G.L. Messing, C.G. Pantano and R.E. Newnham, eds.), Mater. Sci. Research, Vol 20, p. 145, Plenum Press, New York and London, (1986).

[9] R. Fedou, F. Langlais and R. Naslain, "A modeling of the isothermal isobaric chemical vapor infiltration in a straight cylindrical pore. Part 1 : description of the model", J. Mat Synthesis and Processing, 1, [1], 43 (1993).

[10] J.Y. Lee and S.E. Oh, "Structures of pyrolytic carbon matrices in carbon/carbon composites", Carbon, **26**, [6], 763 (1988).

[11] P. Delhaes, M. Trinquecoste, A. Pacault, J. Goma, A. Oberlin and J. Thebault, "Matériaux composites carbone/carbone : conditions de fabrication par dépôt chimique en phase vapeur, microstructures et propriétés physiques", J. Chimie Physique, **81**, [11/12], 809 (1984).

[12] R.O. Grisdale, "The formation of black carbon", J. Appl. Phys., **24**, [9], 1082 (1953).

[13] J.C. Bokros, "Variation in the crystallinity of carbons deposited in fluidized bed", Carbon, **3**, 201 (1965).

[14] J. Linke, K. Koizlik and H. Nickel, "Fundamentals on the agglomerate model and its relation to the physical properties of pyrocarbon", J. Nuclear Technology, **35**, 257 (1977).

[15] J.L. Kaae, "The mechanism of the deposition of pyrolytic carbon", Carbon, **23**, [6], 665 (1985) .

[16] H.O. Pierson and M.L. Liebermann, "The chemical vapor deposition of carbon on carbon fibers", Carbon, **13**, 159 (1975).

[17] R.J. Diefendorf, "The deposition of pyrolytic graphite", J. Chimie Physique, **57**, 815 (1960).

[18] M.H. Back and R.A. Back, "Thermal decomposition and reactions of methane", in "Pyrolysis : Theorie and Industrial Practise", p. 1, **1**, (L.F. Albright, B.L. Crynes and W.H. Corcoran., eds), Academic Press, (1983).

[19] C.J. Chen and M.H. Back, "The simultaneous measurement of the rate of formation of carbon and of hydrocarbon products in the pyrolysis of methane", Carbon, **17**, 175 (1979).

[20] P. Dupel, R. Pailler and R. Naslain, "Pulse chemical vapor deposition (P-CVD) and infiltration (P-CVI) of pyrocarbon in model pores with rectangular cross section, Part 2 : study of the infiltration", to be published in J. Mat. Sciences.

[21] D.H. Doehlert, "Uniform shell designs", Appl. Statistics, 19, 231 (1970)

[22] G. Dumenil, G. Mattei, M. Sergent, J.C. Bertrand, M. Laget and R. Phan-Tan-Luu, "Application of a Doehlert experimental design to the optimization of microbial degradation of crude oil in sea water by continuous culture", Appl. Microbiol. Biotechnol., **27**, 405 (1988).

[23] R.J. Diefendorf and E. W. Tokarsky, "The relationships of structure to properties in graphite fibers", Air Force report AF 33(615)-70-C-1530 (1971).

[24] P. Dupel, X. Bourrat and R Pailler, "Anisotropic pyrocarbon obtained at low temperatures by pulse CVI : Structural characterization", Submitted to Carbon.

[25] L.F. Coffin, "Structure-property relation for pyrolytic graphite", J. Amer. Ceram. Soc., **47**, [10], 473 (1964).

[26] J.Y. Lee, J.H. Je, W.S. Ryu and H.S. Kim, "A study of the properties of pyrolytic carbons deposited from propane in a tumbling and stationary bed between 900 and 1230°C", Carbon, **21**, [6], 523 (1983).

[27] K.M. Sundaram and G.F. Froment, "Kinetics of coke deposition in the thermal craking of propane", Chem. Eng. Sci., **34**, 635 (1979).

[28] K.E. Spear, "Thermochemical modeling of steady state CVD processes", Proc. 9thInt. Conf. CVD, Paris, France (1989), (Mc Robinson et al., eds.), The Electrochem. Soc., Pennington, 81(1989).

[29] C.E. Morosanu, "Thin films in chemical vapor deposition", Elsevier Ed., Amsterdam-Oxford-New York-Tokyo, (1990).

[30] J. Goma, "Pyrocarbone et interfaces silicium-carbone, etude en microscopie et diffraction electroniques", Thèse d'état, UER des sciences Orléans, France, (1983).

[31] P. Lajzerowicz, "Modelisation de l'élaboration de composites carbone-carbone par depot chimique en phase vapeur", Thèse de docteur ingénieur, numéro d'ordre : 606, Institut National Polytechniques de Grenoble, France, (1987).

Chapître 2 : PULSE CHEMICAL VAPOR DEPOSITION (P-CVD) AND INFILTRATION (P-CVI) OF PYROCARBON IN MODEL PORES WITH RECTANGULAR CROSS SECTIONS : PART 1 - STUDY OF THE PULSED PROCESS OF DEPOSITION

Si quelques études expérimentales succinctes ont été consacrées à la P-CVI, aucune, à notre connaissance, n'a étudié de manière détaillée l'influence des paramètres de la P-CVI sur la qualité de l'infiltration d'une porosité donnée, sur la microstructure du dépôt, sur sa composition chimique...etc.

Ce premier chapitre consacré à la P-CVI aborde l'étude des **mécanismes de dépôt du pyrocarbone à partir du propane**. De même qu'en I-CVI, les dépôts sont réalisés ici sur des pores modèles et dans un large domaine de conditions expérimentales (950°C>T>1150°C, 1 kPA<P<10 kPA, 0,2 s<durée du palier<120 s). Les épaisseurs de PyC déposées par pulse en fonction des conditions expérimentales et les observations des dépôts au TEM ont permis de développer un **modèle** mettant en jeu deux mécanismes de dépôt du PyC. L'étude à été complétée par des **analyses ponctuelles de la phase gazeuse** présente dans la zone chaude du réacteur en fonction de la température. De toute évidence l'épuisement de la phase gazeuse avec la durée du palier et la quantité d'hydrogène (qui croît au cours du temps) ont un rôle important sur la vitesse de dépôt et sur la microstructure du dépôt.

Ce chapitre présente les résultats de l'étude sous forme d'un projet de publication adressée au Journal of Material Science.

submitted to the Journal of Materials Science.

PULSE CHEMICAL VAPOR DEPOSITION (P-CVD) AND INFILTRATION (P CVI) OF PYROCARBON IN MODEL PORES WITH RECTANGULAR CROSS-SECTIONS : PART 1 - STUDY OF THE PULSED PROCESS OF DEPOSITION

P. Dupel, R. Pailler and F. Langlais
Laboratoire des Composites Thermostructuraux
UMR-47 CNRS-SEP-UB1, Domaine Universitaire
3, allée de La Boëtie, 33600 Pessac, France.

ABSTRACT

The pulse-CVD/CVI is a promising technique to densify porous substrates. By cycling the reactor pressure, the in-depth depletion of the gas phase is limited. An experimental approach of the deposition process is presented : influence of the residence time, temperature, pressure and nature of the precursor on the gas phase composition and the deposition thicknesses at the external surface and within the pores of the substrates. Two types of mechanisms are involved, governed by the maturation of the gas phase during the pulse. For low pressures, low temperatures and stable precursors such as CH_4, the gas maturation is very limited, the deposition mainly occurs by slow

decomposition of small molecules and good infiltration can be obtained. Conversely, for high pressures, high temperatures and more reactive precursors such as C_3H_8, a high maturation of the gas phase results in (i) rapid condensation of stacks of small carbon layers through heavy aromatic species and (ii) difficult infiltration of porous substrates.

KEY WORDS

Pulse CVD/CVI, pyrocarbon, propane, methane.

1- INTRODUCTION

The ceramic matrix composites (CMC), developed mainly for aerospace applications, consist of ceramic fibers embedded in a ceramic matrix, an interphase being usually introduced between the two constituents in order to control the fiber-matrix bonding. A convenient choice of these three components can lead to materials with outstanding thermomechanical properties even under oxydizing environment [1].

The processing of these materials can be performed according to three classical ways, i.e. from the gaseous, liquid or solid phases [2-4]. The chemical vapor infiltration (CVI) technique, which derives directly from chemical vapor deposition (CVD), permits to densify the pore network of fiber preforms by a ceramic matrix, with several advantages : (i) a processing temperature rather low with respect to that of sintering, melting or decomposition of the ceramic matrix, (ii) a low processing pressure, both preventing a pronounced degradation of the ceramic fibers, and (iii) the possibility of preparing a large range of matrices and/or interphases [5-10]. Nevertheless, the isothermal/isobaric technique (I-CVI) exhibits two drawbacks : (i) a large processing duration resulting from the need of a low deposition rate to decrease the thickness gradient through the preform and (ii) a non negligible residual porosity (about 10-15%).

With a view to solve these problems, derived methods have been proposed. The forced-CVI, i.e. with temperature and/or pressure gradients, permits to increase the infiltration rate but can only be applied to a very few number of specific samples such as tubes or plates [11]. The second technique is **the pulse CVI (P-CVI)** developed by Beatty [12] and more recently by Sugiyama [13-14] for the infiltration of porous carbon or fiber preforms. In this

process, a pressure cycle is applied in order to periodically regenerate the whole gas phase : the pulse consists, after evacuation of the reactor chamber, in instantaneous charge of source gas, holding at desired pressure and again evacuation. The aim of this pressure cycling is to limit the occurrence of the reaction products usually inhibitor within the preform pore network and consequently to favour in-depth deposition and, increase the infiltration rate.

The present paper is the first part of a study of the P-CVI of pyrocarbon. It deals mainly with the surface deposition process (P-CVD) of pyrocarbon through an investigation of the influence of various parameters such as the temperature, pressure, residence time and nature of gaseous precursor. This approach is carried out on model porous substrates which permit to consider both the external surface and in-depth deposition.

2- EXPERIMENTAL

2.1- Pulse - CVD/CVI apparatus

The apparatus used for the CVD/CVI experiments is shown in fig. 1. The precursor gas (here propane or methane) is maintained at the pressure desired for the pulse in a tank from which the gas can be fed to the reactor instantly through a pneumatic valve with an opening time of about 0.1 s. The deposition chamber is an inconel vertical cylindrical tube resistively heated. The temperature is monitored with a thermocouple and a quasi-isothermal zone 27 mm in diameter and 50 mm in height is available. An outlet pneumatic valve permits to evacuate the gas mixture from the reactor chamber to the vacuum pump through a liquid nitrogen trap. An automation can control the opening and closing of the valves as well as the safety devices

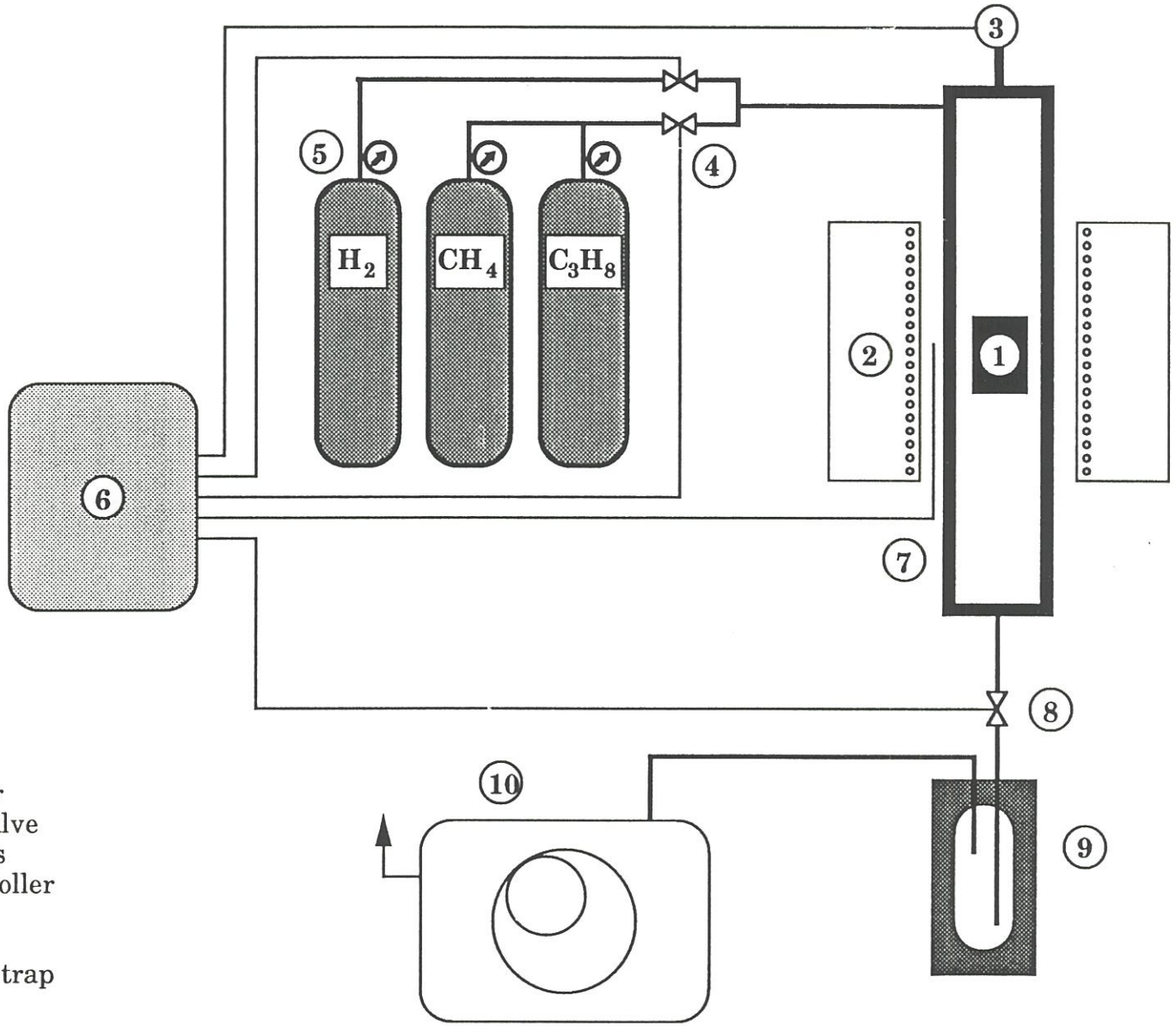

1 - substrate
2 - furnace
3 - pressure sensor
4 - gas injection valve
5 - gaseous sources
6 - automate controller
7 - thermocouple
8 - shut-off valve
9 - liquid nitrogen trap
10 - vacuum pump

Fig. 1 : Apparatus used for the P-CVD/CVI of pyrocarbon (schematic).

for temperature and pressure and at last the total number of pulses. A typical example of pressure cycle is given in fig. 2.

2.2- The model substrates

The model substrate with straight rectangular pores is shown schematically in fig. 3. The model pores are formed by the assembly of two plates made of purified graphite, one of them being machined to obtain three parallel grooves. These grooves 20 mm in length exhibit rectangular cross-sections with the same width (l = 2 mm) and various heights (h = 60, 120 and 320 μm). The pore height is actually dependent on the tightening of both plates and the roughness of the graphite surface, which results in a possible uncertainty on h of about 5 μm. The practical interest of such a substrate is the easy assessment of the profiles of pyrocarbon deposit thickness by optical observations over the whole pore length, the deposits resulting from P-CVD being analyzed on the external parts of the graphite plates.

2.3- Analysis of the gas phase

The chemical composition of the gaseous mixture was semi-quantitatively assessed by probing the gas phase near the substrate external surface with a capillary connected to a quadripole mass-spectrometer. The resulting analysis gave interesting data on the species stable at the ambient temperature, particularly on the variations of thin concentration as a function of residence time, (Ar peak being used as standard and analysis duration being only 0.1 s).

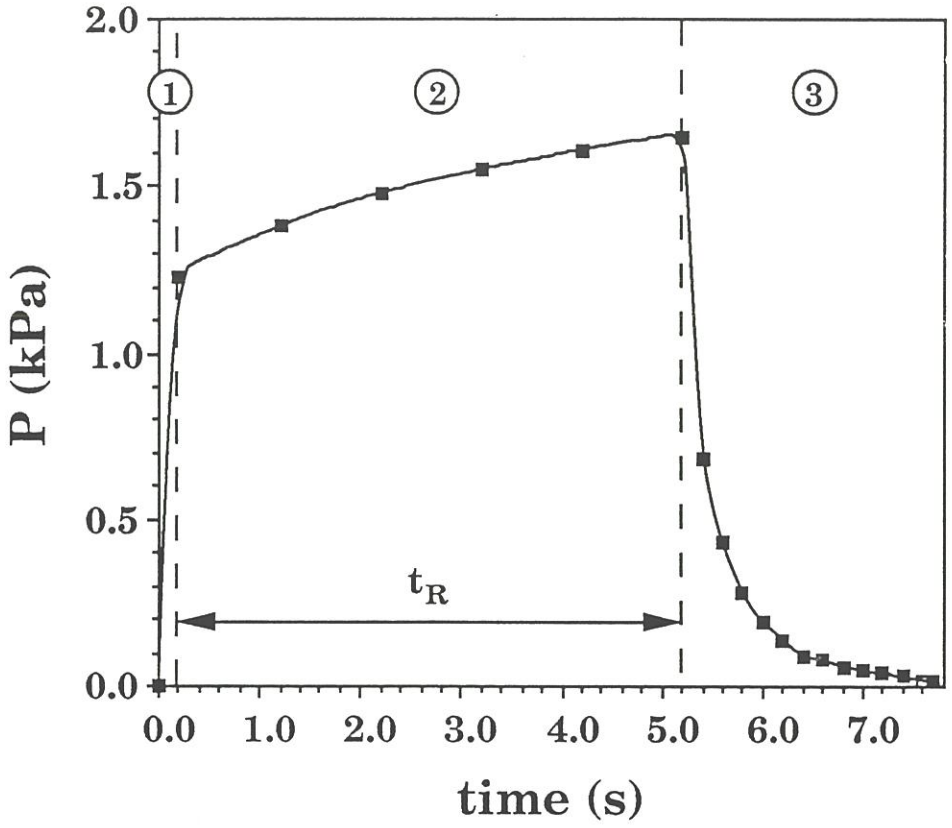

① Introduction (0.2 s)

② Deposition (5 s)

③ Gas evacuation (2.5 s)

Fig. 2 : Example of pressure cycling for t_R = 5 s.

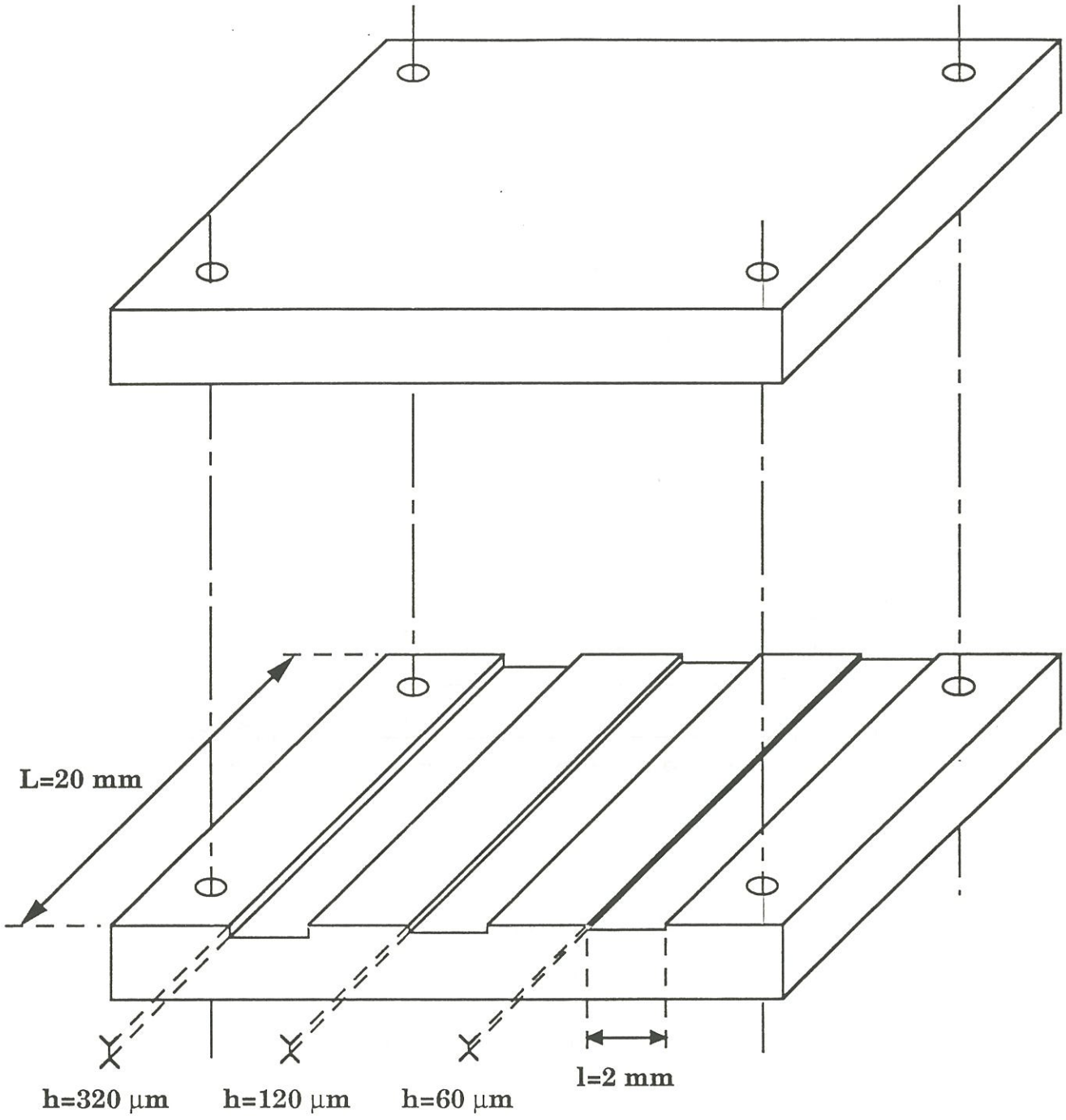

Fig. 3 : Schematic of the model graphite substrate with 3 straight pores with rectangular cross-sections.

2.4- Deposit analysis

The profiles of pyrocarbon deposit thickness were assessed by optical observations over the whole pore length, which needs to cut axially the sample, to embed it in a resin and to perform a conventional polishing. In the present contribution, the thickness of the deposits on the external surface of the substrates was more specifically investigated as a function of various experimental parameters.

The surface morphology of the pyrocabon was observed by scanning electron microscopy (SEM) either on the external deposits or on the in-depth deposits after disconnecting the two plates of the model substrates. A preliminary microstructural approach was carried out by optical microscopy in polarized light.

3- RESULTS

3.1- Analysis of the gas phase

In most of the experimental conditions, the main gaseous species detected by mass spectrometry are : H_2, CH_4, C_2H_6, C_3H_8, C_2H_4, C_3H_6, C_2H_2, C_6H_6. Several of these molecules exhibit mass spectra which overlap to one another. Only the peaks for the masses 2, 16, 29 and 78 corresponding respectively to hydrogen, methane, propane and benzene, are considered in the semi-quantitative analysis. On the other hand, tars are observed in the cold parts of the reactor and analyzed by Steric Exclusion Chromatography suggesting that aromatic compounds such as pyrene and phenantrene are formed.

The relative concentrations of H_2, CH_4, C_3H_8 and C_6H_6 are reported in fig. 4 as a function of the residence time, t_R, for pure propane as precursor, P = 3 kPa and two values of the temperature T = 950 and 1050°C. While C_3H_8 concentration decreases with increasing t_R, those of CH_4 and H_2 rises. These concentration variations are less and less rapid as t_R increases and a stable state seems to be reached beyond a threshold value of t_R.This threshold is about 30 s at 950°C and only 15 s at 1050°C. C_6H_6 is detected, but its concentration remains very low with respect to the other species.

The influence of temperature on the various species concentrations is shown in fig. 5 for t_R=10 s and two precursors : propane under 3 kPa and methane under 10 kPa. By increasing temperature, C_3H_8 source species is more and more consumed giving rise to increasing amounts of CH_4, H_2 and to a less extent C_6H_6. When CH_4 is the precursor species, its concentration is also decreased but no other species can be detected by the mass spectrometer.

3.2 - Morphology of the deposits

The SEM micrograph of fig. 6 shows the aspect of the pyrocarbon deposited at the entrance of a pore 320 μm in height for T =1050°C, P = 10 kPa propane and t_R = 2 s. The deposit thickness seems to be rather uniform in the cross-section, with a more or less smooth surface morphology. The pyrocarbon deposit consists of carbon layers almost parallel to the substrate surface and which appear only weakly bonded to one another.

As shown in fig. 7, the pyrocarbon has grown with a cone/columnar microstructure [15]. Most of the nucleation sites are located on the rough graphite substrate surface for various experimental conditions, e.g. for P = 3

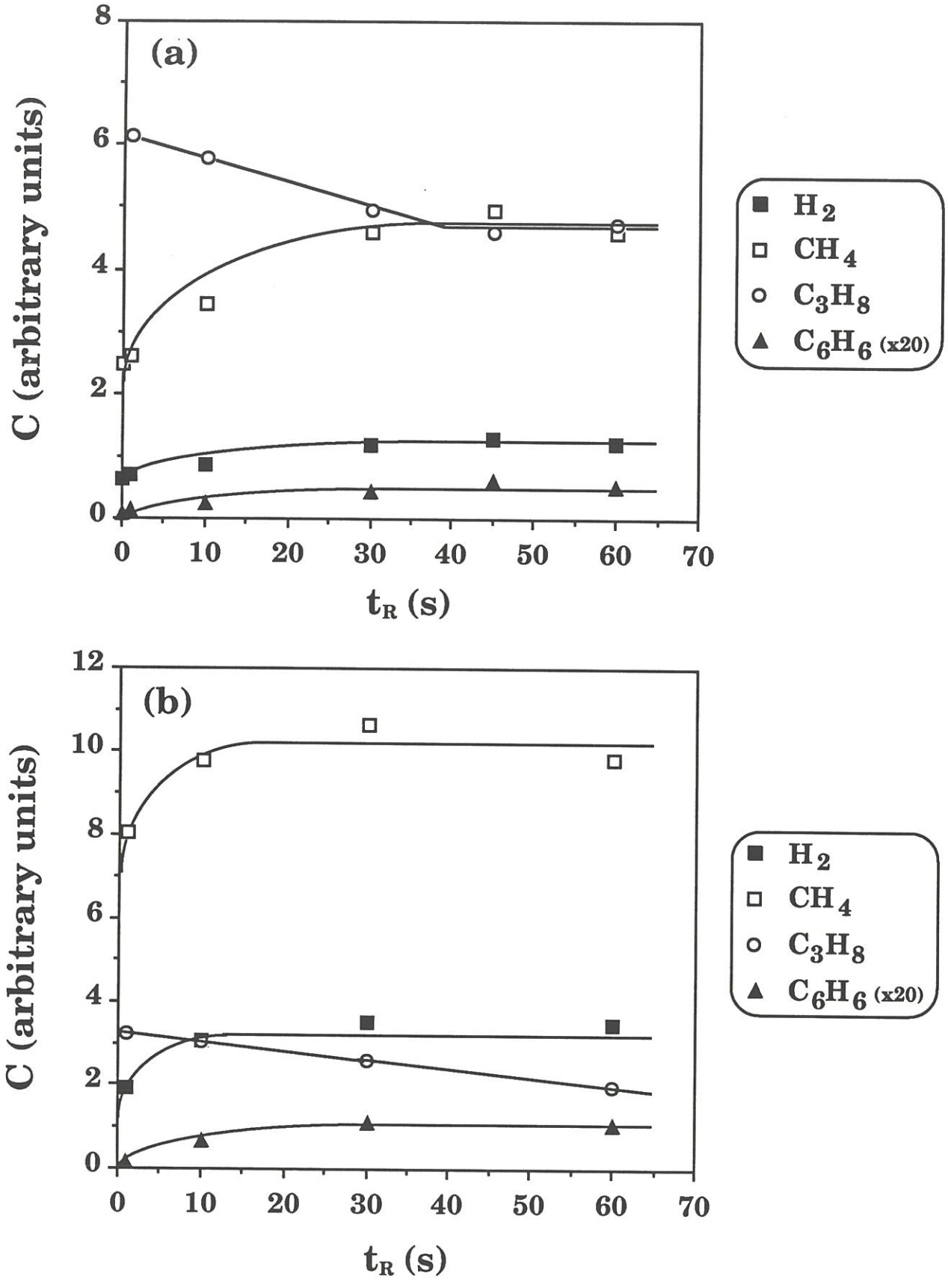

Fig. 4 : Variations of the concentrations of the various gaseous species analyzed by mass spectrometry as a function of the residence time for P= 3 kPa, (a) T=950°C and (b) T=1050°C.

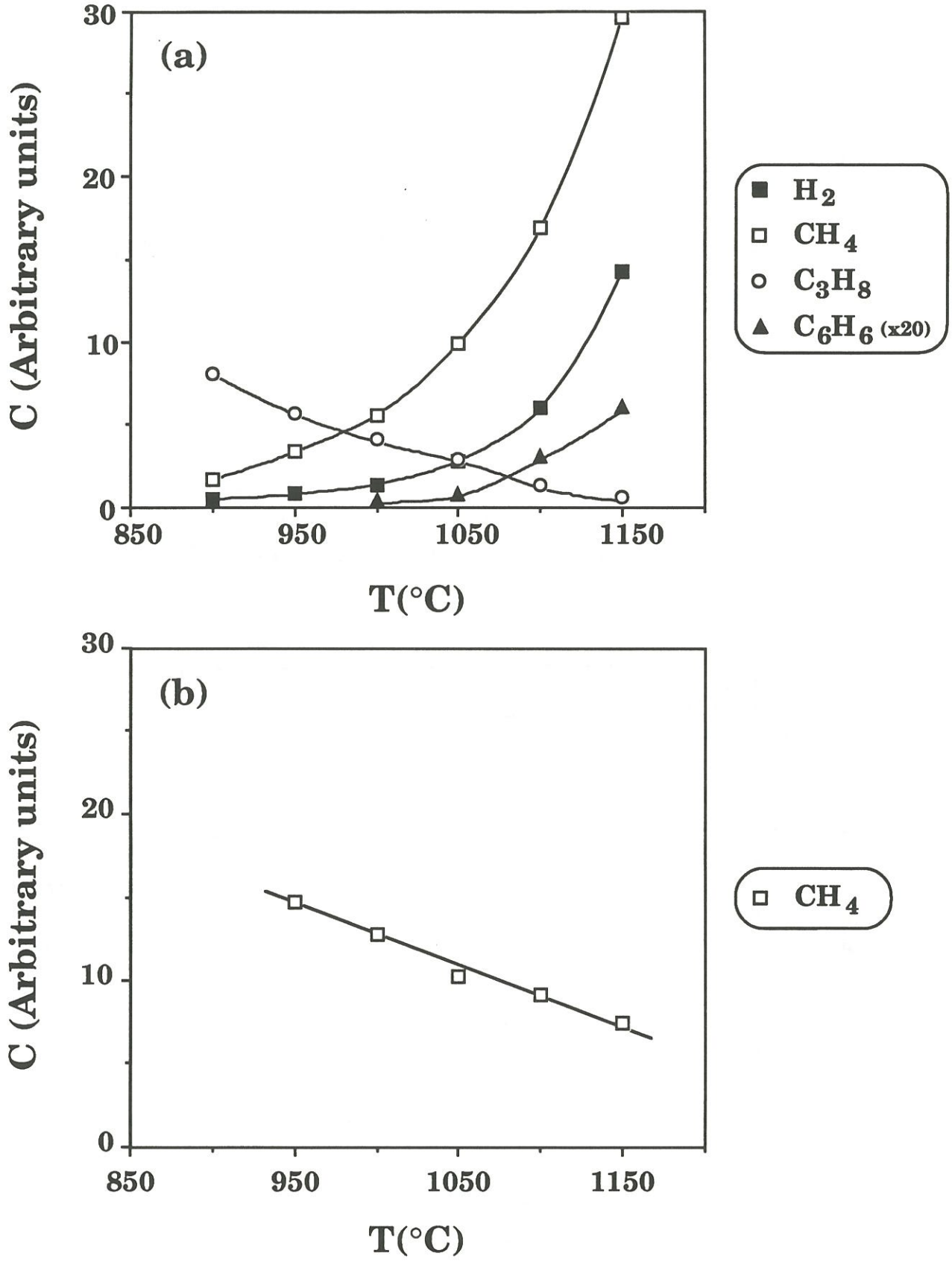

Fig. 5 : Variations of the concentrations of the various gaseous species analyzed by mass spectrometry as a function of the temperature for t_R=10 s, (a) P(C_3H_8)=3 kPa and (b) P(CH_4)=10 kPa.

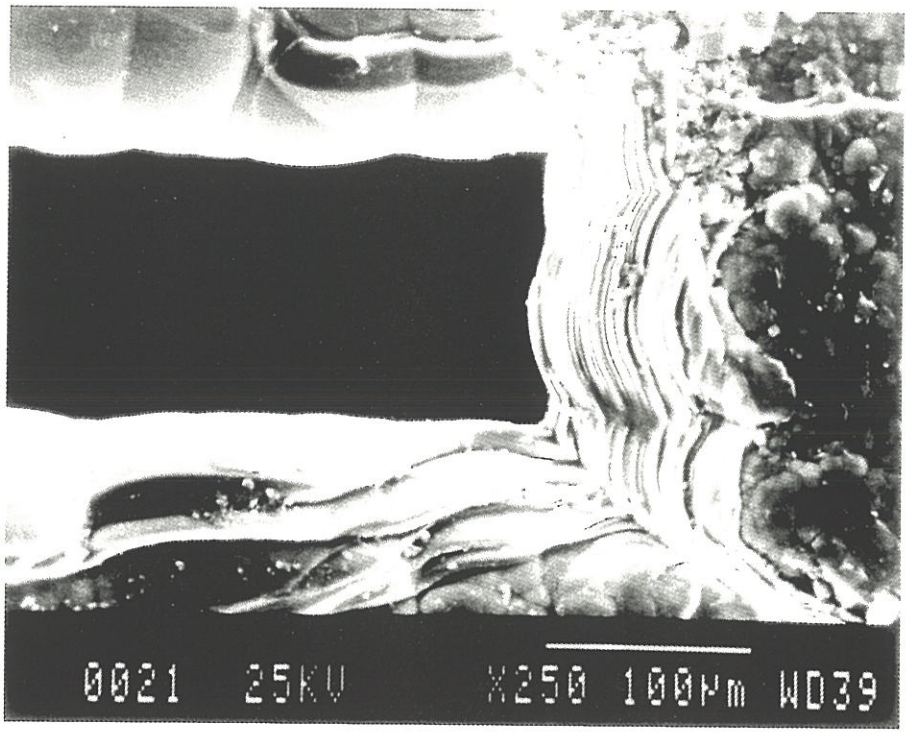

Fig. 6 : SEM. micrograph of pyrocarbon deposited at the entrance of a 320 µm model pore for T=1050°C, $P(C_3H_8)$=10 kPa and t_R=2 s.

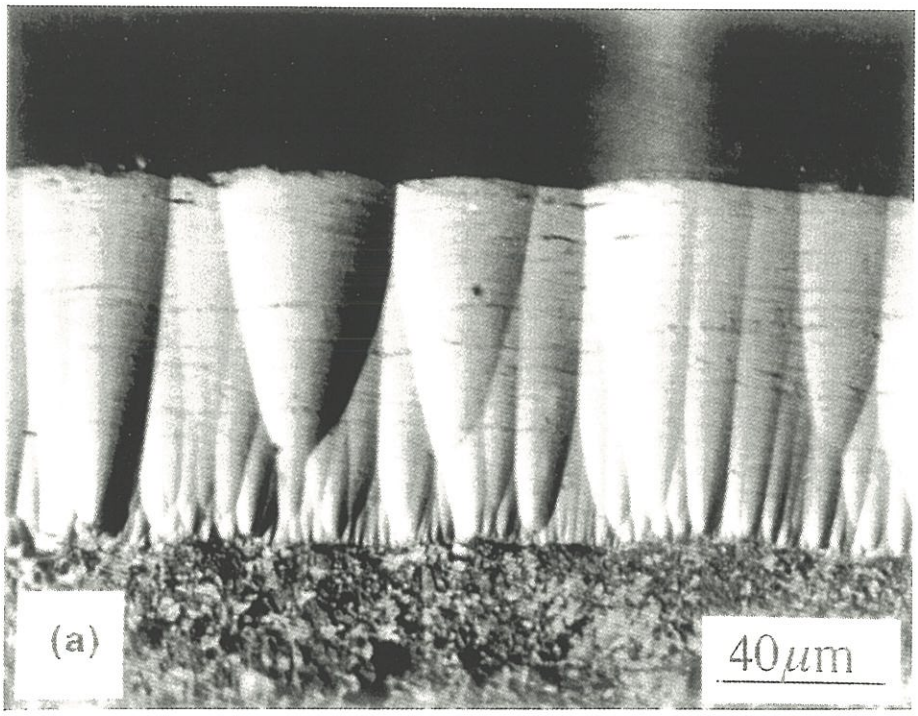

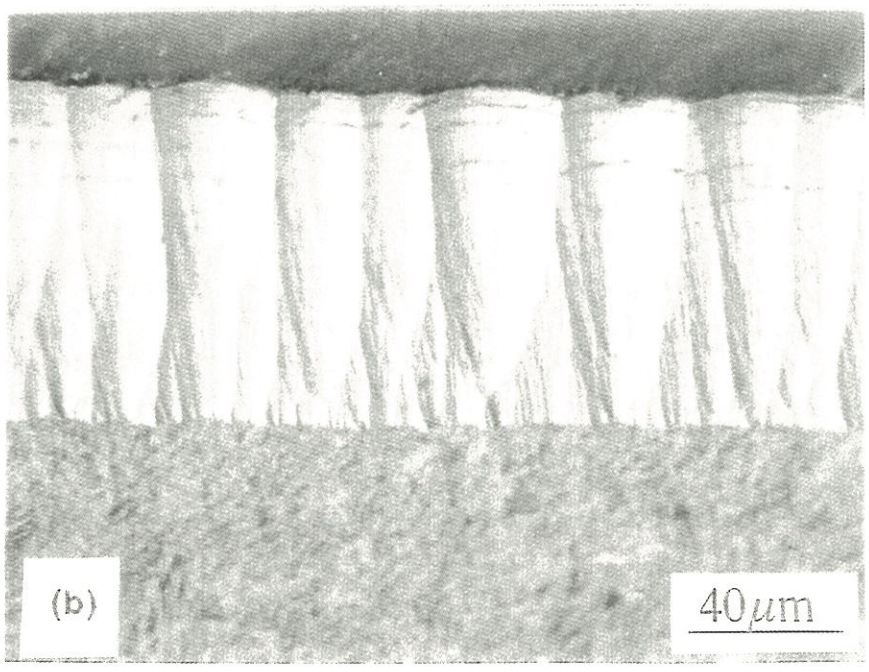

Fig. 7 : Optical micrographs (polarized light) of pyrocarbon deposited from propane for T=1050°C and (a) P=3 kPa, t_R=0.5 s and (b) P=10 kPa, t_R=2 s.

kPa, T = 1050°C and t_R = 0.5 s (fig. 7a). If the propane pressure is high enough (P ≥ 10 kPa), the nucleation frequency is much higher, giving rise to a lot of small growth cones within the pyrocarbon deposit (fig. 7b).

3.3 - Kinetics of the pusled-deposition of pyrocarbon

3.3.1 - Influence of the residence time t_R

Fig 8 shows the variations of the thickness of pyrocarbon deposited during one pulse (overall thickness divided by the pulse number) on the external surface (e_{ps}) and at the center of the pore of 320 μm (e_{p320}) and 60 μm (e_{p60}), as a function of the residence time t_R for a temperature of 1050°C and three values of the propane pressure (P = 1, P=3 and P=10 kPa). All the observed thicknesses seem to increase in a parabolic maner with t_R up to a threshold value (beyond which they are almost constant). This parabolic law is evidenced in the case of surface deposition by drawing the variations in a Ln-Ln scale (fig. 9) :

$$e_{ps} = A\, t_R^{0.5} \qquad (1)$$

where A is a constant which depends on the pressure and temperature deposition conditions. This behaviour means that, during a long enough pulse, the instantaneous deposition rate decreases continuously down to zero.

3.3.2 - Influence of the temperature

Fig. 10 shows the thermal variations of the deposit thiknesses (e_{ps}, e_{p320}, e_{p120} and e_{p60}) (Arrhenius plots) for three typical residence time values. For a

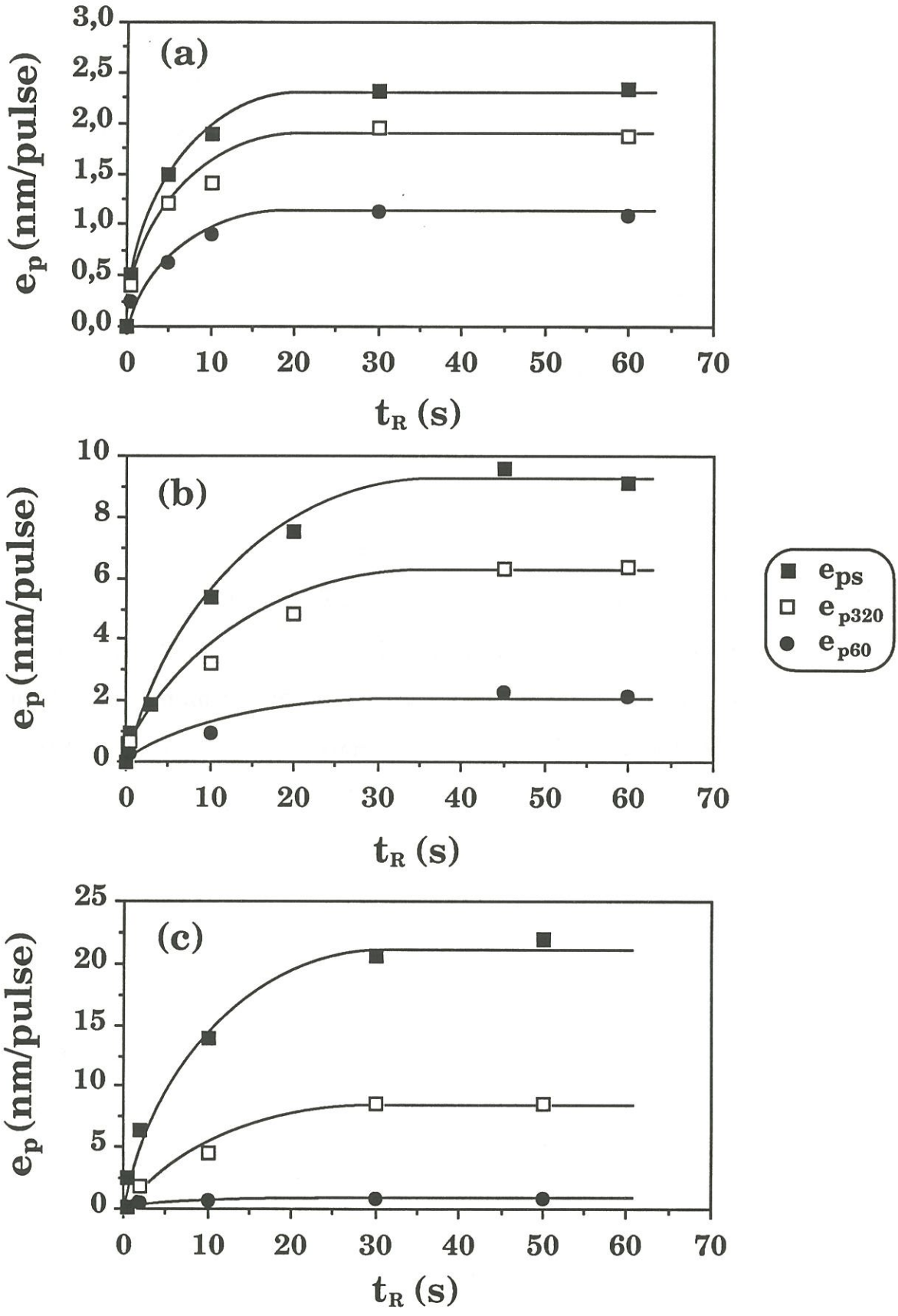

Fig. 8 : Influence of the residence time on the deposit thickness per pulse from propane on the external surface and at the center of 320 and 60 μm model pores for T=1050°C and (a) P=1 kPa, (b) P=3 kPa, (c) P=10 kPa.

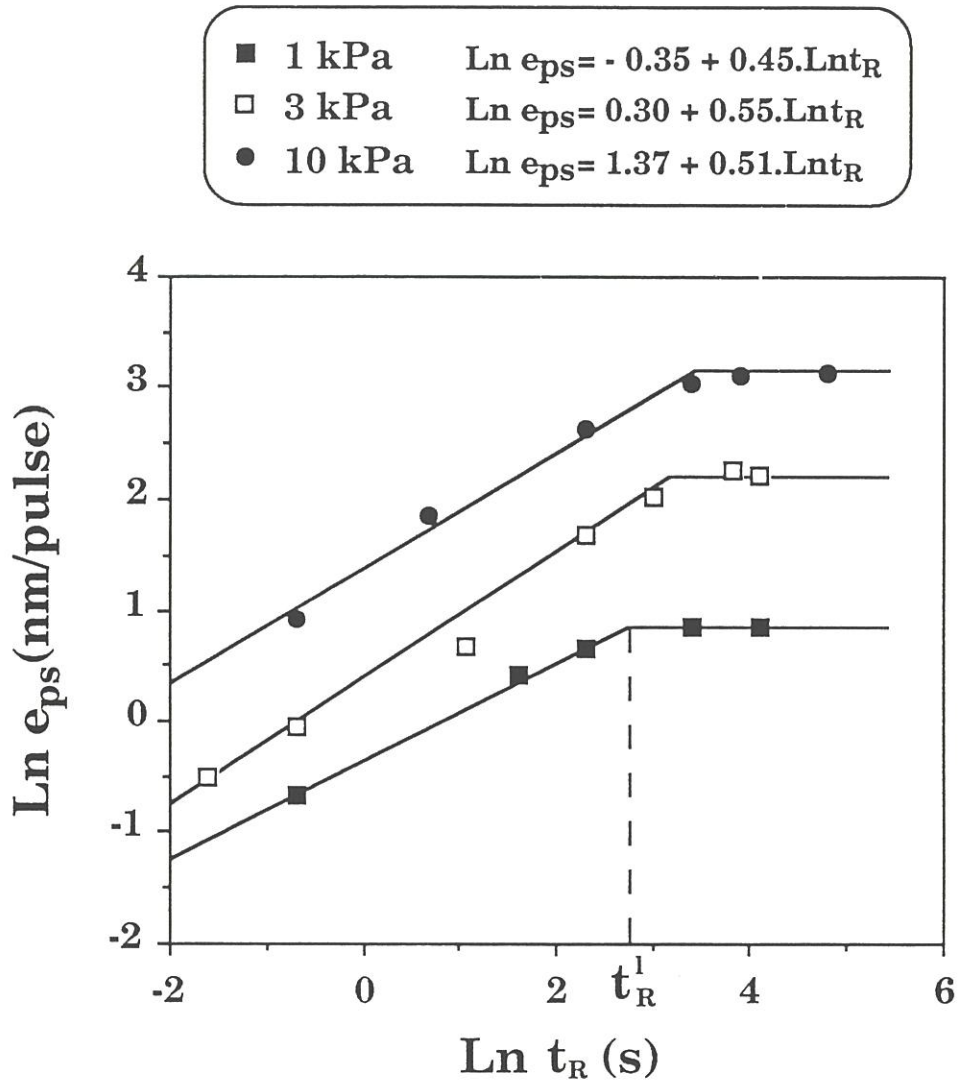

Fig. 9 : Variations of the deposit thickness per pulse on the external surface of the substrate as a function of the residence time, (Ln-Ln scale) for various total propane pressures and T=1050°C.

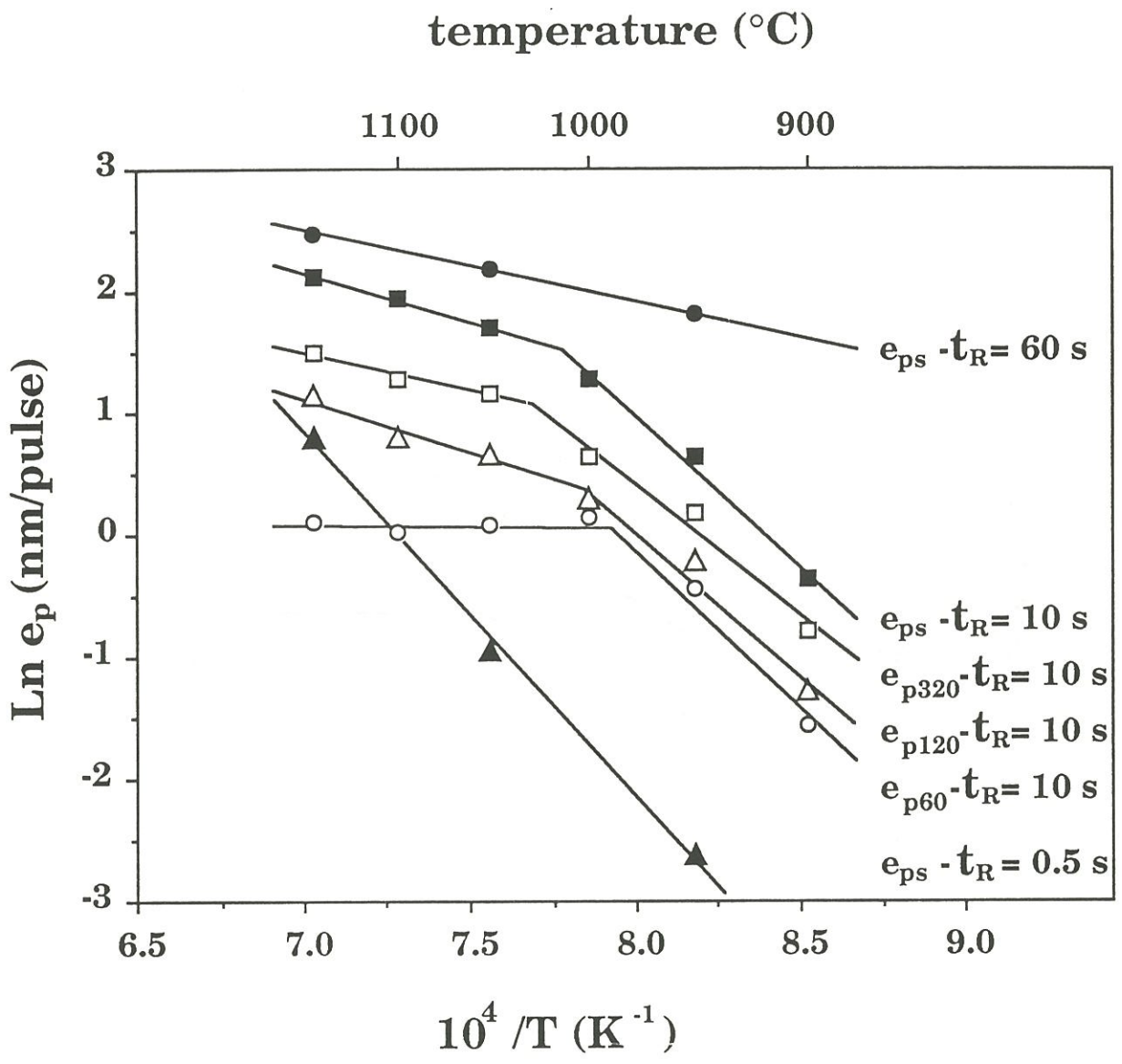

Fig. 10 : Variations of the deposit thickness per pulse on the external surface of substrate for various residence time, and at the center pores for t_R =10 s as a function of the reciprocal temperature for P(C_3H_8)=3 kPa.

short time, (t_R = 0.5 s.), i.e. when the instantaneous deposition rate is relatively high, the thickness of pyrocarbon deposited per pulse on the external surface of the substrate is highly favored by rising the temperature. For a long residence time (t_R = 60 s.), at the end of which the growth rate is nul, the thickness of pyrocarbon deposited after one pulse increases more slowly with temperature. For an intermediate time (t_R = 10 s.), two regimes are observed for both the surface or in-depth depositions : a high dependence at low temperatures and a low dependence at high temperatures, with a transition at about 1025°C. For the smallest pore (h=60 μm), the deposition at its center is not favored by increasing the temperature.

3.3.3 - Influence of the pressure

The variations versus pressure of the pyrocarbon thickness deposited per pulse at the external surface (e_{ps}) are shown in fig. 11 in a Ln-Ln scale for T = 1050°C and the three values of t_R previously given and for T = 950°C and t_R = 10 s. For all the conditions, a linear variation is observed with a slope between 0.7 and 1, which can be expressed by the following law :

$$e_{ps} = B.P^n \qquad (2)$$

with $0.7 \leq n \leq 1$ and B is a constant which depends on the temperature and residence time.

3.3.4 - Influence of the pore size

The deposit thickness per pulse at the center of the pores is reported as a function of the pore height h in fig. 12 for various conditions of propane pressure, temperature and residence time. If the thickness is found to

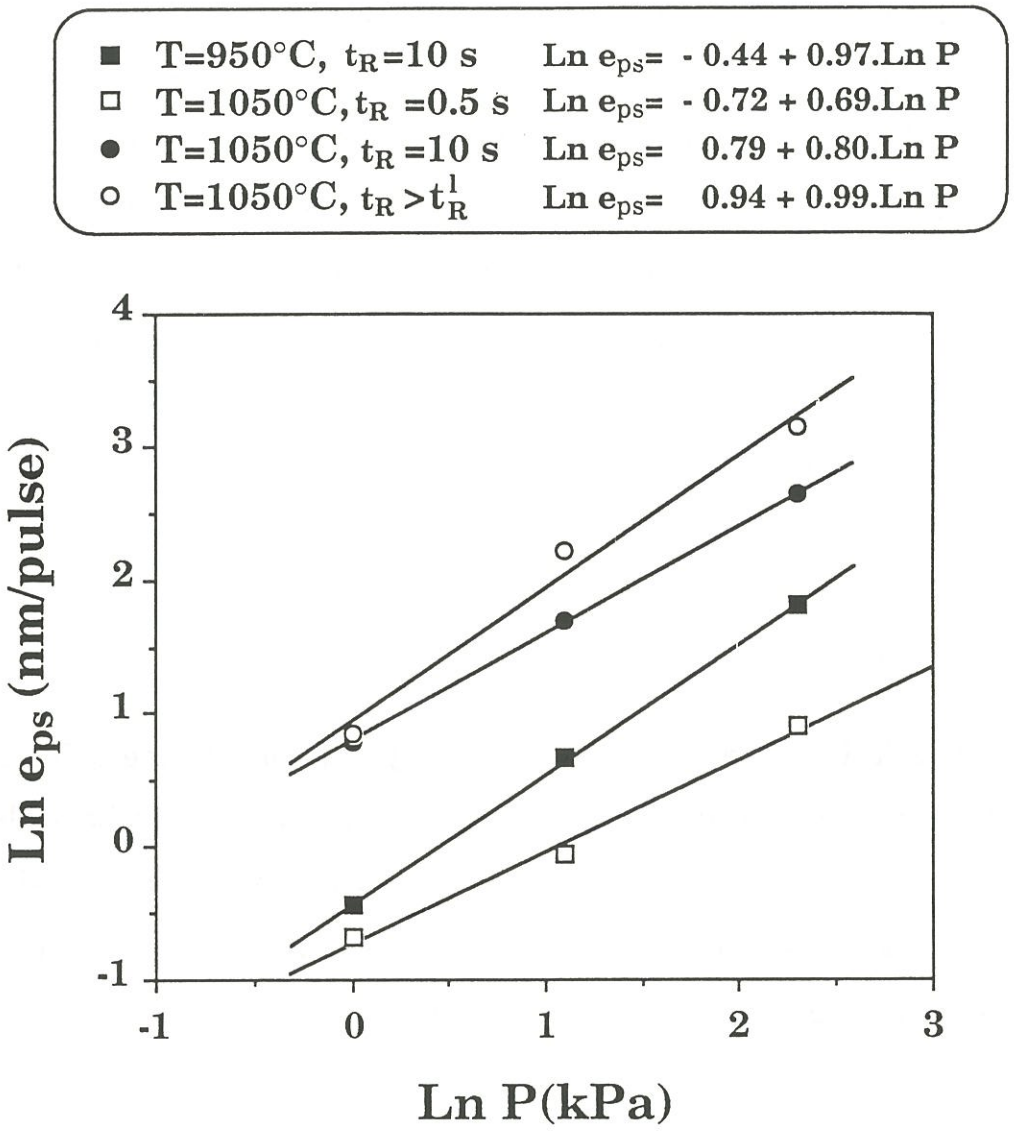

Fig. 11 : Variations of the deposit thickness per pulse on the external substrate surface as a function of propane pressure for various residence times and temperatures.

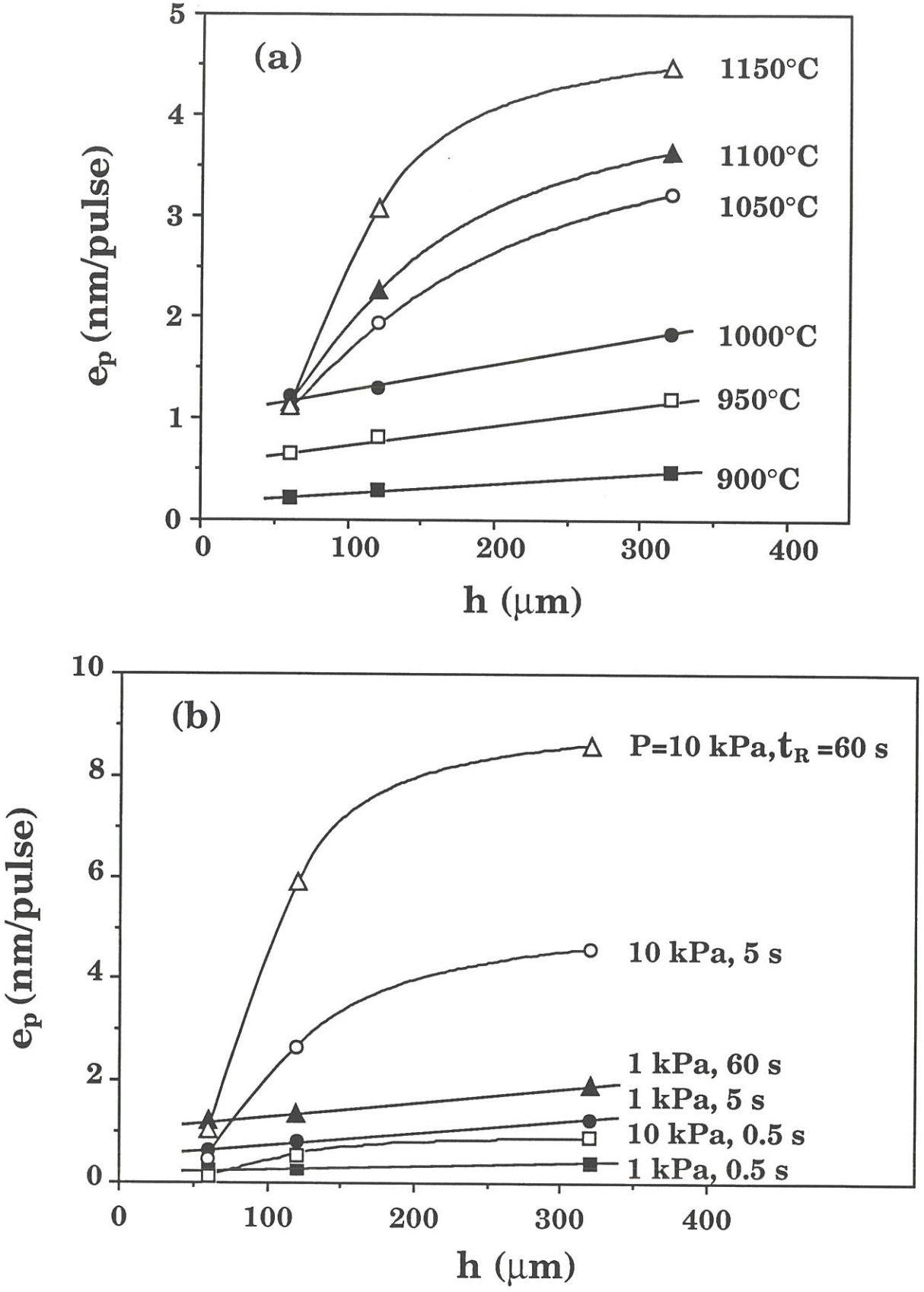

Fig. 12 : Variations of the deposit thickness per pulse from propane at the center of the pores as a function of their height (a) P=3 kPa, t_R=10 s and for various temperatures, (b) for T=1050°C, various pressures and residence times.

increase with pore height in all cases, two different behaviors are observed : (i) for low temperatures (T ≤ 1050°C) and low pressures (P ≤ 3 kPa), a linear variation occurs, while (ii) for high temperatures (T ≥ 1050°C) and high pressures (P ≥ 3 kPa), the small pores (h = 60 μm) are hardly infiltrated giving rise to a non-linear variation. An increase of the residence time increases the deposit thickness per pulse but does not affect the type of variation.

3.3.5 - Influence of the precursor

Table 1 gives a comparison of the various pyrocarbon thicknesses, e_{ps}, e_{p320} and e_{p60}, for propane and methane as source species, P = 1, 3 and 10 kPa, T = 1050°C and t_R = 10 s. The external deposit thickness e_{ps} is highly decreased (by a factor of about 10) if CH_4 replaces C_3H_8 as precursor. On the other hand, CH_4 precursor permits a much better infiltration, the thicknesses per pulse at center of the pores being close to those measured at the external surface. For P = 3 kPa and a pore of 320 μm in height, the in-depth deposit thickness is slightly higher than the surface one.

4 - DISCUSSION

In pulse-CVD/CVI, the chemical system is maintained at a constant pressure during the residence time, without any exchange with the outside, the reactor being a closed system. In such a case, the gaseous phase introduced in the reactor is changed according to a series of reactions which are well-known for methane : cracking, cycling and aromatisation, as shown by Kassel [16], Grisdale [17] or Chen and Back [18]. This "maturation" of the gas phase, which probably controls the deposition process of pyrocarbon,

P (kPa)	gas	e_{ps} (μm)	e_{p320} (μm)	e_{p60} (μm)
3	Propane	5.4	3.2	0.97
	Methane	0.4	0.46	0.30
10	Propane	14.0	4.5	0.46
	Methane	1.4	0.97	0.42

Table. 1 : Thickness of pyrocarbon deposited per pulse at the external substrate surface and at the center of the 320 and 60 μm pores for T=1050°C, t_R =10 s, P=3, 10 kPa, propane and methane as precursors.

depends on the various parameters previously studied, i.e. t_R, T, P, precursor nature and pore size for P-CVI.

4.1 - Influence of t_R, T and P

The variations of pyrocarbon thicknesses per pulse with residence time represented in fig. 8 are very similar to those reported by Sugiyama and Ohzawa for P-CVD/CVI of boron nitride on a Si_3N_4-based preform. They have also to be correlated with the variations of species concentrations (fig. 4). A parabolic increase of both the concentrations of produced species (H_2, CH_4, C_6H_6) and deposit thicknesses per pulse is observed as a function of t_R up to a threshold value t_R^1. Beyond t_R^1, no more reaction seems to occur. Nevertheless, the thermodynamic equilibrium is not achieved because if it was reached under the presently studied conditions, CH_4 should be hardly detected by gas phase analysis, being almost totally consumed to give pyrocarbon [19]. Kinetic factors such as inhibition effect by hydrogen can limit the deposition reactions which lead to the thermodynamic equilibrium. For $t_R = t_R^1$, the gas phase maturation can be considered as finished. When the temperature increases, this maturation is more and more rapid and t_R^1 decreases. t_R^1 increases slowly with the precursor pressure (corresponding to a higher amount of precursor species to be consumed) is, in partly, compensated by the increase of the source consumption rate.

4.2 - Influence of the pore size

The occurrence of two kinds of behaviors in terms of infiltration quality (see 3.3.4 and fig. 12) suggests that different mechanisms with modification of the reactional intermediates are involved in the P-CVD/CVI process. Under conditions of high pressures and high temperatures, the small pores are difficult to infiltrate whatever the residence time (fig. 12). This result means that a high extent of the gas phase maturation is rapidly reached, giving rise to **large aromatic molecules**. The diffusion of such intermediate species towards the center of the small pores is very difficult. They are rather stuck on the external surface of the substrate or at the entrance of the pores according to a process previously described [20]. Conversely, for low pressures and low temperatures, the extent of the gas phase maturation is very limited with the occurrence of only small size molecules. These species easily diffuse along the pores (even the small ones), which results in little differences between the infiltration quality of the pores with various sizes.

4.3 - Influence of the precursor

Owing to its higher thermal stability, the cracking of CH_4 is slower than that of C_3H_8, giving rise to a lower extent of the gas phase maturation for a given residence time. Consequently, (i) the thickness of the external deposits for one pulse is lower in the case of methane and (ii) the infiltration process is better, resulting from the easier diffusion of the small source species occurring in a not very maturated gas phase (table 1). In addition, a reverse infiltration gradient can be obtained for specific conditions such as T = 1050°C, P = 3 kPa and a 320 μm pore. This singular result could be explained on the basis of a

progressive maturation of the gas phase during the mass transport along the pores, the deposition from heavy aromatic species being more rapid than the deposition from light species.

5- CONCLUSION

The process of the pulse-CVD/CVI of carbon from propane can be described as successive identical cycles, each one including three main steps : (i) the inlet of the gaseous precursor by forced convection within the reactor and the pores of the substrate ; (ii) the holding of the gaseous phase at a given pressure which results partly in the deposition of pyrocarbon from small molecules, the production of mainly hydrogen and CH_4, and the diffusion of reactants and products through concentration gradients, partly in the maturation of the gas phase with formation of heavier and more dehydrogenated aromatic species easy to be stuck on the substrate surface ; (iii) the removing of the gaseous mixture from the pores of the substrate and the reactor by forced convection.

On the basis of the present study of pulse-CVD/CVI, at least two types of mechanisms, governed by the gas phase maturation, have been evidenced :
(i) mechanism I, for low pressures, low temperatures and stable precursors such as CH_4, where the gas maturation is very limited, the deposition mainly occurs by slow decomposition of small molecules resulting in a lateral growth of PyC and (ii) mechanism II, for high pressures, high temperatures and more reactive precursors such as C_3H_8, where a high maturation of the gas phase resulting in rapid condensation of heavy aromatic species stacking on the substrate surface.

Actually, according to experimental conditions (T, P, t_R) only the first mechanism or both occur during a pulse and the contribution of one of these mechanisms is probably highly dominant.

The two possible mechanisms derived from the present study of the P-CVD/CVI process result in different microstructures of pyrocarbon and different infiltration qualities. Such correlations will be the aim of the companion article (part 2).

ACKNOWLEDGEMENTS

This work has been supported by SEP. The authors are indebted to C. Robin-Brosse from SEP for valuable discussions.

REFERENCES

[1] R. Naslain, in "Introduction aux materiaux composites 2- Matrices métalliques et céramiques", (Ed. CNRS/IMC, Bordeaux, 1985).

[2] R. Naslain and F. Langlais, in "Fundamental and practical aspects of the chemical vapor infiltration of porous substrates", High Temperatures Sc, (J.W. Hastie, ed), Humana Press, Clifton, New Jersey, **27**, 221 (1990).

[3] S. Yajima, "Special heat-resisting materials from organometallic polymers", Ceramic Bull., **62**, [8], 893 (1983).

[4] J.K. Guo, Z.Q. Mao, C.D. Bao, R.H. Wang and D.S. Yan, "Carbon fiber-reinforced silicon nitride composite", J. Mater. Sc., **117**, 3611 (1982).

[5] F. Christin, R. Naslain and C. Bernard, "A thermodynamic and experimental approach of silicon carbide-CVD. Application to the CVD infiltration of porous carbon-carbon composites", in Proceedings of the 7th Internatinal Conference on CVD, (T.O. Sedgwick et al., eds, The Electrochem. Soc., Princeton, 499-514, 1979).

[6] J.Y. Rossignol, F. Langlais, R. Naslain and C. Bernard, "A tentative modelization of titanium carbide C.V.I. within the pore network of two-dimensional carbon-carbon composite preforms", in Proceedings of the 9th Internatinal Conference on CVD, (Mc.D. Robinson et al., eds, The Electrochem. Soc., Pennington, 596-614, 1984).

[7] H. Hannache, F. Langlais and R. Naslain, "Kinetics of boron carbide chemical vapor deposition and infiltration", in Proceedings of the 5th

European Conference on CVD, (J.O. Carlsson et al, eds, Uppsala, 219-233, 1985).

[8] H. Hannache, R. Naslain and C. Bernard, "Boron nitride chemical vapor infiltration of fibrous materials from BCl_3-NH_3-H_2 or BF_3-NH_3 mixtures : a thermodynamic and experimental approach", J. Less-Common Met., **95**, 221 (1983).

[9] R. Colmet, R. Naslain, P. Hagenmuller and C.Bernard, "Thermodynamic and experimental analysis of chemical vapor deposition of alumina from $AlCl_3$-H_2-CO_2 gas phase mixtures",in Proceedings of the 8th Internatinal Conference on CVD, (J.M. Blocher et al, eds, The Electrochem. Soc., Pennington , 17-31, 1981).

[10] J.Minet, F. Langlais and R. Naslain, "On the chemical vapour deposition of zirconia from ZrO_2-H_2-CO_2-Ar gas mixture II : An experimental approach", J. Less-Common Met, **132**, 273 (1987).

[11] T.M. Besmann, R.A. Lowden, D.P. Stinton and L.L. Starr, "A method for rapid chemical vapor infiltration of ceramic composites", in Proceedings of the 7th European Conference on CVD, Journal de physique, Colloque C5, Supp.5, **50**, 229 (1989).

[12] R.L. Beatty, "Gas pulse impregnation of graphite with carbon", J. Nuclear Applications&Technology., **8**, 488 (1970).

[13] K. Sugiyama and T. Nakamura, "Pulse CVI of porous carbon", J. Materials. Science. Letters, **6,** 331 (1987).

[14] K. Sugiyama and Y. Ohzawa, "Pulse chemical vapor infiltration of SiC in porous or SiC particulate preform using an r.f. heating system", J. Materials. Science, **25**, 4511 (1990).

[15] L.F. Coffin, "Structure-property relation for pyrolytic graphite", J. Amer Ceram Soc, **47**, [10], 473 (1964).

[16] L.S. Kassel, "The thermal decomposition of methane", J. Amer. Chem. Soc., 4, 3949 (1932).

[17] R.O. Grisdale, "The formation of black carbon", J. Applied Physics, **24**, [9], 1082 (1953).

[18] C.J. Chen and M.H. Back, "The simultaneous measurement of the rate of formation of carbon and hydrocarbon products in the pyrolysis of methane", Carbon, **17**, 175 (1979).

[19] H. Mellottée, "Contribution à l'étude théorique et expérimentale de la pyrolyse des oléfines légères", Thèse de l'Université de Paris (1968).

[20] J.L. Kaae, "The mecanism of the deposition of pyrolytic carbon", Carbon, **23** [6] 665 (1985).

Chapître 3 : PULSE CHEMICAL VAPOR DEPOSITION (P-CVD) AND INFILTRATION (P-CVI) OF PYROCARBON IN MODEL PORES WITH RECTANGULAR CROSS SECTIONS : PART 2 - STUDY OF INFILTRATION

Aprés l'étude des mécanismes de dépôt du second chapitre, cette troisième partie expose les résultats de **l'infiltration des pores modèles** en fonction des paramètres de P-CVI (P, T, t_R) et de la nature du gaz. Les essais ont été menés dans les mêmes conditions que ceux réalisés en I-CVI. La **qualité de l'infiltration** d'un pore est exprimée par un pourcentage de remplissage calculé à partir du profil de dépôt le long de l'axe longitudinal du pore. Le rôle de la taille du pore est important. La qualité d'infiltration optimale est fonction non seulement des conditions de P-CVI mais aussi de la taille du pore. En général, une durée de palier intermédiaire (de l'ordre de 10 s) apparaît être très défavorable à la qualité de l'infiltration.

La qualité de l'infiltration a pu être reliée de façon simple à la **maturation de la phase gazeuse**, et par la même aux processus de dépôt.

L'optimisation des conditions d'infiltration en P-CVI permet d'obtenir une infiltration identique voire légèrement meilleure qu'en I-CVI, mais avec des **vitesses de dépôts deux fois plus élevée**. Ce résultat en faveur de la P-CVI ne doit pas cependant faire oublier qu'en P-CVI la durée du palier est fonction de la durée de pompage qui, si elle est courte dans un four de petit volume, serait beaucoup plus importante pour un four industriel.

Ce chapitre présente les résultats de cette étude sous forme d'un projet de publication adressée au Journal of Material Science.

Submitted to Journal of Materials Science.

PULSE CHEMICAL VAPOR DEPOSITION (P-CVD) AND INFILTRATION (P-CVI) OF PYROCARBON IN MODEL WITH RECTANGULAR CROSS-SECTIONS : PART 2 - STUDY OF THE INFILTRATION

P. Dupel, R. Pailler, X. Bourrat and R. Naslain

Laboratoire des Composites Thermostructuraux

(UMR 47 CNRS-SEP-UB1), Domaine Universitaire,

3 allée de La Boëtie, 33600 Pessac, France.

ABSTRACT

Model straight pores with rectangular cross-section (size ranging from 60 to 320 μm) have been infiltrated with pyrocarbon resulting from the cracking of C_3H_8 or CH_4 under pulse CVI-conditions. Three main parameters control the quality of the pore infiltration : temperature and pressure, as previously known for regular I-CVI, and, additionally, residence time, t_R, which appears to be the key parameter in P-CVI. There is a direct correlation between t_R, on the one hand, and both the PyC-thickness gradient and anisotropy along the pores, on the other hand. The experimental results are explained on the basis of a qualitative model assuming two competiting deposition mechanisms depending on whether PyC is formed from small and H-rich molecules (akin to C_3H_8) (low t_R values) or from large aromatic H-poor intermediates resulting from the maturation of the gas phase (high t_R values). The use of CH_4 (more

stable thermally than C_3H_8) shows down the maturation process and favors in-depth infiltration. The best infiltrations, similar to and even better than those reported for I-CVI, are achieved under low t_R, T, P conditions but require very large number of pulses.

P-CVI is an efficient way to control the control the microstructure of the deposit.

KEY WORDS :

Pyrocarbon, pulse CVD/CVI, model pores, microstructure, propane, methane.

1- INTRODUCTION

Chemical vapor infiltraton (CVI), when performed under isothermal/isobaric conditions (I-CVI), has been shown a processing technique well suited to the fabrication of ceramic matrix composites (CMC) particularly when the matrix is a non-oxide material (e.g. carbon, carbides, nitrides) [1-5]. One of its important advantages, from a practical point of view, is its ability to be used for the simultaneous treatment of a large number of fiber preforms even of different sizes and shapes. Conversely, I-CVI is known to exhibit some drawbacks : (i) it requires relatively long processing times and some crust removal and (ii) it yields CMC with a residual porosity of 10-15%.

Attempts have been made to reduce the processing time by applying to the fiber preform pressure/temperature gradients, replacing thus the slow diffusion mass transfer in the pore network by forced-convection mass transfer and increasing the in-depth deposition rate of the matrix by an increase of the temperature. However, the corresponding F-CVI (with F for forced) exhibit strong limitations on preform tooling, on the one hand, and the size and number of preforms, on the other hand [3,6].

Another attractive alternative could be the use of **pulse-CVI** (P-CVI) in which the porous fiber preform is submitted, at a high frequency, to cycles comprising : (i) the injection of the feed gas in the preform by forced convection in a very short time, (ii) holding the feed gas in the preform during a time long enough to permit the deposition of the matrix with a high growth rate but short enough to avoid the poisoning effect of the reaction gaseous products and (iii) vacuuming out the residual gas phase [7-10]. P-CVI is expected to exhibit the following advantages : (i) it may reduce (and even suppress) the deposit density

gradient in the preform and (ii) it may yield high deposition rates, while keeping the main advantage of I-CVI, i.e. its suitability to the simultaneous treatment of a large number of different preforms. Conversely, P-CVI introduces new constraints such as the difficulty related to the fitting and evacuation of large furnaces in very short times.

Generally speaking, P-CVI and particularly that of pyrocarbon has not been extensively studied yet, both from an experimental and theoretical points of view and its suitability to the processing of CMC has still to be established. The aim of present contribution, which is the second part of a series of articles devoted to P-CVD/P-CVI [11,12], was to demonstrate experimentally the interest and limitation of this new processing technique focusing on pyrocarbon and model pore infiltration, on the one hand, and the influence of various parameters (temperature, pressure, residence time, precursor nature, pore aspect ratio), on the other hand, on the infiltration efficiency.

2- EXPERIMENTAL

The P-CVD/P-CVI experiments have been performed with an apparatus and a procedure which have been described in Part 1 [11]. It will be sufficient to recall here that : (i) **pyrocarbon** (PyC) is deposited (or infiltrated) as the result of the cracking of a hydrocarbon (the precursor) which is either **propane** (C_3H_8) or **methane** (CH_4), the former being more reactive than the latter, under the following conditions : $900 < T < 1150°C$; $1 < P < 1000$ kPa ; $0.5 < t_R < 100$ s, t_R being the residence time of the gas in the furnace) and (ii) the substrate consists of a block of purified graphite made of two bolted parts with three straight pores of rectangular cross-sections at the interface. The pores have the

same length (L = 20 mm) and their cross-sections are characterized by the same width (l = 2 mm) but exhibit different heights (namely, 60 ; 120 and 320 μm).

After each deposition/infiltration experiment, the two-parts graphite block is unbolted and the grooved half part cut with a diamond saw along each of the model pores axes. The longitudinal sections are then polished with diamond pastes of decreasing grain sizes (down to 1 μm) and observed with an optical microscope (1). Two kinds of measurements were systematically performed for each longitudinal section : (i) the **thickness** of the PyC-deposit along the z-axis, of the pore (the origin of the z-coordinate being the pore entrance) and (ii) the **extinction angle** Ae used as a representative parameter of the anisotropy of the PyC-microstructure, as discussed with more details elsewhere [12].

The quality of the pore infiltration will be characterized, in the following, by the **thickness profile** along the pore longitudinal z-axis and by the degree of filling of the pore, referred to as **filling ratio** δ_i, calculated by integrating the thickness profile along the pore length and dividing the result by half the initial pore volume.

3- RESULTS

3.1- Thickness profiles and filling ratios

In order to shorten the duration of the experimental study (which consisted of a large number of experiments owing to the number of parameters

(1) MeF3 from REICHERT-JUNG

taken into account), each deposition/infiltration run has been limited to a maximum duration of 200 hr. As a result, under the experimental conditions specified in section 2, it has not been possible to fill totally the two larger pores (which h=120 and 320 μm, respectively). The duration of each run was calculated so that the smaller pore (h = 60 μm) was systematically plugged by the PyC-deposit at its entrance, at the end of the experiment. For the 120 and 360 μm pores, whose filling was not always complete, a constant deposition rate vs time was assumed, in order to calculate the filling ratio value at pore entrance plugging, by extrapolation.

3.2- Influence of the residence time

The **thickness profiles**, measured along the z-axis of the 60 μm pore after pore entrance blocking, are shown in fig. 1a for T = 1050°C, P = 1 kPa and three values of the residence time t_R (t_R being the main part of a pulse duration, as explained in part 1 [11]). The thickness gradient along the pore is minimized at very low (i.e. t_R = 0.5 s) or very large (t_R = 60 s) residence time values.

The **filling ratios δ_i** (with i standing for the size of the pore, respectively 60 ; 120 and 320 μm) are derived from the thickness profiles, as said in section 2. The variations of δ_{60} as a function of t_R are shown in fig. 1b. First, the corresponding curve goes through a rather deep minimum for intermediate residence time values (i.e. t_R = 5 s) and, second, it shows that the **highest filling of the pore** is achieved for the **lowest values of the gas residence time** (δ_{60} = 60% for t_R = 0.5 s).

The variations of the filling ratios δ_i (with i = 60 ; 120 and 320) as a function of the residence time, are shown in fig. 2, for three different values of

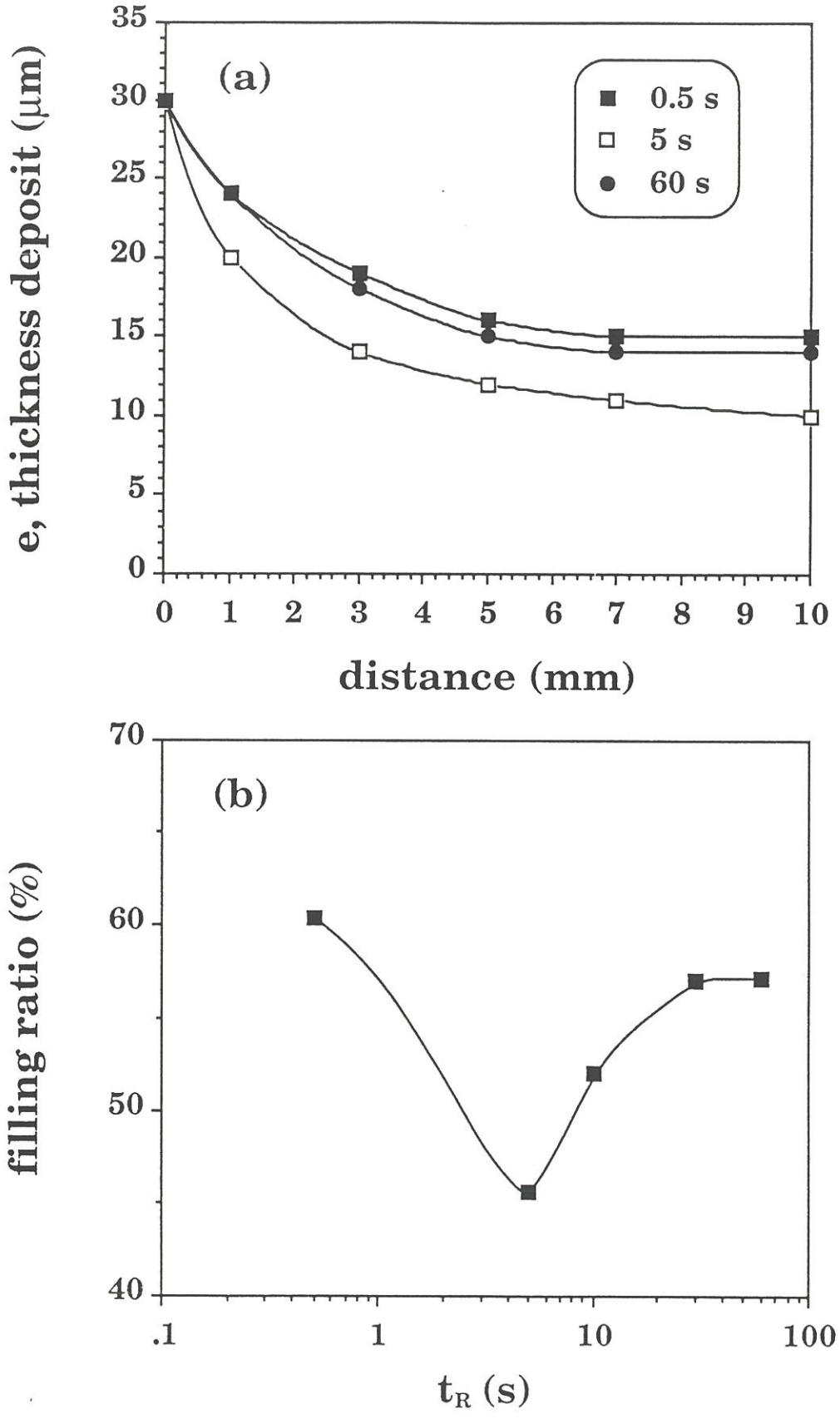

Fig. 1 : PyC-infiltration along the 60 μm model pore for T=1050°C and P=1 kPa : (a) thickness profiles for different t_R values (b) variations of the filling ratio as a function of t_R .

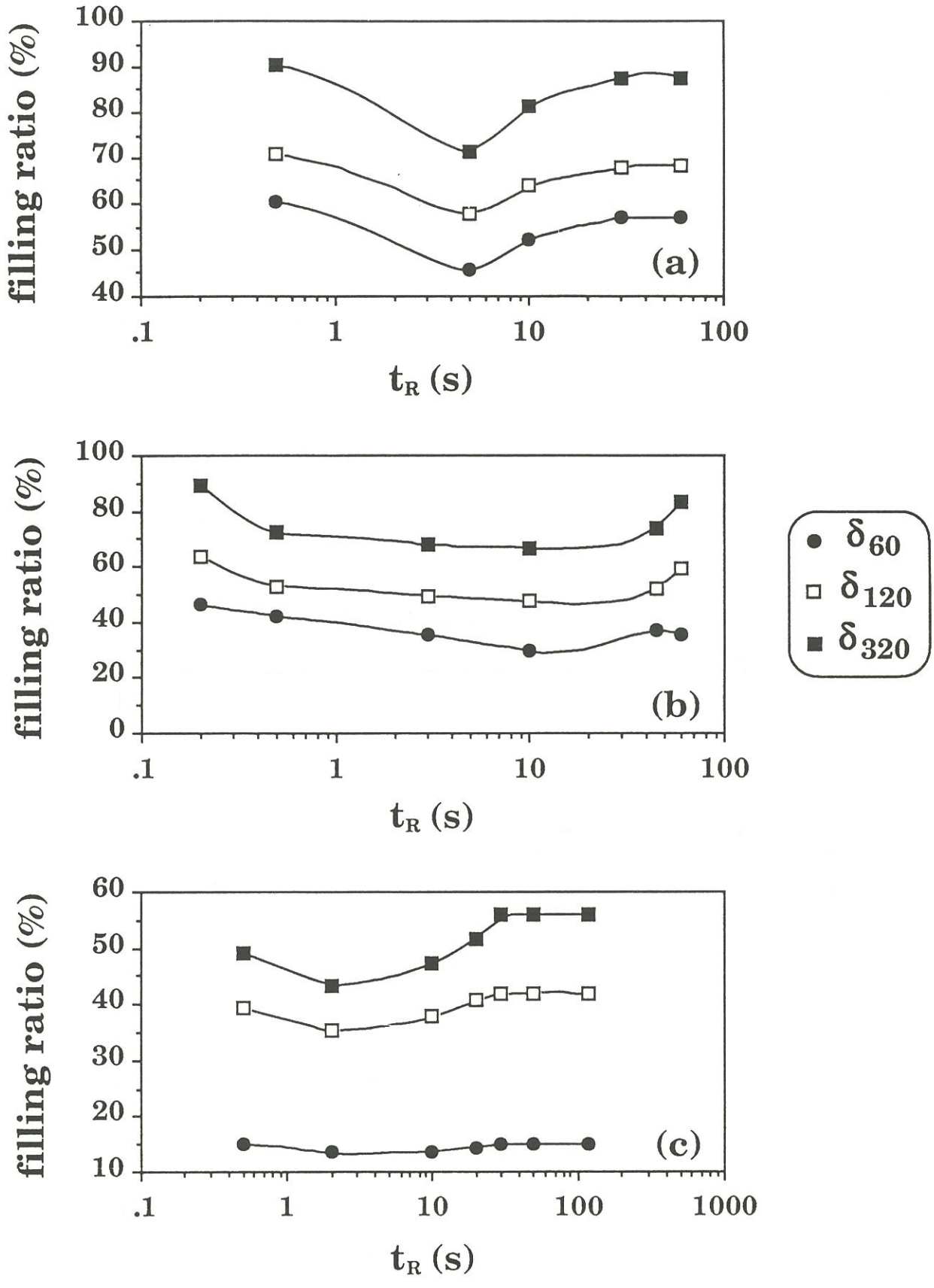

Fig. 2 : Variations of the filling ratio of the three model pores as a function of residence time for T=1050°C and : (a) P=1 kPa, (b) P=3 kPa, (c) P=10 kPa.

the pressure. All the corresponding curves exhibit a minimum and a plateau (for long residence times), which are more or less pronounced depending on the experimental conditions. The value of t_R corresponding to the minimum (see fig. 2a) seems independent of the pore size but changes slightly as pressure is increased.

3.3- Influence of the temperature

The thickness profiles along the 60 μm pore, at pore entrance blocking, are shown in fig. 3a for different temperature values (with $900 < T < 1150°C$) together with the corresponding thermal variations of the filling ratio δ_{60} (fig. 3b). It appears that the PyC-thickness gradient along the pore is reduced for medium temperatures (950-1000°C).

The thermal variations of the filling ratio δ_i exhibit a maximum with the following features : (i) it is well defined for the small size pores (60 and 120 μm), (ii) it is slightly shifted towards the low temperatures and seems to vanish, as the pore size is increased and (iii) the maximum pore filling decreases (roughly from 80% to 50%) as the pore size decreases from 320 to 60 μm, an already well known feature for the I-CVI of model pores [1,2]. Finally, beyond about 1050°C, the values of the filling ratios do not change any longer as temperature is raised, whatever the pore size.

In short, this part of the study emphasizes the interest of performing the P-CVI at medium or low temperatures in order to achieve a high degree of pore-filling by PyC.

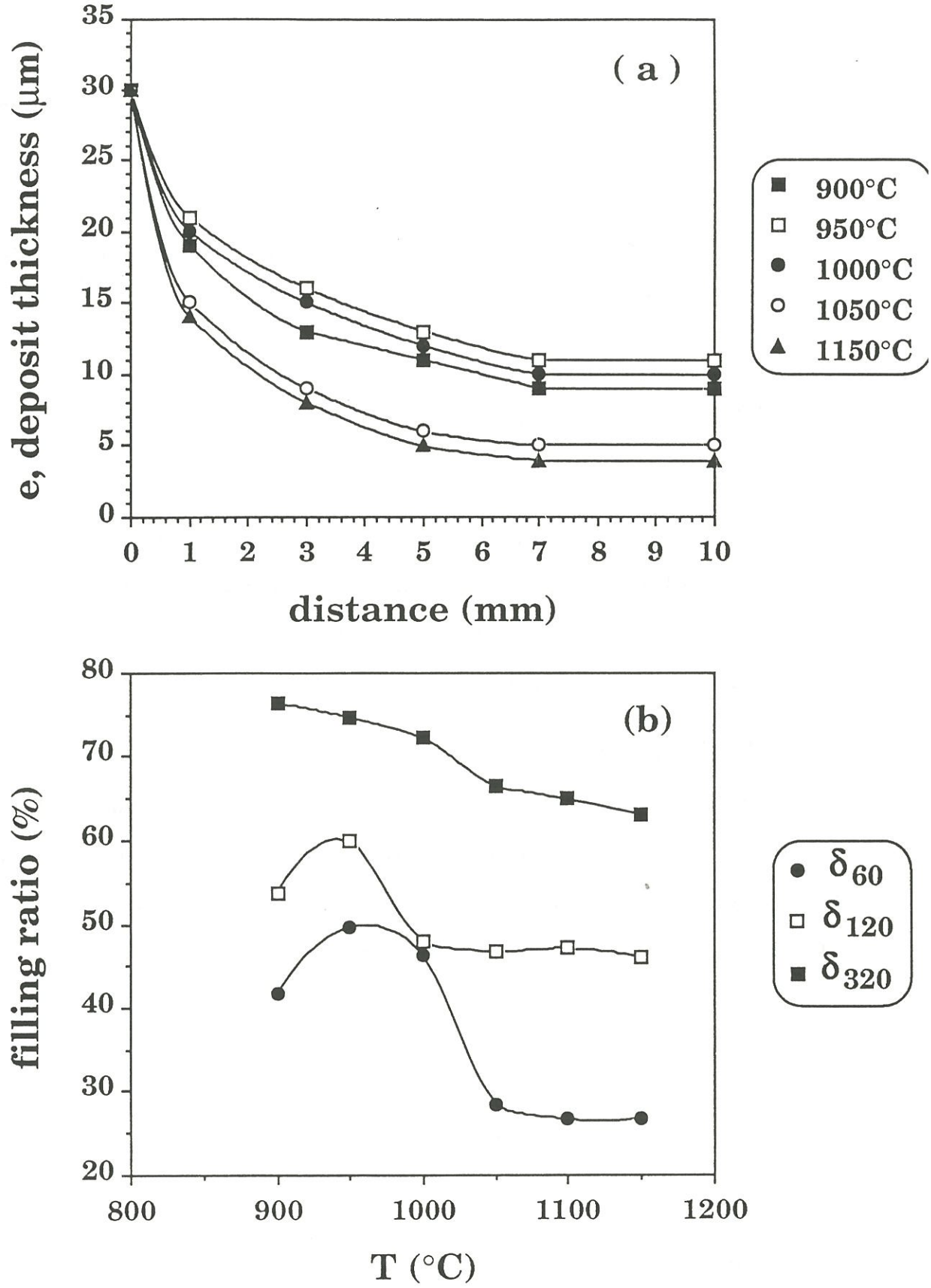

Fig. 3 : PyC-infiltration along the model pores as a function of the temperature for P=3 kPa and t_R =10 s : (a) thickness profiles along the 60 μm-model pore at pore entrance blocking and (b) filling ratio for the three model pores calculated at pore entrance bloking.

3.4- Influence of the pressure

The influence of the propane pressure on the PyC-thickness profile along the 60 μm pore axis (at pore entrance blocking) is shown in fig. 4 for two values of the temperature (950 and 1050°C) and t_R = 10 s.

Generally speaking and as already known for I-CVI [1,2], decreasing the pressure in the infiltration chamber strongly reduces the thickness gradient along the pore (at least under these temperature-residence time conditions).

The corresponding variations of the filling ratio δ_{60} as a function of the pressure of propane are shown in fig. 5 in a Ln-Ln scale. Within the whole pressure range studied here (extending from pressures as low as 1 kPa to pressures as high as 100 kPa), the curves are observed to be linear. As a result, the variations of δ_{60} as a function of the pressure of propane obey the following equation :

$$\delta_{60,\,T,P} = \overset{\circ}{\delta}_{60,T,1}\ P_{C_3H_8}^{-0.56} \qquad \text{with } \overset{\circ}{\delta}_{60,T,1} = \delta_{60,T} \text{ for P=1 kPa} \qquad (1)$$

Thus, decreasing the pressure of propane in the infiltration chamber in the P-CVI of PyC, significally improves the quality of the pore-infiltration (as already reported for I-CVI), very low pressures (1 kPa or less) being apparently necessary to achieve an almost complete filling of the pores of this size.

3.5- Influence of the nature of the gas precursor

The influence of the nature of the source species (propane and methane) on the thickness profile (at pore entrance blocking) is shown in fig. 6, for the 60 μm pore, T = 1050°C, t_R = 10 s and two pressure values. Under such conditions,

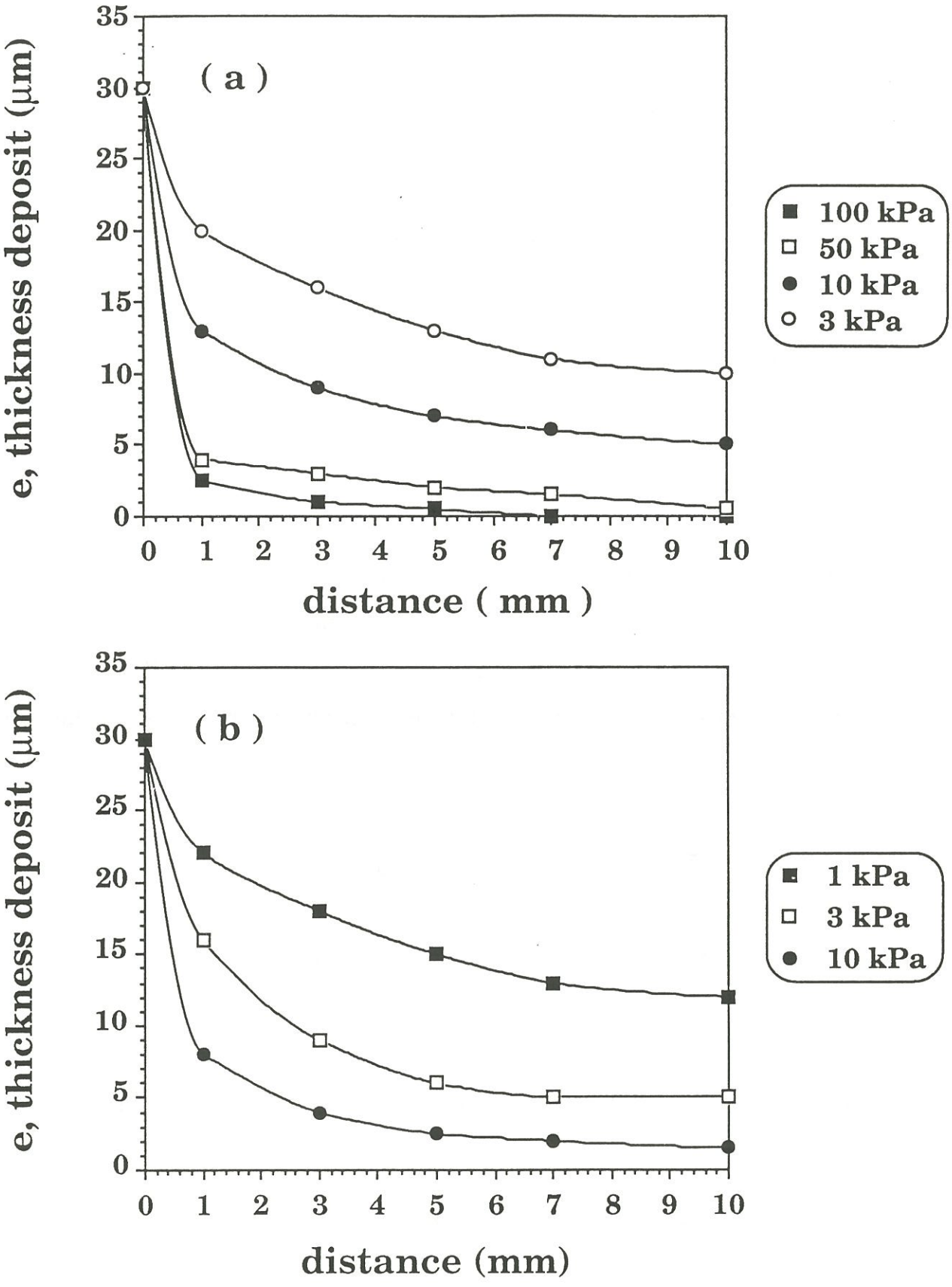

Fig. 4 : PyC-thickness profiles along the 60 µm-model pore (at pore entrance blocking) as a function of the total propane pressure and for t_R =10 s : (a) T= 950°C, (b) T= 1050°C.

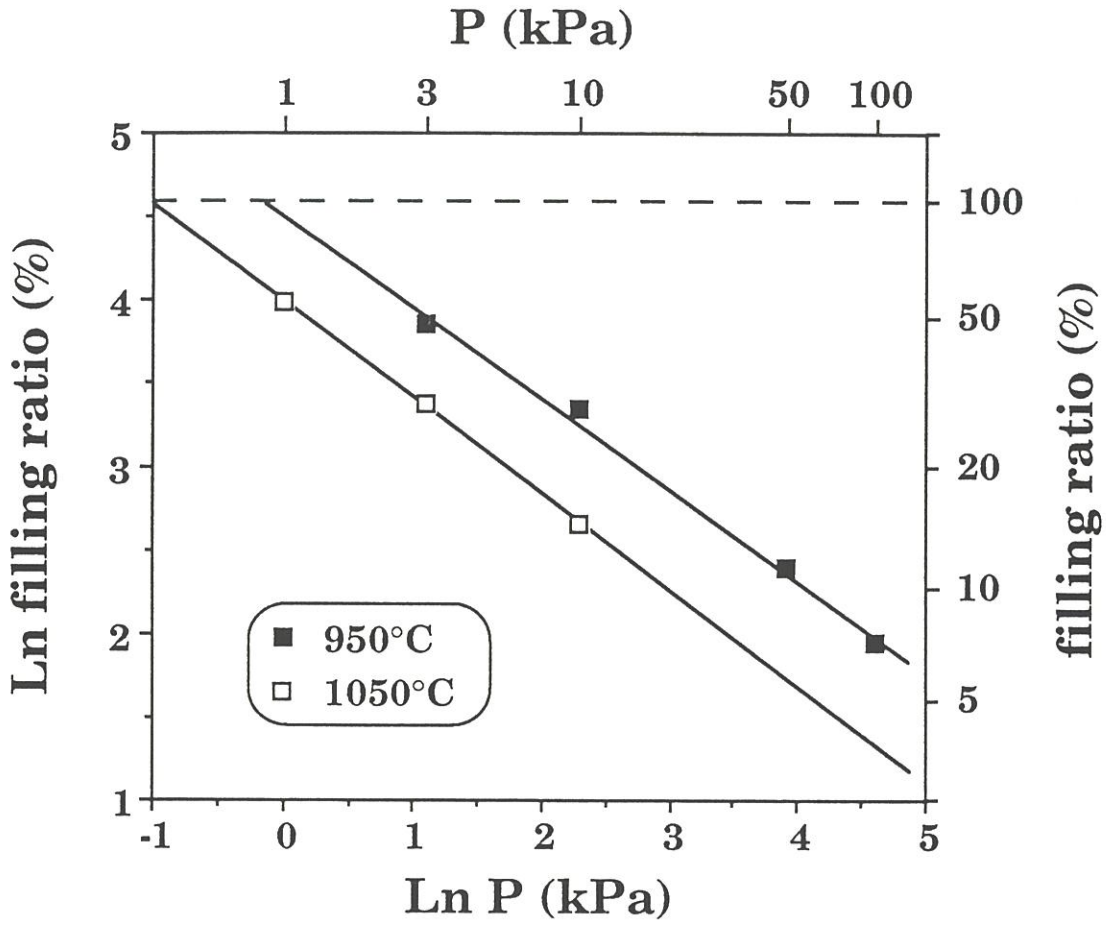

Fig 5 : Variations of the filling ratio of the 60 μm-model pore (at pore entrance blocking) with the total pressure of propane, plotted in an Ln/Ln scale for two temperatures and t_R =10 s.

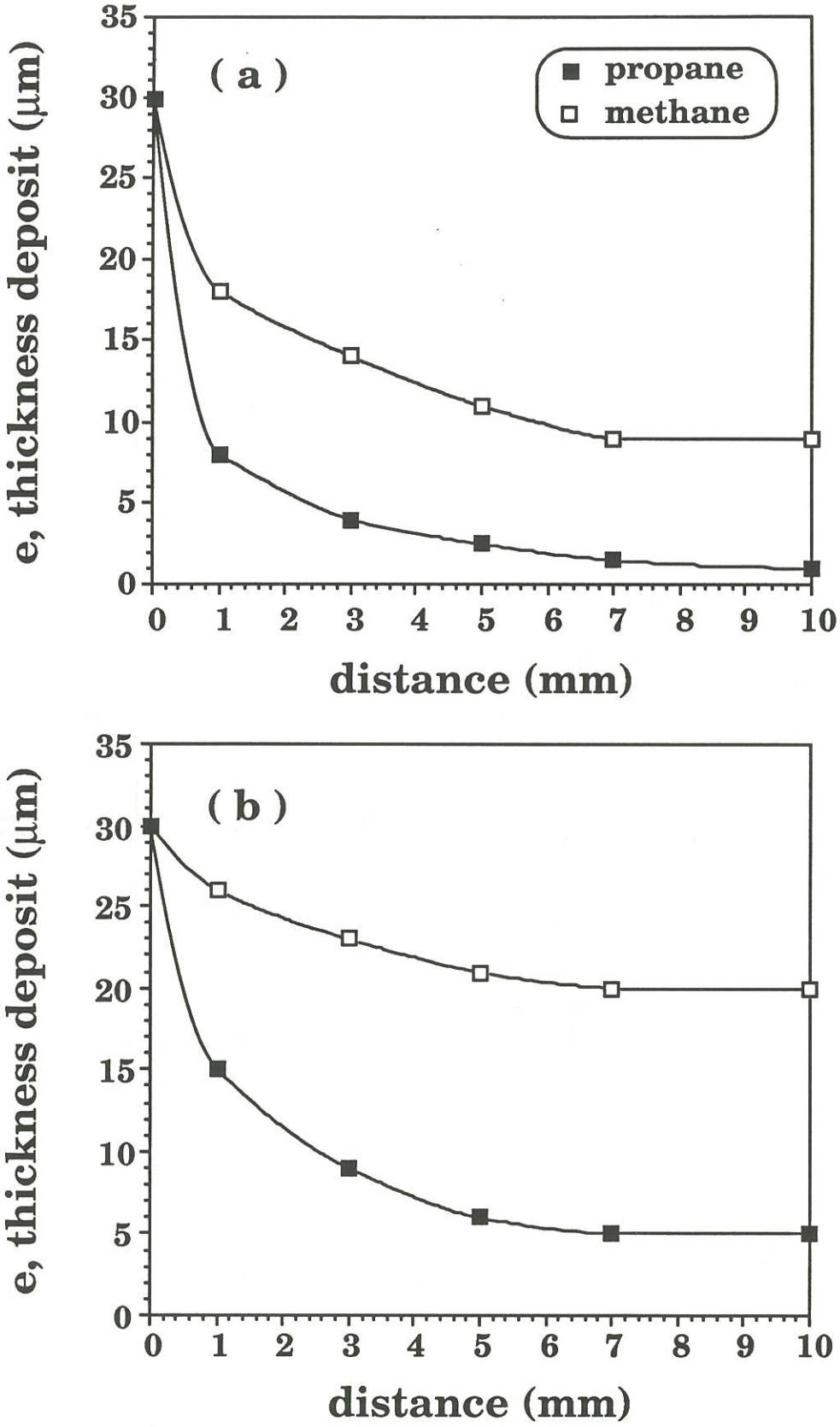

Fig. 6 : Variations of the PyC-thickness profiles along the 60 μm model pore (at pore entrance blocking) with the nature of the gas precursor for T=1050°C and t_R =10 s : (a) P=10 kPa and (b) P=3 kPa.

the quality of the infiltration is **better with methane** whatever the pressure of the hydrocarbon in the infiltration chamber. The improvement in the PyC-thickness profile along the pore, observed when propane is replaced by methane, is more pronounced at low pressures (e.g. 3 kPa) than at high pressures (10 kPa).

Furthermore, the δ_{60} ratio observed for methane is much higher than for propane, their relative value remaining almost unchanged as pressure is lowered : $\delta_{60}(CH_4)/\delta_{60}(C_3H_8) = 2.9$ for P = 10 kPa vs $\delta_{60}(CH_4)/\delta_{60}(C_3H_8) = 2.6$ for P = 3 kPa.

3.6- Influence of the infiltration duration

The influence of the infiltration duration (calculated as the product of the pulse duration by the number of pulses) on the PyC-thickness profile along the 120 μm pore, is shown in fig. 7 together with that (for purpose of comparison) corresponding to I-CVI, both performed under close experimental conditions in the same hot-wall apparatus.

For P-CVI, the data show that the thickness of the PyC-deposit at a given z-abscissa along the pore varies in a linear manner as a function of the infiltration duration. As a consequence, the variations of the related δ_{120} filling ratio as a function of time obey a similar linear law, as shown in fig. 8. This is no longer the case for I-CVI, at least for experimental conditions which have been used in present work. It appears from a comparison of the curves that : (i) the infiltration rate is higher for P-CVI than for I-CVI (the blocking of the pore being achieved for t = 22 hr for the former and only for t = 72 hr, for the latter) and (ii) the filling ratio at pore blocking is higher for I-CVI. One could argue

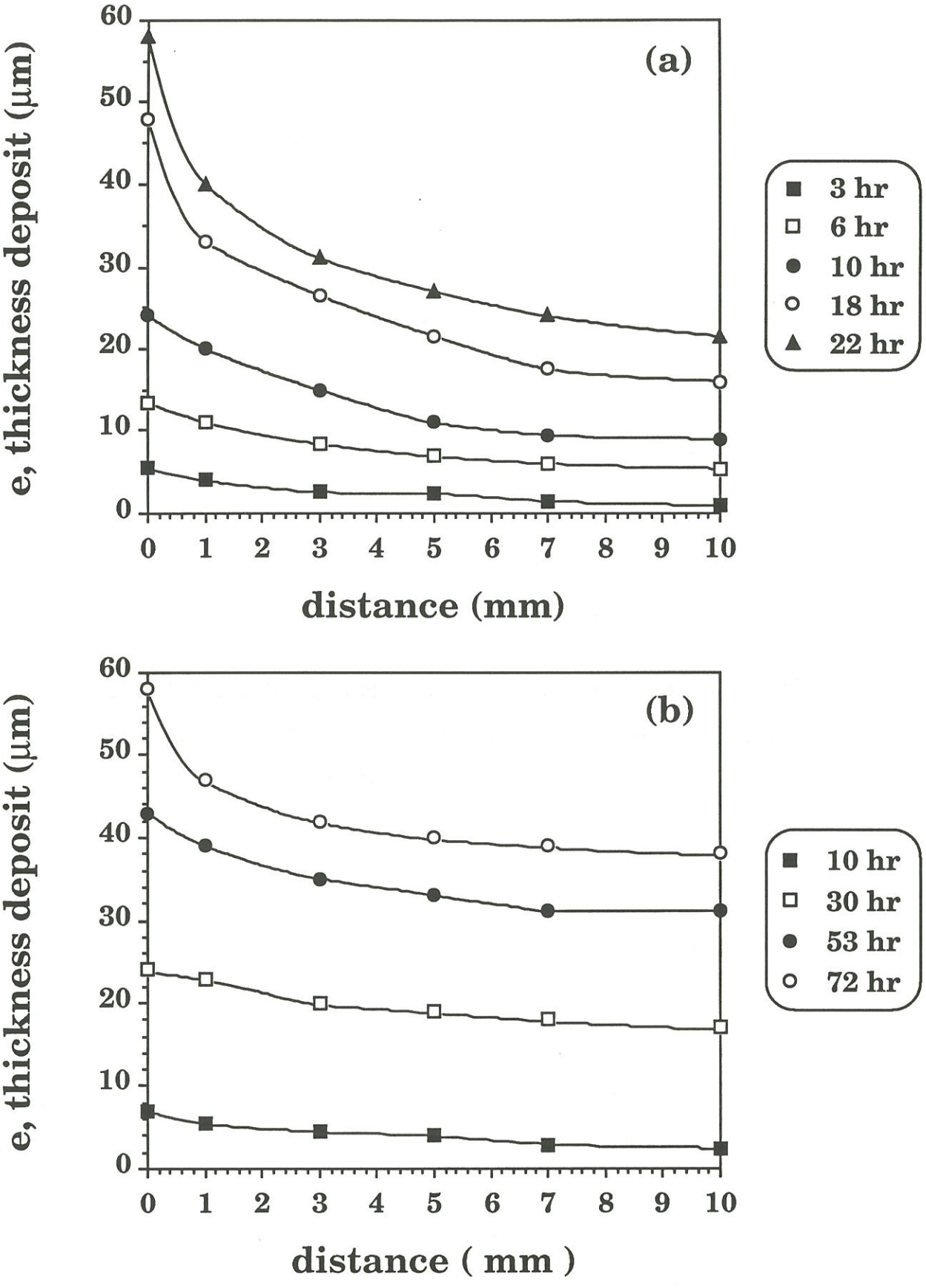

Fig. 7 : Variations of PyC-thickness profiles along the 120 µm-model pore as a function of infiltration total duration : (a) P-CVI; T=1150°C; P=3 kPa; t_R=10 s and (b) I-CVI; T=1050°C; P=3 kPa; Q=60 sccm.

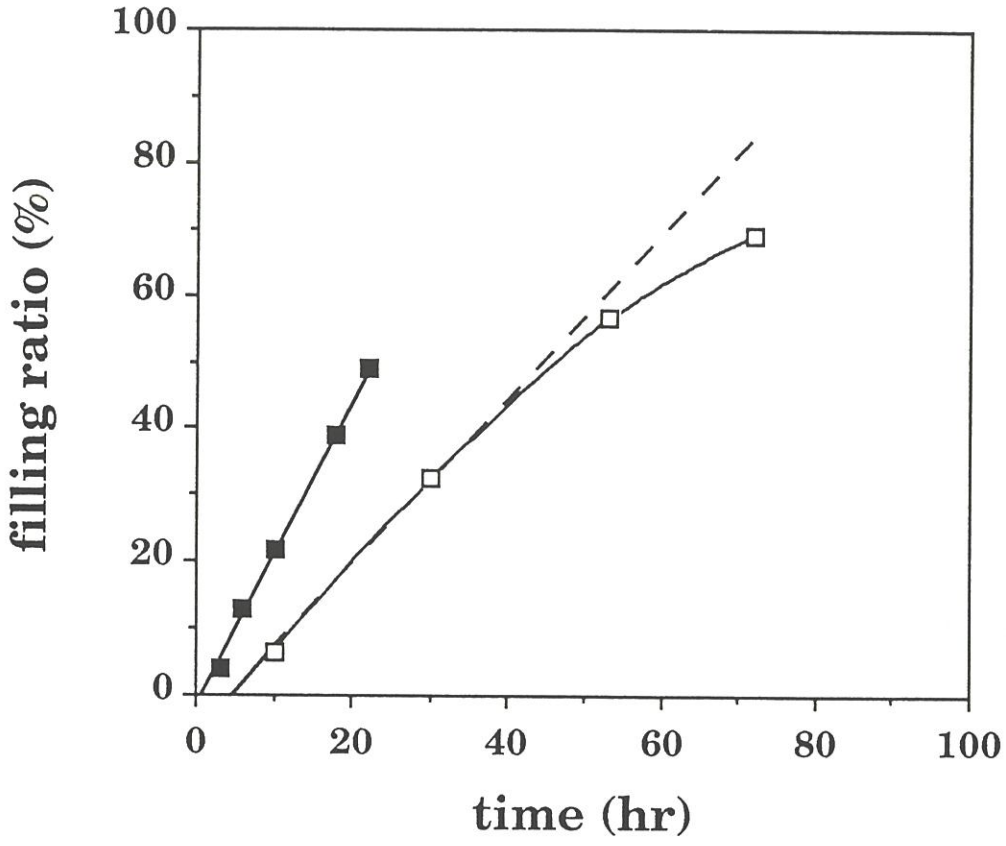

Fig. 8 : Variations of the filling ratio of the 120 μm -model pore as a function of infiltration duration : ■ P-CVI; T=1150°C; P=3kPa; t_R=10 s and □ I-CVI; T=1050°C; P=3 kPa; Q=60 sccm.

that these differences could be due to the fact that the experiments have been performed at different temperatures (1150°C for P-CVI vs 1050°C for I-CVI). However, the PyC thickness profiles shown in fig. 3a suggest that the influence of temperature is weak within the 1050-1150°C range.

3.7 - Anisotropy of the PyC-deposit along the pore

The extinction angle Ae (measured in polarized light with an optical microscope) is know to characterize the PyC-anisotropy. Its value increases from 4° (isotropic PyC) to 20° (rough laminar PyC) as the anisotropy of the PyC-deposit increases. Its variations along the longitudinal axis of the 60 μm-model pore are shown in table Ia for different values of the residence time t_R of the propane precursor in the deposition chamber.

Short residence times (i.e. t_R = 0.2 s) yield a PyC-deposit whose anisotropy is relatively low (Ae = 12°, corresponding to dark/smooth laminar) and homogeneous along the pore axis. Conversely, when t_R is raised (from 0.2 to 60 s), the PyC-microstructure exhibits the following features : (i) the PyC-anisotropy is very high (Ae = 20° ; rough laminar) at the substrate surface (z = 0) and near the pore entrance (z ≤ 1 or 2 mm) and (ii) an anisotropy gradient is observed along the pore which is steep for low (t_R =0.5 s) or high (t_R = 60 s) residence times and less pronounced for intermediate values (t_R = 10 s).

There is thus a clear correlation between the anisotropy of the PyC-deposited at the substrate external surface and along the model pores, on the one hand, and the duration of the pulse, on the other hand, which will be discussed in the next section.

residence time t_R(s)	location along the pore axis, z(mm)				
	0	1	3	5	10
0.2	12	12	12	12	12
0.5	20	20	15	12	12
10	20	20	19	15.5	14.5
60	20	20	17	13	12

(a)

$t_R^{(j)}$ (s)	$t_R^{(i)}$ (s)	location along the pore axis, z(mm)				
		0	1	3	5	10
0	0.2	0.6	0.45	0.33	0.26	0.21
0.2	0.5	0.44	0.26	0.09	0.1	0.07
0.5	10	4.3	2.2	1.2	0.56	0.63
10	60	3.7	3.3	2.1	1.83	1.52

(b)

Table. 1 : Variations of the extinction angle, Ae(°) (a) and of the differential PyC-thickness per pulse, $\Delta e_{p,z}$ (in nm.pulse^{-1}) (b), along the longitudinal 60 µm-pore axis for different residence times t_R (T=1050°C; P=3 kPa).

4 - DISCUSSION

The data which have been presented in section 3 show that the total pressure P and the temperature T are two important parameters for controlling the kinetics of the infiltration process in P-CVI, as already well established for the related I-CVI [1,2]. However, P-CVI provides an additional controlling parameter, the **residence time t_R**, which appears particulary important when the gas phase undergoes chemical change as it is maintained at high temperatures in a closed reactor vessel (which is actually the case for a hydrocarbon precursor such as propane). For the purpose of the discussion, a pulse can be divided into two main stages :

(i) at the beginning of the pulse, a **short stage** (stage 1), whose duration is typically of the order of a few hundredths of a second, during which the C_3H_8 gas precursor is forced to penetrate the pore (the mass transfer of the gaseous reactant being by forced convection).

(ii) in a second stage, which corresponds to the **majority of the pulse** (i.e. a few tenths of a second to a few seconds and even several 10 seconds) the gas phase, entrapped in the closed infiltration chamber and maintened at a high temperature, undergoes a continuous change in chemical composition. During this stage, referred to as stage 2 or **gas phase maturation**, deshydrogenation, condensation and cyclisation phenomena occur giving rise to the formation of aromatic and large size molecules [13]. During stage 2, **two deposit processes** are in competition [9] : **process I** which is characterized by heterogeneous reactions involving molecules akin to propane, i.e. of rather small sizes and highly hydrogenated and **process II** which takes place when the gas phase maturation is more achieved and corresponds to the direct

condensation of the large aromatic species onto the substrate surface. Since in P-CVI, the filling-holding-evacuating sequence is repeated periodically, the corresponding PyC-deposit is itself a sequence of several elemental deposits formed according to processes I or II, depending on the value of t_R.

4.1 - Influence of residence time on thickness profile

The residence time t_R has a great influence on the PyC thickness profile along the model pores and on the related filling ratio (δ_i), as shown in fig. 1 and 2. In P-CVI, the interesting t_R values, i.e. those yielding high filling ratios, are either the **low t_R values** (corresponding mainly to the filling of the pore by forced convection (stage 1) with very limited gas phase maturation and being higher as the pore size is lower) or the **high t_R values** (corresponding mainly to stage 2 and limited by both the gas phase depletion and the inhibiting effect of the increase of the hydrogen partial pressure in the pore).

The effect of t_R on the PyC-thickness profile along the pore axis (e.g. the 60 μm pore), under given T-P conditions (e.g. T = 1050°C and P = 3 KPa) can be discussed on the basis of the two deposition processes (process I and process II) considering the PyC-thicknesses per pulse, $e_{p,z,t_R^{(i)}}$ and $e_{p,z,t_R^{(j)}}$, deposited at a given z abscissa during two pulses of different durations $t_R^{(i)}$ and $t_R^{(j)}$, with $t_R^{(i)} > t_R^{(j)}$, as shown in fig. 9. **The differential thickness per pulse**, $\Delta e_{p,z}$, defined according to the following equation :

$$\Delta e_{p,z} = e_{p,z,t_R^{(i)}} - e_{p,z,t_R^{(j)}} \qquad (2)$$

is assumed to represent that portion of the PyC deposited during a pulse corresponding to a given mean degree of gas phase maturation (defined

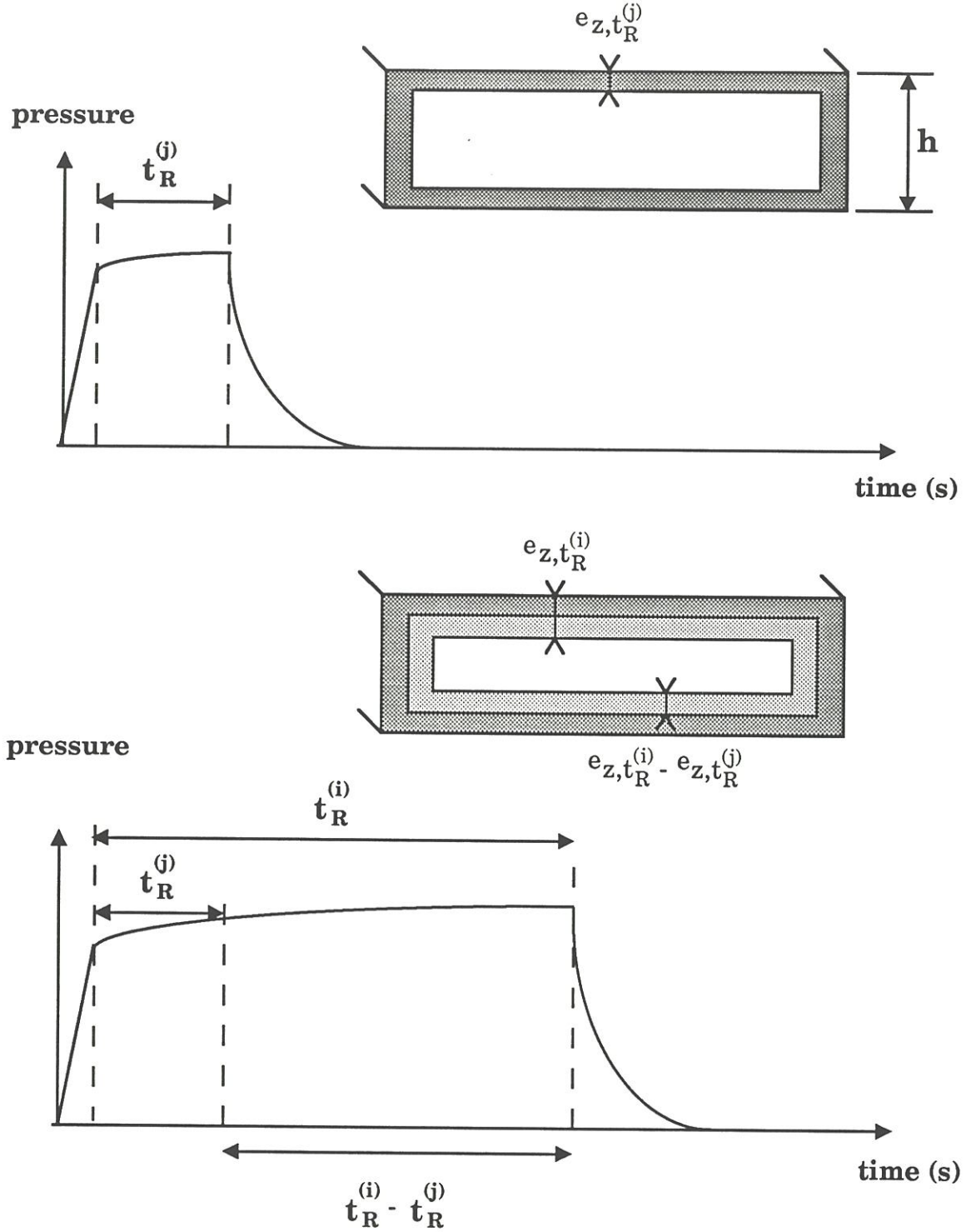

Fig. 9 : PyC- thickness, $e_{z,t_R^{(i)}}$, $e_{z,t_R^{(j)}}$ and $e_{z,t_R^{(i)}} - e_{z,t_R^{(j)}}$, deposited in a pore cross-section at a given abscissa z, during pulses of different durations corresponding to different degrees of gas phase maturation (schematic).

between the two limits $t_R^{(j)}$ and $t_R^{(i)}$). In other words, $\Delta e_{p,z}$ allows one to substract the PyC-thickness deposited at the beginning of a pulse from the overall PyC-thickness per pulse and to consider only that related to a mean degree of gas phase maturation.

Equation (2) can be rewritten, considering the deposit accuring at the pore entrance, i.e. at z = o, as :

$$\Delta e_{p,o} = \Delta e_{p,o}\, t_R^{(i)} - \Delta e_{p,o}\, t_R^{(j)} \qquad (2')$$

The number of pulses, n, which would be necessary for achieving pore blocking at z=o by this specific PyC deposited under such a controlled condition of gas phase maturation is defined by :

$$n = \frac{h/2}{\Delta e_{p,o}} \qquad (3)$$

knowing this value of n, it is thus possible to calculate, for each value of z, the PyC-thickness deposited under the condition of gas phase maturation defined above, at pore entrance blocking :

$$e_z^v = \Delta e_{p,z} \,.\, n \qquad (4)$$

Equation (4) can be rewritten as :

$$e_z^v = \frac{\Delta e_{p,z}}{\Delta e_{p,o}} \cdot \frac{h}{2} \qquad (4')$$

The values of the PyC-thickness deposited per pulse, $e_{p,z}$ are directly calculated from the experimental curves e = f(z) (see for example fig.1a). Their variations as a function of z are shown in fig. 10a for the 60 µm-model pore, T = 1050°C, P = 3 kPa and t_R ranging from 0.2 to 60 s. Introducing these values in equations

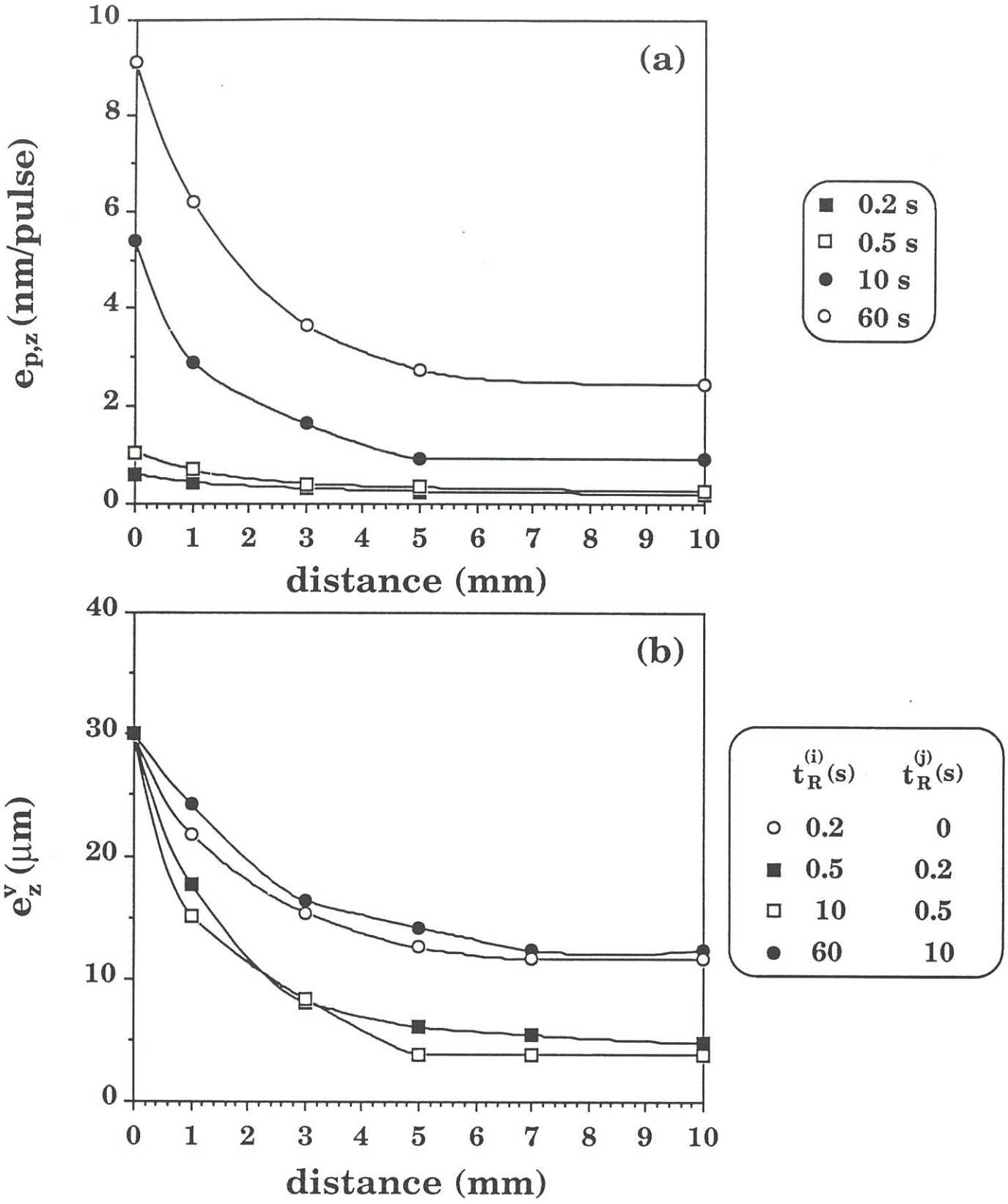

Fig. 10 : PyC-thickness profiles along the model pores : (a) variations of the elementary PyC-thickness deposited per pulse, $e_{p,z}$ as a function of z for the 60 μm-pore and different t_R values (with T=1050°C and P=3 kPa), and (b) virtual PyC-thickness profiles along the 60 μm model pore calculated for different degrees of gas phase maturation (corresponding to various $t_R^{(i)}$ - $t_R^{(j)}$ differential residence times) and T=1050°C; P=3 kPa.

(2), (2') and (4') allows one to draw **virtual thickness** profiles, $e_z^v = f(z)$, that would correspond to PyC deposited along the pore axis under the $t_R^{(i)}$ - $t_R^{(j)}$ gas phase maturation conditions, at pore entrance blocking (table 1a). These profiles are shown in fig. 10b for the 60 μm pore and will be used to discuss the effect of t_R.

4.1.1 - Very low t_R values (t_R < 0.05 s)

When the pulse is of very short duration, majority of the pulse corresponds to the filling of the pore by the C_3H_8 precursor (stage 1) which occurs by forced convection with almost no maturation of the gas phase. Under such conditions, the thickness profile along the pore should be flat (if the pulse duration, i.e. t_R in a first approximation, is sufficient to allow the precursor transport at the pore center). Such a condition is fulfilled, for t_R < 0.05 s, when the pore size is large enough (e.g. for h = 320 μm, as it will be established later) but it may be no longer the case for pores of very small sizes, as established by Sotirchos for the infiltration of < 1 μm pore by SiC deposited from a CH_3SiCl_3/H_2 mixture [9]. This stage 1 corresponds to the real P-CVI, as described by Sugiyama and Ohzawa, where the reactant mass transfer along the pore occurs mainly by forced convection (i.e. almost without diffusion) [8]. However such very short residence time values are too low to be accessible with our apparatus (and a fortiori with a large industrial furnace).

The **theoretical PyC-thickness** deposited per pulse, e_{pp}, under such conditions of very short t_R can be calculated from the amount of propane entrapped in the rectangular cross-section model pore, assuming that each

C_3H_8 molecule is cracked as carbon during t_R. The calculations lead to the following simple equation (see appendix) :

$$e_{pp} = K.h \qquad (A4)$$

where K is a dimensionless constant :

$$K = \frac{1}{2240} \cdot \frac{P}{Po} \cdot \frac{To}{T} \qquad (A5)$$

equal to 2.81×10^{-6} for P = 3 kPa and T = 1050°C. For the three model pores considered here, with h = 60 ; 120 and 320 μm, the corresponding e_{pp} values are 0.168 ; 0.337 and 0.899 nm, respectively. These values are undoubtedly overestimated since all the propane is not actually consumed. However, they can be used to estimate the values of t_R necessary to achieve a flat PyC-thickness profile along the pore axis. With a deposition rate of 3 $nm.s^{-1}$ (derived from the $e_{p,o}$ value, 0.6 $nm.pulse^{-1}$, corresponding to the lowest t_R value, t_R = 0.2 s, in table 1b), a PyC thickness equal to e_{pp}, will be achieved in 56 ; 112 and 300 ms, for h = 60 ; 120 and 320 μm, respectively. These results show that flat profiles along the pore axis could be expected only for the 320 μm pore taking into account the limitation of our apparatus ($t_R \geq 0.2$ s).

Since under the condition of pore filling by forced convection mass transfer (i.e. very low t_R values), the PyC-thickness profile along the pore is assumed to be flat, the pore filling ratio δ_i corresponding to a given number of pulses n can be written as (see appendix 2) :

$$\delta_i = 1 - (1-2K)^n \qquad (A6)$$

with δ_i no longer depending on the pore size. Under such conditions, the infiltration of the model pore is expected to be very good (flat PyC-thickness profile) but a **large number of pulses** is necessary to achieve a high filling ratio.

As an example, a δ_i value of 94 % will require n = 500.000 pulses for T = 1050°C and P = 3 kPa. It is worthly of note that a δ_{320} value of the order of 90 % has been observed for t_R = 0.2 s, T = 1050°C and P = 3 kPa (fig. 2b) suggesting that the infiltration may have proceeded mainly according to this mode (stage 1) for these specific conditions (low t_R value and pore of large size).

4.1.2 - Low t_R values ($0.05 < t_R < 0.2$ s)

Within the $0.05 < t_R < 0.2$ s range, the infiltration of the model pores involves now the two stages (stage 1 and stage 2) and the PyC-thickness profile is no longer expected to be flat. In other words, a PyC-thickness gradient is present along the pore, as already reported for the related I-CVI process [1,2,14]. This feature is clearly apparent from both the experimental curves (fig. 1a and fig. 10a) and the calculated virtual thickness profiles (fig. 10b).

For these t_R values, the gas phase composition in the dead volume (i.e. that corresponding to the closed reaction vessel) is **only slightly changed** during the pulse, since the amount of PyC deposited is low. As an example, the PyC-thickness deposited on the external substrate surface (z = 0) during a pulse of 0.2 s is only 7 % of that corresponding to a 60 s pulse (fig. 10a). The PyC-deposition occuring during such short pulses is thought to result from the surface adsorption and reaction of small and highly hydrogenated species akin to propane, i.e. mainly according to process I with little gas phase maturation. These molecules diffuse easily along the pores and the filling ratios are very good (fig. 1b), whatever the pore size, with a PyC-thickness gradient along the pore not too steep.

4.1.3 - Intermediate t_R values ($0.2 < t_R < 10$ s) :

The e_z^v profiles calculated for significant degrees of gas phase maturation, i.e. between $t_R^{(i)} = 0.5$ and $t_R^{(j)} = 0.2$ or between $t_R^{(i)} = 10$ and $t_R^{(j)} = 0.5$ s, which are shown in fig. 10b, exhibit strong gradients along the pore axis. It is thought that the PyC-deposit on the external substrate surface and in the pore near its entrance grows according to process II. As a matter of fact, the **large molecules** formed in the gas phase (such as pyrene and phenanthrene) as the result of deshydrogenation-cyclization-condensation processes and which have been actually detected experimentally [11] have indeed a high probability to stack near the pore entrance and their diffusion along the pore is limited (particularly when the pore size is limited e.g. for the 60 μm-pore). As a consequence, at z = 10 mm (pore center) the PyC is thought to grow mainly according to process-I, i.e. as the result of the cracking of small and hydrogenated molecules (whose life time and mobility are higher). The PyC-thickness at the pore center is much lower owing to the gas phase depletion and the inhibition effect of hydrogen. These intermediate t_R values correspond to the worst conditions, in terms of thickness gradient and pore filling ratio (fig. 1b and 10b).

4.1.4- For high t_R values ($t_R > 10$s)

The e_z^v thickness profile, which has been calculated for $t_R^{(i)} = 60$ s and $t_R^{(j)} = 10$ s and is shown in fig. 10b, exhibits a less pronounced gradient. This might be due to a strong decrease of the amount of the large aromatic molecules because of the gas phase depletion and/or the increase of the hydrogen

concentration. As a result, the species present in the gas phase (for these high degrees of maturation) might be again smaller and more hydrogenated. This assumption is also supported by the methane concentration (methane leads to weak gradients in P-CVI and even to inverse gradients in I-CVI [15]) which has been reported to be high for long pulses. These smaller molecules diffuse well along the pore, as previously mentioned. The PyC-growth occurs according to a process which is not yet fully elucidated but which could be a mixt process.

4.2- Correlation between the residence time and the PyC anisotropy

For **short** residence times, e.g. t_R = 0.2 s, the extinction angle is low (Ae = 12°) whatever the value of the abscissa z along the pore axis (table 1a). As discussed in section 4.1, the chemical species which lead to PyC are small and highly hydrogenated. As a consequence, their diffusion in the pore is easy (with the result that the thickness gradient along the pore is not too steep; table 1b and fig. 10b) but the PyC is poorly organized (table 1a).

For **intermediate** residence times (e.g. t_R = 0.5 or 10 s) both an Ae gradient (table 1a) and a thickness gradient (table 1b and fig. 10b) are present along the model pore. The gas phase maturation (which is significant for these values of t_R) leads to the formation of large and deshydrogenated (aromatic) molecules, as already discussed, which tend to preferentially stack on the pore wall near the pore entrance (i.e. at about 0<z<1mm). The improvement of Ae (and thus of the PyC-anisotropy) observed near the pore entrance (Ae = 20°) is thought to result from the direct condensation of these molecules onto the wall and the external surface of the substrate. The higher the PyC-thickness deposited according to process II (with respect to that formed according to

process I), the higher is the Ae-gradient along the pore (table 1). As an example, at z = 10 mm (pore center) :

Δe_p = 0.21 nm and Ae = 12°, for $t_R^{(i)}$ = 0.2 $t_R^{(j)}$ = 0 s

Δep = 0.07 nm and Ae=12°, for $t_R^{(i)}$ = 0.5 $t_R^{(j)}$ = 0.2 s (process I only)

Δep = 0.63 nm and Ae=14.5°, for $t_R^{(i)}$ = 10 $t_R^{(j)}$ = 0.5 s (process I and II)

For **high** residence times (e.g. t_R = 60 s), the gas phase maturation is almost fully achieved. The concentration of the large aromatic species is much lower and the formation of both methane and hydrogen enhanced. As a result, the PyC-rate deposition decreases and tends to zero (inhibition by hydrogen). At the substrate external surface (z = 0) Ae is still very high (20°) but in the middle of the pore (z = 10 mm) Ae decreases (12°) because the PyC-thickness deposited during the last part of the pulse is poorly organized and important with respect to the overall PyC thickness at this location ($e_{p10,\ 0.2\text{-}10}$ = 0.7 nm and $e_{p10,\ 10\text{-}60}$ = 1.52 nm).

There is thus a rather clear correlation between the PyC-anisotropy, on the one hand, and the residence time, on the other hand. More details about the anisotropy of the PyC-deposited are given elsewhere [12].

4.3- Influence of both temperature and pressure on the thickness profile

Both temperature and pressure have a strong influence on the PyC thickness profile along the model pores in P-CVI, at least for the t_R range studied in present work, as previously reported for I-CVI [1,2,14].Generally speaking, decreasing T and P favors in-deph deposition (fig. 3a and 4).

The variations of the filling ratio δ_i as a function of **temperature** are more important as the pore is smaller (fig. 3b). At t_R=10 s, process II mainly controls the deposit particularly when temperature is high (the gas phase maturation being faster). Under such conditions, a fast blocking of the pore entrance occurs because of the condensation of the large (aromatic) molecules, with the result that the filling ratio is low particularly for the small size pores (δ_{60} = 25 % and δ_{120} = 45 % for T=1100°C). Finally, the filling ratio decreases, from an optimun value which is achieved at about 950°C, as the temperature is lowered. This feature, which is observed only for the 60 μm and 120 μm-pores, is still incompletely understood and might be related to soot formation (which has been actually observed experimentally).

An increase of the pressure, at 950 < T <1050°C and t_R = 10 s (conditions corresponding to a significant degree of gas phase maturation) is thought to lead to a rapid control of the PyC-deposition by process II and is thus unfavorable to in-depth infiltration (fig. 4).

4.4- Influence of the precursor nature on the thickness profile

The nature of the precursor (and thus its thermal stability and ability to yield carbon) is another parameter which has a great influence on the PyC-thickness profiles along the model pores (fig. 6). As an example, when propane is replaced by methane, the filling ratio is raised from 28% to 74% for the 60 μm pore under the same experimental conditions (T = 1050°C ; P = 3 kPa and t_R = 10 s). As the thermal stability of methane is higher, its maturation is slower than that of propane, for a given t_R value and thus the in-depth diffusion of the source species (as small size molecules) is favored, resulting in a higher filling

of the pore by the PyC-deposit (process-I). In other words, the deposition process (mainly process-I) of PyC from CH_4 for t_R = 10 s might be close to that for C_3H_8 at t_R = 0.2 s, the same degree of gas phase maturation being achieved at different residence times.

Another important feature is that the PyC-deposition rate per pulse is one order of magnitude higher with C_3H_8 than with CH_4, under the same deposition conditions (which unfavors in-depth infiltration). However, if the experimental conditions are chosen different, in order to yield the same deposition rate per pulse, propane appears as a better source than methane, for infiltration [11].

4.5- Influence of the total infiltration duration on the thickness profile

The P-CVI experiments performed with the 120 μm model pore (fig 7a) show that surprisingly the PyC-deposition rate remains almost constant as infiltration proceeds, i.e. as the pore size decreases versus time. As a result, the thickness of the PyC deposited at a given z value, $e_z(t)$, is proportional to the number of pulses and can be expressed as :

$$e_z(t) = e_{p,z} (n - n_0) \qquad (5)$$

where n_0 is the initial number of pulses which are necessary to fill the porosity/rugosity of the pore wall and to measure a deposit. The reason why the PyC-deposition rate remains constant in P-CVI is not yet known.

5- CONCLUSION

The experimental data reported in section 3 and the discussion presented in section 4, lead to the following main conclusions :

(i) - model straight pores with rectangular cross-sections and sizes ranging from 60 to 320 μm have been infiltrated with pyrocarbon deposited from CH_4 and C_3H_8 precursors under pulse CVI-conditions,

(ii) - the main experimental parameters controlling the quality of the infiltration are temperature and pressure, as previously reported for I-CVI, but also the **residence time** which appears as a key parameter in P-CVI (in as much as it controls both the filling ratio and the anisotropy of the PyC-deposit),

(iii) - there are two important steps during a pulse. At the beginning of the pulse (stage I), a mass transfert of the source species occurs by **forced convection** along the pore during a few hundredths or tenths of a second (depending on the pore size). Then during the majority of the pulse (stage II), the hydrocarbon gas phase undergoes a key **maturation** phenomenon,

(iv) - during stage II, the PyC deposition occurs according to two successive or simultaneous processus mechanisms. In process I, PyC is formed from small highly hydrogenated molecules whereas in process II, it is formed by simple condensation on the pore wall of large aromatic intermediate species. The former is favorable to in-depth infiltration and yields a PyC deposit with a low anisotropy whereas the latter takes place preferentially near the pore entrance and results in a highly anisotropic PyC. The respective contributions of the two processes are highly dependent on the residence time t_R (which controls the degree of the gas phase maturation at given T, P) and there is a direct

correlation between t_R, on the one hand, and the thickness gradient on PyC anisotropy along the pore, on the other hand,

(v) - very short pulses might yield flat PyC-thickness profiles along the pore. Unfortunately, such conditions could not be achieved in present work due to experimental limitation (as it would be also the case for large size furnaces at the plant level),

(vi) - short residence times (e.g. $t_R \approx 0.5$ s) associated with low propane pressures (e.g. a few kPa) and temperature ranging from 900 to 1000°C, yield filling ratios equivalent to and even higher than those reported for I-CVI with the restriction that , under such conditions, a large number of pulses is necessary,

(vii) - replacing propane by methane results, under the same experimental conditions, in better infiltrations owing to the higher thermal stability of CH_4 which limits the gas phase maturation (i.e. the formation of large size aromatic molecules),

(viii) - although P-CVI may appears to exhibit a limited interest with respect to I-CVI (its advantages being mitigated by its constraints at the industrial level), it offers an efficient way for controlling the microstructure of the solid which is deposited.

ACKNOWLEDGEMENTS

This work has been supported by SEP through a grant given to P.D. The authors are indebted to S. Goujard and C. Robin-Brosse from SEP for technical assistance and valuable discussions.

REFERENCES

[1] R. Naslain and F. Langlais, "CVD-processing of ceramic-ceramic composites materials", in "Tailoring multiphase and composite ceramics" (R.E. Tressler, G.L. Messing, C.G. Pantano and R.E. Newnham, eds.), Mater. Science. Res, **20** (1986) 145 , Plenum Press, New York and London.

[2] R. Naslain, "CVI-composites" in "Ceramic matrix composites" (R. Warren, ed., Glasgow and London, 199, 1992).

[3] W.J. Lackey and T.L. Starr, "Fabrication of fiber-reinforced ceramic composites by chemical vapor deposition : processing, structure and properties", in "Fiber reinforced ceramic composites" (K.S. Mazdiyasni, ed., Noye Publ, Park Ridge (NJ), [14], 397, 1990) .

[4] S. Middleman, "The interaction of chemical kinetics and diffusion in the dynamics of chemical vapor infiltration", J. Mater. Res., **4**, [6],1515 (1989).

[5] Y.S. Lin, "Analysis of CVI process for porous material densification using a continuous model", Proceeding of the 11th International Conference on CVD, Seattle, (K.E. Spear and G.W. Cullen, eds, The Electrochem. Soc. Pennington, 532, 1990).

[6] T.M. Besmann, R.A. Lowden, D.P. Stinton and L.L. Starr, "A method for rapid chemical vapor infiltration of ceramic composites", J physique, Colloque C5, Supp.5, **50**, 229, (1989).

[7] K. Sugiyama and T. Nakamura, "Pulse CVI of porous carbon", J. Mater. Sci. Let., **6** 331, (1987).

[8] K. Sugiyama and Y. Ohzawa, "Pulse chemical vapor infiltration of SiC in porous or SiC particulate preform using an r.f. heating system", J. Mater. Sci. Let. , **25** , 4511, (1990) .

[9] S.V. Sotirchos, "Dynamic modeling of chemical vapor infiltration", AIChE, **37**, 1365, (1991).

[10] S.V. Sotirchos and M. Tomadakis, "Modelling tranport, reaction, and pore structure evolution during densification of cellular or fibrous structures", in Chemical Vapor Deposition of Refractory Metals and Ceramics, (T.M. Besmann and B.M. Gallois, eds, MRS, Pittsburgh, 73, 1990).

[11] P. Dupel, R. Pailler and F. Langlais, "Pulse chemical vapor deposition (P-CVD) and infiltration (P-CVI) of pyrocarbon in model pores with rectangular cross section : Part 1 - study of the pulsed process of deposition", this journal, to be published.

[12] P. Dupel, X. Bourrat and R. Pailler , "Anisotropic pyrocarbon obtained at low temperature by pulse-CVI : structural characterization", submitted to Carbon.

[13] C.J. Chen and M.H. Back, "The simultaneous measurement of the rate of formation of carbon and hydrocarbon products in the pyrolysis of methane", Carbon, **17**, 175, (1979).

[14] P. Dupel, R. Pailler, F. Langlais, R. Naslain and A. Costecalde, "CVD/CVI of pyrocarbon from propane on flat substrates and in model pores with rectangular croos-sections", To be published in Carbon.

[15] P. Lajzerowicz, "Modelisation de l'élaboration de composites carbone-carbone par dépot chimique en phase vapeur", Thèse doct-ing, numéro d'ordre : 606,INPG, Grenoble 1987.

APPENDIX

1- The potential PyC-thickness deposited per pulse, epp, related to the force convection step (stage 1) is defined as the thickness of PyC that would be formed on the wall of an elementary section of the model pore, located at an abscissa z, from the C_3H_8 molecules present in this section, assuming that the C_3H_8/C conversion is total.

Let us consider an elementary pore cross-section of thickness ΔL. It contains at T, P, a C_3H_8-volume $\Delta V = l.h.\Delta L$ and the area of the pore cross-section wall is $\Delta S \approx 2.\Delta L.l$, neglecting $2.\Delta l.h$ (since h is assumed to be negligible with respect to l).

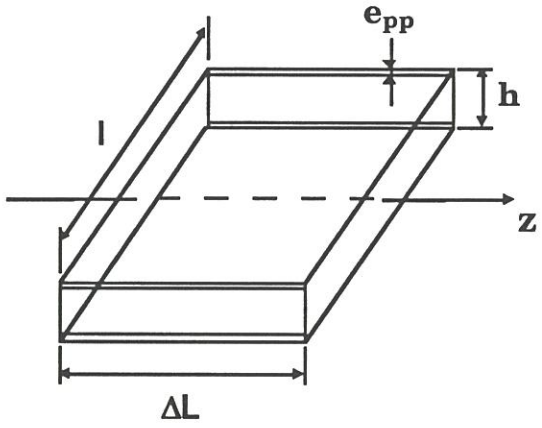

Assuming that propane obeys the perfect gas law, the number of moles of C_3H_8 entrapped in the elementary volume under the standard T, P conditions is :

$$\eta = (l.h.\Delta L).\frac{P}{P_0}.\frac{T_0}{T}.\frac{1}{22400} \qquad (A1)$$

l, h and Δl being expressed in cm.

Since $M(C_3H_8) \approx 36$ g. mol^{-1} and assuming that the density of PyC is 1.8 g. cm^{-3}, the volume of carbon that could be formed is :

$$v_c^{th} = \frac{36}{1.8}\eta = 20\,\eta \qquad (A2)$$

and e_{pp} expressed as :

$$e_{pp} = \frac{20\,\eta}{2.\Delta L.1} \qquad (A3)$$

or $$e_{pp} = K.h \qquad (A4)$$

with $$K = \frac{1}{2240} \cdot \frac{P}{P_o} \cdot \frac{T_o}{T} \qquad (A5)$$

For P = 3 kPa and T = 1050 + 273 = 1323 K, the value of K is : $K = 2.81 \times 10^{-6}$.

2- Under the condition of pore filling by forced convection mass transfer, i.e. for very low t_R values, the PyC-thickness profile along the pore z-axis is expected to be flat. Thus, the pore filling ratio δ_i corresponding to a given number of pulses n can be calculated by considering the cumulative thickness of PyC deposited onto the pore wall.

During the **first pulse** (n = 1), the size of the pore decreases from h to :

$$h - 2\,e_{pp} = h - 2\,Kh = h(1 - 2K)$$

and during the **second pulse**, from $h(1 - 2K)$ to :

$$h(1 - 2K) - 2e_{pp} = h(1 - 2K) - 2h(1 - 2K)\,K$$

$$= h(1 - 2K)\,(1 - 2K) = h(1 - 2K)^2$$

thus, after **n pulses**, the size of the pore is $h(1 - 2K)^n$ and the cumulative thickness of PyC is :

$$h - h(1 - 2K)^n = h[1 - (1 - 2K)^n]$$

Finally, the pore filling ratio is :

$$\delta_i = \frac{h\,[1 - (1 - 2K)^n]}{h}$$

or : $\delta_i = 1 - (1 - 2K)^n$ (A6)

Chapître 4 : ANISOTROPIC PYROCARBON OBTAINED AT LOW TEMPERATURE BY PULSE -CVD/CVI : STRUCTURAL CHARACTERIZATION

Le chapitre suivant est relatif à la **microstructure du pyrocarbone** déposé en surface et dans les pores modèles. L'observation microstructurale est réalisée à deux échelles complémentaires : (i) par microscopie optique en lumière polarisée, qui permet la mesure de l'angle d'extinction du pyrocarbone et ainsi de classer les pyrocarbones selon leur degré d'anisotropie, (ii) par microscopie électronique en transmission (TEM), méthode qui donne accès aux paramètres cristallographiques et qui conduit à une analyse plus fine de la taille et de l'organisation des couches de carbone entres elles.

La comparaison en terme de microstructure des dépôts de pyrocarbone I-CVI et P-CVI montre des différences nettes. Ceci conduit a supposer que les mécanismes de dépôt sont différents.

Un résultat important est que la P-CVI permet d'obtenir des dépôts présentant une **forte anisotropie** au sein même des pores modèles (même ceux de 60 μm), ce qui n'a pas été observé en I-CVI où l'anisotropie du pyrocarbone se dégrade rapidement dans le pore.

Ce chapitre présente les résultats de l'étude sous forme d'un projet de publication adressée à Carbon.

submitted to Carbon.

ANISOTROPIC PYROCARBON OBTAINED AT LOW TEMPERATURES BY PULSE-CVD/CVI : STRUCTURAL CHARACTERIZATION.

P. Dupel, X. Bourrat and R. Pailler

Laboratoire des composites thermostructuraux, (UMR-47 CNRS-SEP-UB1), 3 Allée de La Boétie, 33600 Pessac, France.

ABSTRACT

Compared to classical chemical vapor infiltration (CVI) where the deposition of pyrocarbon (PyC) is mainly controlled by temperature, pressure and precursor type, pulse chemical vapor infiltration (P-CVI) provides an additional controlling parameter : the residence time (t_R), i.e. the reaction duration. Controlling the reaction by this way, P-CVI can be managed to grow highly anisotropic PyC in the C-H binary system at temperatures as low as 900°C with an heterogeneous reaction and a lateral growth mechanism. This PyC is characterized by a large layer size (L_2>10 nm), a high preferred orientation and a reduced turbostratic coherency. It is able to yield a highly dense infiltrated carbon. In regular isothermal/isobaric CVI (I-CVI) there is a lost of preferred orientation with the infiltration depth, it is due to the decrease of L_2, the layer size, as well as, N, the number of layers coherently stacked one on the other: I-CVI PyC has a classical columnar growth.

KEY WORDS

Pyrocarbon, Pulse CVD/CVI, structure, TEM, optical microscope, anisotropy.

1- INTRODUCTION

Chemical vapor infiltration of carbon by thermal decomposition of hydrocarbon precursors have been extensively studied for several decades. It is now revisited for application in composites where it is needed to get an homogeneous deposition all over the preform : e.g. a pyrocarbon coating acting as **interphase** on ceramic fibers in ceramic matrix composites (CMC). Many papers in the past were dealing with the control on the PyC-structure [1-4] but the fine control on preferred orientation inside the porosity all over the preform is not resolved at all. Till now, I-CVI at low depositing rates is the classical route for achieving such deposits [5]. It is generally performed with methane as precursor at low temperatures (less than 1100°C) where the depositing rate is controlled by the heterogeneous surface reactions and under reduced pressures (a few kPa). To our knowledge, conditions where PyC is **infiltrated with a high preferred orientation**, have never been reported. In this context, pulse CVI was thought to be a promising alternative.

Only few works have been reported on P-CVI [6-8]. This paper focusses on the structure of pyrocarbon obtained by means of P-CVI as compared to I-CVI. The PyC structure deposited, from propane, was studied at two different scales. First, an optical method is adapted from Diefendorf *et al* [9] to measure the value of the **extinction angle, Ae**. The extinction angle is indirectly a measurement of the reflecting power of the carbon. Reflecting power is an optical property widely varying with the preferred orientation, mainly during the pre-graphitization process. In this sense, it gives a quantitative variation of the long-range textural variations occurring among the different PyC types : isotrope, dark, smooth or rough laminar. The variations of Ae are detailed

regarding the variations of temperature, pressure, gas nature and especially regarding residence time.

Secondly, the structure was studied by transmission electron microscopy (TEM). This technique has access to the crystallographic parameters necessary to characterize the turbostratic carbon structure. As earlyer demonstrated for aerosol growth of carbon (acetylene blacks) [10] L_2, the carbon layer size is the fundamental parameter guiding the structural properties of those pyrocarbons.

2- EXPERIMENTAL

The experimental approach was detailed elsewhere [11, 12]. In short, P-CVI can be described as a static isothermal process periodically re-set after a more or less long time. In this work only the pressure is allowed to vary : at each cycle or pulse, the reactor is evacuated and for a large part the sample porosity too (or expected so). Then, the reactor is re-filled. Filling is stopped when nominal pressure is achieved, typically 1 to 10 kPa. In such a process, there is a control on reaction duration : it is the pulse duration or the residence time (t_R), (typically 0.2 to 120 s in this work). The PyC-precursor was mainly propane, but methane and propylene were also used. The vessel was of a hot-wall type, isothermally working. The volume was 70 cc. Loading up was kept unchanged. Then the surface/volume ratio was equivalent for each of the runs involved in this work. For completeness, the same device was used in I-CVI [13] in the same range of temperature and pressure.

In order to study the infiltration, porosity model straight pores machined in a double graphite bloc were used, as shown in fig. 1. At each run, three

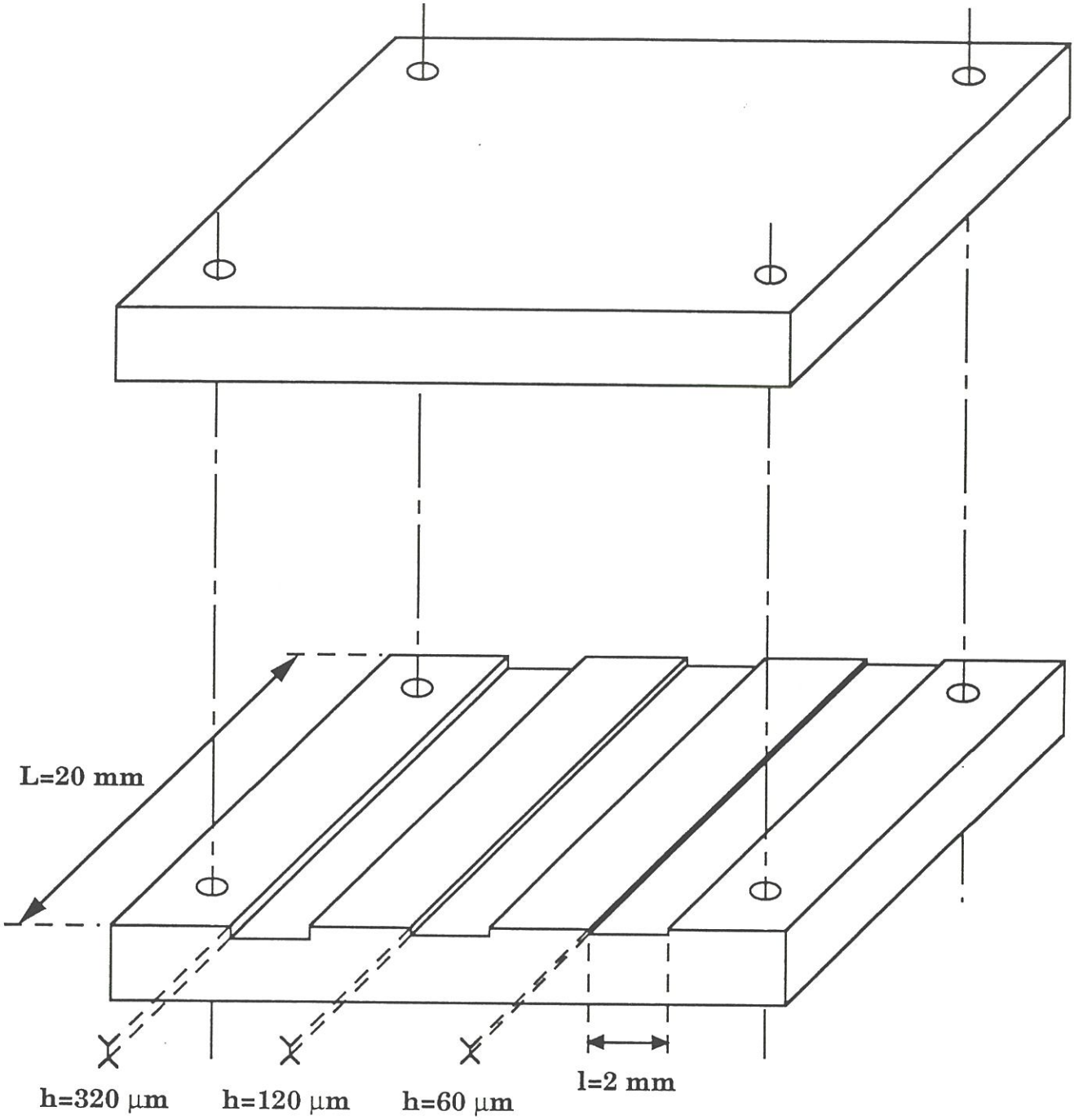

Fig. 1 : Schematic of the model graphite substrate with 3 straight pores with rectangular cross-sections.

different pores were infiltrated : 60 μm-, 120 μm- and 320 μm in size. After infiltration, the graphite bloc was sawn along the pore axis z and optical microscopy measurements were performed on polished longitudinal sections. The deposit thickness, e, as well as the extinction angle, Ae, were measured as follows.

The optical measurements were performed on a Reichert-Jung microscope (MeF_3) in polarized light. The extinction angle Ae is obtained in cross polars by rotating the analyzer of the microscope as a compensator [9]. Then, this angle depends on the amplitude of the beam transmitted parallel to the anisotropic plane regarding the normal direction; the larger the angle Ae, the higher is the anisotropy. The physical meaning of Ae is somewhat complex. This measurement sums different variations up : i.e. mainly the intrinsic bireflectance and the averaging effect related to the degree of anisotropy. The extensive use of this technique by Doux [14] has pointed it out as a relevant method to characterized the different PyC. The following correspondence between Ae and the classical structural classification can be done but is not univocal :

rough laminar			Ae	>	18°
smooth laminar	18°	<	Ae	<	12°
dark laminar	12°	<	Ae	<	4°
isotrope	Ae	<	4°		

Then, generally three thin cross-sections of the smaller pore (h=60 μm) were cut : first, at the entrance (z=0), then in the middle of the pore (z=10 mm) and finally at an intermediate depth (z≈3mm). The thin cross-sections were embedded in a resin, mechanically thinned and at last ion-milled. TEM was

performed using a JEOL 2000FX (±60° goniometer). The lattice fringes technique was mainly used (with a PR=.3 nm). Three measurement series were performed on each sample in order to determine the main parameters of the carbon layer. First, L_2, was measured (see fig.2), L_2 being the layer diameter : i.e. the real size of the layer, comprising its defects (or distorted layer). Then, L_1, was measured, L_1 being the straight part of the fringe which is close from L_a (L_a, is the defect-free part of the layer). Finally, N, the number of layers stacked each on the other, was measured. The measurements were not automatically performed in this work. A special care was taken to get a statistical image of the structure.

3- RESULTS

3.1- Residence time control on the anisotropy.

The basic interest of P-CVI is its controlling the gas phase reaction duration by re-setting the process at each pulse. So, a low residence time, t_R, means limiting the series of reactions to the transient state, whereas a long residence time produces conditions evolving like in a closed vessel. In order to point out the effect of the residence time, Ae profiles inside the 60 μm-model pore are presented for three different temperatures and two different pressures in figs. 3 and 4.

3.1.1- T=1050°C and different pressures

-At a low pressure, P=1 kPa, 3 different Ae profiles were observed, depending on the residence time.

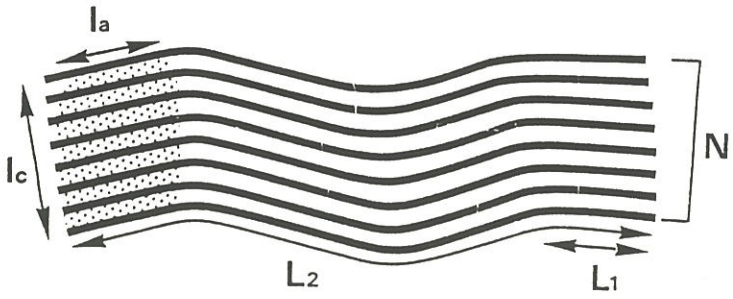

Fig. 2 : Schematic diagram of a layer stack : L_a is the size of distorted layer, N the number of layers piled together, L_d the defect free part of the layer. Superposed dashed is the coherent length as measured by means of 002 dark-field : L_2 and L_1, the coherent lengths in the plane and in the normal direction respectively.

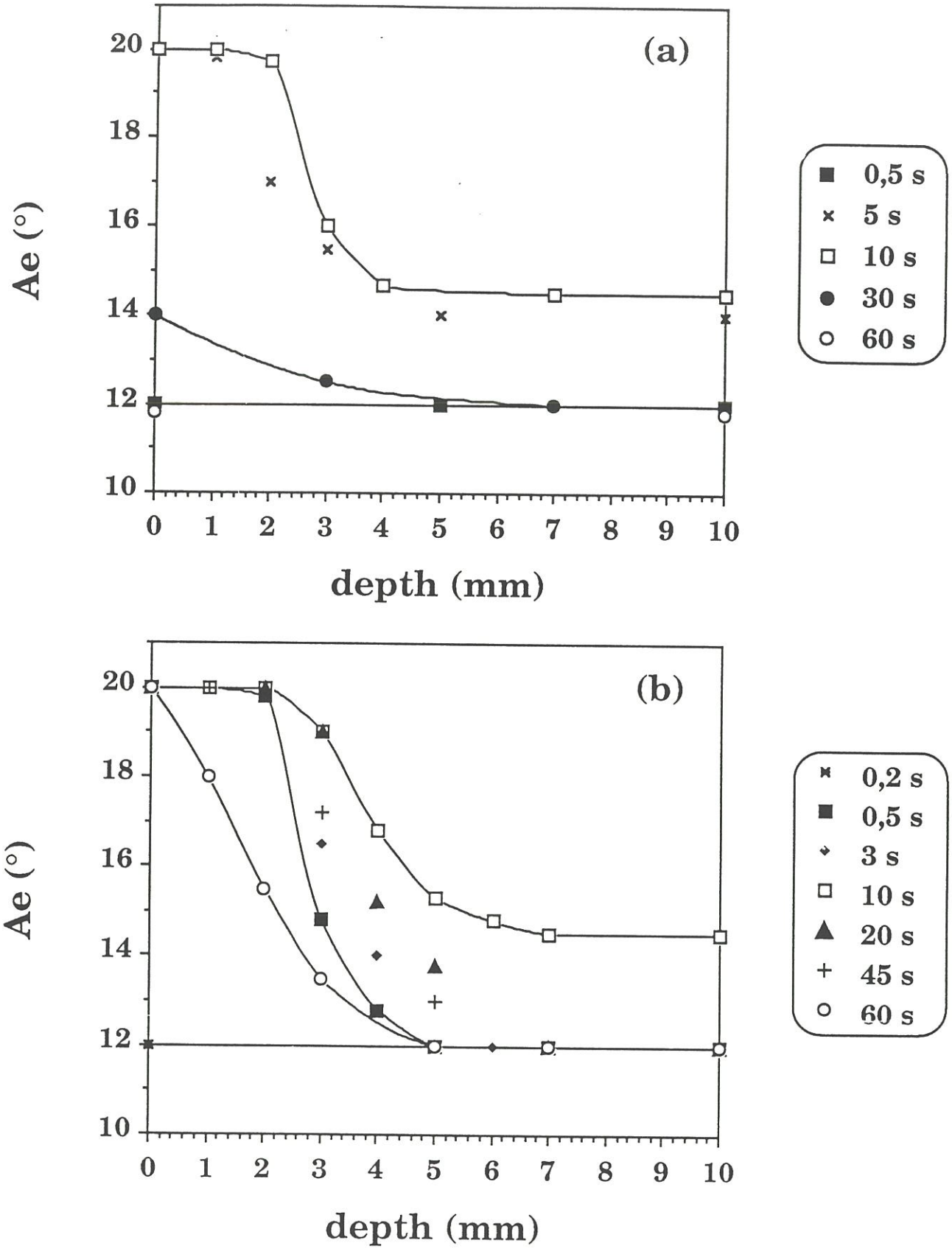

Fig. 3 : Ae profiles along the 60 μm-model pores as a function of t_R for T=1050°C : (a) P=1 kPa, (b) P=3 kPa and (c) P=10 kPa.

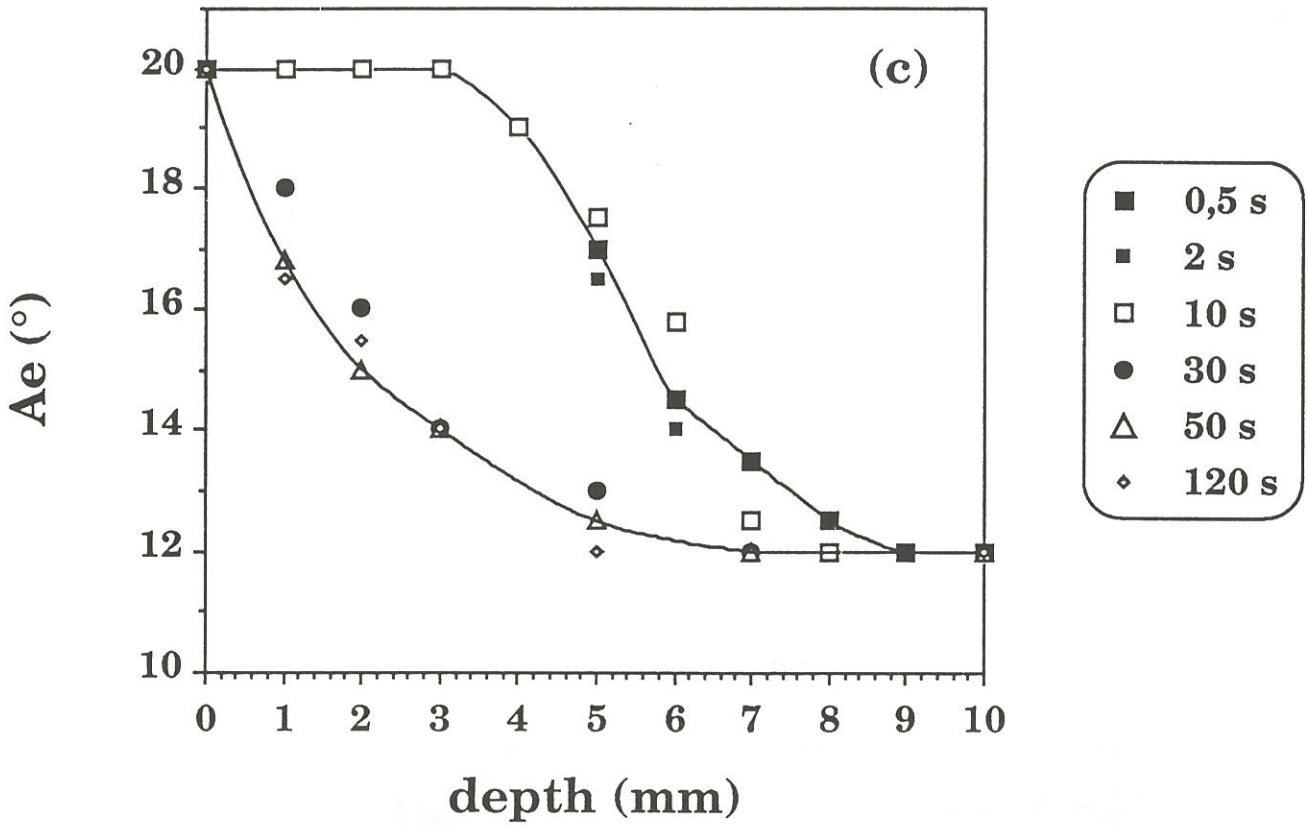

Fig. 3 : continued.

- **(i) For a short residence time**, t_R=0.5 s, a flat profile was observed with a poor PyC-texture (but not isotropic) : Ae=12°. The **deposit is homogeneous all along the pore**.

- **(ii) For an intermediate residence time**, t_R=5 s, the texture at the surface of the pore (z=0) is improved up to the best value : Ae=20°. Inside the pore, a gradient is appearing : Ae=15° at the middle of the pore. The profile exhibits a bell-like shape. For a residence time of 10 s, this gradient is minimized.

- **(iii) For longer residence times** the profiles get worst. When t_R=30 s, the texture on the surface (z=0) is a smooth laminar (14°) whereas the texture inside the pore is rapidly (for 5<z<10) a dark laminar (12°). The flat profile with the homogeneous but poor texture is observed again for very long durations, e.g. t_R=60 s

-At an intermediate pressure, P=3 kPa. The same stages as previously reported for low pressures are observed.

- **(i) For short residence times**, a flat profile is observed but for a shorter residence time : t_R=0.2s. Under these conditions, a dark laminar texture (12°) can be homogeneously infiltrated in the smaller pore with a high rate : 0.64 µm/hour at the entrance and half in the center.

- **(ii) For intermediate residence times**, as previously, an optimal deposition is obtained characterized by a low gradient of texture : 20° down to 15° at the middle. This profile is the best with C_3H_8 at high temperatures (1050°C) regarding the anisotropy and the rate.

- **(iii) For the longer residence times**, (t_R=45 s), the profile is getting worst but not so much as previously seen for the low pressures (P=1 kPa). The gradient increases (20° down to 12°). Especially, any flat profile was observed in this

case. Pyrocarbon deposited during the stage is still characterized by a poor ordering but a better infiltration is achieved [12].

-At a high pressure, P=10 kPa.

The flat profiles with a poor PyC-texture is not observed. The optimum profile, the one with the highest anisotropy and the smallest gradient, is observed for t_R=0.5 s. A shift is thus noticeable toward the short durations as the pressure is increasing. Also in this case, the texture in the middle of the pore is not as good as the one measured at lower pressures : Ae=12° compared to 15°. This effect is apppearing first in the smaller pore and for a higher pressure in the larger ones (120 and 320 μm pores).

3.1.2- T=1150°C and P=3 kPa

Those temperature/pressure conditions point out the equivalent control of temperature and pressure on the carbon anisotropy. This is shown in fig. 4, by continuity with the previous series, pressure being compensated by temperature. As t_R increases only the second process is appearing, profiles look worst and worst.

3.2- Temperature control on the anisotropy

Pressure and residence time were fixed at 3 kPa and 10 s respectively. Temperature was then allowed to vary in the 900°C-1150°C range. Profiles of the extinction angle, Ae, are plotted in fig. 5 for different temperatures.

- **At 900°C** the CVD deposition (z=0) yield smooth laminar PyC (Ae=17°). The Ae profile along the pore is of the logarithmic-decrease-type, comparable to the

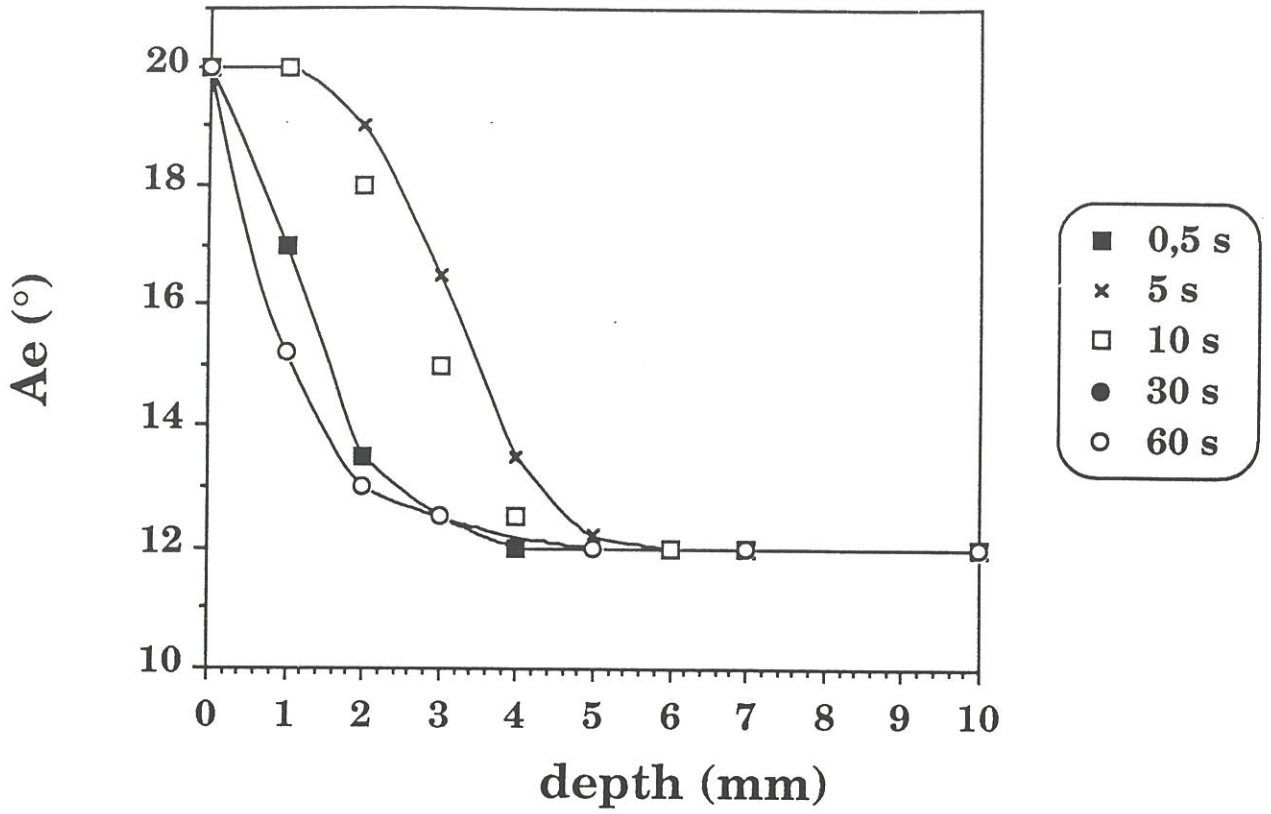

Fig. 4 : Extinction angle vs depth in the pore (60 μm large). Conditions are T=1150°C and P=3 kPa. The different plots are drawn for different residence times.

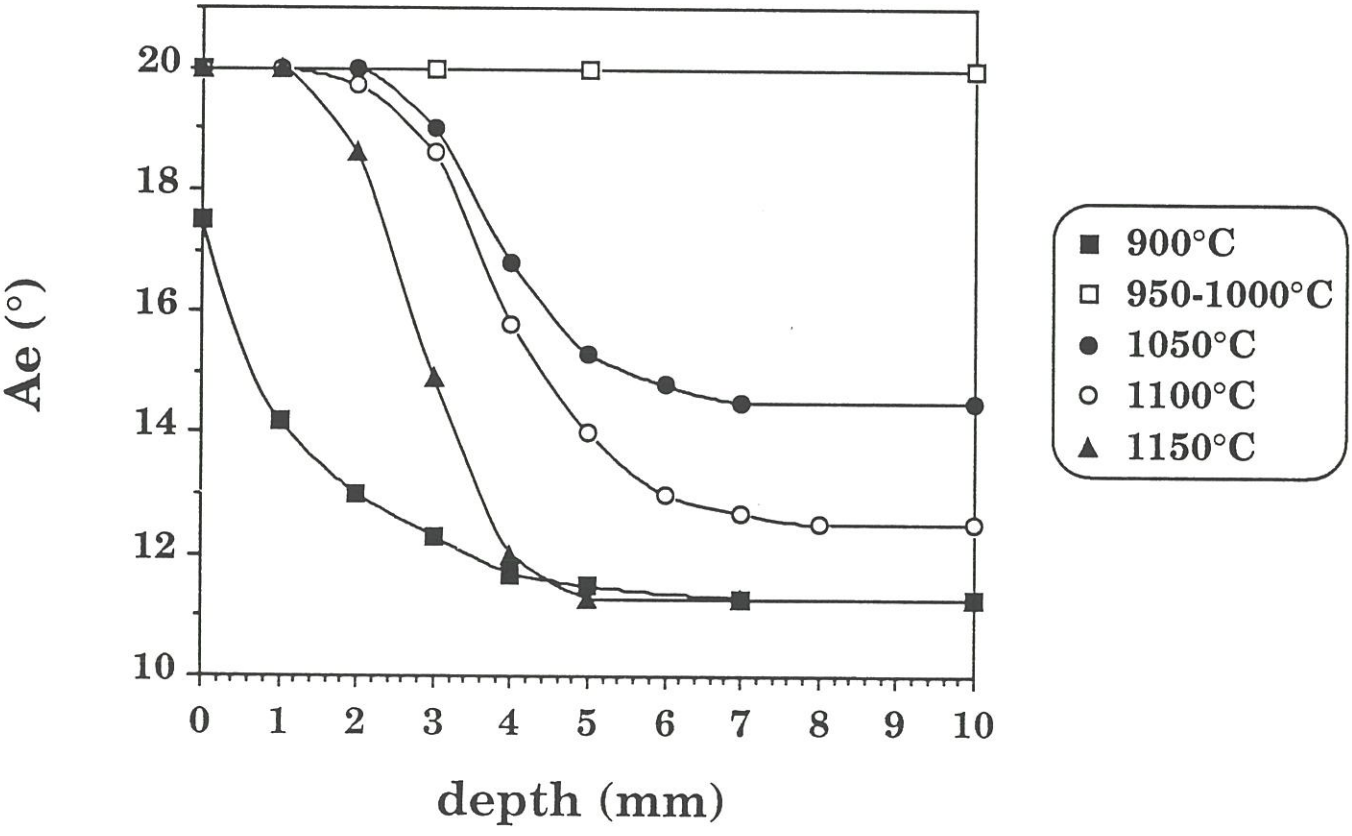

Fig. 5 : Extinction angle vs depth in the pore (60 μm large). Conditions are P=3 kPa and t_R =10 s. The different plots are drawn for different temperatures.

curves observed previously for the low residence times (figs. 3 and 4). The same profile (17° down to 13°) is observed even in the largest pore (320 μm) for the same run. This means that the effect of the geometric factor is not concerned. At this temperature or pressure, chemical reactions are not completed.

- **950-1000°C**. The profiles observed in this range of temperatures appear as optimized : **the profile is flat with the best texture (Ae=20°) all along the pore (small or large). That means achieving infiltration conditions for texture-controlled pyrocarbon.** This experience was reproduced at different times (for both temperatures 950°C or 1000°C). In the larger pore (320 μm) this optimized window is even larger, i.e. the same flat profile can be seen in the 950-1100°C range. The gradient (i.e. from 20° at the surface (z=0) down to 16° at the center (z=10)) is seen again at 1150°C for the larger pores.

In short, there is a set of peculiar conditions (950< T<1000°C, P=3 kPa) for which the use of P-CVI (t_R=10 s) enables one to minimize the geometric effect of the porosity. Thus, the control on the highly ordered texture deep inside the porosity is maximized.

In the same range of temperature (e.g. T=950°C), t_R was allowed to vary from 0.5 s to 60 s (fig. 6). An optimum reaction time is necessary to produce in the gas phase the species able to diffuse inside the porosity and condense correctly on the surface. For the longer residence times, a degradation of the deposit ordering is observed inside the pore. So this mechanism needs a weak but necessary gas phase "maturation".

- **1050°C-1150°C**. In the 60 μm pore, the aspect ratio of the pore is such that the rate is diffusion- limited : 50°C is sufficient to get out of the window (compared to 100°C for the 320 μm pore). The profile recovers the bell-like shape (fig. 5). As

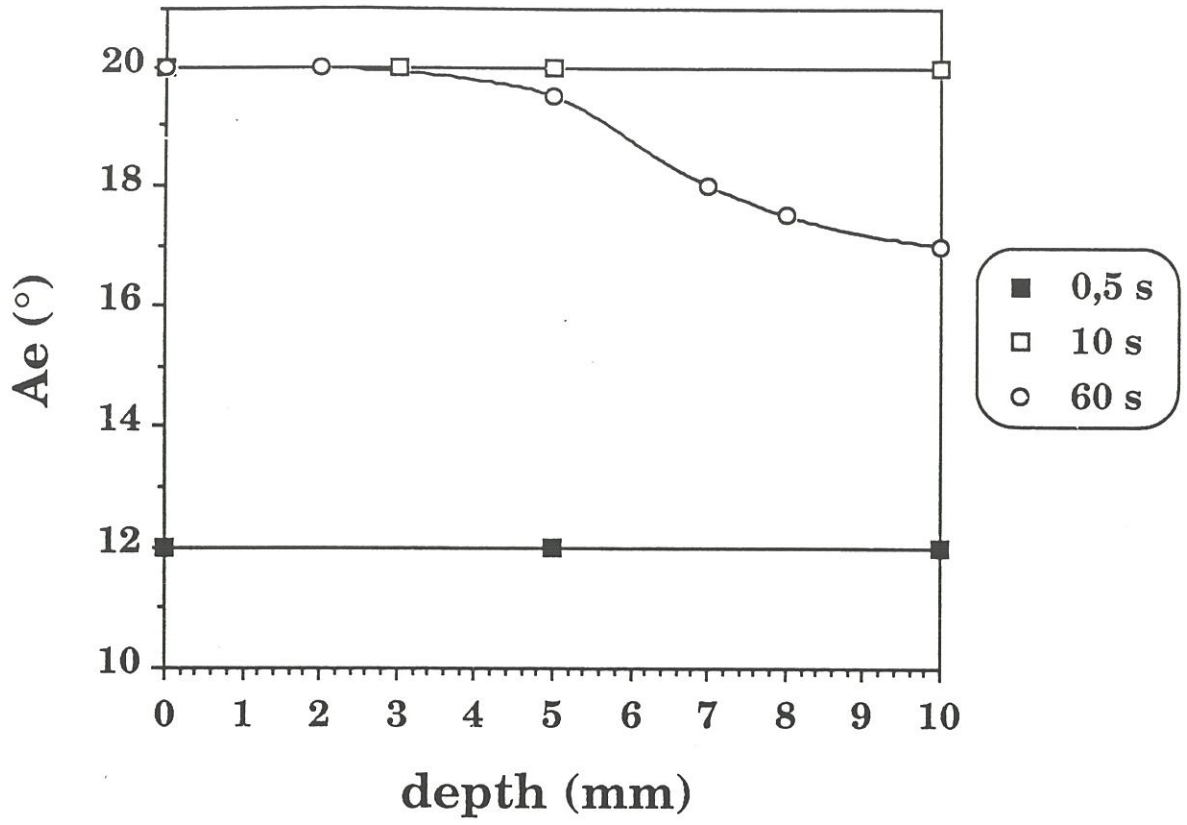

Fig. 6 : Ae profiles in the 60 µm-model pore for different residence times for T=950°C and P=3 kPa.

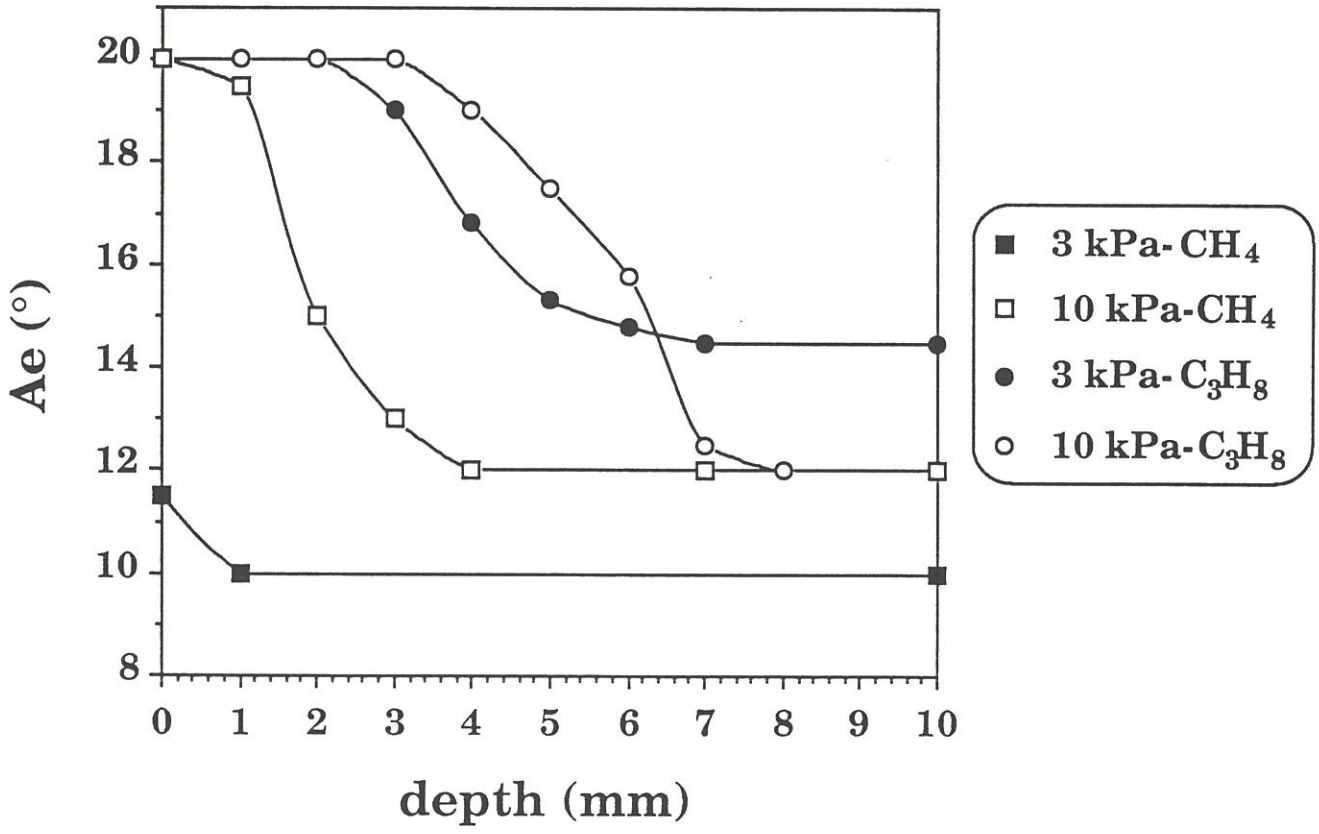

Fig. 7 : Ae profiles in the 60 µm-model pore for different total pressures and gas precursors for T=1050°C and t_R =10 s.

the temperature increases the gradient is increasing too. In the middle of the pore (z=10), Ae is equal to 15° at 1050°C, 13° at 1100°C and finally 11.5° at 1150°C.

In short, the **P-CVI control on the PyC-anisotropy inside the porosity** is an important result. Pulse duration is seen acting as a residence time, but being controlled in a much larger range as compared to the I-CVI process. Its main interest is to achieve the right completion of the gas phase reactions with time at low temperatures and/or pressures. Under these conditions, the mean free path is increased and the geometric effect of the porosity minimized. The choice of the right precursor was suspected to play a role in achieving the right maturation of the gas phase. That is the object of the following section.

3.3- Influence of gas nature on anisotropy

First, **methane** which is characterized by a high H/C atomic ratio (H/C=4) was used in the same temperature range. Profiles observed at 1050°C and P=3 kPa or 10 kPa are plotted in fig. 7 with those obtained for **propane** C_3H_8 (H/C=2.7) under the same deposition conditions. With CH_4, the PyC-texture cannot be obtained in depth with a high anisotropy.

Secondly, **propylene** C_3H_6 was used (H/C=2). Ae profiles are plotted in fig. 8 with those observed under close conditions with propane. It is appearing that **the optimized profile is observed 50°C lower with C_3H_6, i.e. at 900°C, with respect to 950°C for C_3H_8.** Thus, it is expected that infiltration is enhanced just by using a precursor with a lower H/C ratio and/or a better configuration to produce aromatic pyrocarbogenic species.

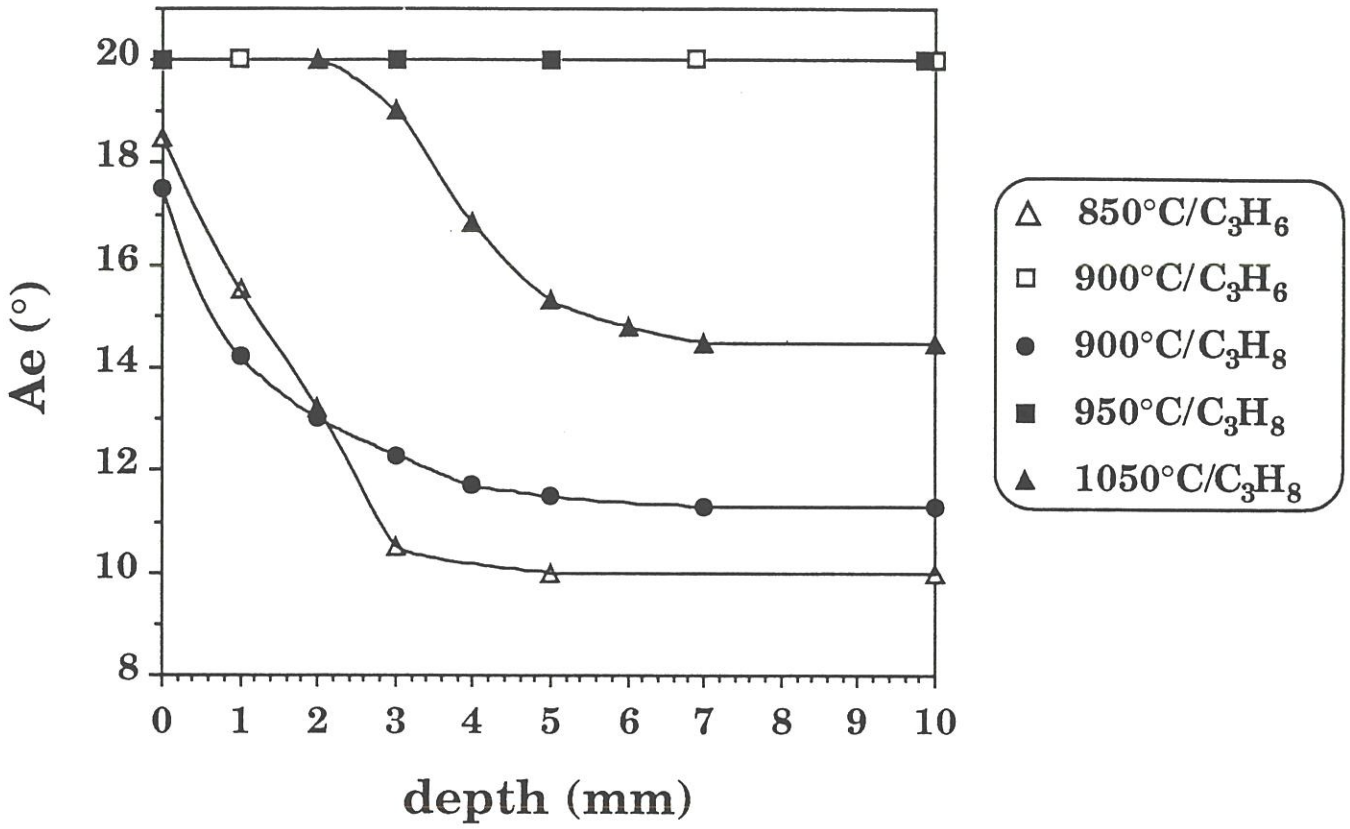

Fig. 8 : Ae profiles along the 60 μm-model pore as a function of temperature and gas nature for P=3 kPa and t_R =10 s.

3.4-TEM study of the optimized pyrocarbon

The texture of the PyC obtained under the optimized conditions (T=1000°C, P=3 kPa and t_R=10 s) was characterized at the nano/micro scale by TEM, using the lattice fringes technique. fig. 9a shows that the PyC deposit is highly anisotropic but also characterized by a good close-packing. There is no porosity (i.e. needle-like pore). The structure of the layers are characterized first by a **large layer diameter L_2** (up to 15 nm, see arrows). Data obtained on the carbon layers are reported in table 1.

The mean layer diameter $\bar{L}_2$ is 4 nm (line 1, table 1) , L_1 is about 1 nm whereas $\bar{N}$ is 3.1. **Such diameters are quite high for a low temperature pyrocarbon. The growth mechanism is obviously a lateral growth of the layers.** This means that the large layers are built up in-place by the surface reaction of little aromatic units and small species homogeneously produced in the gas phase. The second feature of this carbon is also related to its **low temperature deposition**. The coherent lengths of this turbostratic order (i.e. La and Lc) are very reduced. It is worthy of note that the resultant anisotropy, with less coherence and more distorted layers, is only related to the high L_2 diameter. As a comparison, fig. 9b shows the structure of a regular "columnar" PyC obtained by processuss II in I-CVI. In this last case, L_2 is smaller but N is much higher (see arrows).

3.5- The control of residence time on layer structure

Three samples obtained at the entrance of the pore (z=0) were selected for being deposited at same temperature (1050°C), same C_3H_8 total pressure (1 kPa) and increasing residence time : 0.5 s, 10 s and 30 s. The extinction angle

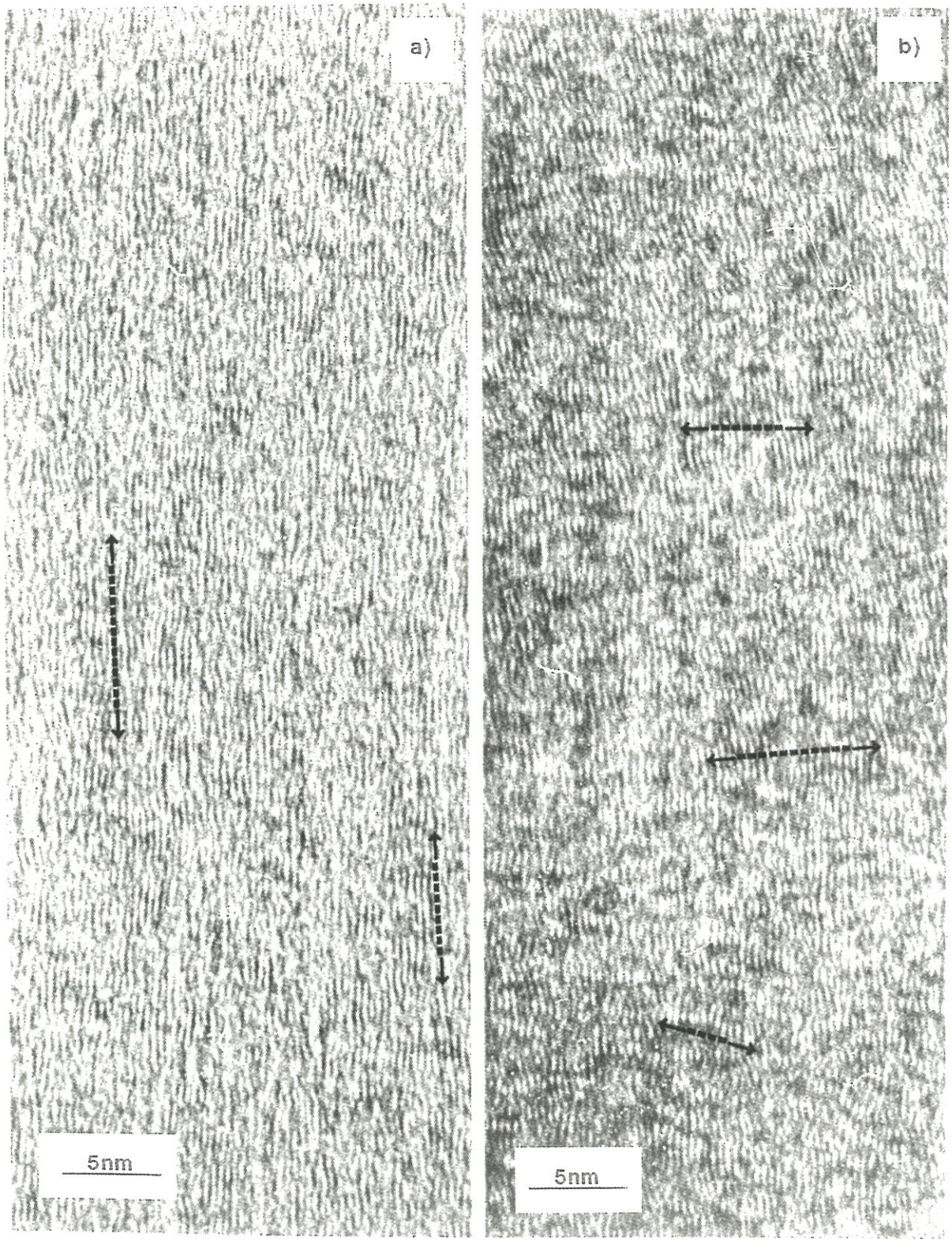

Fig. 9 : a) Structure of the optimized PyC deposited by P-CVI : arrows show the lateral extension of the fringes and b) structure of a regular anisotrope PyC as obtained by I-CVI (or P-CVI process II) with a columnar structure, for comparison (arrows show the columns).

process	experimental conditions				sampling	$\overline{L_1}$ (nm)	L_{2max} (nm)	$\overline{L_2}$ (nm)	$\overline{N}$	Ae (°)
	P (kPa)	T (°C)	Dp (s)	Q (sccm)						
P-CVI	3	1000	10	---	entrance	1	15	4.0	3.1	20
P-CVI	1	1050	0.5	---	entrance	0.7	4.5	1.9	2.5	12
P-CVI	1	1050	10	---	entrance	0.8	8	2.9	3.1	20
P-CVI	1	1050	30	---	entrance	0.8	6	1.9	2.6	14
P-CVI	1	1050	10	---	entrance	0.8	8	2.9	3.1	20
P-CVI	1	1050	10	---	3 mm-deep	0.9	7	2.2	3.8	18
P-CVI	1	1050	10	---	center	0.8	4	1.9	2.5	15
I-CVI	4.7	1050	---	40	entrance	0.85	6	2.3	4.8	20
I-CVI	4.7	1050	---	40	3 mm-deep	0.65	5	1.9	2.6	15
I-CVI	4.7	1050	---	40	center	0.7	5	2.0	2.2	11

Table. 1 : Structural data for the different carbons analysed by TEM.

increases from Ae=12° for the shortest duration up to 20° for the optimum of 10 s. Under this low pressure, the anisotropy decreases again for long durations, say 30 s. Those variations are only controlled by the residence time.

- t_R=0.5 s (Ae=12)

The residence time is low. The nano-texture of this carbon is illustrated in fig. 10 a. The carbon layer stack is characterized by $\bar{L}_2$=1.9 nm and $\bar{N}$=2.5 (line2, table 1). The only main difference with respect to the optimized PyC (T=1000°C, P=3 kPa and t_R=10 s) is L_{2max}=4.5 nm, consistant with a low Ae=12° as compared to 8 nm at 10 s. The absence of large layers, even in small amount, is responsible for the lost of preferred orientation.

- t_R=10 s (Ae=20°)

The carbon deposited is highly anisotropic: this is apparent in fig. 10 b.. The close-packing is also very high. It is noticeable that the L_2 diameter is large : 2.9 nm in average, up to 8 nm for the largest (line 3, table 1). The higher coherent lengths and the lower L_2 values indicate that the growth mechanism is essentially columnar. This mechanism is characterized by the direct deposition of **large aromatic molecules**. As a consequence, the layer diameter L_2 is lower but the layer itself is better organized as compared to the lateral mechanism. Thus the stacking, N, is higher.

The carbon observed for t_R=10 s should be composed in fact as a sequence: first, a thin layer of poorly organized carbon is expected, then highly organized carbon; in the reality, it is difficult to distinguish any sequence within the deposit. On the contrary the whole deposit is homogeneous.

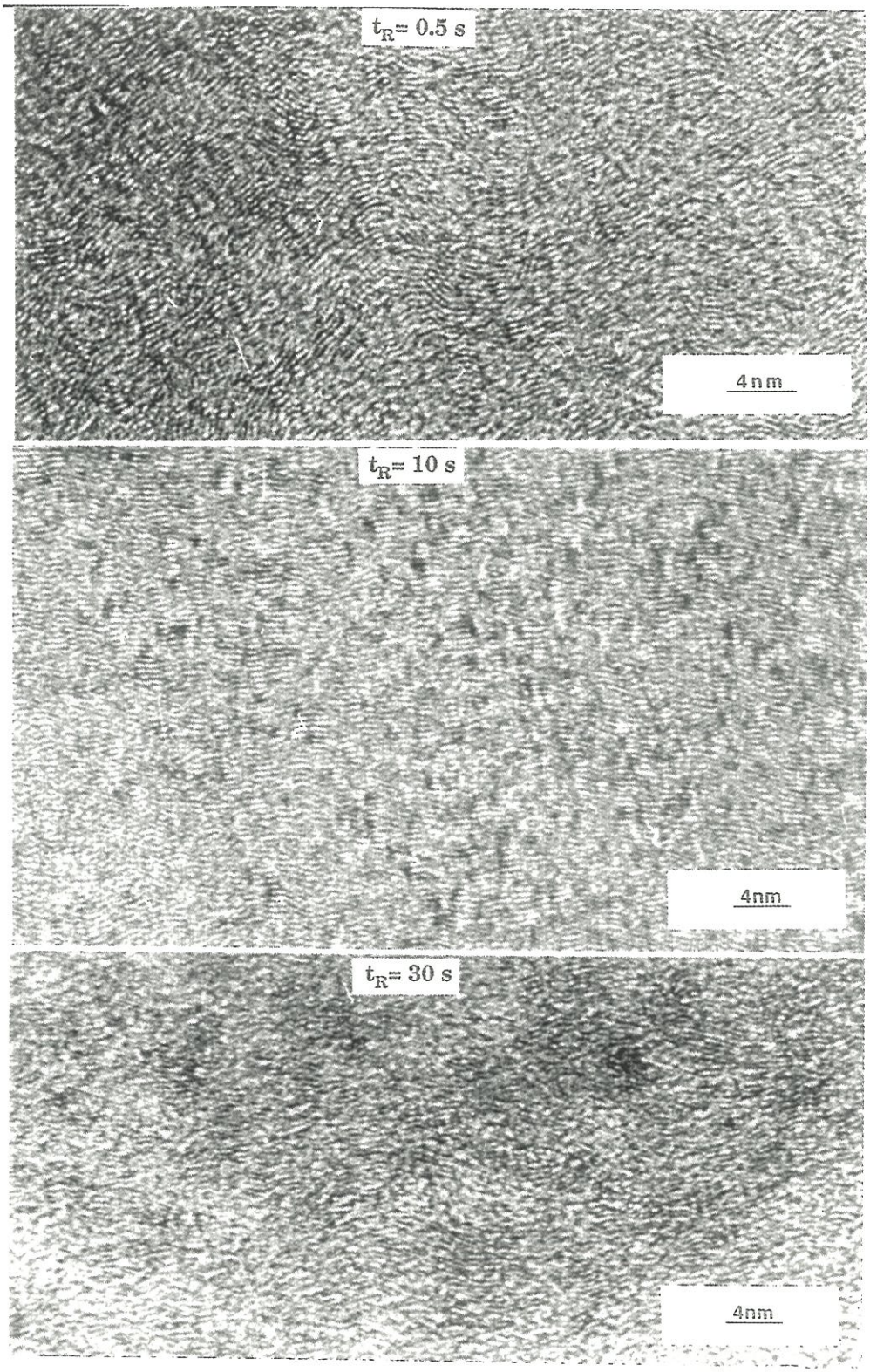

Fig. 10 : TEM lattice fringes of the pyrocarbon obtained by P-CVI at the external surface for T=1050°C; P=1 kPa and various residence times.

- t_R=30 s (Ae=14°)

The organization of the carbon is shown in fig. 10 c. The high anisotropy is lost as compared to t_R= 10 s. Such a pyrocarbon is characterized by lower $\bar{L}_2$ and $\bar{N}$ values (line 4, table 1). It is worthy of note that the size of the largest layers measured in this case is smaller than for the 10 s residence time : 6 nm compared to 8 nm.

Because this sample is deposited under the same conditions than the previous one except that the residence time is not 10 s but 30 s, it could be expected that the deposit get similar during the 10 first seconds then different for the rest of the pulse. As a matter of fact, there is clearly no sequence in the deposit, also the large layers observed for a 10 s residence time (8 nm) are no more present after a long residence time : the pyrocarbon is clearly homogeneous in the bulk.

3.6- Infiltration disturbance in the porosity (P-CVI).

The pore infiltrated with a 10 s pulse (T=1050°C, P=1kPa) was sampled at z=0; z=3 and z=10 mm. Ae (and thus the anisotropy) decreases from 20° at the entrance (z=0) down to 15° in the middle of the pore (z=10) (table 1). fig.11 a-c shows the ordering of the carbon. The data (line 5-7, table 1) point out a decrease of $\bar{L}_2$ as well as a decrease of $L_{2max.}$ from 8 nm to 7 nm down to 4 nm in the middle. The decrease of Ae with the infiltration depth, z, is clearly connected to the layer size decrease. The control of the layer size on the preferred orientation, as measured by Ae, is the same as previously shown for the surface deposition (CVD). As for $\bar{N}$, first it is significantly increasing from 3.1 up to 3.8 as the size decreases: in others words, it is easier to stack small

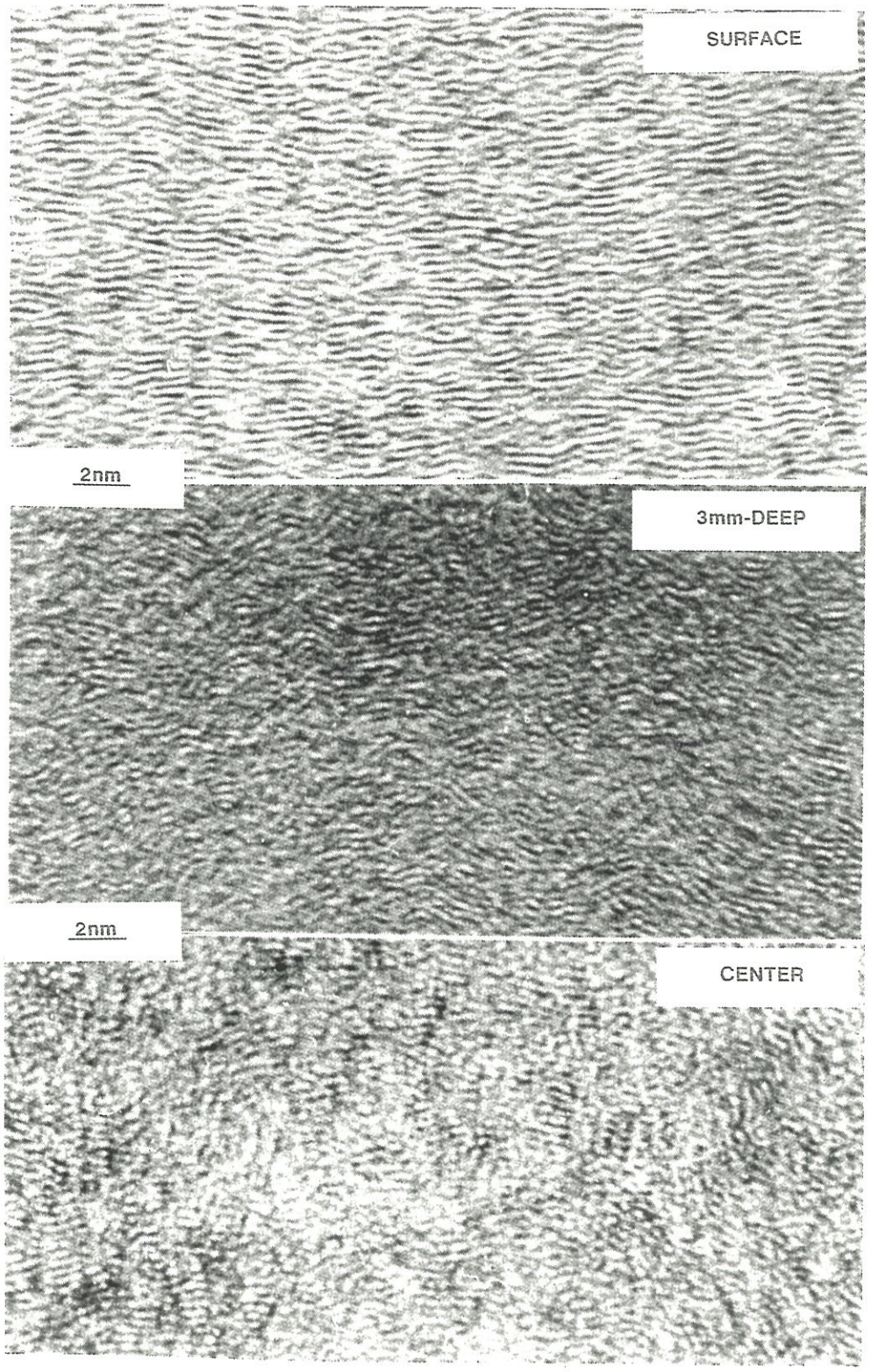

Fig. 11 : TEM lattice fringes of the pyrocarbon obtained by P-CVI in the 60 μm model pore for T=1050°C; P=1 kPa and t_R=10 s. (a) entrance of the pore : Ae=20°, (b) about 3 mm-deep inside the pore : Ae=17°, (c) at the center of the pore : Ae=12°.

layers ones upon the others.Then it drops down with the smaller layer size at the center of the pore (2.5).

3.7 Pyrocarbon deposited from C_3H_8 in I-CVI.

It is of interest to compare the layer organization obtained by the regular I-CVI process, under optimized conditions, with regard to the P-CVI process. The conditions selected were : T=1050°C, P=4.7 kPa and Q (C_3H_8)=40 sccm. The smaller infiltrated pore was sampled at z=0 (Ae=20); z=3 (Ae=15.5) and z=10 mm (Ae=11). fig. 12 a-c shows the degradation of the carbon ordering with the infiltration depth.

At the pore entrance (z=0), the pyrocarbon deposited in I-CVD is different : the layer size, $\bar{L}_2$ (2.3 nm) is not as large as in P-CVD but $\bar{N}$ is far more larger (4.8). The growth is columnar based on better ordered units : layers are less distorted.

The contrast with infiltration is important (z=3 and 10 mm, figs 12. b-c). There is only a slight difference in the $\bar{L}_2$ values. Those were recognized to be important for the long range orientation in P-CVI. The only large variations are $\bar{N}$ and $\bar{L}_1$. As the units are smaller, and more defectuous (L_1) the ability to stack coherently is diminished and the anisotropy is lost.

The same level of anisotropy is observed in I-CVI as in P-CVI with a different turbostratic ordering. As the growth mechanism gives rise to smaller layers, even with C_3H_8 as precursor [15], a better ordering of the layer is needed. This is achieved at higher temperatures with a columnar carbon : N, the number of layers in the pile is higher, a sign of layer ordering [16,10]

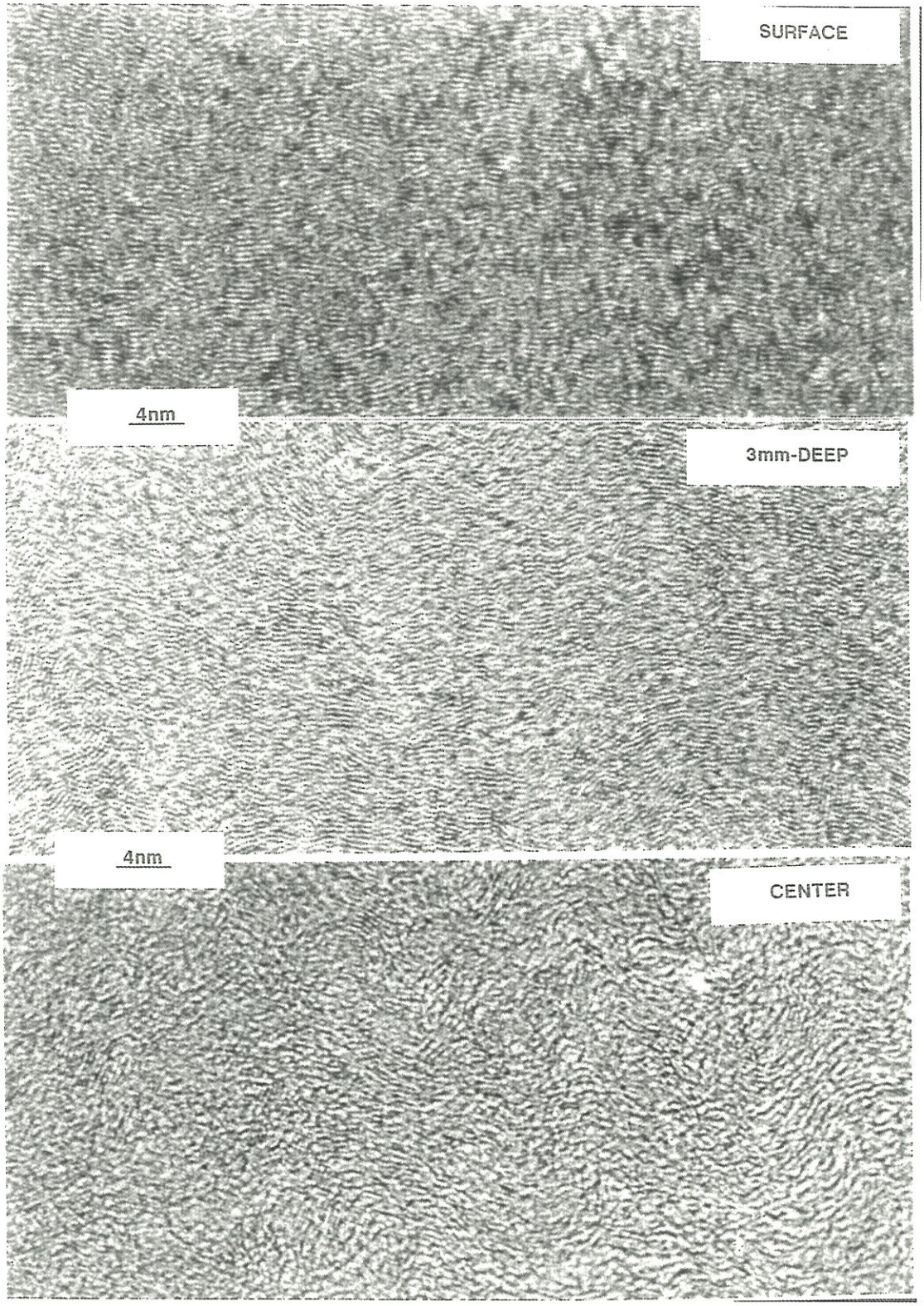

Fig. 12 : TEM lattice fringes of the pyrocarbon obtained by I-CVI in the 60 μm model pore for T=1050°C; P=4.7 kPa and Q=40 sccm : (a) entrance of the pore : Ae=20°, (b) about 3 mm-deep inside the pore : Ae=15°, (c) at the center of the pore : Ae=12°.

5- DISCUSSION

Residence time, t_R, in P-CVI is a macroscopic variable which controls the **gas phase maturation** and thereafter the pyrocarbon texture and infiltration. In previous works [11, 12], two different stages were recognized: a very short convectional start and then a long and complex diffusional phase. At the beginning of the pulse, a convectional transport forces the mother gas phase to penetrate the porosity. This stage lasts a few hundredths of second. The PyC thickness deposited is probably uniform inside the porosity but carbon yield is very low. Moreover, it necessitates a high pulse frequency.

During the diffusionnal stage, a continuum of processes is observed. In order to be clear this continuum is divided in **three different processes** depending on the reaction duration, i.e. the gas phase maturation.

(i) A first process was recognized (process I [11]). It is occurring for the lower residence time or low temperature/pressure conditions. It is characterized by a good infiltration and the higher deposition rates.

(ii) The second stage is a process occurring at longer residence times, i.e. for a more complete gas phase maturation (process II [11]). The growth rate is high at the surface and infiltation is limited. This is the process usualy described in closed vessel, as for example by Chen and Back [17].

(iii) At last, a third process is characterized by a low rate and its better capability of infiltrating the porosity. It ends up with an equilibrium of the gas phase which is poisoned by a high H_2 pressure.

Depending on which species are formed in the gas phase as t_R is increased, either a lateral or a columnar growth mechanisms were observed.

(i) When the residence time is of few tenths of a second to few seconds (according to P, T), the situation is typically equivalent to a short residence time in I-CVI. The chain reactions, say cracking, cyclisation, *etc...* are not completed. Molecules produced in the gas phase could be **low molecular weight radicals highly hydrogenated**. The kinetic study [11] has shown that the deposition rate is high and the process highly thermally activated : heterogeneous reactions are rate-limiting and controlling the growth of PyC. The carbon deposited is probably very hydrogenated; it contains a lot of defects. In this case, the preferred orientation remains poor (dark laminar). At low pressures, the texture observed all over the porosity is very homogeneous and the deposit gradient minimized. As soon as the pressure (or temperature) increases the process I duration is shortened: gas phase reactions go on, species nature changes and thereafter deposition mechanism changes too (process II). If the pressure is increased (P=3kPa) but the temperature lowered (T=950°C), it is possible to enhance these transient conditions with a longer residence-time (t_R=10s). Under these conditions texture is optimized (anisotropy). The mechanism is still of the processus I-type : infiltration is rather good, deposit gradients are minimized but now the pyrocarbon is highly oriented. The growth mechanism itself is lateral: the layers built up by reaction on the surface of low molecular species. The layer size of this pyrocarbon was observed to be as large as 15nm. As the carbon layer remains very large inside the porosity, it is thought that the species developing under those optimized conditions, and which condense on the surface, are easily diffusing inside the porosity. The use of C_3H_6 as mother precursor enhances the mechanism either because of the lower hydrogen content or because of the molecular structure. At the end of the pulse, the pressure falls off during the vacuum stage. The

dehydrogenation step is thus suspected to accelerate rapidly at that time. As a consequence carbon could undergo a re-arrangement.

(ii) For intermediate residence times, the gas phase maturation goes on. The growth is referred to as the process II. It is characterized by a high deposition rate at the surface (z=0 mm) with a high preferred orientation. In the pores, as the porosity diameter decreases the rate and the preferred orientation decrease as well. The deposition mechanism of process II can be tentatively described following, for a large part, the mechanism proposed by Chen and Back [17] : cyclisation and aromatisation have completed and then, large (planar) molecules are concentrating in the gas phase. Preferred orientation and growth rate match very well because the higher the aromaticity the easier the "electrostatic" deposition. The growth mechanism is columnar. Thereafter, these planar molecules stack preferencially at the surface (z=0 mm), the amount of defects is low and the preferred orientation is high. On the other hand, in the porosity diffusion is the limiting process. It is suspected that only the cyclic or small aromatic molecules are allowed to diffuse; as a consequence, the deeper the diffusion inside the porosity, the lower the growth rate and the preferred orientation. Dehydrogenation is not critical at the surface because the large aromatic species are well stacked one on the other. On the contrary, inside the porosity dehydrogenation is very important to ensure a long distance orientation. Precisely, this dehydrogenation looks too limited, then layers are more distorted and the preferred orientation is reduced.

(iii) For longer residence times, deposition conditions change again: a third process is happening. Once again, deposition mechanism is controlled by the gas phase composition. As noticed by Kassel [18] and Dupel et all [11], the

hydrogen content of the gas phase increases with time and lowered the deposition rate. Depositing rates decrease and in the same time infiltration is enhanced regarding process II. This is because diffusion is enhanced by the lower concentration gradients, then infiltration is increased but in the meantime the rate is lowered. Texture degradates inside the porosity, whatever the pressure and temperature conditions as t_R increases. This also supports the assumption that the species developing in the gas phase with the third process are more hydrogenated. The surface reaction itself which is more or less suspected to be a de-hydrogenation process, get inhibited by the high H_2 partial pressure. Those last deposits, plus those of next process I (following pulse) are bad enough to limit the texture of the process II in between. This is systematically true inside the porosity and at low pressures (and low temperatures) at the surface only. As a result, sequence were rarely evidenced, only the texture of the dominant deposited carbon is observed. Deposition ends up after a while; gas phase reactions get rapidly inhibited by the increasing H_2 partial pressure like in all classical static systems.

6-CONCLUSIONS

This work shows the capability of P-CVI to grow different types of pyrocarbon and also its capability to control the homogeneity of the texture (anisotropy) inside the porosity. A continuum of different processes occurs. Among them, at low residence times, one is able to grow large diameter carbon layers with a high preferred orientation and to infiltrate such carbon layers in small pores. This can be obtained by controlling the gas phase reactions at low temperatures and growing the carbon by a lateral growth mechanism (process

I of P-CVI). This carbon looks like smooth laminar but Ae falls in the range of the rough laminar (20°, whereas graphite has theoretically the same value : 19.5°). This apparent descreapency is due to the fact that the pyrocarbon is obtained with a real **high anisotropy** but at a **low temperature** without a high crystallinity (L_a, L_c).

The structural results obtained in this work, especially at low temperatures, already indicate that P-CVI of carbon is a promising alternative to achieve infiltration of complex preforms with a highly oriented pyrocarbon.

ACKNOWLEDGEMENTS

This work has been supported by SEP (through a grant given to P.D). The authors are indebted to M. Alrivie for samples preparation and C. Robin-Brosse from SEP for fruitful discussions.

REFERENCES

[1] J.C. Bokros, "The structure of carbon deposited in a fluidized bed", Carbon, **3,** 17 (1965).

[2] M.L. Lieberman, "Chemical vapor deposition of carbon : kinetic process in methane pyrolysis", Internal report Sandia Lab. Albuquerque, NM, SLA-74-0233 (1963).

[3] T. Jachlewski and R.J. Diefendorf, "Chemical vapor of carbon matrices", Proceed. 15th biennial Conf. on Carbon, (American Carbon Society, eds), 284 (1981).

[4] P. Loll, P. Delhaes, A. Pacault and A Pierre, "Diagramme d'existence et propriétés de composites carbone-carbone", Carbon, **15**, 383 (1977).

[5] K. Hedden and E. Wicke, Proc. 3d Int. Conf. on Carbon, (American Carbon Society, eds.) 249 (1957).

[6] R.L. Beatty, "Gas pulse impregnation of graphite with carbon", J. Nucl Applications & Technology., **8**, 488 (1970).

[7] K. Sugiyama and Y. Ohzawa, "Pulse chemical vapor infiltration of SiC in porous or SiC particulate preform using an r.f. heating system", J. Mat. Sc. Let. , **25**, 4511 (1990).

[8] S.V. Sotirchos and M. Tomadakis, "Modelling tranport, reaction, and pore structure evolution during densification of cellular or fibrous structures, Chemical Vapor Deposition of Refractory Metals and Ceramics", (T.M. Besmann and B.M. Gallois, eds), MRS, Pittsburgh, p. 73 (1990).

[9] R.J. Diefendorf and E. W. Tokarsky, "The relationships of structure to properties in graphite fibers", Air Force report AF 33(615)-70-C-1530 (1971).

[10] X. Bourrat, "Electrically conductive grades of carbon blacks : structure and properties", Carbon, (1993), in print.

[11] P. Dupel, R. Pailler and F. Langlais, "Pulse chemical vapor deposition (P-CVD) and infiltration (P-CVI) of pyrocarbon in model pores with rectangular cross section : Part 1 - Study of the pulsed process of deposition", Submitted to J. Mat. Sciences.

[12] P. Dupel, R. Pailler and R. Naslain, "Pulse chemical vapor deposition (P-CVD) and infiltration (P-CVI) of pyrocarbon in model pores with rectangular cross section, Part 2 - Study of infiltration", Submitted to J. Mat. Sciences.

[13] P. Dupel, R. Pailler, F. Langlais, R. Naslain and A. Costecalde, "CVD/CVI of pyrocarbon from propane on flat substrates and in model pores with rectangular croos-sections", Submitted to Carbon.

[14] F. Doux, "Les carbones en lumière polarisée", (1989) SEP internal report MC 949308 - FD/1f.4.

[15] M.H. Back and R.A. Back, "Thermal decomposition and reaction of methane", in "Pyrolysis : Theory and Industial Practice", pp. 1-24, **1,** (L.F. Albright, B.L. Crynes and W.L. Corcoran, eds), Academic Press Inc, (1983).

[16] A. Oberlin, "Carbonization and graphitization", Carbon, **22** [6] 521 (1984).

[17] C.J. Chen and M.H. Back, "The simultaneous measurement of the rate of formation of carbon and hydrocarbon products in the pyrolysis of methane", Carbon, **17**, 175 (1979).

[18] L.S. Kassel, "The thermal decomposition of methane", J. Amer. Chem. Soc., 54, 3949 (1932).

Chapître 5 : INFLUENCE D'INTERPHASES PYROCARBONE DEPOSEES PAR CVI PULSEE SUR LES CARACTERISTIQUES MECANIQUES DE MATERIAUX COMPOSITES UNIDIRECTIONNELS

Le dernier chapitre est consacré à une étude des propriétés mécaniques de composites unidirectionnels C/PyC/SiC et SiC/PyC/SiC présentant une interphase PyC déposée par I-CVI ou par P-CVI. Les interphase sont déposées à l'aide du même appareillage, et les conditions expérimentales de dépôt (P,T) sont voisines. L'épaisseur de l'interphase PyC P-CVI a été optimisée dans le cas des composites SiC/PyC/SiC.

L'emploi d'une interphase P-CVI a permis d'obtenir de meilleures propriétés mécaniques. Une étude par microscopie électronique à transmission a permis de mettre en évidence le rôle particulier de l'anisotropie de l'interphase P-CVI.

Ce chapitre présente les résultats de cette étude sous forme d'un projet de publication adressée au Journal de Physique III.

soumis au Journal de Physique III.

INFLUENCE D'INTERPHASES PYROCARBONE DEPOSEES PAR CVI PULSEE SUR LES CARACTERISTIQUES MECANIQUES DE MATERIAUX COMPOSITES UNIDIRECTIONNELS

P. Dupel, J.L. Bobet, R. Pailler et J. Lamon
Laboratoire des Composites thermostructuraux
UMR-47 CNRS-SEP-UB1, Domaine Universitaire
3, allée de La Boëtie, 33600-Pessac, France.

RESUME

Il a été montré que la CVI pulsée (P-CVI) permet de réaliser de manière controlée des dépôts de Pyrocarbone (PyC) à microstructure anisotrope. Aussi, était il intéressant d'élaborer des composites unidirectionnels SiC/PyC/SiC et C/PyC/SiC, possédant ce type d'interphase et de comparer leur propriétés mécaniques à celles de composites semblables à interphase PyC déposée par CVI. Les résultats de tests en traction ont montré :

(i) un accroissement notable des caractéristiques mécaniques lié à l'utilisation de P-CVI,

(ii) que l'optimun d'épaisseur de l'interphase PyC (P-CVI) est de l'ordre de 0,2 μm dans le cas de composites unidirectionnel SiC/PyC/SiC,

(iii) qu'il est possible de corréler les caractéristiques mécaniques , d'une part, avec les contraintes résiduelles d'origine thermique créées lors de

l'élaboration des CMC et dépendant notamment de l'épaisseur de l'interphase, et d'autre part, à la nature plus orientée du PyC déposé en P-CVI.

MOTS CLE

CMC, interphase pyrocarbone, propriétés mécaniques, CVI pulsée.

1- INTRODUCTION

Les composites à matrice céramique renforcée par des fibres longues sont une classe de matériaux prometteurs [1]. L'introduction d'un renfort fibreux leur confère un caractère endommageable. Différents mécanismes d'endommagement interviennent alors - tels la multifissuration matricielle, la décohésion fibre-matrice, le glissement et le frottement des fibres vis à vis de la matrice aux interfaces, et le déchaussement des fibres rompues [2] - et permettent d'obtenir des caractéristiques mécaniques intéressantes. Cependant, l'existence de ces mécanismes d'endommagement est conditionnée par la qualité de la liaison fibre-matrice. Dans le cas d'une liaison trop forte, aucun des phénomènes cités plus haut n'est observé et le comportement mécanique est purement fragile. Par contre, une liaison trop faible limite les transferts de charge à l'interface et ne permet qu'une faible libération d'énergie par décohésion ce qui se traduit par une contrainte à rupture faible associée à une déformation à rupture élevée. Afin d'optimiser les transferts de charge, et d'obtenir une contrainte et une déformation à rupture élevées, un troisième constituant est souvent déposé entre les fibres et la matrice : l'interphase.

Les matériaux d'interphase les plus fréquemment utilisés sont le pyrocarbone [3] et le nitrure de bore hexagonal [4]. Ces deux matériaux possédent des caractéristiques très voisines : (i) une faible rigidité (≈50GPa) comparée à celles des autres constituants du composite et (ii) une structure lamellaire fortement anisotrope. De plus, l'épaisseur de l'interphase joue un rôle important sur les propriétés mécaniques du composite comme l'ont montré Ménessier et al [5] dans le cas d'un composite SiC/vitrocéramique ou

Lowden et Stinton [6] et Naslain [7] dans le cas de composites ex-PCS/PyC/SiC testés respectivement en flexion et en traction .

La méthode la plus couramment employée pour déposer une interphase est l'infiltration chimique en phase vapeur (CVI). Cette méthode se traduit le plus souvent par l'obtention d'une interphase de qualité plus ou moins controlée dans l'épaisseur [8].

Dupel et coll ont montré que la P-CVI de carbone à partir de propane conduit, selon les conditions expérimentales, à un contrôle de la microstructure et de l'épaisseur du PyC déposé et ceci même au sein de pores modèles [9-10].

L'objectif de ce travail est double : d'une part, évaluer les caractéristiques mécaniques de composites unidirectionnels dont l'interphase PyC a été déposée soit par I-CVI, soit par P-CVI, et d'autre part, définir dans le cas d'interphases PyC (P-CVI) l'optimun en épaisseur conduisant aux caractéristiques mécaniques maximales.

2- PROCEDURE EXPERIMENTALE

2.1- Préparation des composites unidirectionnels

Les matériaux composites unidirectionnels ont été réalisés à partir de deux types de mèches : (i) des mèches de fibres de carbone T300[1] composées de 1000 filaments, et (ii) des mèches de fibres ex-PCS[2] composées de 500 filaments. L'élaboration se décompose en 4 étapes successives :

---

(1) fournies par la SEP-Bordeaux
(2) Nicalon NL202 de NIPPON Carbide

- (i) le maintien en tension des mèches de 50 mm de longueur sur des cadres en graphite par une colle céramique,

- (ii) le désensimage des mèches par pyrolyse à 500°C sous vide pendant 4 heures,

- (iii) le dépôt de l'interphase pyrocarbone à partir de propane selon des procédures décrites par ailleurs [9,11]. Quelle que soit la méthode, le PyC a été déposé sous une pression de 3 kPa et une température de 1000°C. En I-CVI le débit est égal à 60 sccm, et en P-CVI la durée du palier est égale à 10 s, le nombre de pulses varie selon l'épaisseur de l'interphase (e_i) déposée (20 pulses pour $e_i \approx 0,05$ nm, 800 pulses pour $e_i \approx 1000$ nm). Les fig. 1 et 2 montrent à titre d'exemples des interphases déposées par P-CVI sur des fibres de carbone et de Si-O-C ex-PCS (la matrice, à ce stade, n'est pas encore déposée).

- (iv) le dépôt par I-CVI de la matrice SiC sur les mèches dans un four industriel(3) [12].

Le tableau 1 donne les différentes valeurs de l'épaisseur de l'interphase pyrocarbone déposée au sein des mèches SiC/PyC/SiC et C/PyC/SiC, ainsi que les pourcentages volumiques moyens de fibre (V_f), de matrice (V_m), d'interphase (V_i) et le nombre de mèches testées. Les diamètres des fibres de carbone (d=7 µm) et ex-PCS (d=14 µm) sont supposés constants. La section moyenne de la mèche a été déterminée par pesée en considérant que la porosité résiduelle est nulle (fig. 3).

---

(3) selon un procédé développé par la S.E.P

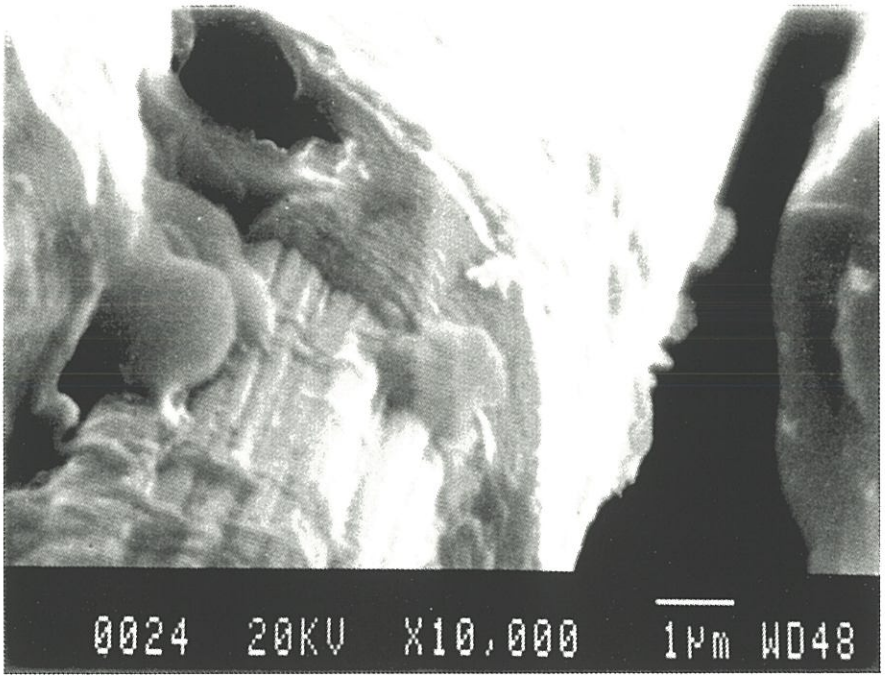

Fig. 1 : Observation au MEB de l'interphase pyrocarbone I-CVI sur une fibre carbone T300 (lot C).

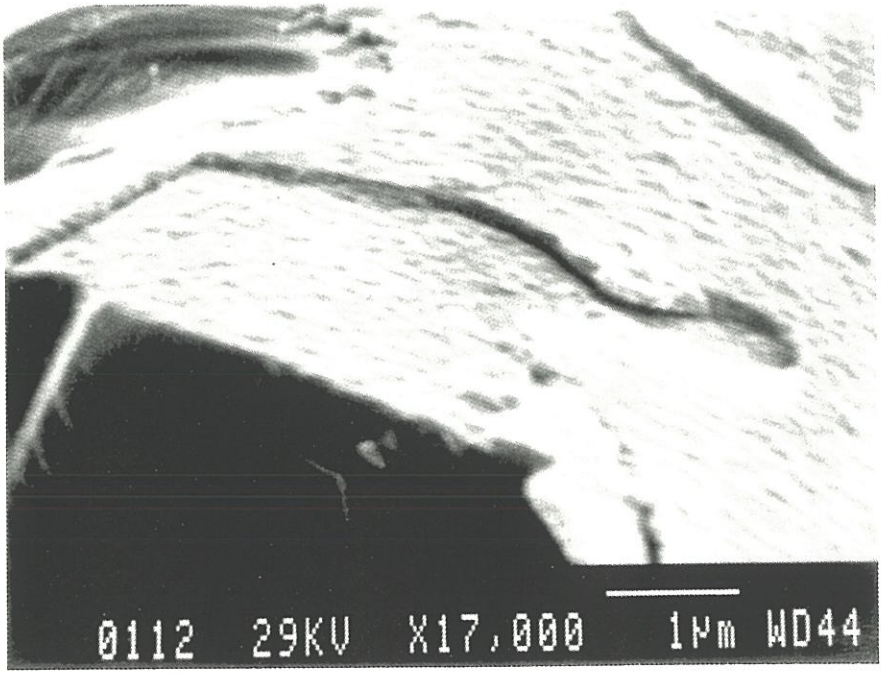

Fig. 2 : Observation au MEB de l'interphase pyrocarbone P-CVI sur une fibre ex-PCS (lot E).

lot	type de fibre	mode de dépôt	épaisseur * interphase (μm)	V_f (%)	V_m(%)	V_i (%)	N
A	C	P-CVI	0,5	44,8	42,3	12,9	10
B	"	"	1,0	38,6	37,2	24,2	22
C	"	I-CVI	1,0	39	37,0	24,0	17
D	ex-PCS	P-CVI	0,05	64,3	35,5	0,2	9
E	"	"	0,09	65,7	32,8	1,4	15
F	"	"	0,12	56,3	41,3	2,4	18
G	"	"	0,22	47,0	49,4	3,6	18
H	"	"	1,0	57,9	32,2	9,8	9
I	"	I-CVI	0,1	62,4	36,5	1,0	10

*** mesures réalisées au MEB à effet de champ N : nombre de composites unidirectionnels testés**

Tableau.1 : Epaisseur de l'interphase pyrocarbone, mode de dépôt, et pourcentages volumiques moyens de matrice, de fibres, et d'interphase de chacun des lots.

Fig. 3 : Observation au MEB. d'une mèche composite (T300/PyC/SiC, lot C).

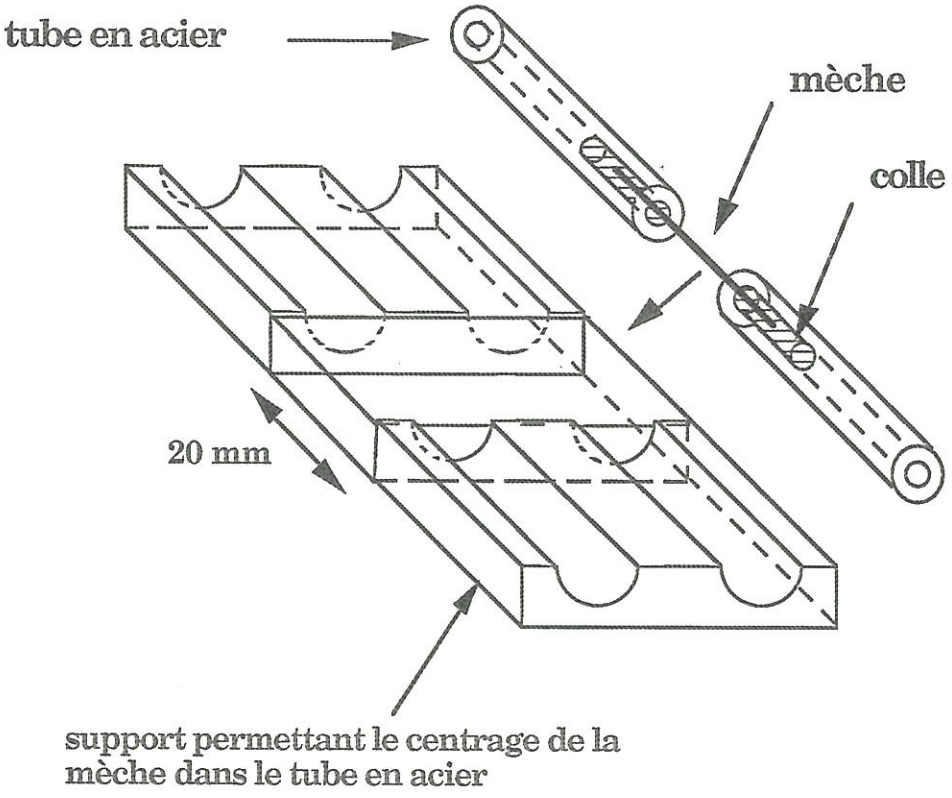

Fig. 4 : Technique de collage de la mèche.

2.2- Essais mécaniques

2.2.1- Procédure d'essai de traction

Les extrémités des mèches ont été collées dans des tubes en acier selon une technique permettant un centrage précis de l'échantillon (fig. 4). La longueur de jauge est de 20 mm. Les tubes en acier ont été serrés dans les machoires de la machine de traction. Les essais ont été menés avec une vitesse de déplacement constante de 0,1 mm/min. Un capteur de déplacement monté sur les mors permettait de mesurer l'élongation des mèches.

2.2.2- Exploitation des résultats

Les principales caractéristiques mécaniques du composite telles les contraintes et déformations à la limite élastique, à saturation de la fissuration matricielle et à rupture ont été déduites de la courbe force-déplacement enregistrée lors de chaque essai de traction

La contrainte à rupture est calculée de deux façons :

(i) en rapportant la force à rupture à la section totale de la mèche, en supposant que la matrice contribue à supporter les efforts (σr_1),

(ii) en rapportant la force à rupture à la section totale des fibres seulement, en supposant que ce sont elles qui supportent l'essentiel de l'effort lorque le processus de fissuration matricielle a atteint la saturation (σr_2), et que le nombre de fibres qui se sont rompues avant la rupture est négligeable devant le nombre total de fibres au sein de la mèche.

Pour chacun des lots, la dispersion statistique des contraintes à rupture σr_1 a été décrite par l'analyse statistique de Weibull [13].

Les propriétés de l'interphase ont été caractérisées par (i) le pas de fissuration de la matrice à saturation, d_s, mesuré soit par microscopie optique(4) sur des échantillons enrobés et polis, soit au MEB(5) sur des mèches après rupture en traction (figs. 5 et 6) et (ii) la contrainte de cisaillement interfacial τ_c qui refléte les transferts de charge entre les fibres et la matrice. τc a été déduite du pas de fissuration de la matrice d_s à saturation grâce à l'équation suivante proposée par Marshall [14],

$$\tau_c = \frac{\sigma_s . r_f}{4 . v_f . d . (1 + \frac{E_f V_f}{E_m V_m})} \qquad (1)$$

où V_f et V_m sont respectivement les fractions volumiques de fibre et de matrice, r_f est le rayon de la fibre ($r_{f\ carbone}$=3,5 µm, $r_{f\ SiC}$=7,5 µm), E_f le module d'Young de la fibre ($E_{f\ carbone}$=200 GPa, $E_{f\ SiC}$=180 GPa), Em le module d'Young de la matrice (E_m=400 GPa) et σ_s la contrainte à saturation déterminée à partir de la courbe force-déplacement. Cette formule donne une estimation acceptable et comparative des propriétés interfaciales, compte tenu que les fissures créées dans la matrice traversent les échantillons dans toute leur largeur. Les valeurs obtenues pour τc sont satisfaisantes pour comparer les interphases entre elles.

---

(4) MeF_3 de REICHERT-JUNG
(5) JEOL 840

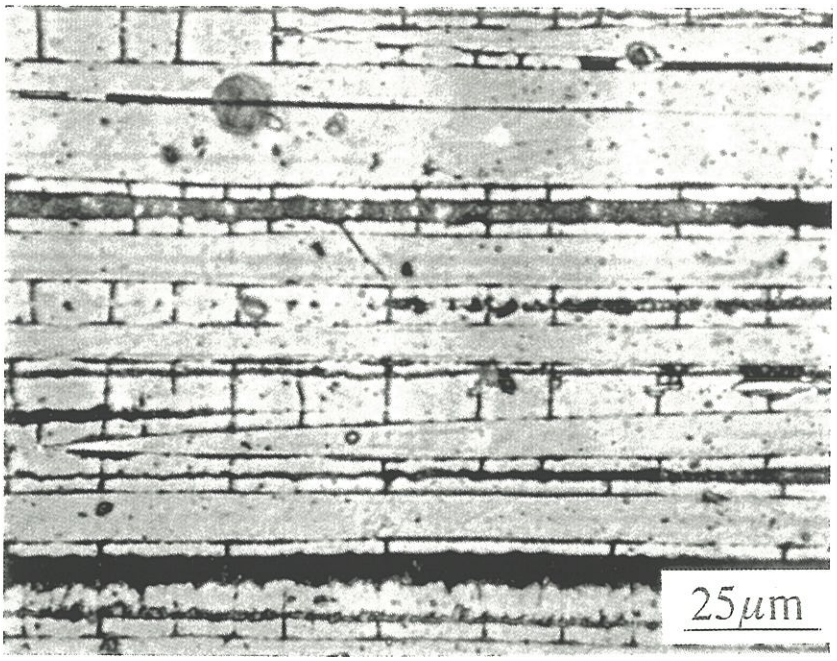

Fig. 5 : Observation au microscope optique du pas de fissuration sur une mèche après rupture en traction (T300/PyC/SiC, lot C).

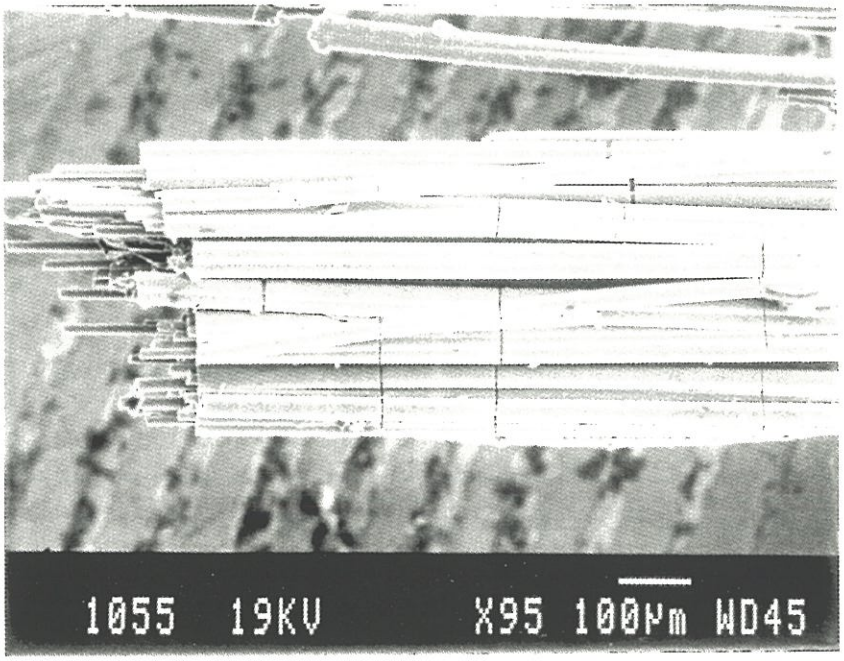

Fig. 6 : Observation au MEB. du pas de fissuration sur une mèche après rupture en traction (fibre ex-PCS/PyC/SiC, lot E).

3- RESULTATS ET DISCUSSION

3.1- Composites unidirectionnels C/PyC/SiC

3.1.1- Analyse des courbes contrainte-déplacement

Les courbes types contrainte-déplacement relatives à chacun des lots de C/PyC/SiC sont présentées à la figure 7. Les éprouvettes des trois lots montrent le comportement classique des composites à matrice fragile. Trois domaines sont présents sur les courbes :

(i) un domaine linéaire élastique de faible importance car la matrice est endommagée après élaboration et avant essai en raison de la différence des coefficients de dilatation axiaux ($\alpha_{a\ matrice}$-$\alpha_{a\ fibre}$=4,6 E-6) et radiaux (-15 E-6 <$\alpha_{r\ matrice}$-$\alpha_{r\ fibre}$<-20 E-6) de la matrice et de la fibre,

(ii) un domaine non linéaire induit par la fissuration de la matrice,

(iii) un domaine linéaire dans la dernière partie de la courbe résultant de la déformation des fibres dans la région des fissures matricielles. A noter que lors de la quasi totalité des essais de traction, l'état de saturation matricielle a été atteint.

Les composites appartenant au lot C (I-CVI) se distinguent de ceux des lots A et B (P-CVI) par une déformation et une contrainte à rupture plus faibles. L'emploi d'une épaisseur de PyC (P-CVI) plus importante pour le lot B par rapport au lot A permet d'accroître légèrement déformation et contrainte à rupture.

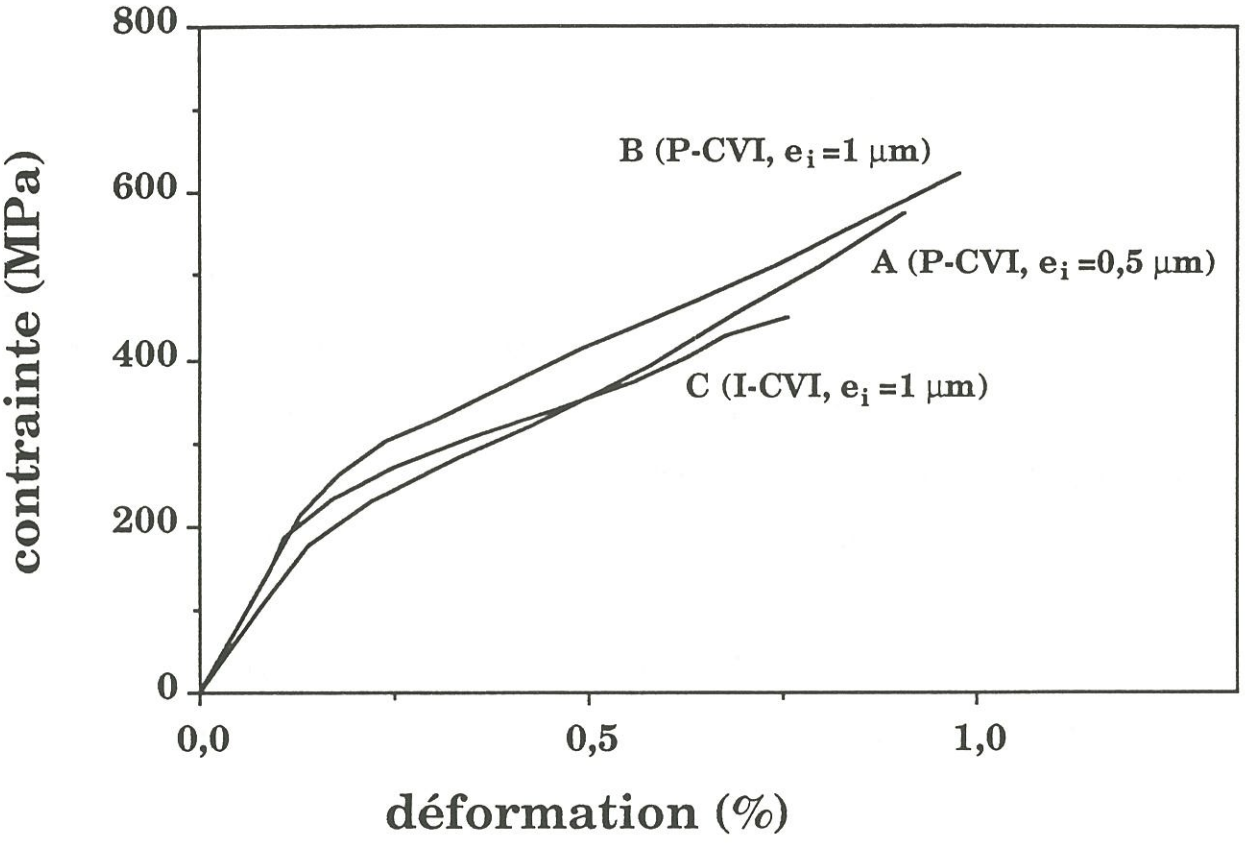

Fig. 7 : Courbes types de comportement en traction des lots A,B,C (fibres carbone/PyC/SiC).

3.1.2- Propriétés interfaciales

Les valeurs moyennes des grandeurs mécaniques calculées à partir des courbes force-déplacement sont reportées au tableau 2.

Les caractéristiques mécaniques moyennes des mèches du lot B (P-CVI, e_i=1µm) sont supérieures à celles des mèches du lot A (P-CVI, e_i=0,5µm), mais de façon peu significative : la variation d'épaisseur de pyrocarbone entre les deux lots P-CVI influe peu sur les caractéristiques mécaniques des mèches C/PyC/SiC testées en traction. Cependant, le lot B présente une dispersion plus faible (module de Weibull des contraintes à rupture plus élevé).

Les différences essentielles entre ces deux lots de mèches résident dans les caractéristiques des interphases, d_s et τc. En effet, le passage de e_i= 0,5 µm à e_i=1 µm se traduit par une diminution du pas de fissuration et un accroissement de la contrainte de cisaillement interfaciale (tableau 2). Cet effet peut être attribué à l'influence de l'épaisseur de l'interphase sur les contraintes résiduelles après élaboration. Une simulation numérique [15] basée sur une adaptation du modèle de Eshelby [16] a permis le calcul des contraintes résiduelles d'origines thermiques dans le cas de microcomposites C/PyC/SiC (fig. 8) en respectant les épaisseurs moyennes de matrice et d'interphase mesurées sur les lots A, B et C. Les valeurs des grandeurs mécaniques (E_1=12 GPa, E_3=30 GPa et G=2 GPa) de l'interphase PyC (P-CVI) ont été considérées, en première approximation, identiques à celles de l'interphase PyC (I-CVI). L'utilisation de microcomposites à la place de mèches conduit à négliger l'effet des fibres voisines, ce qui a une influence essentiellement sur le calcul des contraintes résiduelles radiales. Toutefois, le raisonnement tenu par la suite prend en compte cet effet.

lot	σ_{r1} (MPa)	m	σ_{r2} (MPa)	σ_e (MPa)	σ_s (MPa)	ε_e %	ε_s %	ε_r %	ds (µm)	τ_c (MPa)
A (P-CVI, e_i=0,5 µm)	570 [107]	5,9	1374 [216]	150 [62]	415 [78]	0,09 [0,03]	0,55 [0,11]	0,90 [0,12]	90	13,3 [2,1]
B (P-CVI, e_i=1 µm)	605 [85]	9,3	1621 [167]	164 [21]	319 [53]	0,13 [0,03]	0,46 [0,12]	1,0 [0,17]	30	32,5 [6,7]
C (I-CVI, e_i=1 µm)	416 [85]	6,2	1133 [216]	132 [34]	305 [32]	0,09 [0,03]	0,51 [0,10]	0,78 [0,25]	50	20,3 [2,1]

[ ] écart type

Tableau. 2 : Résultats des lots A,B,C (fibres carbone T300/PyC/SiC).

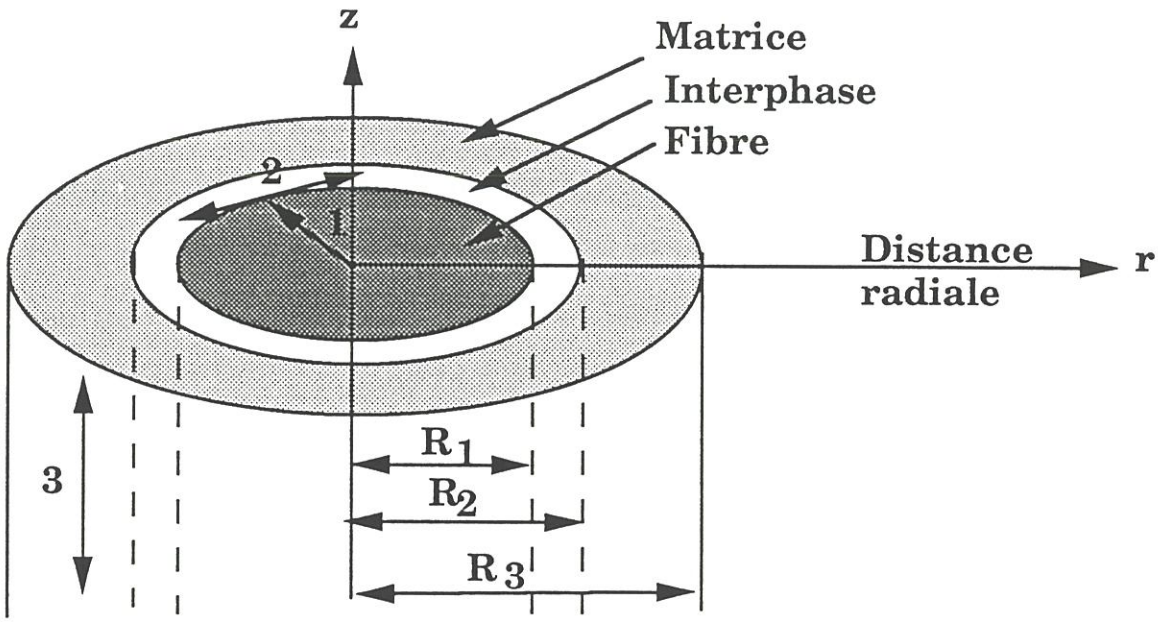

1 = Contraintes radiales (σ^R)

2 = Contraintes circonférentielles (σ^H)

3 = Contraintes longitudinales ou axiales (σ^A)

Fig. 8 : Représentation schématique d'un microcomposite et directions principales des contraintes résiduelles d'origine thermique.

La fig. 9 présente les variations des contraintes résiduelles calculées dans le cas de deux microcomposites C/PyC/SiC d'épaisseurs d'interphase e_i=0,5 µm (fig. 9 a) et e_i=1 µm (fig. 9 b).

La contrainte longitudinale σ^A dans la matrice diminue lorsque e_i augmente. Celle-ci est donc soumise à une contrainte de tension d'autant plus faible que e_i est élevée, ce qui permet d'augmenter la limite d'élasticité ε_e entre les lots A et B (tableau 2). Toutefois, l'interphase étant peu rigide, cet effet est assez faible, la contrainte longitudinale dans la matrice passant de 260 MPa à 210 MPa lorsque e_i passe de 0,5 µm à 1 µm.

L'étendue de la zone d'endommagement est fonction des contraintes résiduelles radiales σ^R et circonférentielles σ^H. Les contraintes résiduelles radiales conduisent à un frettage de la fibre lorsqu'elles sont négatives ou à une décohésion fibre/interphase lorsqu'elles sont positives. Quelle que soit la valeur de e_i, σ^R est positive (traction) dans l'interphase et est d'autant plus élevée que e_i est faible. La décohésion fibre/interphase sera donc moindre (d_s plus petit) et les transferts de charge meilleurs (τ_c plus élevée) lorsque e_i=1 µm. Toutefois, la variation du pas de fissuration observée (d_s est multiplié par trois lorsque e_i passe de 1 µm à 0,5 µm) ne peut être expliquée uniquement par la variation de σ^R qui augmente de 20 % lorsque e_i diminue.

Les valeurs moyennes des caractéristiques mécaniques des mèches du lot C (I-CVI, e_i=1 µm) sont plus faibles et plus dispersées (module de Weibull plus faible) que celles du lot B (P-CVI, e_i=1 µm). (Pour le lot C , $\bar{\sigma}_{r1}$=416 MPa alors que pour le lot B, $\bar{\sigma}_{r1}$=605 MPa, soit une différence de 45 %).

La comparaison du comportement mécanique de ces deux lots suggère que **l'interphase produite par P-CVI est plus souple**. En effet, malgré un pas de fissuration plus faible et corrélativement une contrainte interfaciale plus forte

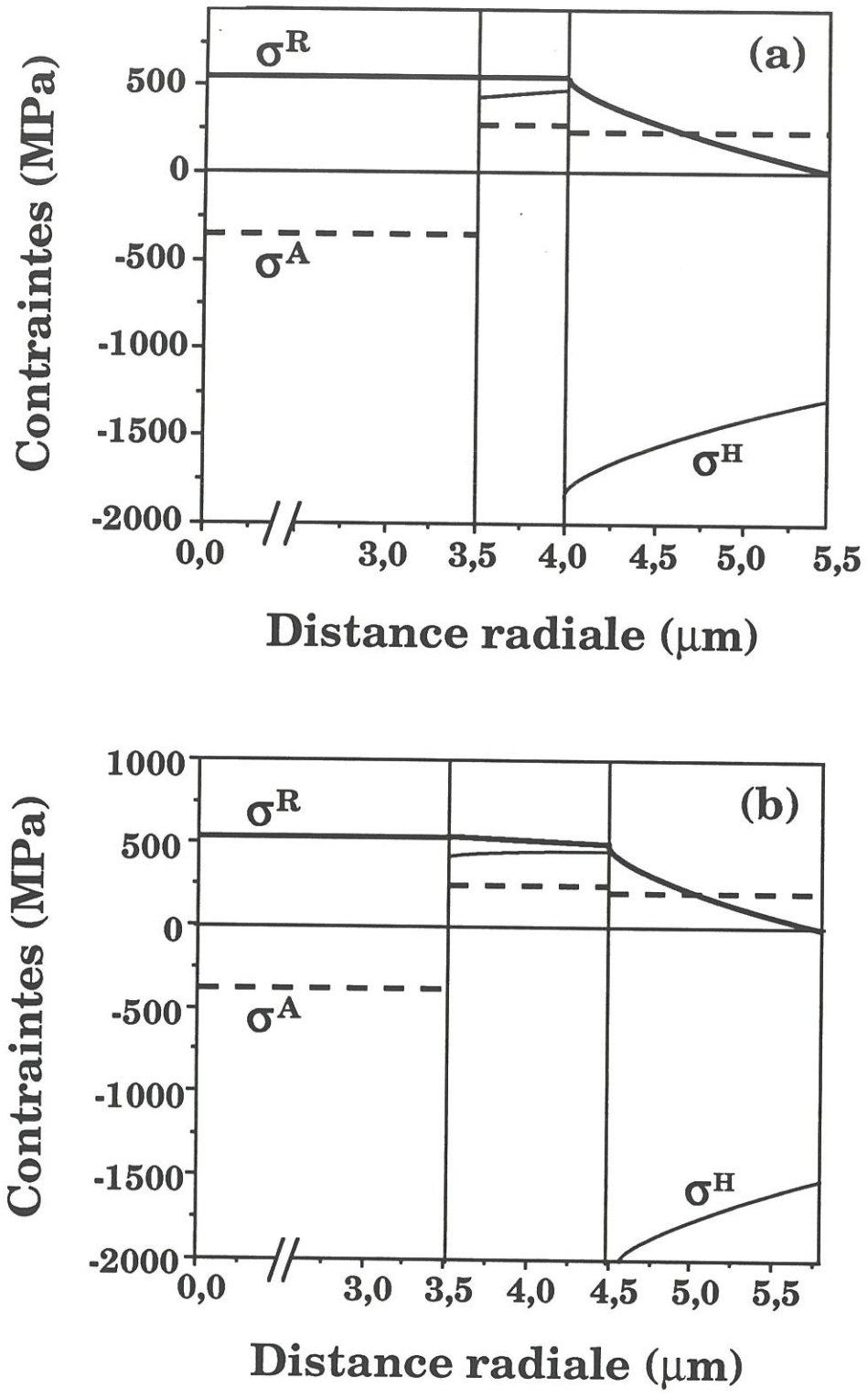

Fig. 9 : Comparaison entre la distribution des contraintres résiduelles d'origine thermique pour des microcomposites C/PyC/SiC (a) e_i=0,5 μm et (b) e_i=1 μm.

pour les mèches du lot B, celles-ci se déforment davantage que les mèches du lot C.

Les calculs de contraintes résiduelles effectués sur des microcomposites possédant les mêmes épaisseurs d'interphase et de matrice que les mèches du lot C indiquent que les performances de ce lot devraient être voisines voire supérieures à celles des mèches du lot B, ce qui est en opposition avec les résultats expérimentaux. Ceci conduit à penser que les valeurs des grandeurs thermomécaniques de l'interphase PyC (P-CVI) sont différentes de celles de l'interphase PyC (I-CVI). Afin de corréler les résultats expérimentaux et les calculs théoriques, il est nécessaire d'augmenter l'anisotropie des modules d'Young de l'interphase PyC (P-CVI) ($E_3/E_1 \approx 4,0$, alors que pour l'interphase PyC (I-CVI) $E_3/E_1 \approx 2,5$). La variation des contraintes résiduelles radiales avec e_i serait alors plus importante et expliquerait la forte variation de d_s lorsque e_i diminue. Cette différence s'explique par la différence d'organisation du PyC obtenu en P-CVCI et en I-CVI. En effet, une étude précédente [11] a montré que en P-CVI, dans les conditions utilisées, l'organisation des couches de carbone est latérale (fig. 10 a). Dans ce cas, la taille des couches peut être très importante même si la cohésion suivant l'axe c reste faible (voir flèches). Par contre en I-CVI la croissance est colonnaire (flèches, fig. 10b).

La structure latérale du PyC (P-CVI) permettrait à la fibre de se déformer plus aisément au niveau des régions situées entre les zones de décohésion interfaciale (de longueur l), où elle est cependant liée à la matrice (fig. 11).

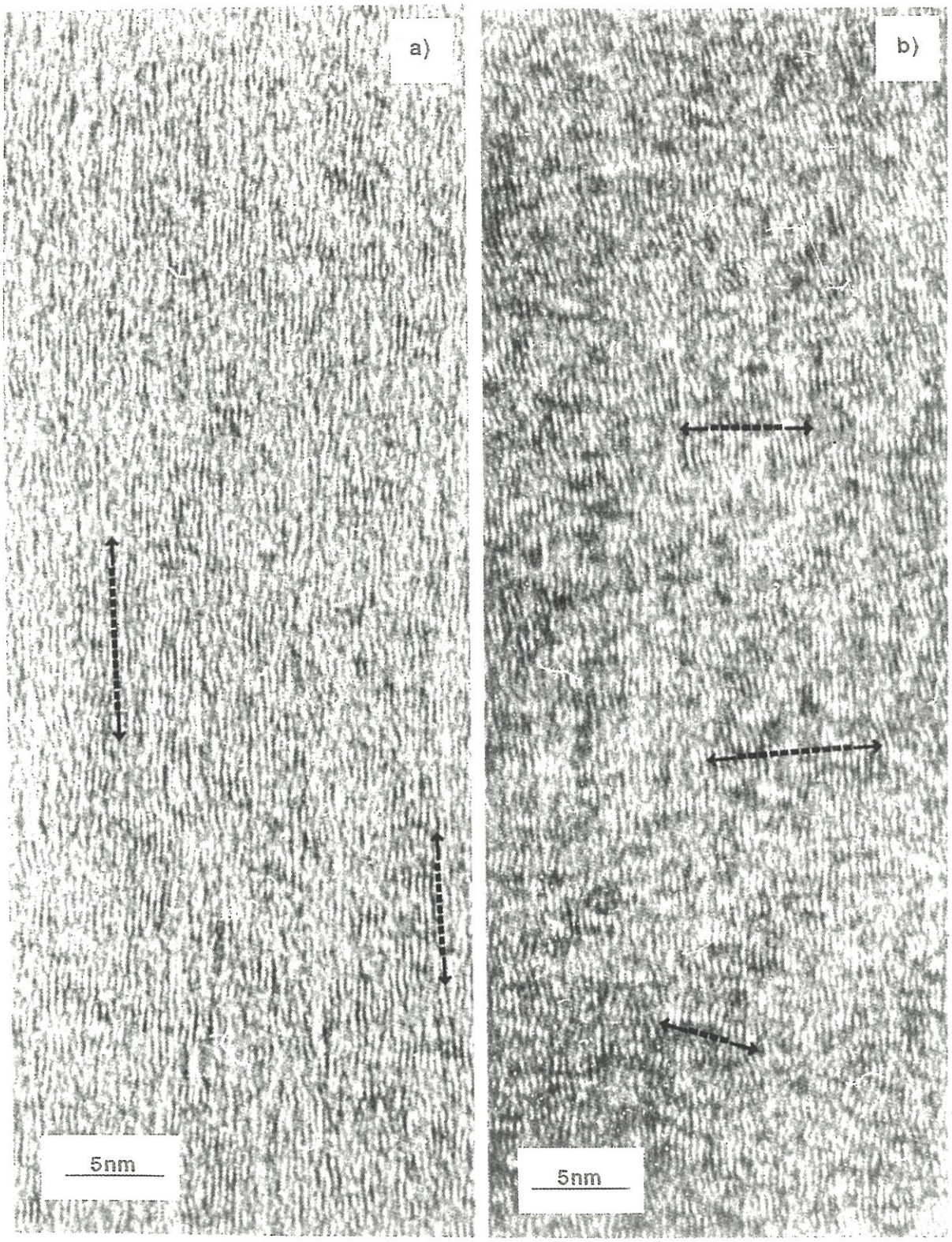

Fig. 10 : Comparaison de la structure des PyC obtenus en I-CVI et P-CVI : (a) I-CVI, T=1050°C, P=4.7 kPa et Q=40 sccm (montrant une croissance colonnaire) et (b) P-CVI T=1000°C, P=3 kPa et t_R=10 s (montrant une croissance latérale).

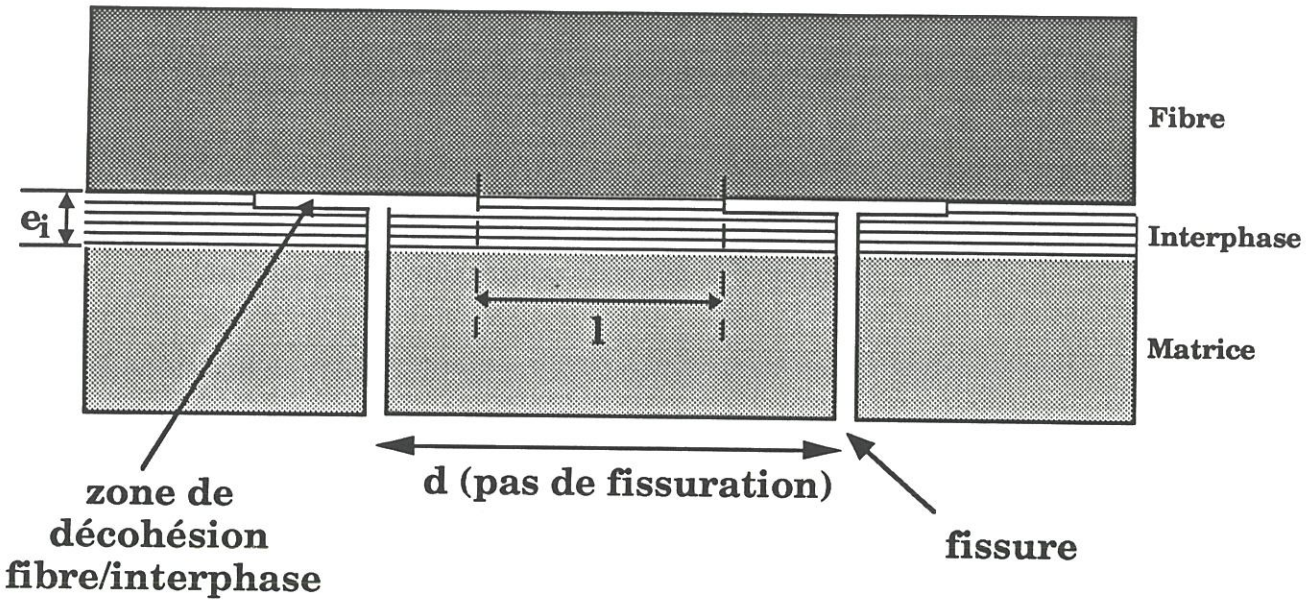

Fig. 11 : Schéma de la rupture interfaciale à saturation.

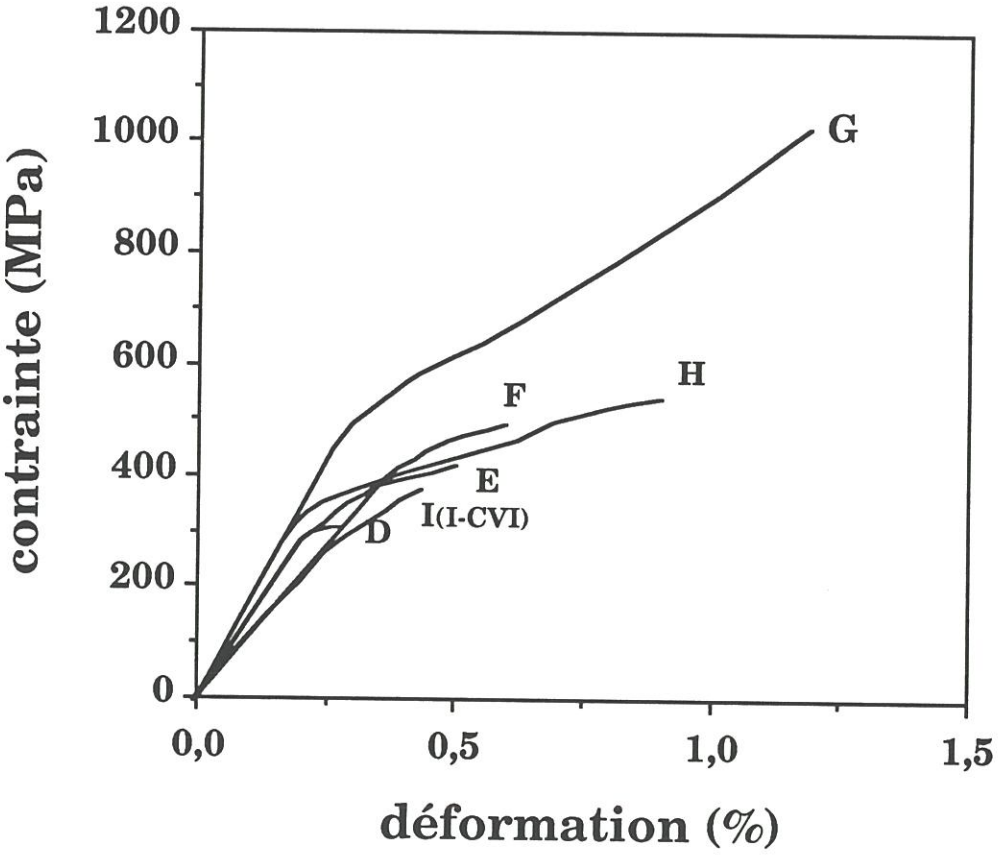

Fig. 12 : Courbes types de comportement en traction des lots D,E,F,G,H,I (fibres ex-PCS/PyC/SiC).

3.2- Composites unidirectionnels SiC/PyC/SiC

3.2.1- Analyse des courbes contrainte-déplacement

Les courbes types contrainte-déplacement relatives aux lots D à I sont présentées à la figure 12. Les trois domaines observés classiquement sont présents. Le domaine élastique est beaucoup plus étendu que dans le cas des mèches C/PyC/SiC. Le domaine de multifissuration est très large, sauf pour le lot D qui ne semble pas atteindre la saturation matricielle. Les mèches des lots E,F montrent un comportement proche. Deux lots se mettent en évidence : le lot D qui subit une rupture prématurée sous une faible contrainte, le lot G dont l'allongement et la contrainte à rupture sont beaucoup plus élevés que ceux des autres lots.

3.2.2- Propriétés interfaciales

Les valeurs des grandeurs mécaniques calculées à partir des courbes contrainte-déplacement sont rassemblées au tableau 3.

Il apparaît que le lot D présente les résultats les plus dispersés, alors que les résultats des lots E et G sont très groupés.

L'influence pure de l'épaisseur de l'interphase sur les propriétés mécaniques est difficile à analyser car les fractions volumiques de matrice et de fibres varient d'un lot à l'autre. Cependant, l'ensemble des caractéristiques mécaniques des composites unidirectionnels SiC/PyC (P-CVI)/SiC évolue avec la valeur de e_i, passant par un optimun pour le lot G (e_i=0,22 µm). Ceci est en bon accord avec divers travaux montrant une variation semblable des contraintes à rupture avec l'épaisseur d'interphase PyC obtenue par I-CVI dans le cas de matrices SiC ou vitrocéramique [5,6,17].

lot	σ_{r1} (MPa)	m	σ_{r2} (MPa)	σ_e (MPa)	σ_s (MPa)	ε_e %	ε_s %	ε_r %	ds (µm)	τ_c (MPa)
D (P-CVI, e_i=0,05 µm)	300 [120]	2,6	871 [330]	228 [127]	---	0,18 [0,07]	---	0,26 [0,04]	200	---
E (P-CVI, e_i=0,09 µm)	470 [106]	10,9	1439 [310]	300 [38]	370 [58]	0,21 [0,04]	0,35 [0,11]	0,65 [0,20]	180	18,0
F (P-CVI, e_i=0,12µm)	549 [58]	5,5	1371 [125]	386 [52]	472 [31]	0,31 [0,10]	0,40 [0,08]	0,64 [0,16]	70	43,0
G (P-CVI, e_i=0,22 µm)	939 [144]	7,9	1910 [209]	387 [29]	566 [67]	0,26 [0,05]	0,58 [0,10]	1,30 [0,16]	30	90,7
H (P-CVI, e_i=1,0 µm)	470 [87]	6,0	1471 [306]	200 [44]	304 [47]	0,17 [0,03]	0,43 [0,12]	0,97 [0,15]	260	10,2
I (I-CVI, e_i=0,1 µm)	408 [76]	6,2	1108 [172]	280 [57]	347 [53]	0,21 [0,05]	0,31 [0,03]	0,46 [0,12]	70	37,5
[18] (I-CVI, e_i=0,2 µm)	458 [82]	---	---	237 [42]	---	0,081	---	0,63	35	---

[ ] écart type

Tableau. 3 : Résultats des lots D,E,F,G,H,I et de [18] (fibres ex-PCS/PyC/SiC).

Les contraintes thermiques résiduelles ont été calculées dans le cas de microcomposites SiC/PyC/SiC pour différentes épaisseurs d'interphase (0,05 µm< e_i < 1 µm) et une épaisseur de matrice fixée à 4 µm (fig. 13). Cette simulation numérique montre que la contrainte longitudinale dans la matrice (qui intervient sur la valeur de la limite d'élasticité ε_e) diminue légèrement lorsque e_i croît. ε_e devrait donc augmenter avec e_i, ce qui est effectivement observé pour les lots D, E et F. Dans le cas du lot H (e_i=1 µm) ε_e est plus faible, ceci pourrait être lié à un affaiblissement des interfaces induit par des contraintes résiduelles (circonférentielles aux interfaces et radiales dans l'interphase) qui croissent avec e_i et deviennent de tension pour e_i>0,4 µm.

Des contraintes résiduelles radiales de **compression** sont présentes dans l'interphase pour **e_i<0,4 µm** et de **tension lorsque e_i>0,4 µm**. Les contraintes résiduelles de compression assurent le frettage de la fibre et de l'interphase par la matrice causant ainsi une décohésion interfaciale fibre/interphase limitée et un bon transfert de charges fibre/matrice. Inversement, en présence de contraintes résiduelles de tension, le système est décohésif. Ceci explique l'évolution de d_s et de τ_c avec e_i. Le comportement particulier des mèches du lot G pourrait provenir d'une épaisseur d'interphase optimum associée à une épaisseur de matrice plus faible que celle des autres lots (3 µm au lieu de 4,5 µm).

La comparaison des résultats obtenus à épaisseur d'interphase constante pour les mèches du lot I (I-CVI, e_i=0,1 µm) avec ceux des lots E et F (P-CVI, e_i=0,09 et 0,12 µm) montre que l'emploi **d'une interphase P-CVI améliore les propriétés mécaniques.**

Cette amélioration des propriétés mécaniques lors de l'utilisation d'une interphase PyC (P-CVI) est aussi mise en évidence en comparant les résultats obtenus par Fretty [18] (tableau 3) (qui a testé en traction des composites

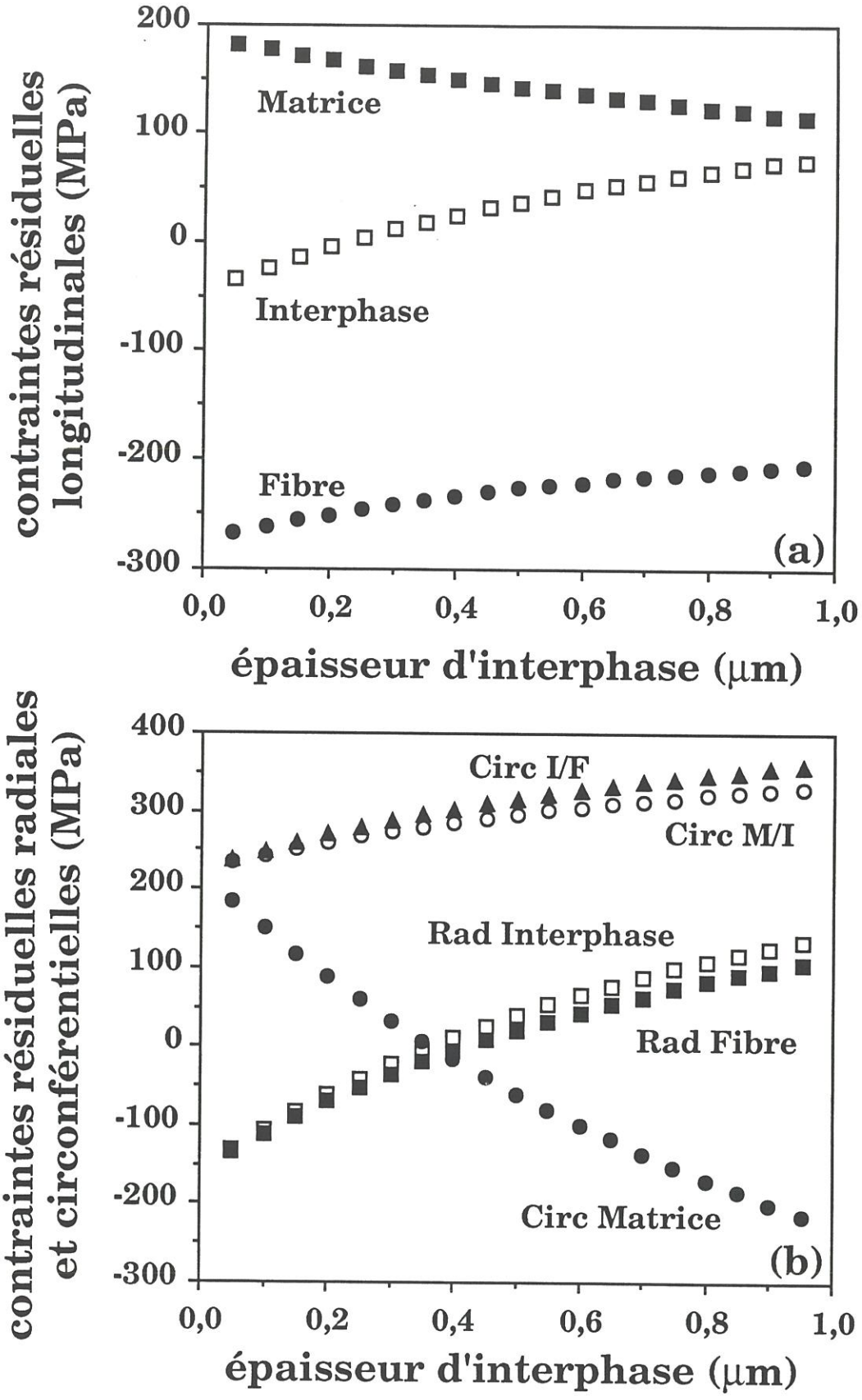

Fig. 13 : Variations des contraintes résiduelles d'origine thermique dans un microcomposite SiC / PyC / SiC en fonction de l'épaisseur de l'interphase pyrocarbone : (a) contraintes longitudinales et (b) contraintes radiales et circonférentielles.

SiC/PyC/SiC unidirectionnels, d'une longueur de 50 mm, à interphase pyrocarbone I-CVI, e_i=0,2 µm, Vf=45 %) avec ceux du lot G (P-CVI, e_i=0,22 µm, Vf=47 %). Les valeurs moyennes de contrainte et d'allongement à rupture sont nettement supérieures dans le cas du lot G. La différence du volume testé bien qu'importante ne permet pas d'expliquer l'écart entre les résultats des deux lots, d'ailleurs Fretty obtient des mesures peu différentes avec des composites unidirectionnels d'une longueur de 180 mm. Il est donc probable que l'interphase P-CVI est à l'origine de l'amélioration des propriétés mécaniques. Ceci pourraît être dû à la **microstructure particulière du PyC déposé en P-CVI** qui améliorerait la souplesse de l'interphase. Comme dans le cas des composites C/PyC/SiC, pour corréler les calculs numériques et les résultats expérimentaux il est nécessaire de considérer que l'interphase P-CVI est plus anisotrope ($E_1/E_3 \approx 5$) que l'interphase I-CVI ($E_1/E_3 \approx 2,5$).

4- CONCLUSION

Les deux familles de mèches (C/PyC/SiC et SiC/PyC/SiC) présentent le comportement classique de composites à matrice céramique testés en traction.

La comparaison des propriétés mécaniques (limites et contraintes élastiques, à saturation, et de rupture) des différents lots de mèches a permis de mettre en évidence une forte variation des propriétés mécaniques avec **l'épaisseur de l'interphase** PyC (P-CVI), surtout dans le cas de mèches SiC/PyC/SiC. L'épaisseur de l'interphase semble avoir une influence moindre dans le cas de mèches C/PyC/SiC, bien que les valeurs obtenues avec e_i=1µm soient beaucoup moins dispersées que celles obtenues avec e_i=0,5µm. Des études sur les contraintes résiduelles de microcomposites C/PyC/SiC et

SiC/PyC/SiC permettent d'expliquer l'évolution des caractéristiques mécaniques avec e_i.

La comparaison des lots à interphase PyC (P-CVI) et PyC (I-CVI) a montré une nette amélioration des caractéristiques mécaniques lors de l'utilisation d'une interphase PyC (P-CVI). Ceci semble être lié à la **microstructure particulière du PyC déposé en P-CVI** [10] qui permettrait un meilleur transfert de charge tout en évitant le délaminage aux interfaces, et autoriserait les déformations de la fibre dans les régions situées entre les zones de décohésion où elle est liée à la matrice.

REMERCIEMENTS

La présente étude a été réalisée avec l'aide de SEP, sous la forme d'une bourse d'étude attribuée à P. Dupel et la fourniture de matériaux. Elle a, par ailleurs, bénéficié de l'assitance technique de B. Humez.

REFERENCES

[1] R. Naslain, Introduction aux materiaux composites 2- Matrices métalliques et céramiques, Ed. CNRS/IMC, Bordeaux, (1985).

[2] A. G. Evans, F. W. Zok et J. Davis, The role of interfaces in fiber-reinforced brittle matrix composites, Composites Science and Technology, (1991) 3 .

[3] L. Grateau, Etude du comportement mécanique de composites monofilamentaires SiC/SiC- Rôle de l'interface, Thèse de doctorat, numéro d'ordre : 779, université de Paris -Sud (Centre d'Orsay), décembre 1987.

[4] R. Naslain, O. Dugne, A. Guette, J. Sevely, C. Robin-Brosse, J.P. Rocher et J. Cotteret, Boron nitride in ceramic-matrix composites, J. Am. Ceram. Soc., **74** [10] (1991) 2482 .

[5] E. Menessier, A. Guette, A. Pailler et R. Naslain, Influence de l'épaisseur d'un dépôt pyrocarbone sur les propriétés mécaniques d'un matériaux composite (fibre Nicalon/matrice vitrocéramique), Comptes rendus des Sixièmes Journées Nationales sur les Composites, Paris, 11-13 octobre 1988, p 195.

[6] R.A. Lowden et D.P. Stinton, The influence of the fiber-matrix bond on the mechanical behaviour of Nicalon/SiC composites, Oak Ridge National Laboratory, 1987, P 44, Rapport n° ORNL/TM-10667, DE88006155.

[7] R. Naslain, Interfaces et interphases in MMC and CMC : A comparative approach, Actes de Mechanical Properties and Applications of MMC, Japan-France Worrkshop on MMC, 1992, Paris.

[8] D. Cojean, Composites SiC/C/SiC : Relation entre les propriétés mécaniques et la microtexture des interphases, Thèse de doctorat, numéro d'odre : 104, université de Pau, septembre 1991.

[9] P. Dupel, R. Pailler et R. Naslain, Pulse chemical vapor deposition (P-CVD) and infiltration (P-CVI) of pyrocarbon in model pores with rectangular cross section, Part 2 : Study of infiltration, soumis au J. Mat Sciences.

[10] P. Dupel, X. Bourrat et R. Pailler, Anisotropic pyrocarbon obtained at low temperature by pulse-CVI : Structural characterization, soumis à Carbon.

[11] P. Dupel, R. Pailler, F. Langlais, R. Naslain et A. Costecalde, CVD/CVI of pyrocarbon from propane on flat substrate and in model pores with rectangular cross-sections, soumis à Carbon.

[12] L. Heraud, F. Christin et R. Naslain, Brevet Français du 06/09/1977, n° FR-A-2 401 888.

[13] W.A. Weibull, A statistical distribution of wide applicability, J. Applied Mechanics, sept. 1951, 525-532.

[14] D.B. Marshall et A.G. Evans, Failure mechanisms in ceramic-fiber/ceramic-matrix composites, J. Am. Ceram. Soc., **68** [5] (1985) 225.

[15] J.L. Bobet et J. Lamon, Thermal residual stress field in continuous fiber reinforced ceramix matrix microcomposites, Proc of MAT-TEC 92, (A. Niku-Lari, ed.), Grenoble, (1992) 35.

[16] J. D. Eshelby, The elastic field outside an ellipsoidal inclusion, Proc of the Royal Society, London, Serie A, 252 (1959) 561.

[17] P. Pluvinage, Etude expérimentale et simulation numérique du comportement mécanique de matériaux composites SiC/SiC. Influence des paramètres de stratification et d'élaboration, Thèse de doctorat, numéro d'ordre 584, Université de Bordeaux I, Avril 1991.

[18] N. Fretty, Comportement et endommagement mécaniques de torons densifiés et de matériaux 1D et 2D SiC/SiC. Influence de vieillissement sous air à haute température, Thèse de doctorat, Ecole Nationale Supérieure des Mines de Paris, septembre 1991.

CONCLUSIONS GENERALES

Ce travail s'inscrit dans le cadre général des études visant à améliorer le procédé d'élaboration des CMC par la voie gazeuse (CVI). Il a été appliqué à un système chimique, à priori, simple : le dépôt de **pyrocarbone** à partir d'un précurseur gazeux. L'essentiel de l'étude est basé sur des dépôts réalisés à partir de **propane**, mais d'autres gaz comme le méthane et le propylène ont été également utilisés.

La comparaison entre ces deux méthodes d'infiltration a été réalisée à l'aide de substrats en graphite comprenant trois types de **pores modèles** de 320 µm, 120 µm et 60 µm de hauteur sur 2 mm de largeur et 20 mm de long. Ces substrats ont été préférés à des préformes fibreuses en raison d'une plus grande facilité d'exploitation. En effet, il a été possible de mesurer avec précision le profil de dépôt en épaisseur le long de l'axe du pore. De même, la qualité du pyrocarbone déposé en toute position d'un pore a pu être quantifiée par la mesure en microscope optique de l'angle d'extinction.

Le premier chapitre de ce mémoire était consacré au dépôt du pyrocarbone à partir de propane dans les pores modèles par I-CVI. Une étude cinétique dans un domaine restreint a permis d'établir une **loi cinétique**. Celle-ci a été employée par Fedou pour calculer les profils de dépôt dans les pores modèles à partir d'une approche théorique qu'il a développée sur l'infiltration d'un pore rectiligne à section rectangulaire. Il a observé une bonne adéquation entre les résultats expérimentaux d'infiltration et les profils de dépôt théoriques. Dans un second temps, **l'infiltration des pores modèles** a été optimisée à l'aide d'un plan d'expériences simple ne prenant en compte que la

pression et le débit gazeux. Il apparaît que contrairement à ce qui aurait dû être, la meilleure qualité d'infiltration n'est pas obtenue pour la pression minimale, mais pour une pression intermédiaire (3 kPa), le débit ayant peu d'influence dans le domaine expérimental considéré. La température joue un rôle important sur l'infiltration des pores, une température élevée réduisant fortement le taux de remplissage du pore. En I-CVI, une decroissance de la qualité du dépôt est toujours observée le long de l'axe des pores, celle-ci étant d'autant plus prononcée que la taille du pore est petite. La valeur de l'angle d'extinction a pu être reliée à un facteur empirique (Fap) fonction de la quantité de benzène présent dans le four et évaluée par spectromètrie de masse.

Le second chapitre abordait la P-CVI sous son aspect "cinétique", bien qu'il soit difficile d'utiliser ce terme en P-CVI puisqu'il s'agit de dépôt réalisé pulse après pulse. C'est pourquoi la notion d'épaisseur de pyrocarbone déposée par pulse a été choisie. Cette étude met en exergue l'importance de **l'état de maturation** dans lequel se trouve la phase gazeuse. En effet, le dépôt étant réalisé en milieu clos, la composition de la phase gazeuse évolue rapidement et tend vers un équilibre. Dans les premiers instants du pulse, le dépôt est réalisé à partir de molécules proches du propane qui doivent réagir directement avec la surface par des réactions hétérogènes (**processus I**) conduisant à une croissance latérale du carbone. Puis, des réactions homogènes de cyclisation, aromatisation.. conduisent à la formation de molécules de plus grande taille qui doivent se déposer par condensation sur la surface du substrat (**processus II**) conduisant à une croissance colonnaire du carbone. Ces réactions en phases homogène et hétérogène produisent de l'hydrogène qui inhibe les processus de dépôt en fin de pulse : au-dessus d'une durée de palier limite,

l'épaisseur de PyC déposée par pulse devient pratiquement indépendante du temps.

En fonction des conditions expérimentales, l'importance relative des deux processus varie car la phase gazeuse se modifie plus ou moins rapidement selon la pression et la température. Ainsi, une température et une pression élevées conduisent à un dépôt essentiellement formé à partir de molécules aromatiques de grande taille alors que faibles température et pression conduisent à un PyC formé par des molécules très hydrogènées de petite taille.

Le troisième chapitre était consacré à **l'infiltration des pores modèles par P-CVI**. Trois paramètres jouent un rôle important : la température, la pression et la durée du palier. Tout comme en I-CVI, la qualité de l'infiltration est améliorée pour les basses températures. Il en est de même pour la pression contrairement à l'I-CVI où un optimun proche de 3 kPa a été observé.

La variation de la qualité de l'infiltration avec la durée du palier est plus complexe. Schématiquement un pulse peut se décomposer en deux phases :

(i) pour les durées de palier très courte, une phase de convection forcée du gaz source dans les pores, et (ii) une seconde phase au cours de laquelle la diffusion et la maturation de la phase gazeuse interviennent.

Au cours de la première phase, le gaz présent dans le pore conduit à un dépôt de pyrocarbone par l'intermédiaire de réactions hétérogènes. Cette phase correspond à la P-CVI proprement dite conduisant en théorie à une très bonne infiltration. Cependant, les durées de palier nécessaires sont très courtes (<0,05 s) et peu compatibles avec un appareillage de laboratoire, et encore moins avec des fours industriels.

Au cours de la seconde étape, qui intervient très rapidement surtout à haute température ou haute pression, la taille et la quantité des molécules conduisant au dépôt va dans un premier temps croître, et conduire à une qualité d'infiltration qui decroît avec la durée du palier. En effet, les molécules de grande taille auront tendance à se déposer à l'entrée des pores, leur diffusion étant limitée par leur taille et leur nombre, cette tendance est d'autant plus forte que leur taille est grande. Puis, la quantité d'hydrogène croissant et celle en gaz source diminuant, les réactions en phase homogène deviennent plus limitées, et la taille moyenne des molécules décroît, ce qui favorise leur diffusion dans les pores et conduit à une forte amélioration de la qualité de l'infiltration pour les durées de palier longues. Ainsi, la qualité de l'infiltration des pores modèles passe par une durée de palier minimun se situant en général entre 2 et 10 s.

Le quatrième chapitre était consacré à l'étude microstructurale, en microscopie optique en lumière polarisée et en microscopie électronique en transmission, des pyrocarbones déposés en I-CVI et en P-CVI.

En I-CVI, les observations confirment la dégradation de l'anisotropie du pyrocarbone déposé dans les pores, ceci quelles que soient les conditions opératoires.

C'est en général le cas en P-CVI, mais il existe une fenêtre expérimentale pour laquelle le pyrocarbone déposé est **anisotrope dans tout le pore**, et ou la qualité de l'infiltration est relativement satisfaisante. Ces conditions expérimentales particulières correspondent au processus I. Le processus I peut donc conduire à un PyC de mauvaise qualité dans les premiers instants du pulse, puis la taille moyenne des molécules croissant, à

un dépôt anisotrope. Ce processus est supposé être associé à une croissance latérale de la couche de carbone. Lorsque la durée du palier augmente, le processus II est majoritaire et entraîne la formation d'un pyrocarbone très anisotrope, avec empilement des molécules. En fin de palier, la qualité du pyrocarbone se dégrade en raison de l'intégration de molécules très hydrogènées au dépôt qui viennent perturber les couches de carbone.

Il est étonnant de constater que le pyrocarbone déposé avec des durées de palier longues peut être tout à fait différent de celui obtenu avec des durées de palier intermédiaires. Il faut concevoir que lors de la dernière phase de dépôt, le pyrocarbone de mauvaise qualité empêche un dépôt correct au cours du pulse suivant.

Le cinquième chapitre était une étude des propriétés mécaniques de composites unidirectionnels dont l'interphase a été déposée par I-CVI ou par P-CVI. Il apparaît que la méthode de dépôt de l'interphase joue un rôle effectif sur les propriétés mécaniques des composites. Ainsi, à épaisseur d'interphase identique, l'interphase P-CVI a conduit à un accroissement d'environ 30 % des caractéristiques mécaniques.

L'épaisseur de l'interphase a été optimisée dans le cas de composites SiC/PyC/SiC, l'optimun se situant vers 0,2 µm. Les contraintes résiduelles après élaboration pourraient expliquer l'existence de cette optimun. Cette étude, très limitée, appelle un travail complémentaire d'analyse au TEM des interphases P-CVI et I-CVI, qui n'a malheuresement pu être entrepris faute de temps, afin de mettre en évidence les raisons de cette amélioration des propriétés mécaniques.

En résumé, ce travail représente **la première étude approfondie de la P-CVI**, appliquée plus particulièrement au dépôt de pyrocarbone à partir de propane.

L'importance des réactions en phase homogène sur la qualité de l'infiltration et sur l'anisotropie du dépôt de pyrocarbone dans les pores modèles a été mise en évidence. Le principal avantage de la P-CVI apparaît être sa capacité à contrôler, par l'intermédiaire du temps de résidence, la taille des espèces intermédiaires gazeuses conduisant au dépôt de pyrocarbone. Cette technique permet, d'une part , d'accroître la vitesse moyenne par rapport à l'I-CVI et, d'autre part, à qualité d'infiltration proche, d'obtenir une meilleure qualité et homogénéité du PyC déposé au sein des pores. En outre, si elle semble difficile à transposer au niveau industriel sous sa forme actuelle, elle constitue un moyen d'analyse fine des **systèmes transitoires** et ainsi peut permettre de définir des compositions de phases gazeuse qui, en I-CVI, conduiraient à une bonne infiltration tout en conservant une bonne qualité du PyC déposé, ce qui n'est pas le cas en général.

Un autre intérêt de la P-CVI est de pouvoir réaliser des dépôt de très fine épaisseur (de l'ordre du nm), pouvant mener à l'élaboration d'interphase séquencée sur une très fine échelle. Une étude est d'ailleurs en cours au laboratoire sur ce sujet.

RESUME :

Les limites inhérentes à la CVI isotherme-isobare (I-CVI) ont conduit à explorer de nouvelles voies d'infiltration chimique en phase vapeur dont la **CVI pulsée (P-CVI)**. La P-CVI consiste à faire varier cycliquement un paramètre (e.g. la pression) pendant le dépôt.
Ce travail, avait pour objectif de réaliser une étude exhaustive de la P-CVI du pyrocarbone (PyC). Il s'est orienté autour de trois axes principaux :
(i) en I-CVI, l'optimisation de la qualité d'infiltration de pores modèles a été réalisée et la microstructure des dépôts reliée à la **concentration en espèces aromatiques** de la phase gazeuse,
(ii) en P-CVI, l'étude de la qualité de l'infiltration associée à l'observation microstructurale des dépôts dans les pores (MET ou microscope optique en lumière polarisée) a permis de montrer l'importance du **temps de séjour** des espèces gazeuses dans le réacteur et de proposer un modèle explicatif permettant de rendre compte des différents résultats expérimentaux,
(iii) la P-CVI permet de déposer un pyrocarbone présentant une **anisotropie particulière**, celui-ci testé en tant qu'interphase dans des composites unidirectionnels conduit à une amélioration notable des propriétés mécaniques vis à vis d'un PyC conventionnel (laminaire rugueux).

MOTS CLES :

- CVD/CVI isotherme-isobare
- CVD/CVI pulsée
- Pyrocarbone
- Propane
- Microstructure
- Pores modèles
- Composites
- Interphase